STUDIES OF THE N-END RULE PATHWAY IN *SACCHAROMYCES CEREVISIAE*

Thesis by

Anna Shemorry

In Partial Fulfillment of the Requirements

for the Degree of

Doctor of Philosophy

California Institute of Technology

Pasadena, California

2013

(Defended January 18, 2013)

ACKNOWLEDGEMENTS

I would like to first thank my advisor, Alexander Varshavsky: without him this work would not be possible. His enthusiasm for scientific discovery is contagious.

In addition, I would like to thank Cheol-Sang Hwang, a major collaborator in all my work. With his scientific rigor and prolific work ethic, we were able to open up two major lines of research. These discoveries would not be possible without his support.

I also want to thank my thesis committee, Judith Campbell, William Dunphy, and Shu-ou Shan, for all your support over the years.

Lastly, I would like to thank my husband and partner in life, Piotr Dollar. Without his daily support, I would not have reached this point.

I would like to dedicate this dissertation to my grandfather, Ernest Thesman. I wish you could have seen me finish, but I know you had no doubt in your mind that I would. I do not think I would have aspired to such great heights if you had not shown me what was possible in life.

ABSTRACT

Many intracellular proteins are either conditionally or constitutively short-lived, with in vivo half-lives that can be as brief as a few minutes. The regulated and processive degradation of intracellular proteins is carried out largely by the ubiquitin (Ub)-proteasome system (UPS). In eukaryotes, the N-end rule pathway is a part of the UPS. The N-end rule relates the regulation of the in vivo half-life of a protein to the identity of its N-terminal residue. Degradation signals (degrons) that are targeted by the N-end rule pathway include a set called N-degrons. E3 Ub ligases of the N-end rule pathway are called N-recognins. They bind to primary destabilizing N-terminal residues of N-end rule substrates. The N-end rule pathway comprises two major branches, the Arg/N-end rule pathway and the Ac/N-end rule pathway.

The Arg/N-end rule branch involves the N-terminal arginylation of protein substrates and also the targeting of specific unmodified N-terminal residues by E3 N-recognins. The *S. cerevisiae* Arg/N-end rule pathway contains a single N-recognin, Ubr1. The Ub-fusion degradation (UFD) pathway is also a part of the UPS. This pathway recognizes a ‘‘nonremovable’’ N-terminal Ub moiety of a Ub fusion as a primary degron. My collaborator, Cheol-Sang Hwang, and I demonstrated that the RING-type Ubr1 E3 and the HECT-type Ufd4 E3 interact, both physically and functionally. We showed that the Ubr1-Ufd4 complex targets the *S. cerevisiae* Mgt1 DNA repair enzyme through a degron near its N-terminus, in addition to mediating the Arg/N-end rule pathway and a part of the UFD pathway as well. We also further characterized the physical interaction between Ubr1 and Ufd4.

I also report the discovery of the other branch of the N-end rule pathway, the Ac/N-end rule pathway, which recognizes N-terminally acetylated residues as N-degrons, termed Ac/N-degrons. We showed that Ac/N-degrons are recognized by the Doa10 E3 Ub ligase and apparently by other E3s as well. Given the prevalence of Ac/N-degrons, as nearly 90% of human proteins are Nt-acetylated, we also demonstrated the physiological role of Ac/N-degrons in protein quality, including the regulation of input stoichiometries of subunits in oligomeric proteins.

TABLE OF CONTENTS

LIST OF FIGURES

Figure **Page**

CHAPTER 1:

AN INTRODUCTION TO THE N-END RULE PATHWAY

The Ubiquitin-Proteasome System

Intracellular proteolysis involves both nonprocessive (single) cleavages of polypeptide chains of cellular proteins and the processive (complete or nearly complete) degradation of specific proteins to short peptides and/or individual amino acids. Many intracellular proteins are either conditionally or constitutively short-lived, with in vivo half-lives that can be as brief as a few minutes. One major role of proteolytic pathways is the selective destruction of regulatory proteins whose concentrations must vary with time and alterations in the state of a cell. Among the other functions of intracellular proteolysis are the elimination of misfolded or otherwise abnormal proteins, the maintenance of amino acid pools in cells affected by stresses such as starvation, and the generation of protein fragments that act as hormones, antigens, or other effectors (1). A short in vivo half-life of a protein provides a way to generate its spatial gradient and to rapidly adjust its concentration or subunit composition through changes in the rate of its degradation (2). In conjunction with molecular chaperones, autophagy, and lysosomal proteolysis, selective degradation of proteins largely occurs through the ubiquitin-proteasome system (UPS) (1,3). In this multipathway system, proteins are marked for degradation by the covalent conjugation of ubiquitin (Ub) to the target protein (4).

Ub is a 76-residue protein that mediates proteolysis through the enzymatic conjugation of Ub to proteins that contain primary degradation signals, called degrons (5). Ub-protein conjugation marks proteins for their recognition and degradation by the 26S proteasome, a processive, ATP-dependent protease (6). Ub

is conjugated to proteins either as a single moiety or as a poly-Ub chain that is linked (in most cases) to the ε-amino group of an internal Lys residue in a substrate protein, although other residues have been shown to conjugate Ub (7). The number of topologically distinct poly-Ub chains can be very large, as all seven Lys residues of Ub can contribute, in specific in vivo contexts, to the synthesis of poly-Ub linked to protein substrates. The delivery of ubiquitylated proteins to the 26S proteasome can be mediated by either K48-type, K11-type or K29-type chains, and possibly by poly-Ub of other topologies as well (8-10).

The 26S proteasome is a multisubunit ATP-dependent protease that degrades polyubiquitylated proteins (11,12). The 26S proteasome is composed of the 19S regulatory particle (RP) and the 20S core particle (CP) (3,6,13). The RP is responsible for recognizing the proteins to be degraded, to a large extent through conjugated poly-Ub chains. Substrates are recognized by specific ubiquitin receptor proteins located in the RP. The substrate-linked poly-Ub chains are disassembled by deubiquitylating enzymes (DUBs), some of which are subunits of the RP. The targeted substrate is at least partially unfolded by ATPase subunits of the RP and thereafter is threaded through a channel into the CP, which processively degrades the protein to short peptides.

The conjugation of Ub to other proteins involves a preliminary ATP-dependent step in which the last residue of Ub (Gly^{76}) is joined, via a thioester bond, to a Cys residue of the E1 (Ub-activating) enzyme. The ‘‘activated’’ Ub moiety is transferred to a Cys residue in one of several Ub-conjugating (E2) enzymes, and from there, through an isopeptide bond, to a Lys residue of an ultimate acceptor. E2

enzymes function as subunits of E2-E3 Ub ligase complexes that can produce substrate-linked poly-Ub chains. This process is illustrated in figure 1.1.

One role of the E3 is the recognition of a substrate's degradation signal (degron (5)). Individual mammalian genomes encode at least 1000 distinct E3 Ub ligases. There are 2 major types of E3 ligases in eukaryotes, defined by their catalytic domain (14). One type of E3 contains a RING (or RING-like) domain and a conserved cysteine and histidine residue that coordinate 2 zinc ions (15). The RING E3s mediate the direct transfer of the Ub moiety from the E2 to the target protein. The other type of E3, with a HECT domain, transfers the Ub molecule to a cysteine within itself and then transfers the Ub molecule to the substrate (16).

The N-end Rule Pathway

The 1986 discovery of the N-end rule pathway identified the first specific pathway of the Ub system (17-20). The N-end rule relates the regulation of the in vivo half-life of a protein to the identity of its N-terminal residue. N-terminal degradation signals of the N-end rule pathway are called N-degrons. The main determinant of an N-degron is a destabilizing N-terminal residue of a protein. Recognition components of the N-end rule pathway are called N-recognins and in eukaryotes, these are the E3 Ub ligases that bind to specific N-degrons. In eukaryotes, the N-end rule pathway comprises two branches, the Arg/N-end rule pathway and the Ac/N-end rule pathway.

The Arg/N-end Rule Pathway

This branch involves the N-terminal arginylation (Nt-arginylation) of protein substrates and also the targeting of specific unmodified N-terminal residues by E3 N-recognins. N-terminal Arg, Lys, His, Leu, Phe, Tyr, Trp, Ile, Asp, Glu, Asn, Gln, and Cys comprise the main determinants of N-degrons in the Arg/N-end rule pathway. These residues become N-terminal by either the cotranslational removal of Met by Met-aminopeptidases (MetAPs) or by the posttranslational (and conditional) cleavage by nonprocessive proteases that include caspases, calpains, or separases. Among these N-degrons, the unmodified basic (Arg, Lys, His) and bulky hydrophobic (Leu, Phe, Tyr, Trp, Ile) N-terminal residues are recognized directly by cognate E3 N-recognins. These E3s contain highly spalogous (spatially similar (21)) ~80-residue regions called UBR domains or Type-1 binding sites. Folded around 3 zinc ions, a UBR domain binds to N-terminal Arg, Lys, or His, the Type-1 primary destabilizing residues of N-end rule substrates (22,23). Another (usually adjacent) region of UBR-type N-recognins, called the Type-2 binding site, recognizes N-terminal Leu, Phe, Tyr, Trp, or Ile, which are called the Type-2 primary destabilizing residues. Together, the directly recognized N-terminal Arg, Lys, His, Leu, Phe, Tyr, Trp, and Ile are denoted as primary destabilizing residues (24,25).

In contrast to these residues, the N-terminal Asp, Glu, Asn, Gln, and Cys function as secondary or tertiary destabilizing residues through their preliminary modification, depending on the number of specific modifications that precede their targeting by N-recognins. One of these modifications is Nt-arginylation. Arg-tRNA-protein transferase (R-transferase) conjugates Arg to N-terminal Asp, Glu, or

oxidized Cys of proteins or short peptides, with Arg-tRNA as the cosubstrate and the donor of Arg (26). R-transferases are encoded by Ate1 and its sequelogs from yeast to mammals but are absent from examined prokaryotes. In contrast to N-terminal Asp, Glu and oxidized Cys, the N-terminal Asn and Gln residues cannot be arginylated by R-transferase. However, the Arg/N-end rule pathway contains specific N-terminal amidases (Nt-amidases) that convert N-terminal Asn and Gln to Asp and Glu, respectively, followed by their Nt-arginylation (27).

The unmodified N-terminal Cys residue of a protein substrate is formally a tertiary destabilizing residue in the Arg/N-end rule pathway, as it must undergo two modifications (oxidation and arginylation) prior to substrate's binding by an N-recognin. If the protein's N-terminal Cys can be oxidized through (apparently nonenzymatic) reactions that require both nitric oxide (NO) and oxygen, and if these compounds are present in a cell at sufficient levels, the resulting N-terminal Cys-sulfinate or Cys-sulfonate (but not the original Cys) can be Nt-arginylated by the Ate1 R-transferase. The necessity of NO and oxygen for the destabilizing activity of N-terminal Cys makes the Arg/N-end rule pathway a sensor of both NO and oxygen (28).

Until recently, polyubiquitylation of substrates by the *S. cerevisiae* Arg/N-end rule pathway was thought to be mediated by a dimer comprising the 225-kDa Ubr1 E3 and the Ubr1-bound 20-kDa Rad6 E2 enzyme (25,29-31). As described in chapters 2 and 3 and appendix 1, we discovered that the targeting ensemble is more elaborate. It comprises a physical complex of the RING-type Ubr1 E3 (N-recognin) and the HECT-type Ufd4 E3, in association with their cognate E2s Rad6 and

Ubc4/Ubc5, respectively (32,33). Ufd4 is the 168 kDa HECT-type E3 of the Ub-fusion degradation (UFD) pathway that recognizes a ‘‘nonremovable’’ N-terminal Ub moiety of a Ub fusion as a primary degron and polyubiquitylates the Ub moiety, a prerequisite for the fusion’s degradation by the 26S proteasome (34,35). The UFD pathway was discovered by this laboratory in 1986 through analyses of N-terminal Ub fusions in which an alteration of either the Ub moiety or a junctional amino acid residue inhibits the cleavage of a fusion by deubiquitylases and thereby results in the fusion’s degradation by the UFD pathway. The UFD pathway is present in both yeast and mammals, suggesting that the Ubr1-Ufd4 double-E3 organization of the *S. cerevisiae* Arg/N-end rule pathway is universal among eukaryotes (36,37). Figure 1.A, B diagram the Arg/N-end rule pathway in mammals (A) and *S. cerevisiae* (B).

Physiological functions of the N-end rule pathway are strikingly broad and continue to be discovered. Regulated degradation of proteins by the eukaryotic Arg/N-end rule pathway mediates the sensing of heme, NO, oxygen, and short peptides; the selective elimination of misfolded proteins; the regulation of DNA repair (through degradation of Mgt1, a DNA repair protein); the cohesion/segregation of chromosomes (through degradation of a subunit of cohesin); the signaling by transmembrane receptors (through degradation of the G-protein regulators Rgs4, Rgs5, and Rgs16); the control of peptide import (through degradation of Cup9, the import’s transcriptional repressor); the regulation of apoptosis, meiosis, viral and bacterial infections, fat metabolism, cell migration, actin filaments, cardiovascular development, spermatogenesis, neurogenesis, and memory; the functioning of adult organs, including the brain, muscle, testis, and

pancreas; and the regulation of leaf and shoot development, leaf senescence, and seed germination in plants (24,27,38-66). Mutations in UBR1, an E3 N-recognin of the human Arg/N-end rule pathway, cause Johanson–Blizzard syndrome (JBS)(67).

The Ac/N-End Rule Pathway

The other branch is termed the Ac/N-end rule pathway. The Ac/N-end rule pathway was discovered by us in 2010, 24 years after the Arg/N-end rule pathway (chapter 4) (68). It involves the cotranslational Nα-terminal acetylation (Nt-acetylation) of nascent proteins whose N-termini bear either Met or the small uncharged residues Ala, Val, Ser, Thr, or Cys. These residues become N-terminal after the cotranslational removal of N-terminal Met by Met-aminopeptidases (MetAPs) (69,70).

The Nt-acetylated Met, Ala, Val, Ser, Thr, and Cys residues of newly formed proteins comprise a specific class of N-degrons, termed Ac/N-degrons. The cotranslational Nt-acetylation of nascent proteins is both enzymatically and functionally distinct from the largely posttranslational acetylation of internal residues in many proteins. The Nt-acetylation and internal acetylation are carried out by (mostly) nonoverlapping sets of specific acetylases. Previous studies of Nt-acetylation have characterized Nt-acetylated proteins and Nα-terminal acetyltransferases (Nt-acetylases) that catalyze this cotranslational modification (71-76). A diagram of the specificities of Nt-acetylases is shown in figure 1.4. Nt-acetylation is apparently irreversible. No Nt-deacetylases have been identified, in

contrast to a dynamic internal acetylation/deacetylation, with specific deacetylases removing internally conjugated acetyl groups.

In *S. cerevisiae*, Ac/N-degrons of the Ac/N-end rule pathway are recognized by the Doa10 E3 Ub ligase and apparently by other E3s as well, as shown in chapter 5. The 151-kDa RING-type Doa10 E3 is a multispanning integral membrane protein located in the ER membrane and in the inner nuclear membrane (77-79). The Doa10 E3 functions together with the Ubc6 and Ubc7 E2 enzymes and targets both ‘‘soluble’’ (nuclear and cytosolic) and transmembrane proteins (78). Isolated *S. cerevisiae* Doa10 selectively binds to the Nt-acetylated N-terminal Met, Ala, Val, Ser, Thr, Cys, Gly, and Pro residues of model peptides. Remarkably, the binding of Doa10 to Nt-acetylated residues of these peptides is precluded by the presence of a basic residue such as Lys at Position 2. Thus, the *S. cerevisiae* Ac/N-end rule pathway avoids the targeting of proteins with a basic residue at Position 2 through two independent constraints: first, such proteins are not Nt-acetylated in yeast (75); and second, the cognate Doa10 E3 apparently does not recognize Nt-acetylated proteins that bear a second-position basic residue.

The proteolytic function of Nt-acetylation is likely to be relevant to more than 80% of the entire proteome, that is, to many thousands of Nt-acetylated proteins. In contrast, either an identified or inferred necessity of Nt-acetylation for other (nonproteolytic) functions involves, at present, only ~10 Nt-acetylated proteins (80-85). What functions are subserved by such a massive production of degradation signals (Ac/N-degrons) in nascent proteins, if many of these proteins are destined for long half-lives? In 2010, we suggested that a major role of these

degradation signals involves quality-control mechanisms and the regulation of protein stoichiometries in a cell. A key feature of such mechanisms would be conditionality of AcN-degrons. We went on to verify and prove this hypothesis, as shown in chapter 5.

FIGURE 1.1. The ubiquitin-proteasome system (UPS). The conjugation of Ub to other proteins involves a preliminary ATP-dependent step in which the last residue of Ub (Gly^{76}) is joined, via a thioester bond, to a Cys residue of the E1 (Ub-activating) enzyme. The ‘‘activated’’ Ub moiety is transferred to a Cys residue in one of several Ub-conjugating (E2) enzymes, and from there, through an isopeptide bond, to a Lys residue of an ultimate acceptor, denoted as ‘‘protein.” E2 enzymes function as subunits of E2-E3 Ub ligase complexes that can produce substrate-linked poly-Ub chains. Such chains have specific Ub-Ub topologies, depending on the identity of a Lys residue of Ub (which contains several lysines) that forms an isopeptide bond with C-terminal Gly^{76} of the adjacent Ub moiety in a chain. Specific poly-Ub chains can confer the degradation of a substrate by the 26S proteasome or other metabolic fates. Monoubiquitylation of some protein substrates can also occur, and has specific functions. One role of E3 is the recognition of a substrate’s degradation signal (degron). Individual mammalian genomes encode at least a 1000 distinct E3 Ub ligases.

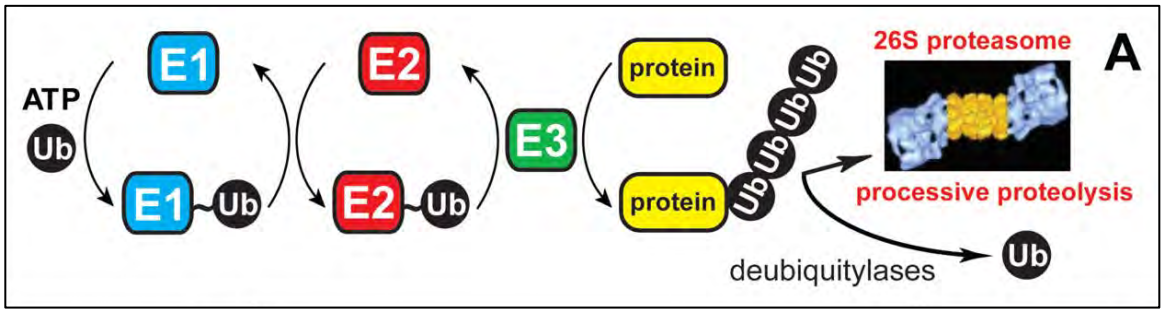

FIGURE 1.2. Overview of the Arg/N-end rule pathway

A. The mammalian Arg/N-end rule pathway. N-terminal residues are indicated by single- letter abbreviations for amino acids. Yellow ovals denote the rest of a protein substrate. ‘‘Primary,’’ ‘‘secondary,’’ and ‘‘tertiary’’ denote mechanistically distinct subsets of destabilizing N-terminal residues. C* denotes oxidized N-terminal Cys, either Cys- sulfinate or Cys-sulfonate, produced in vivo through reactions that require both nitric oxide (NO) and oxygen. The mammalian N-recognins Ubr1, Ubr2, Ubr4, and Ubr5 (Edd) have multiple substrate binding sites that also recognize internal (non-N-terminal) degrons in other substrates of the Arg/N-end rule pathway, the ones that lack N-degrons. A question mark after Trip12 (which mediates the mammalian UFD pathway (36,37) and is a sequelog of the *S. cerevisiae* Ufd4 E3) denotes the untested possibility that mammalian Ubr1 and/or Ubr2 form complexes with Trip12, by analogy with the Ubr1–Ufd4 complex in *S. cerevisiae*.

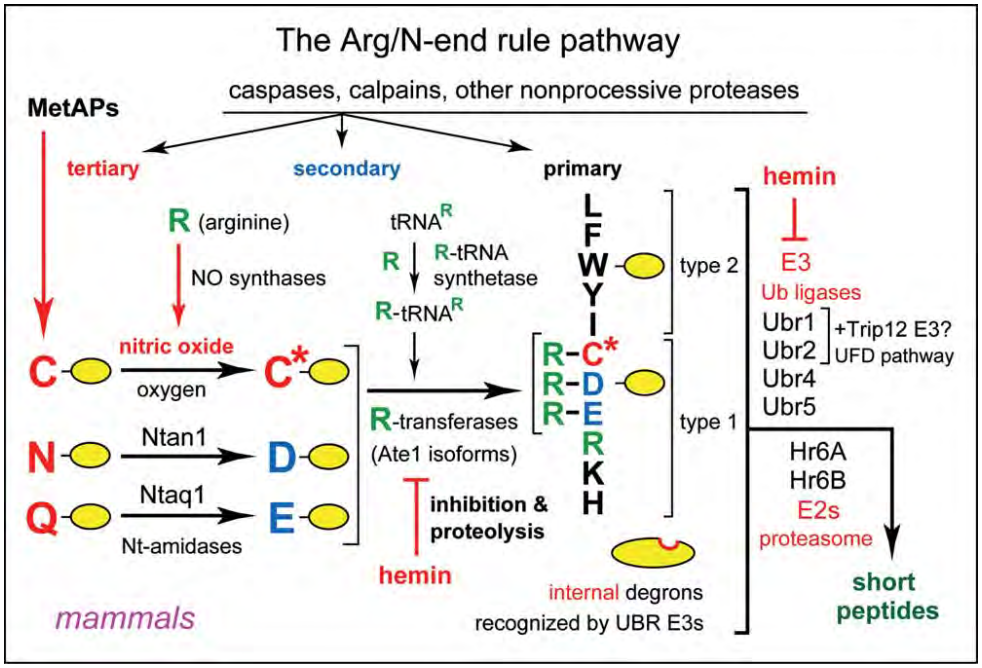

B. The Arg/N-end rule pathway in *S. cerevisiae.* Yellow ovals denote the rest of a protein substrate. ‘‘Primary,’’ ‘‘secondary,’’ and ‘‘tertiary’’ denote mechanistically distinct subsets of destabilizing N-terminal residues. The physically associated Ubr1 (N-recognin) and Ufd4 E3s have substrate-binding sites that recognize internal (non-N-terminal) degrons in substrates of the Arg/N-end rule pathway that lack N-degrons. Ubr1 (but not Ufd4) recognizes N-degrons as well.

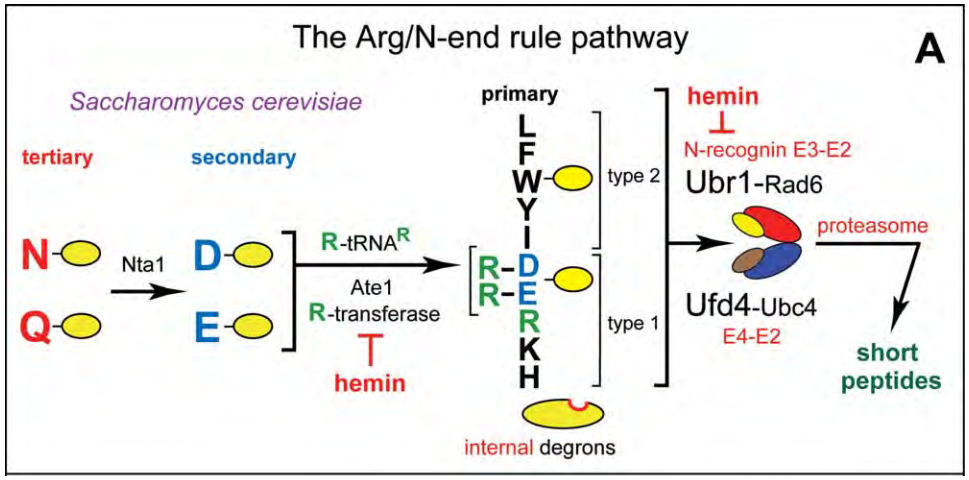

FIGURE 1.3. Overview of the Ac/N-end rule pathway. Red arrow on the left indicates the removal of N-terminal Met by Met-aminopeptidases (MetAPs). This Met residue is retained if a residue at Position 2 is nonpermissive (too large) for Met-aminopeptidases. If the (retained) N-terminal Met or N-terminal Ala, Val, Ser, Thr and Cys are followed by residues that allow Nt-acetylation, these N-terminal residues are usually Nt-acetylated. The resulting N-degrons are called Ac/N-degrons. The term ‘‘secondary’’ refers to the necessity of modification (Nt-acetylation) of a destabilizing N-terminal residue before a protein can be recognized by a cognate Ub ligase. Proteins containing AcN-degrons are targeted for ubiquitylation and proteasome-mediated degradation by the Doa10 E3 N- recognin, in conjunction with the Ubc6 and Ubc7 E2 enzymes. Although Gly and Pro can be made N-terminal by MetAPs, and although Doa10 can recognize Nt-acetylated Gly and Pro, few proteins with N-terminal Gly or Pro are Nt-acetylated.

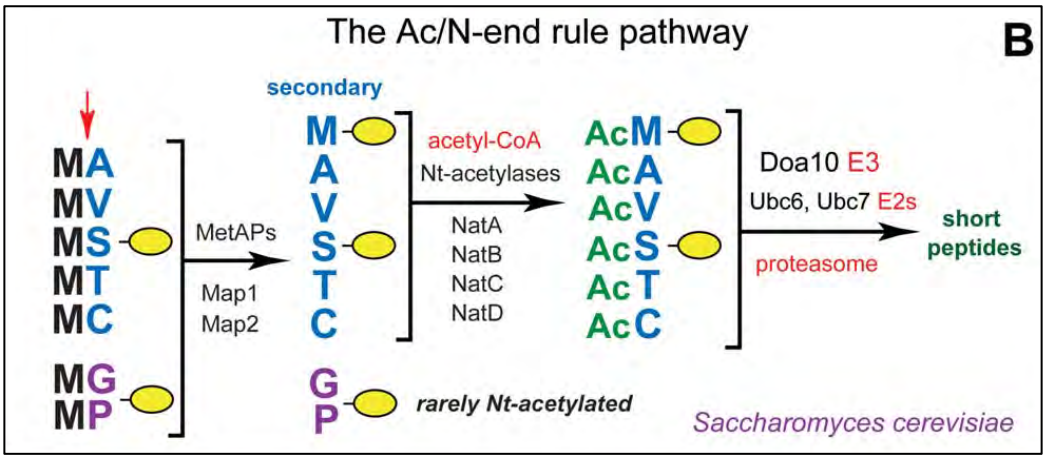

FIGURE 1.4 Substrate specificities and subunit compositions of *S. cerevisiae* Nt-acetylases. This compilation is derived from data in the literature. The present paper uses the revised nomenclature for specific subunits of Nt-acetylases and cites the older names of these subunits in parentheses.

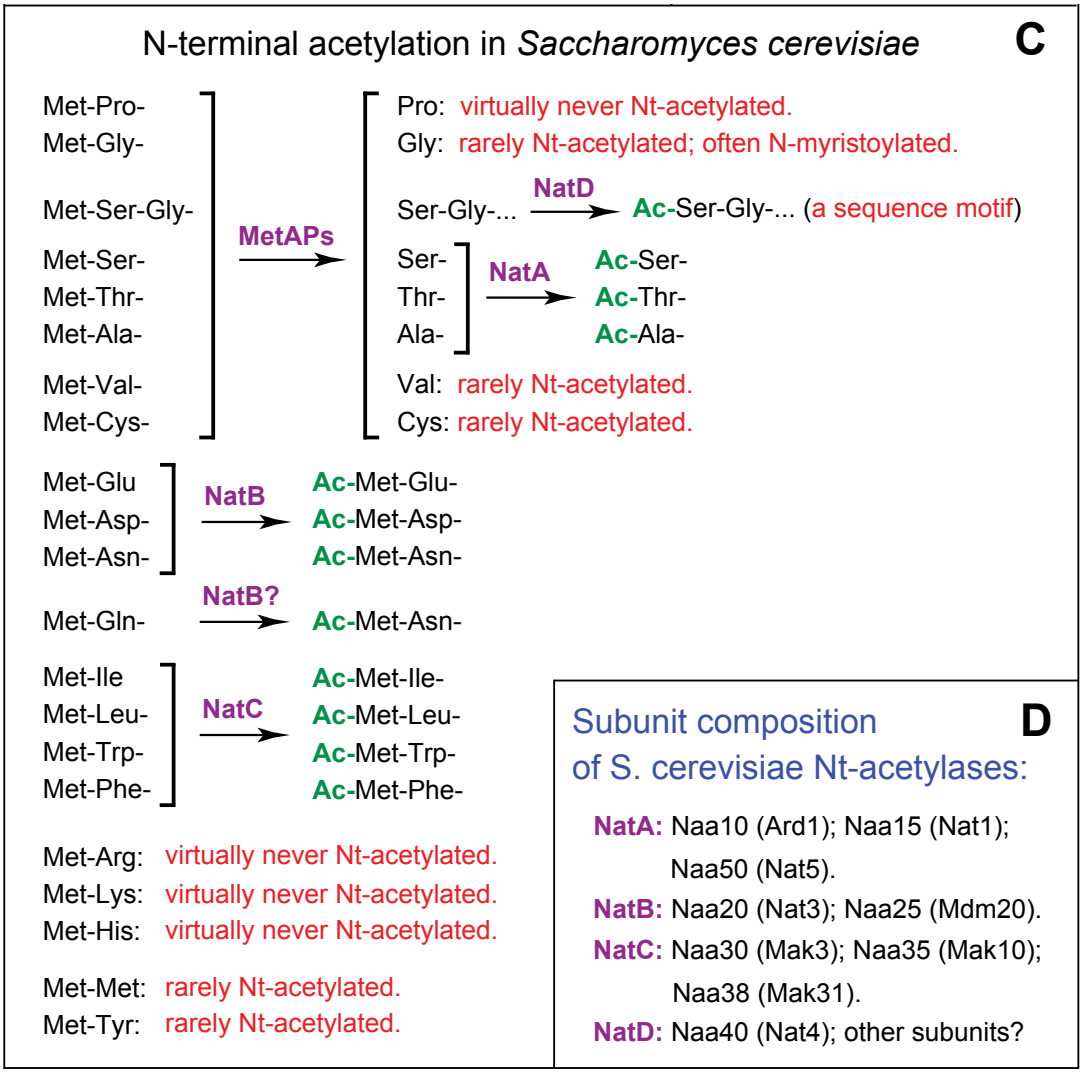

REFERENCES

1. Varshavsky, A. (2011) *Protein science : a publication of the Protein Society*
2. Ang, X. L., and Wade Harper, J. (2005) *Oncogene* **24**, 2860-2870
3. Finley, D., Ulrich, H. D., Sommer, T., and Kaiser, P. (2012) *Genetics* **192**, 319-360
4. Varshavsky, A. (2006) *Protein science : a publication of the Protein Society* **15**, 647-654
5. Varshavsky, A. (1991) *Cell* **64**, 13-15
6. Finley, D. (2009) *Annual review of biochemistry* **78**, 477-513
7. Kravtsova-Ivantsiv, Y., and Ciechanover, A. (2012) *Journal of cell science* **125**, 539-548
8. Hochstrasser, M. (2006) *Cell* **124**, 27-34
9. Kulathu, Y., and Komander, D. (2012) *Nature reviews. Molecular cell biology* **13**, 508-523
10. Behrends, C., and Harper, J. W. (2011) *Nature structural & molecular biology* **18**, 520-528
11. Gallastegui, N., and Groll, M. (2010) *Trends in biochemical sciences* **35**, 634-642
12. Marques, A. J., Palanimurugan, R., Matias, A. C., Ramos, P. C., and Dohmen, R. J. (2009) *Chemical reviews* **109**, 1509-1536
13. Xie, Y., and Varshavsky, A. (2000) *Proceedings of the National Academy of Sciences of the United States of America* **97**, 2497-2502

14. Metzger, M. B., Hristova, V. A., and Weissman, A. M. (2012) *Journal of cell science* **125**, 531-537

15. Deshaies, R. J., and Joazeiro, C. A. (2009) *Annual review of biochemistry* **78**, 399-434

16. Rotin, D., and Kumar, S. (2009) *Nature reviews. Molecular cell biology* **10**, 398-409

17. Bachmair, A., Finley, D., and Varshavsky, A. (1986) *Science* **234**, 179-186

18. Bachmair, A., and Varshavsky, A. (1989) *Cell* **56**, 1019-1032

19. Varshavsky, A., Bachmair, A., and Finley, D. (1987) *Biochemical Society transactions* **15**, 815-816

20. Varshavsky, A., Bachmair, A., Finley, D., Gonda, D. K., and Wunning, I. (1989) *Biotechnology* **13**, 109-143

21. Varshavsky, A. (2004) *Current biology : CB* **14**, R181-183

22. Choi, W. S., Jeong, B. C., Joo, Y. J., Lee, M. R., Kim, J., Eck, M. J., and Song, H. K. (2010) *Nature structural & molecular biology* **17**, 1175-1181

23. Matta-Camacho, E., Kozlov, G., Li, F. F., and Gehring, K. (2010) *Nature structural & molecular biology* **17**, 1182-1187

24. Tasaki, T., and Kwon, Y. T. (2007) *Trends in biochemical sciences* **32**, 520-528

25. Xia, Z., Webster, A., Du, F., Piatkov, K., Ghislain, M., and Varshavsky, A. (2008) *The Journal of biological chemistry* **283**, 24011-24028

26. Hu, R. G., Brower, C. S., Wang, H., Davydov, I. V., Sheng, J., Zhou, J., Kwon, Y. T., and Varshavsky, A. (2006) *The Journal of biological chemistry* **281**, 32559-32573

27. Wang, H., Piatkov, K. I., Brower, C. S., and Varshavsky, A. (2009) *Molecular cell* **34**, 686-695

28. Hu, R. G., Sheng, J., Qi, X., Xu, Z., Takahashi, T. T., and Varshavsky, A. (2005) *Nature* **437**, 981-986

29. Xia, Z., Turner, G. C., Hwang, C. S., Byrd, C., and Varshavsky, A. (2008) *The Journal of biological chemistry* **283**, 28958-28968

30. Du, F., Navarro-Garcia, F., Xia, Z., Tasaki, T., and Varshavsky, A. (2002) *Proceedings of the National Academy of Sciences of the United States of America* **99**, 14110-14115

31. Dohmen, R. J., Madura, K., Bartel, B., and Varshavsky, A. (1991) *Proceedings of the National Academy of Sciences of the United States of America* **88**, 7351-7355

32. Hwang, C. S., Shemorry, A., Auerbach, D., and Varshavsky, A. (2010) *Nature cell biology* **12**, 1177-1185

33. Hwang, C. S., Shemorry, A., and Varshavsky, A. (2009) *Proceedings of the National Academy of Sciences of the United States of America* **106**, 2142-2147

34. Johnson, E. S., Ma, P. C., Ota, I. M., and Varshavsky, A. (1995) *The Journal of biological chemistry* **270**, 17442-17456

35. Johnson, E. S., Bartel, B., Seufert, W., and Varshavsky, A. (1992) *The EMBO journal* **11**, 497-505

36. Park, Y., Yoon, S. K., and Yoon, J. B. (2009) *The Journal of biological chemistry* **284**, 1540-1549

37. Park, Y., Yoon, S. K., and Yoon, J. B. (2008) *Biochemical and biophysical research communications* **374**, 294-298

38. Hu, R. G., Wang, H., Xia, Z., and Varshavsky, A. (2008) *Proceedings of the National Academy of Sciences of the United States of America* **105**, 76-81

39. Varshavsky, A. (2008) *The Journal of biological chemistry* **283**, 34469-34489

40. Mogk, A., Schmidt, R., and Bukau, B. (2007) *Trends in cell biology* **17**, 165-172

41. Graciet, E., and Wellmer, F. (2010) *Trends in plant science* **15**, 447-453

42. An, J. Y., Seo, J. W., Tasaki, T., Lee, M. J., Varshavsky, A., and Kwon, Y. T. (2006) *Proceedings of the National Academy of Sciences of the United States of America* **103**, 6212-6217

43. Kwon, Y. T., Xia, Z., An, J. Y., Tasaki, T., Davydov, I. V., Seo, J. W., Sheng, J., Xie, Y., and Varshavsky, A. (2003) *Molecular and cellular biology* **23**, 8255-8271

44. Kwon, Y. T., Kashina, A. S., Davydov, I. V., Hu, R. G., An, J. Y., Seo, J. W., Du, F., and Varshavsky, A. (2002) *Science* **297**, 96-99

45. Kwon, Y. T., Xia, Z., Davydov, I. V., Lecker, S. H., and Varshavsky, A. (2001) *Molecular and cellular biology* **21**, 8007-8021

46. Kwon, Y. T., Balogh, S. A., Davydov, I. V., Kashina, A. S., Yoon, J. K., Xie, Y., Gaur, A., Hyde, L., Denenberg, V. H., and Varshavsky, A. (2000) *Molecular and cellular biology* **20**, 4135-4148

47. Hwang, C. S., and Varshavsky, A. (2008) *Proceedings of the National Academy of Sciences of the United States of America* **105**, 19188-19193

48. Brower, C. S., and Varshavsky, A. (2009) *PloS one* **4**, e7757

49. Graciet, E., Walter, F., Maoileidigh, D. O., Pollmann, S., Meyerowitz, E. M., Varshavsky, A., and Wellmer, F. (2009) *Proceedings of the National Academy of Sciences of the United States of America* **106**, 13618-13623

50. Eisele, F., and Wolf, D. H. (2008) *FEBS letters* **582**, 4143-4146

51. Heck, J. W., Cheung, S. K., and Hampton, R. Y. (2010) *Proceedings of the National Academy of Sciences of the United States of America* **107**, 1106-1111

52. Prasad, R., Kawaguchi, S., and Ng, D. T. (2010) *Molecular biology of the cell* **21**, 2117-2127

53. Nillegoda, N. B., Theodoraki, M. A., Mandal, A. K., Mayo, K. J., Ren, H. Y., Sultana, R., Wu, K., Johnson, J., Cyr, D. M., and Caplan, A. J. (2010) *Molecular biology of the cell* **21**, 2102-2116

54. Ouyang, Y., Kwon, Y. T., An, J. Y., Eller, D., Tsai, S. C., Diaz-Perez, S., Troke, J. J., Teitell, M. A., and Marahrens, Y. (2006) *Mutation research* **596**, 64-75

55. Yoshida, S., Ito, M., Callis, J., Nishida, I., and Watanabe, A. (2002) *The Plant journal : for cell and molecular biology* **32**, 129-137

56. Holman, T. J., Jones, P. D., Russell, L., Medhurst, A., Ubeda Tomas, S., Talloji, P., Marquez, J., Schmuths, H., Tung, S. A., Taylor, I., Footitt, S., Bachmair, A., Theodoulou, F. L., and Holdsworth, M. J. (2009) *Proceedings of the National Academy of Sciences of the United States of America* **106**, 4549-4554

57. Rai, R., Wong, C. C., Xu, T., Leu, N. A., Dong, D. W., Guo, C., McLaughlin, K. J., Yates, J. R., 3rd, and Kashina, A. (2008) *Development* **135**, 3881-3889

58. Zhang, F., Saha, S., Shabalina, S. A., and Kashina, A. (2010) *Science* **329**, 1534-1537

59. Kurosaka, S., Leu, N. A., Zhang, F., Bunte, R., Saha, S., Wang, J., Guo, C., He, W., and Kashina, A. (2010) *PLoS genetics* **6**, e1000878

60. Saha, S., Mundia, M. M., Zhang, F., Demers, R. W., Korobova, F., Svitkina, T., Perieteanu, A. A., Dawson, J. F., and Kashina, A. (2010) *Molecular biology of the cell* **21**, 1350-1361

61. de Groot, R. J., Rumenapf, T., Kuhn, R. J., Strauss, E. G., and Strauss, J. H. (1991) *Proceedings of the National Academy of Sciences of the United States of America* **88**, 8967-8971

62. Lloyd, A. G., Ng, Y. S., Muesing, M. A., Simon, V., and Mulder, L. C. (2007) *Virology* **360**, 129-135

63. Mulder, L. C., and Muesing, M. A. (2000) *The Journal of biological chemistry* **275**, 29749-29753

64. Lecker, S. H., Solomon, V., Price, S. R., Kwon, Y. T., Mitch, W. E., and Goldberg, A. L. (1999) *The Journal of clinical investigation* **104**, 1411-1420

65. Lecker, S. H., Solomon, V., Mitch, W. E., and Goldberg, A. L. (1999) *The Journal of nutrition* **129**, 227S-237S

66. Carpio, M. A., Lopez Sambrooks, C., Durand, E. S., and Hallak, M. E. (2010) *The Biochemical journal* **429**, 63-72

67. Zenker, M., Mayerle, J., Lerch, M. M., Tagariello, A., Zerres, K., Durie, P. R., Beier, M., Hulskamp, G., Guzman, C., Rehder, H., Beemer, F. A., Hamel, B., Vanlieferinghen, P., Gershoni-Baruch, R., Vieira, M. W., Dumic, M., Auslender, R., Gil-da-Silva-Lopes, V. L., Steinlicht, S., Rauh, M., Shalev, S. A., Thiel, C., Ekici,

A. B., Winterpacht, A., Kwon, Y. T., Varshavsky, A., and Reis, A. (2005) *Nature genetics* **37**, 1345-1350

68. Hwang, C. S., Shemorry, A., and Varshavsky, A. (2010) *Science* **327**, 973-977
69. Moerschell, R. P., Hosokawa, Y., Tsunasawa, S., and Sherman, F. (1990) *The Journal of biological chemistry* **265**, 19638-19643
70. Li, X., and Chang, Y. H. (1995) *Proceedings of the National Academy of Sciences of the United States of America* **92**, 12357-12361
71. Van Damme, P., Lasa, M., Polevoda, B., Gazquez, C., Elosegui-Artola, A., Kim, D. S., De Juan-Pardo, E., Demeyer, K., Hole, K., Larrea, E., Timmerman, E., Prieto, J., Arnesen, T., Sherman, F., Gevaert, K., and Aldabe, R. (2012) *Proceedings of the National Academy of Sciences of the United States of America* **109**, 12449-12454
72. Starheim, K. K., Gevaert, K., and Arnesen, T. (2012) *Trends in biochemical sciences* **37**, 152-161
73. Van Damme, P., Arnesen, T., and Gevaert, K. (2011) *The FEBS journal* **278**, 3822-3834
74. Helsens, K., Van Damme, P., Degroeve, S., Martens, L., Arnesen, T., Vandekerckhove, J., and Gevaert, K. (2011) *Journal of proteome research* **10**, 3578-3589
75. Arnesen, T., Van Damme, P., Polevoda, B., Helsens, K., Evjenth, R., Colaert, N., Varhaug, J. E., Vandekerckhove, J., Lillehaug, J. R., Sherman, F., and Gevaert, K. (2009) *Proceedings of the National Academy of Sciences of the United States of America* **106**, 8157-8162

76. Polevoda, B., Brown, S., Cardillo, T. S., Rigby, S., and Sherman, F. (2008) *Journal of cellular biochemistry* **103**, 492-508

77. Kreft, S. G., and Hochstrasser, M. (2011) *The Journal of biological chemistry* **286**, 20163-20174

78. Ravid, T., Kreft, S. G., and Hochstrasser, M. (2006) *The EMBO journal* **25**, 533-543

79. Kreft, S. G., Wang, L., and Hochstrasser, M. (2006) *The Journal of biological chemistry* **281**, 4646-4653

80. Behnia, R., Panic, B., Whyte, J. R., and Munro, S. (2004) *Nature cell biology* **6**, 405-413

81. Setty, S. R., Strochlic, T. I., Tong, A. H., Boone, C., and Burd, C. G. (2004) *Nature cell biology* **6**, 414-419

82. Jackson, C. L. (2004) *Nature cell biology* **6**, 379-380

83. Hofmann, I., and Munro, S. (2006) *Journal of cell science* **119**, 1494-1503

84. Graham, T. R. (2004) *Current biology : CB* **14**, R483-485

85. Coulton, A. T., East, D. A., Galinska-Rakoczy, A., Lehman, W., and Mulvihill, D. P. (2010) *Journal of cell science* **123**, 3235-3243

CHAPTER 2:

THE N-END RULE PATHWAY IS MEDIATED BY A COMPLEX OF THE RING-TYPE UBR1 AND HECT-TYPE UFD4 UBIQUITIN LIGASES

From Hwang, C. S., Shemorry, A., Auerbach, D., and Varshavsky, A. (2010) *Nature cell biology* **12**, 1177-1185

Abstract

Substrates of the N-end rule pathway are recognized by the Ubr1 E3 ubiquitin ligase through their destabilizing N-terminal residues. Our previous work showed that the Ubr1 E3 and the Ufd4 E3 co-target an internal degron of the Mgt1 DNA repair protein. Ufd4 is an E3 of the ubiquitin-fusion degradation (UFD) pathway that recognizes an N-terminal ubiquitin moiety. Here we report that the RING-type Ubr1 E3 and the HECT-type Ufd4 E3 interact, both physically and functionally. Although Ubr1 can recognize and polyubiquitylate an N-end rule substrate in the absence of Ufd4, the Ubr1-Ufd4 complex is more processive in that it produces a longer substrate-linked polyubiquitin chain. Conversely, Ubr1 can function as a polyubiquitylation-enhancing component of the Ubr1-Ufd4 complex in its targeting of UFD substrates. We also found that Ubr1 can recognize the N-terminal ubiquitin moiety. These and related advances unify two proteolytic systems that have been studied separately over two decades.

Introduction

Here we report that the RING-type Ubr1 E3 and the HECT-type Ufd4 E3 interact, both physically and functionally. Using in vitro and in vivo approaches, we show that the Ubr1-Ufd4 complex mediates the Arg/N-end rule pathway and a part of the UFD pathway as well. Cooperation, in their physical complex, between Ubr1 and Ufd4 includes their ability to increase the processivity of polyubiquitylation of both Arg/N-end rule and UFD substrates, in comparison to targeting by Ubr1 or Ufd4 alone. Thus, operationally, the complex of Ubr1 and Ufd4 functions as an E3–

E4 pair in which the 'assignment' of an E3 or E4 function depends on the substrate and the nature of its degron. We also found that Ubr1, similarly to Ufd4, contains a domain that specifically binds to N-terminal Ub but not to free Ub. S. cerevisiae lacking the Ufd4 component of the Ubr1-Ufd4 complex retained the Arg/N-end rule pathway but its proteolytic activity was lower than in wild-type cells. This could be seen not only with Arg/N-end rule substrates (i.e., substrates containing N-degrons) but also with Cup9, a transcriptional repressor of peptide import that is targeted by Ubr1 through an internal degron of Cup9. These and other results unified two proteolytic systems that have been studied separately over two decades.

The Arg/N-end rule pathway in the yeast *Saccharomyces cerevisiae* is mediated by the 225 kDa RING-type Ubr1 E3 Ub ligase (Fig. 1a). The type-1 and type-2 substrate-binding sites of Ubr1 recognize the unmodified basic (Arg, Lys, His) and bulky hydrophobic (Leu, Phe, Tyr, Trp, Ile) N-terminal residues, respectively (3, 11, 22, 23). The type-1 binding site of Ubr1 resides in the ~70-residue UBR domain (3, 17) that was recently solved at atomic resolution (24–26). In addition to the type-1/2 sites, Ubr1 contains binding sites that recognize internal (non-N-terminal) degrons of proteins that include the Cup9 transcriptional repressor, the Mgt1 DNA repair protein (O^6-alkylguanine DNA alkyltransferase) (5, 12, 22, 27), and misfolded proteins (28–31). In contrast to the 'primary' destabilizing N-terminal residues (Arg, Lys, His, Leu, Phe, Tyr, Trp, Ile), the N-terminal residues Asp, Glu, Asn and Gln can be targeted by Ubr1 only after their Nt-arginylation by the Ate1 Arg-tRNA-protein transferase (R-transferase) (Fig. 1a). These destabilizing residues are called 'secondary' or 'tertiary', depending on the number of steps (arginylation of Asp and

Glu; deamidation/arginylation of Asn and Gln) that precede the targeting and polyubiquitylation, by Ubr1, of Nt-arginylated N-end rule substrates (8, 10, 15, 16, 32).

Regulated degradation of specific proteins by the Arg/N-end rule pathway mediates a legion of physiological functions, including the sensing of haem, nitric oxide, oxygen, and short peptides; the degradation of misfolded proteins; the fidelity of chromosome segregation; the regulation of DNA repair and peptide import; the signaling by G-coupled transmembrane receptors; the regulation of apoptosis, meiosis, fat metabolism, cell migration, cardiovascular development, spermatogenesis and neurogenesis; the functioning of adult organs, including the brain, muscle, testis and pancreas; and the regulation of leaf and shoot development, leaf senescence and seed germination in plants (refs. 3, 5, 6, 8–12, 15, 16, 18, 22, 28–35, and refs. therein). The recently discovered Ac/N-end rule pathway is likely to mediate, among other things, protein quality control and degradation of long-lived proteins (18). Partial Nt-arginylation of apparently long-lived proteins such as β-actin and calreticulin (36, 37) suggests that Nt-arginylation may have nonproteolytic roles as well.

Our previous study showed that the *S. cerevisiae* Mgt1 DNA repair protein is co-targeted for degradation by the Ubr1/Rad6-mediated Arg/N-end rule pathway and the Ufd4/Ubc4-mediated Ub-fusion degradation (UFD) pathway (12). Rad6 and Ubc4/Ubc5 are E2 enzymes that function with the E3s Ubr1 and Ufd4, respectively. Ufd4 is the 168 kDa HECT-type E3 of the UFD pathway (38–43). The UFD pathway

was discovered through analyses of N-terminal Ub fusions in which the Pro residue at the Ub-reporter junction or mutations of the Ub moiety were found to inhibit the cleavage of a fusion by deubiquitylases (DUBs) (1, 38, 44, 45). Such UFD substrates are targeted for polyubiquitylation and degradation through their N-terminal Ub moieties (Fig. 1b).

A priori, the number of topologically distinct poly-Ub chains can be very large, as all seven Lys residues of Ub can contribute, in specific in vivo contexts, to the synthesis of poly-Ub linked to protein substrates (46, 47). The delivery of ubiquitylated proteins to the 26S proteasome can be mediated by either K48-type, K11-type or K29-type chains, and possibly by poly-Ub of other topologies as well (refs. 3, 19, 46–48 and refs. therein). A single E3 can cooperate, in some settings, with two distinct E2 enzymes that mediate, sequentially, the synthesis of a substrate-linked poly-Ub chain (49). Two E3s can also cooperate in producing a poly-Ub chain. Studies by Jentsch and colleagues (45) (see also refs. 46, 50, 51 and refs. therein) introduced the concept of an E4 as an E3-like enzyme that cooperates with a specific E3 and its cognate E2 enzyme to increase the processivity of polyubiquitylation. Given the mechanistic and regulatory complexity of polyubiquitylation that remains to be understood, it would be constructive, at present, to define E4 operationally, as an E3-like enzyme that cooperates with a substrate-specific ubiquitylation machinery to increase the efficacy (including processivity) of polyubiquitylation, and in some cases to alter topology of a poly-Ub chain as well. This definition of E4 does not constrain its possible modes of action.

Here we report that the RING-type Ubr1 E3 and the HECT-type Ufd4 E3 interact, both physically and functionally. Using *in vitro* and *in vivo* approaches, we show that the Ubr1-Ufd4 complex mediates the Arg/N-end rule pathway and a part of the UFD pathway as well. Cooperation, in their physical complex, between Ubr1 and Ufd4 includes their ability to increase the processivity of polyubiquitylation of both Arg/N-end rule and UFD substrates, in comparison to targeting by Ubr1 or Ufd4 alone. Thus, operationally, the complex of Ubr1 and Ufd4 functions as an E3–E4 pair in which the 'assignment' of an E3 or E4 function depends on the substrate and the nature of its degron. We also found that Ubr1, similarly to Ufd4, contains a domain that specifically binds to N-terminal Ub but not to free Ub. *S. cerevisiae* lacking the Ufd4 component of the Ubr1-Ufd4 complex retained the Arg/N-end rule pathway but its proteolytic activity was lower than in wild-type cells. This could be seen not only with Arg/N-end rule substrates (i.e., substrates containing N-degrons) but also with Cup9, a transcriptional repressor of peptide import that is targeted by Ubr1 through an internal degron of Cup9. These and other results unified two proteolytic systems that have been studied separately over two decades.

Results

Ubiquitylation of Mgt1 by Ubr1 and Ufd4.

Although Mgt1 could be ubiquitylated (and subsequently degraded) by either the Arg/N-end rule or UFD pathways, strong polyubiquitylation of Mgt1 was observed only in the presence of both pathways (12). To further address this interplay between Ubr1 and Ufd4, we employed a ubiquitylation assay that

comprised ^{35}S-labeled Mgt1$_{f3}$ (C-terminally tagged with flag epitopes) that had been produced in reticulocyte extract (12), and the following purified components: Ub; Uba1 (E1); Rad6 and/or Ubc4 (cognate E2s); Ubr1 and/or Ufd4; and ATP.

The assays were performed using wild-type Ub, Ub^{K29R}, Ub^{K48R}, or Ub^{K63R}, with Ub mutants of this set precluding formation of Ub-Ub isopeptide bonds of the K48, K29 or K63 topologies, respectively. Ubr1/Rad6 alone polyubiquitylated Mgt1 to comparable extents with either wild-type Ub, Ub^{K29R}, or Ub^{K63R} (Fig. 2, lanes 2, 3, 5). In contrast, little polyubiquitylation was observed with Ub^{K48R} (Fig. 2, lane 4), in agreement with evidence that Ubr1/Rad6 preferentially produces K48-type chains (48). Together, Ubr1/Rad6 and Ufd4/Ubc4 polyubiquitylated Mgt1 both more strongly and more processively than Ubr1/Rad6 alone. Specifically, ubiquitylated ^{35}S-Mgt1$_{f3}$ produced with wild-type Ub and Ubr1/Rad6 plus Ufd4/Ubc4 migrated as high-yield polyubiquitylated derivatives in a narrow size range, ~200 kDa on average, corresponding to ~21 Ub moieties in a substrate-linked chain (Fig. 2, lane 7). In contrast, a broader distribution of much shorter chains was observed with Ubr1/Rad6 alone (Fig. 2, lane 2; cf. lane 7). When Ubr1/Rad6 and Ufd4/Ubc4 were assayed together in the presence of UbK29R, both high yield and processivity of Mgt1 polyubiquitylation were diminished, in comparison to results with wild-type Ub (Fig. 2, lane 8; cf. lanes 2, 3 and 7). When Ubr1/Rad6 and Ufd4/Ubc4 were assayed in the presence of Ub^{K48R}, the yield of Mgt1-linked chains was also much lower than with wild-type Ub, but their large average size and narrow size distribution were retained (Fig. 2, lane 9; cf. lanes 4 and 7). Similar results were obtained with Ufd4/Ubc4 alone, using either wild-type Ub or its mutants (Fig. 2,

lanes 11–15). Thus, the presence of both Ubr1/Rad6 and Ufd4/Ubc4, and also of Ub containing wild-type Lys48 and Lys29 are required for the high-yield production of larger Mgt1-linked chains, and for their narrow size distribution as well (Fig. 2, lanes 7 and 10).

Physical interaction between Ubr1 and Ufd4.

To test for a possible interaction between Ubr1 and Ufd4, we performed coimmunoprecipitations with extracts from cells expressing flag-tagged Ubr1 (^{f}Ubr1) and ha-tagged Ufd4 (^{ha}Ufd4) (Fig. 3a–c). ^{ha}Ufd4 was coimmunoprecipitated with ^{f}Ubr1 by anti-flag (Fig. 3a). Conversely, ^{f}Ubr1 was coimmunoprecipitated with ^{ha}Ufd4 by anti-ha (Fig. 3b). To determine whether these results signified a direct interaction between Ubr1 and Ufd4, we also performed a coimmunoprecipitation with equal amounts of purified ^{f}Ubr1 and ^{f}Ufd4. The results (Figs. 3c and S1a) confirmed a direct interaction between Ubr1 and Ufd4.

To examine the Ubr1-Ufd4 interaction in vivo, we employed the split-Ub technique (52, 53). Co-expression of Ubr1 as the bait and Ufd4 as the prey produced the interaction-positive Ade+ His+ phenotype reproducibly and robustly, whereas no Ade+ His+ cells were observed with negative controls (Fig. 3d). A reciprocal assay, with Ufd4 as the bait and Ubr1 as the prey, also indicated an in vivo interaction between Ubr1 and Ufd4 (Fig. 3d). To delineate the Ufd4-interacting region of Ubr1, coimmunoprecipitations (Fig. 3a, b) were carried out using anti-ha and extracts from S. cerevisiae that expressed full-length ^{ha}Ufd4 and one of the following Ubr1 fragments: ^{f}Ubr1$^{1\text{-}1175}$, ^{f}Ubr1$^{1\text{-}717}$, ^{f}Ubr1$^{1\text{-}510}$, Ubr1$^{454\text{-}1140f}$ and

^{f}Ubr1$^{454-795}$ (Fig. 3e). ^{ha}Ufd4 was coimmunoprecipitated with all of these fragments except ^{f}Ubr1$^{1-510}$ (Fig. 3f, g). A reciprocal coimmunoprecipitation with anti-flag confirmed that ^{f}Ubr1$^{454-795}$, encompassing 342 residues of the 1,950-residue Ubr1, could interact with ^{ha}Ufd4 (Fig. 3h).

Ufd4 contributes to ubiquitylation and degradation of Arg/N-end rule substrates.

Since the degradation signal of Mgt1 is distinct from an N-degron (12), we asked whether cooperation between Ubr1 and Ufd4 could also be detected with Arg/N-end rule substrates, i.e., with proteins containing N-degrons. Ubiquitylation of purified X-DHFR$_{ha}$ (X=Met, Arg, Leu), a set of previously characterized Arg/N-end rule reporters based on the mouse dihydrofolate reductase (DHFR) moiety and produced from Ub-X-DHFR$_{ha}$ by the Ub fusion technique (54, 55) (Fig. S1b), was examined with wild-type Ub using either purified ^{f}Ubr1/Rad6 alone, ^{f}Ufd4/Ubc4 alone, or ^{f}Ubr1/Rad6 plus ^{f}Ufd4/Ubc4 (Fig. 4a). As expected (38), Ufd4/Ubc4 alone did not polyubiquitylate Arg/N-end rule substrates (Fig. 4a, lanes 11 and 17), confirming that Ufd4 is not an N-recognin. As also expected (5, 23), Ubr1/Rad6 polyubiquitylated both Arg-DHFR$_{ha}$ and Leu-DHFR$_{ha}$ (type-1 and type-2 Arg/N-end rule substrates, respectively) but was virtually inactive with Met-DHFR$_{ha}$ (Fig. 4a). Addition of Ufd4/Ubc4 to Ubr1/Rad6 resulted in longer substrate-linked poly-Ub chains (Fig. 4a), similarly to processivity enhancement that was observed with Mgt1 (Fig. 2).

Ubiquitylation assays were also carried out with Arg-DHFR$_{ha}$ and the Ub mutants Ub^{K29} (Ub in which all lysines except K29 were replaced by Arg) (Fig. 4b,

lanes 1–3); Ub^{K48} (Ub in which all lysines except K48 were replaced by Arg) (Fig. 4b, lanes 4–6); an equimolar mixture of Ub^{K29} and Ub^{K48} (Fig. 4b, lanes 7–9); Ub^{K29R} (Ub in which one lysine, K29, was replaced by Arg) (Fig. 4b, lanes 10–12); Ub^{K48R} (Ub in which one lysine, K48, was replaced by Arg) (Fig. 4b, lanes 13–15); and an equimolar mixture of Ub^{K29R} and Ub^{K48R} (Fig. 4b, lanes 16–18). There was virtually no polyubiquitylation of Arg-$DHFR_{ha}$ by Ufd4/Ubc4 alone in the presence of any Ub mutant (Fig. 4b, lanes 1, 4, 7, 10, 13, and 16), in agreement with Ufd4 not being an N-recognin. In contrast, Ubr1/Rad6 polyubiquitylated Arg-$DHFR_{ha}$ in the presence of either Ub^{K29R}, Ub^{K48R}, or both of them together (Fig. 4b, lanes 11, 14 and 17, cf. lanes 10, 13 and 16, respectively). To our knowledge, this is the first evidence that Ubr1/Rad6 can produce, at least in vitro, non-K48 poly-Ub chains. Similarly to results with wild-type Ub (Fig. 4a, lane 12; cf. lane 9), both the yields and average sizes of substrate-linked poly-Ub chains were significantly larger in the presence of Ubr1/Rad6 plus Ufd4/Ubc4, using either Ub^{K29R}, Ub^{K48R}, or two of them together (Fig. 4b, lanes12, 15 and 18; cf. lanes 11, 14 and 17).

With Ub^{K29}, either Ubr1/Rad6 alone or Ubr1/Rad6 plus Ufd4/Ubc4 could produce only short poly-Ub chains, i.e., no significant increase in processivity was observed with Ubr1/Rad6 and Ufd4/Ubc4 together (Fig. 4b, lanes 2, 3). It is possible that Ub^{K29} was too perturbed by six mutations to be an efficacious substrate for polyubiquitylation by Ubr1/Rad6-Ufd4/Ubc4. In contrast, with Ub^{K48} (only K48-type chains could be produced with this Ub mutant), there was a significant increase in the yield and processivity of polyubiquitylation in the presence of Ubr1/Rad6 plus Ufd4/Ubc4 (Fig. 4b, lanes 5, 6; cf. lanes 2, 3 and 11, 12). In one model that is

consistent with our findings (Figs. 2 and 4a, b), a physical interaction between Ubr1 and Ufd4 (Fig. 3) increases, allosterically, the efficacy and processivity of the Ubr1/Rad6 Ub ligase that is bound to Ufd4/Ubc4. In another plausible model, the Ufd4/Ubc4 component of the Ubr1/Rad6-Ufd4/Ubc4 complex may utilize a specific Lys residue of Ub (e.g., Lys48; see above) to elongate a poly-Ub chain that had been initiated ('primed') by Ubr1/Rad6.

We also employed a degradation assay with the purified 26S proteasome (56) (Fig. 4c). The in vitro half-lives of Leu-DHFR$_{ha}$ that had been polyubiquitylated by Ubr1 alone versus Ubr1 plus Ufd4 were ~23 min versus ~7 min, respectively (Fig. 4d, e). To increase the yields of polyubiquitylated reporters before the addition of the 26S proteasome, ubiquitylation was carried out for 18 hr at 30°C, as opposed to 15 min in the assay of Fig. 4a (lanes 13–18), resulting in the absence of non-ubiquitylated Leu-DHFR$_{ha}$ and most likely accounting for a marginal difference, in this experiment, between the longest chains in the presence of Ubr1 versus Ubr1 plus Ufd4 (Fig. 4d, lanes 1 and 4). In addition to effects of poly-Ub chains, the faster degradation of polyubiquitylated Leu-DHFR$_{ha}$ that had been produced by Ubr1-Ufd4 (Fig. 4d, e) may also stem from previously described (and possibly synergistic) interactions of Ubr1 and Ufd4 with the 26S proteasome (41, 42). These issues await more detailed studies with proteasome-based assays.

To determine whether the *in vitro* effect of Ufd4 on Arg/N-end rule substrates (Fig. 4) occurred *in vivo* as well, we employed X-β-galactosidase (X-β gal) reporters, produced by the cotranslational deubiquitylation of Ub-X-β gal (X=His,

Tyr) (1, 57). The activity of β gal in extracts from cells that express X-βgal is a reliable measure of the reporter's metabolic stability (54). In agreement with in vitro data (Fig. 4), His-βgal and Tyr-βgal became partially stabilized in the absence of Ufd4 (Fig. 5a). ^{35}S-pulse-chases confirmed these results: the *in vivo* half-life of His-βgal was ~18 min in wild-type cells and doubled to ~41 min in *ufd4Δ* cells (Fig. 5b, d). The in vivo half-life of Tyr-β gal was ~28 min in wild type cells and ~99 min in *ufd4Δ* cells (Fig. 5c, d). Half-lives of X-βgals in *ubr1Δ* cells exceeded 20 h (data not shown), in agreement with earlier data (1, 3).

Ufd4 contributes to regulation of peptide import by the Arg/N-end rule pathway.

The binding of short peptides with destabilizing N-terminal residues to the type-1/2 sites of Ubr1 (see Introduction) allosterically activates the third substrate-binding site of Ubr1 that recognizes an internal degron of Cup9, a transcriptional repressor (5, 22). Genes down-regulated by Cup9 include PTR2, which encodes the transporter of di- and tripeptides (33). This positive-feedback circuit, in which Cup9 degradation is induced by type-1/2 peptides, allows *S. cerevisiae* to sense the presence of extracellular peptides and to react by accelerating their uptake (5, 22, 27). In agreement with earlier findings (5, 23), ubiquitylation assays with ^{35}S-labeled Cup9 and Ubr1/Rad6 showed that low-μM levels of the type-1/2 dipeptides Arg-Ala/Leu-Ala greatly increased the Ubr1-mediated polyubiquitylation of Cup9 (Fig. 5e, lanes 1–8). Ufd4/Ubc4 plus Ubr1/Rad6 significantly increased the processivity of Cup9 polyubiquitylation at an even lower (0.1 μM) concentration of the same dipeptides (Fig. 5e, lanes 12, 13). Moreover, in the presence of Ufd4/Ubc4

plus Ubr1/Rad6, dipeptides increased the average size of Cup9-linked poly-Ub chains, in comparison to chains (at the same levels of dipeptides) by Ubr1/Rad6 alone (Fig. 5e, lane 14; cf. lane 5). The effect of dipeptides required the presence of both type-1 and type-2 dipeptides together, and also the presence of Ub that was able to form K29-type chains (Fig. 5f).

In vivo induction of the transporter Ptr2 by low-μM levels of Arg-Ala/Leu-Ala dipeptides (5, 23) was diminished in the absence of Ufd4 (Fig. 5g), in agreement with *in vitro* results (Fig. 5e, f). To determine whether Ufd4 contributes to degradation of Cup9 in vivo, we employed the Ub-reference technique (URT), a method that increases the accuracy of a pulse-chase assay by providing a 'built-in' reference protein (5,27,54) (see the legend to Fig. S2a, b). In agreement with other data (Fig. 5e-g), the in vivo half-life of Cup9 was ~5 min in wild-type cells and ~14 min in *ufd4Δ* cells (Fig. S2a, b).

The Ubr1-Ufd4 complex and the UFD pathway.

Ufd4, as a part of the Ubr1-Ufd4 complex, augments the Ubr1-based Arg/N-end rule pathway (Figs. 4 and 5). Might Ubr1 have a 'reciprocal' effect on the Ufd4-mediated UFD pathway? We employed a ubiquitylation assay with purified UFD substrates such as Ub-ProtA (Protein A) and Ub-GST (glutathione S-transferase) (Fig. S1c). As expected (38, 45), the cognate Ufd4/Ubc4 Ub ligase of the UFD pathway ubiquitylated, with a low processivity, both Ub-ProtA and Ub-GST (Fig. 6a, b, lanes 3; cf. lanes 1). Remarkably, the Ubr1/Rad6 Ub ligase of the Arg/N-end rule pathway could also ubiquitylate (with a low processivity) these UFD substrates in

the absence of Ufd4 (Fig. 6a, b, lanes 2; cf. lanes 1). Moreover, the processivity of polyubiquitylation of Ub-ProtA and Ub-GST was strongly increased in the presence of both Ubr1/Rad6 and Ufd4/Ubc4 (Fig. 6a, b, lanes 4; cf. lanes 1–3). Ufd2, an E4-type enzyme of the UFD pathway (38, 45, 58, 59), also increased the processivity of the Ufd4 E3 in this system (Fig. 6a, b, lanes 7; cf. lanes 1–3, 5). However, in contrast to Ufd4, Ufd2 had only a weak effect on ubiquitylation by Ubr1 (Fig. 6a, b, lanes 6; cf. lanes 1–3, 5). In sum, Ufd4 and Ubr1 can function as mutually cooperative, physically interacting E3 enzymes not only with Arg/N-end rule substrates but with UFD substrates as well. To gauge the extent of substrate specificity of Ubr1 and Ufd4 in these assays (Figs. 2, 4a, b, 5e, f, and 6a, b), we asked whether an unrelated substrate could be ubiquitylated by Ubr1 and/or Ufd4. These experiments employed purified Sic1PY (Fig. S1c), an engineered substrate of the Rsp5 E3 Ub ligase. Whereas purified Rsp5 (with the cognate Ubc4 E2) polyubiquitylated $Sic1^{PY}$, neither Ubr1/Rad6 nor Ufd4/Ubc4 could utilize $Sic1^{PY}$ as a substrate (Fig. 6e).

Because Ubr1 could ubiquitylate UFD substrates in the absence of Ufd4 (Fig. 6a, b), we asked whether Ubr1 contained a Ub-binding site. GST-pulldowns showed that the binding of ^{f}Ubr1 to Ub-GST could be efficaciously competed out by other UFD-type fusions such as Ub-ProtA or Ub-Met-DHFRha, whereas a large molar excess of free Ub did not significantly decrease the binding of ^{f}Ubr1 to Ub-GST (Fig. 6c). Thus Ubr1 contains a previously overlooked Ub-binding site that can distinguish between conjugated and free Ub (Fig. 6c), analogously to a Ub-binding site of the Ufd4 E3 Ub ligase (40).

Neither Ubr1 nor Ufd4 are essential proteins under normal growth conditions (3, 38). Both *ufd4Δ* and *ubr1Δ* mutants were moderately hypersensitive to treatments that increased protein misfolding, such as 6% ethanol or canavanine, an analog of arginine (45) (Fig. 6f, g). Interestingly, *ubr1Δ ufd4Δ* double mutants were much more sensitive to ethanol or canavanine than their single-mutant counterparts (Fig. 6f, g), in agreement with demonstrated interactions and interdependence between the Arg/N-end rule and UFD pathways.

Given the *in vivo* interaction between Ubr1 and Ufd4 (Fig. 3), we wished to determine their approximate molar ratio in wild-type cells. Previous work indicated that haploid *S. cerevisiae* contained ~7300 Ufd4 molecules per cell (60), but there was no information about Ubr1 levels in that study or elsewhere. To estimate in vivo levels of Ubr1, we immunoblotted extracts of wild-type *S. cerevisiae* using the previously characterized, affinity-purified anti-Ubr1 antibody (11) and calibrated these assays with known amounts of purified ^{f}Ubr1. The results (Fig. 6d) indicated that 'wild-type', haploid *S. cerevisiae* in YPD medium contained 500 to 1,000 Ubr1 molecules per cell. Thus Ubr1 is ~10-fold less abundant than the Ufd4, suggesting a minor contribution of Ubr1 to the activity of the UFD pathway. Indeed, no significant decrease in the rate of degradation of Ub^{V76}-Val-βgal, a UFD substrate, was observed in *ubr1Δ S. cerevisiae*, whereas in *ufd4Δ* cells this UFD reporter was nearly completely stabilized (Fig. S2c, d).

Discussion

The Arg/N-end rule and UFD pathways have been studied separately for more than two decades (1, 3, 38, 40, 44, 45). In 2009, we found that an internal degron of *S. cerevisiae* Mgt1 was co-targeted by the Arg/N-end rule and UFD pathways (12). We now report that the Arg/N-end rule pathway is mediated by a physical complex of the RING-type Ubr1 E3 and the HECT-type Ufd4 E3, together with their cognate E2 enzymes Rad6 and Ubc4/Ubc5, respectively (Fig. 1c). The earlier examples of a complex between a RING-type E3 and a HECT-type E3 are distinct from the present case. Specifically, the complexes of the RING-type CBLC E3 with the HECT-type AIP/ITCH E3 and of the RING-type Rnf11 E3 with the HECT-type WWP1 E3 remain to be analyzed functionally (61, 62). Furthermore, specific HECT-type E3s were shown to bind RING-type E3s and target them for polyubiquitylation and degradation (63, 64), in contrast to Ubr1-Ufd4 (Fig. 1c), where intra-complex targeting has not been observed, thus far. Multicellular eukaryotes contain functionally overlapping E3 N-recognins that are sequelogous (similar in sequence) (65) to yeast Ubr1, in part because they contain the UBR domain (3, 17, 24–26). Trip12, a human HECT-type E3, is a sequelog (65) of *S. cerevisiae* Ufd4 and mediates degradation of human UFD substrates (66). Thus our results with yeast Ubr1-Ufd4 are likely to be relevant to all eukaryotes.

S. cerevisiae Ufd4 is not an N-recognin, i.e., it does not, by itself, recognize N-degrons, in contrast to Ubr1 (Fig. 4a, b). But through its physical interaction with the Ubr1 E3, the Ufd4 E3 functions as a novel component of the Arg/N-end rule pathway that increases the efficacy of Ubr1, at least in part by augmenting the processivity of

polyubiquitylation of Arg/N-end rule substrates (Fig. 1a, c). Interestingly, the function of Ufd4 in the Arg/N-end rule pathway is broader than that of a processivity-enhancing component of the Ubr1-Ufd4 complex because Ufd4 can target the internal degron of Mgt1 even in *ubr1Δ* cells (12). Although Ufd4 is not strictly essential for the ability of Ubr1 to mediate the Arg/N-end rule pathway, this pathway is detectably impaired in *ufd4Δ* cells (Figs. 5a–d and S2a, b).

As mentioned above, Ufd4 does not recognize N-degrons but functions to increase the processivity of polyubiquitylation of Arg/N-end rule substrates. Conversely, Ubr1 can function as a processivity-increasing component of the Ubr1-Ufd4 complex in its polyubiquitylation of UFD substrates. Moreover, Ubr1 recognizes the N-terminal Ub moiety of UFD substrates (Fig. 6c). Thus Ubr1 can bind to such substrates independently of Ufd4. Because Ubr1 is ~10-fold less abundant than Ufd4 in wild-type cells (see Results), the Ubr1/Rad6-Ufd4/Ubc4 complex is expected to mediate the bulk of the Arg/N-end rule pathway, whereas the same complex mediates only a subset of the UFD pathway (Fig. 1).

Given the existence of the Ubr1-Ufd4 complex, it is possible that some functions of Ubr1 might be mediated by its functionally relevant associations with other, non-Ufd4 E3s as well, for example with San1, a nuclear E3 Ub ligase that recognizes misfolded proteins (67). In addition, the molar excess of Ufd4 relative to Ubr1 in vivo suggests that Ufd4 might also interact with other E3s. One possibility is that the UFD pathway comprises a dynamic 'mosaic' of reversible binary Ufd4 complexes with several E3s, including Ubr1. These are just some of the ramifications

suggested by results of the present study, which unified, in a novel way, two multifunctional proteolytic systems (Fig. 1).

Methods

Yeast strains, media, genetic techniques, and β-galactosidase assay.

S. cerevisiae strains are described in Table S1. Standard techniques were employed for strain construction and transformation. The strains CHY233 and CHY251 (Table S1) were constructed by PCR-mediated gene disruption of UFD4 in *S. cerevisiae* RJD347, using the pFA6a-KanMX6 plasmid (68). *S. cerevisiae* media included YPD medium (1% yeast extract, 2% peptone, 2% glucose; only most relevant media components are cited); SD medium (0.17% yeast nitrogen base, 0.5% ammonium sulfate, 2% glucose); SRGal medium (0.17% yeast nitrogen base, 0.5% ammonium sulfate, 2% raffinose, 2% galactose); SHM medium (0.1% allantoin, 2% glucose, 0.17% yeast nitrogen base); and synthetic complete (SC) medium (0.17% yeast nitrogen base, 0.5% ammonium sulfate, 2% glucose, plus a drop-out mixture of compounds required by a given auxotrophic strain). Assays for β-galactosidase (β gal) activity in yeast extracts were carried out using Yeast β-Galactosidase Assay Kit (Thermo scientific, Rockford, IL). *S. cerevisiae* strains that expressed His-β gal or Tyr-β gal were prototrophic for all 20 amino acids and were grown in a minimal medium in the absence of amino acids, to bypass the previously characterized activation of the Ubr1/Rad6 Ub ligase by added amino acids (11, 27).

Plasmids.

They are described in Table S2. In the high copy (2μ-based) pCH522 plasmid, $^{f}Ubr1^{1-510}$ (N-terminally tagged with flag) was expressed from the P_{ADH1} promoter. To construct pCH522, a region of the UBR1 ORF was PCR-amplified from

pFlagUBR1SBX using the primers OCH820 (ACACCATGGACTACAAGGACGAT GATGACAAGGGTTCTATGTCCGTTGCTGATGATGATTTA; the *NcoI* site is underlined) and OCH518 (AAACTCGAGCTAATCAAAATAAAGAATATGTTGTAA; the XhoI site is underlined). The resulting DNA fragment was digested with *NcoI/XhoI* and subcloned into *NcoI/XhoI*-cut pNTFlag717UBR1. The plasmids pCH230, pCH231, pCH232, which encoded His_{10}-Ub-X-$DHFR_{ha}$ (X=Met, Arg, Leu), were constructed by ligating *NdeI/HindIII*-digested pEJJ1-M, pEJJ1-R, and pEJJ1-L, respectively (38), into the *NdeI/HindIII*-cut pH_{10}UE plasmid (10). Construction details for other plasmids (Table S2) are available upon request. All final constructs were verified by DNA sequencing.

Yeast-based split-ubiquitin assay.

A version of split-Ub assay (52) used was described (53). The bait *S. cerevisiae* proteins Ubr1 and Ufd4 were cloned via *SfiI* sites downstream of the OST4 sequence into pDHB1. The prey proteins were cloned downstream of the NubG-coding segment into prey vector pPR3-N using full-length UBR1 and UFD4 ORFs. All constructs were verified by sequencing. *S. cerevisiae* NMY51 (*MATa trp1 leu2 his3 ade2 LYS2::lexA-HIS3 ade2::lexA-ADE2 URA3::lexA-lacZ*) (Dualsystems Biotech AG, Schlieren, Switzerland) was cotransformed with bait and prey plasmids using the lithium acetate method (69). Transformants were selected for the presence of bait and prey plasmids during 3 days of growth at 30°C on SC(-Trp, -Leu) medium (minimal medium containing 2% glucose, 0.67% yeast nitrogen base, 2% bacto-agar, and complete amino acid mixture lacking Leu and Trp). Several colonies were

transferred to liquid SC(-Trp, -Leu) and grown overnight to A_{600} of ~1. Five-fold serial dilutions were spotted onto SC(-Trp, -Leu) and SC(-Trp, -Leu, -His, -Ade) plates (53) and grown for 2 days at 30°C.

Immunoblotting, coimmunoprecipitation, and GST-pulldown assays.

Whole yeast cell extracts were prepared using a modification of Kushnirov's method (11, 18, 70). Immunoblotting was performed as described (11, 12, 18). Co-immunoprecipitation (co-IP) assays with ^{f}Ubr1 and ^{ha}Ufd4 were carried out as follows. Extracts (0.2 mg) from JD52 *S. cerevisiae* that co-expressed, from indicated plasmids, the full-length ^{ha}Ufd4 and either full-length ^{f}Ubr1 (pFlagUBR1SBX), ^{f}Ubr1$^{1-1175}$ (pFlagUBR1NT1-1175), ^{f}Ubr1$^{1-717}$ (pFlagUBR1NT1-717), ^{f}Ubr1$^{1-510}$ (pCH522), or ^{f}Ubr1$^{454-795}$ (pCH487), were immunoprecipitated using anti-ha antibody and protein G-magnetic beads (Invitrogen) in lysis buffer (0.1 M NaCl, 0.1% NP40, 0.5 mM EDTA, 5 mM β-mercaptoethanol, 1 mM phenylmethylsulfonyl fluoride (PMSF), 25 mM HEPES, pH 7.5) containing the above-cited protease-inhibitor cocktail (Sigma). Bound proteins were eluted from thrice-washed beads in 0.5 ml of lysis buffer, followed by SDS-4-12% NuPAGE, and immunoblotting with anti–ha or anti-flag. In a different assay, purified ^{f}Ubr1 (0.125 μg) and ^{f}Ufd4 (0.125 μg) were incubated together for 2 h at 4°C in 0.25 ml of reaction buffer (10% glycerol, 0.1 M NaCl, 0.1% NP40, 0.5 mM EDTA 25 mM HEPES, pH 7.5), followed by immunoprecipitation with affinity-purified anti-Ubr1 antibody (1 μg) (11) pre-bound to Protein A immobilized on magnetic beads (Invitrogen). Bound proteins were washed 4 times in 0.5 ml of the same buffer, followed by SDS-4-12% NuPAGE and immunoblotting with anti-

flag. In the assay for a direct interaction between purified ^{f}Ubr1 and ^{f}Ufd4 (see Fig. 3c), immunoprecipitates were washed three times in the binding buffer, followed by elution of retained proteins, SDS-PAGE, and immunoblotting with anti-flag.

GST pulldown assays with purified ^{f}Ubr1 were carried out using a slight modification of the earlier procedure (22). Either GST alone or Ub-GST fusion proteins (5 μg) were incubated with glutathione-Sepharose beads (15 μl; 50% slurry) in 0.5 ml of GST-loading buffer (10% glycerol, 0.5 M NaCl, 1% NP40, 1 mM EDTA, 50 mM Tris-HCl, pH 8.0) for 20 min at 4° C. The beads were washed once with 0.5 ml of GST-binding buffer (10 % glycerol, 0.05% NP40, 50 mM NaCl, 50 mM HEPES, pH 7.8). Washed beads in 0.25 ml of GST-binding buffer were incubated with 1 μl of purified ^{f}Ubr1 (1 μg) in the absence or presence of 1 (or 10) μM Ub, Ub-ProtA, or Ub-Met-DHFR$_{ha}$ at 4° C for 1 h. Beads-associated proteins were eluted and fractionated by SDS-4-12% NuPAGE, followed by immunoblotting with anti-flag. Blots were also Coomassie-stained, to verify the expected amounts of GST fusions pre-bound to glutathione-Sepharose beads.

Production and purification of X-DHFRha test proteins.

The plasmids pCH230, pCH231, pCH232, which encoded His$_{10}$-Ub-X-DHFR$_{ha}$ (X=Met, Arg, Leu) (54, 55) (see also the legend to Fig. 4) were transformed into KSP22 (*aatΔ*) *E. coli*. Purification of these fusions and their in vitro deubiquitylation (55) were carried as described previously (15).

Pulse-chases.

^{35}S-pulse-chase experiments, with 5-min pulses and chases of 20 and 60 min (Fig. 5b, d) were performed as described (11, 12, 23), using *S. cerevisiae* JD52, JD55 (*ubr1Δ*), CHY194 (*ufd4Δ*) or CHY195 (*ubr1Δ ufd4Δ*) that carried plasmids expressing either Ub^{V76}-Val-βgal, Ub-His-βgal, Ub-Tyr-βgal, or ^{f}DHFR-Ub^{K48R}-Cup9$_{NSF}$ (the latter from the plasmid p416^{f}UPRCUP$_{NSF}$; see the legend to Fig. S2).

In vitro ubiquitylation assay.

Unless indicated otherwise, in vitro ubiquitylation assays were carried out as described (12). Purified *S. cerevisiae* Uba1 (E1 enzyme) as well as Ub and its mutant derivatives were from Boston Biochem. The ^{S35}-labelled Mgt1 and Cup9 test proteins were expressed as described (12) for Mgt1, using the in vitro transcription/translation TNT T7 Quick for PCR DNA system, derived from rabbit reticulocyte extract (Promega). Thus far, we could not produce soluble Mgt1 (a relatively hydrophobic protein) in *E. coli*. All experiments with Cup9 utilized Cup9$_{NSF}$, a previously characterized missense mutant that exhibited reduced specific binding to DNA, reduced toxicity in vivo, but no significant changes in the kinetics of in vivo degradation (5). The unlabeled Ub-ProtA, Ub-GST or Sic1^{PY} test proteins, purified from *E. coli* (see above), were examined in ubiquitylation assays directly, whereas purified X-DHFR$_{ha}$ proteins (X=Met, Arg, Leu) were incubated, at first, with N-ethylmaleimide (NEM; 5 mM) for 5 min at 30° C to inactivate traces of the remaining Usp2-cc DUB, followed by removal of NEM, using Zeba desalting columns (Thermo Scientific). 2 μl of either ^{35}S-labeled Mgt1, ^{35}S-labeled Cup9, unlabeled,

purified X-DHFR$_{ha}$ (X=Met, Arg, Leu), Ub-ProtA, Ub-GST, or Sic1^{PY} were incubated with purified ^{f}Ubr1, ^{f}Ufd4, Rad6, and/or Ubc4 at 30° C for 15 or 30 min in 20 µl of the final reaction sample (4 mM ATP, 0.15 M NaCl, 5 mM MgCl2, 1 mM dithiothreitol (DTT), 50 mM HEPES, pH 7.5) containing 100 nM Uba1 and 80 µM Ub. The final concentrations of other purified proteins (if present in the assay) were as follows: 125 nM X-DHFR$_{ha}$; 125 nM Ub-ProtA; 125 nM Ub-GST; 125 nM Sic1^{PY}; 200 nM ^{f}Ubr1; 200 nM ^{f}Ufd4; 1 µM Rad6; 1 µM Ubc4. The reactions were terminated by adding 8 µl of 4xSDS-sample buffer. The samples were heated at 95°C for 5 min, followed by SDS-4–12% NuPAGE and either autoradiography or immunoblotting with antibodies to the ha epitope (1:2000; mouse monoclonal antibody; Sigma); to ProtA (polyclonal rabbit antibody; 1:10000) (Sigma); to GST (polyclonal rabbit antibody; 1:10000) (ZYMED Laboratories); and to the T7 epitope (polyclonal rabbit antibody; 1:10000) (Novagen).

Purification of the 26S proteasome and degradation assay.

A slight modification of the earlier procedure (56) was employed. *S. cerevisiae* YYS40, in which the Rpn11 subunit of the 26 proteasome contained a triple-flag tag, were grown to A_{600} of 3–4 in 2 l of YPD medium. Cells were harvested by centrifugation at 5000*g* for 5 min, washed in phosphate-buffered saline (PBS) and stored at −80° C. Cell pellets were resuspended in 10 ml of the lysis buffer (10% glycerol, 0.1 M NaCl, 10 mM MgCl2, 1 mM DTT, 4 mM ATP, 20 mM creatine phosphate, creatine phosphokinase (20 µg/ml), 50 mM Tris-HCl, pH 7.5). Cells were disrupted using a FastPrep-24 instrument (MP Biomedicals) at the speed setting of

4.5, at 20 s/cycle for 10 cycles. After removal of glass beads, extract was cleared by centrifugation at 11200g for 30 min, followed by incubation with 0.2 ml of anti-flag M2 agarose beads (Sigma) for 2 h at 4°C. The beads were washed twice in 10 ml of storage buffer (10% glycerol, 2 mM ATP, 5 mM MgCl2, 1 mM DTT, 50 mM Tris-HCl, pH 7.5), then once with 5 ml of the same buffer containing also 0.2% Triton X-100, and thereafter again once with 5 ml of the storage buffer. The proteasomes were eluted with the triple-flag peptide (0.1 mg/ml; Sigma) in storage buffer and dialyzed against 1 l of storage buffer overnight at 4° C. Polyubiquitylated Leu-$DHFR_{ha}$, the N-end rule substrate for degradation assay, was prepared by incubating the above in vitro ubiquitylation assay at 30° C for 18 h. The reaction mixture was prepared by adding 1 µl of the purified 26S proteasome (~500 nM; its final concentration was ~50 nM) to 8 µl of reaction buffer (2 mM ATP, 10% glycerol, 0.1 M NaCl, 1 mM DTT, 5 mM MgCl2, 50 mM Tris-HCl, pH 7.5), and thereafter adding 1 µl of polyubiquitylated Leu-$DHFR_{ha}$ (1.25 µM; its final concentration was 125 nM). The reaction was performed at 30°C for 10 and 20 min, followed by the addition of 3 µl of the 4xSDS-sample buffer, heating the samples at 95°C for 5 min, and carrying out SDS-4-12% NuPAGE, following by immunoblotting with anti-ha.

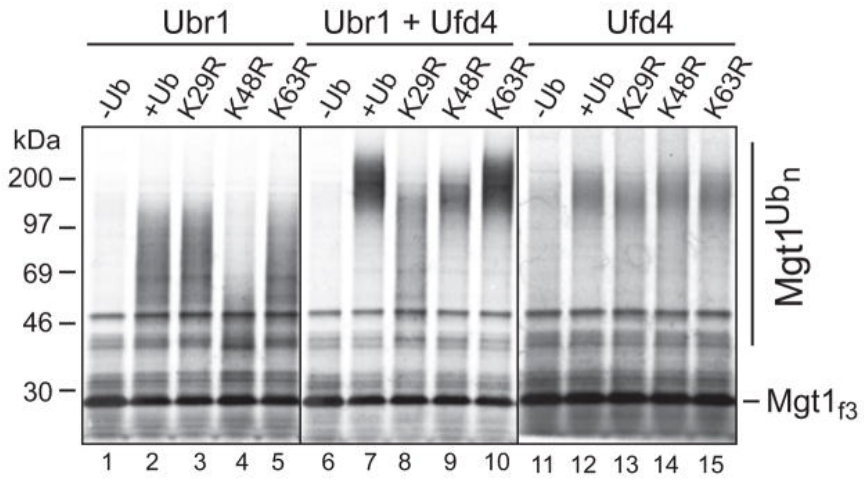

Figure 2.1. Ubiquitylation of Mgt1 by Ubr1-Ufd4. The *in vitro* ubiquitylation assay (12) is described in Methods. Reaction mixtures were incubated at 30° C for 15 min, followed by SDS-PAGE and autoradiography. ^{35}S-Mgt1$_{f3}$ and its polyubiquitylated derivatives are indicated on the right. Lane 1, Mgt1$_{f3}$ in the complete reaction but without added Ub and with Ubr1 as the sole E3. Lane 2, same as lane 1 but with wild-type Ub. Lane 3, same as lane 1 but with Ub^{K29R}. Lane 4, same as lane 1 but with Ub^{K48R}. Lane 5, same as lane 1 but with Ub^{K63R}. Lane 6, ^{35}S-Mgt1$_{f3}$ in the complete reaction (containing both Ubr1 and Ufd4) but without added Ub. Lane 7, same as lane 6 but with wild-type Ub. Lane 8, same as lane 6 but with Ub^{K29R}. Lane 9, same as lane 6 but with Ub^{K48R}. Lane 10, same as lane 6 but with Ub^{K63R}. Lane 11, Mgt1$_{f3}$ in the complete reaction but without added Ub and with Ufd4. Lane 12, same as lane 11 but with wild-type Ub. Lane 13, same as lane 11 but with Ub^{K29R}. Lane 14, samas lane 1 but with Ub^{K48R}. Lane 15, same as lane 11 but with Ub^{K63R}.

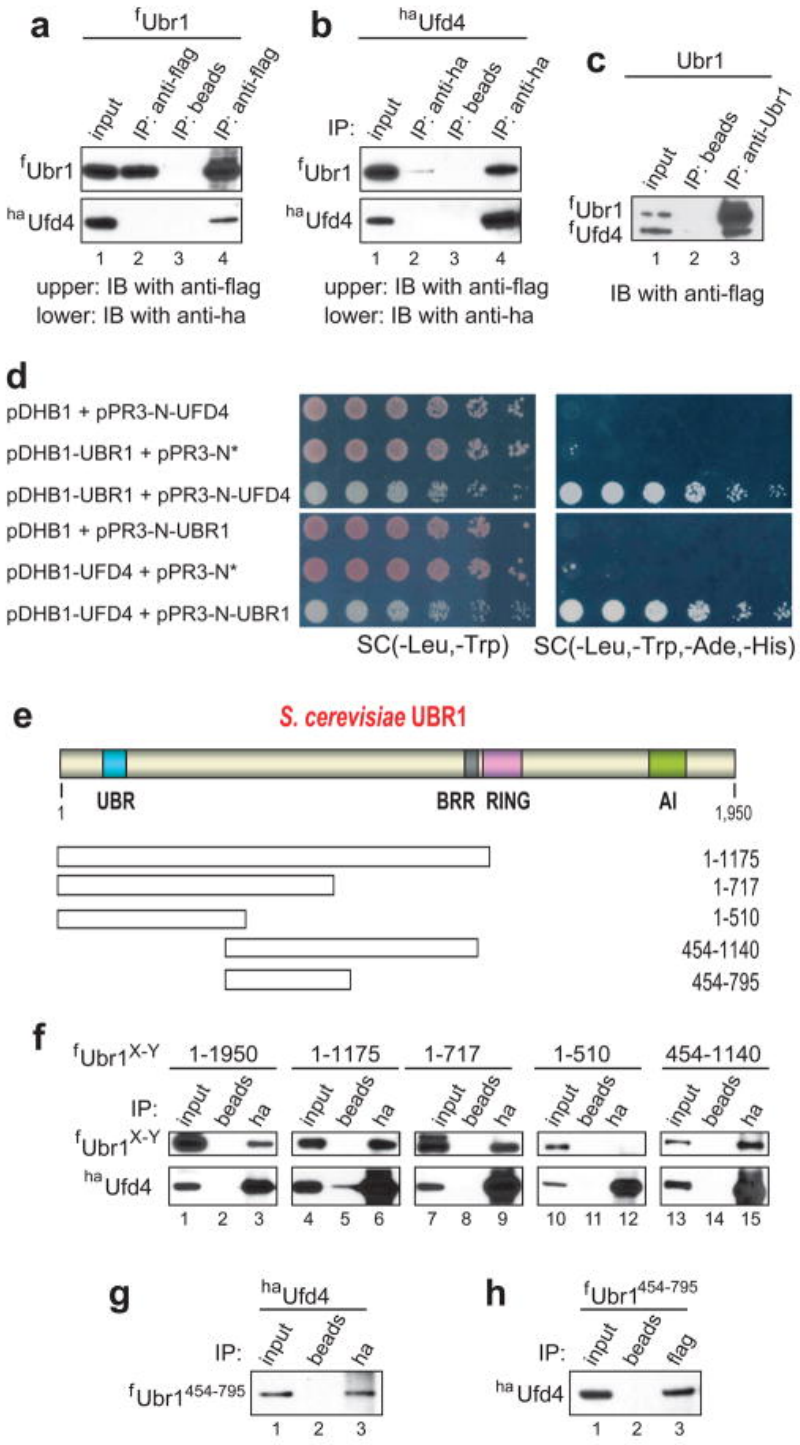

Figure 2.2. Physical interaction between Ubr1 and Ufd4. (a) Coimmunoprecipitation of ^{f}Ubr1 and ^{ha}Ufd4 with anti-flag antibody. JD52 *S. cerevisiae* expressed N-terminally flag-tagged Ubr1 (^{f}Ubr1), either alone (lane 2) or together with N-

terminally ha-tagged Ufd4 (^{ha}Ufd4) (lanes 3 and 4). Cell extracts were immunoprecipitated with anti-flag (lanes 2 and 4) or with antibody-free beads (lane 3). The upper and lower panels show the results of immunoblotting with anti-flag (detection of ^{f}Ubr1) and with anti-ha (detection of ^{ha}Ufd4), respectively. Lane 1, 1% input of extract from cells expressing both ^{f}Ubr1 and ^{ha}Ufd4. Lane 2, extract from cells expressing only ^{f}Ubr1 was incubated with anti-flag pre-bound to beads. Immunoblotting with anti-flag and anti-ha (upper and lower panels, respectively). Lane 3, extract from cells expressing both ^{f}Ubr1 and ^{ha}Ufd4, but with beads lacking antibody. Lane 4, same as lane 3 but immunoprecipitation with anti-flag. (b) Same as in a but extracts were immunoprecipitated with anti-ha pre-bound to beads (lanes 2 and 4) or with beads lacking antibody (lane 3), followed by SDS-PAGE of immunoprecipitates and immunoblotting with anti-flag and anti-ha. (c) Direct interaction of ^{f}Ubr1 and ^{f}Ufd4. Lane 1, 10% inputs of ^{f}Ubr1 and ^{f}Ufd4 (purified as described in ref. 12; see also Fig. S1a). ^{f}Ubr1 (125 ng) and ^{f}Ufd4 (125 ng) were mixed and incubated with beads lacking antibody (lane 2) or with previously characterized (11) affinity-purified anti-Ubr1 antibody pre-bound to beads (lane 3), for 1 hr at 4° C in 0.25 ml of binding buffer, followed by SDS-PAGE and immunoblotting with anti-flag. (d) In vivo detection of Ubr1-Ufd4 interactions using split-Ub assay (53). *S. cerevisiae* coexpressing bait (pDHB1, pDHB1-UBR1, or pDHB1-UFD4) and prey (pPR3-N*, pPR3-N-UFD4, or pPR3-N-UBR1) plasmids were grown to A600 of ~1, serially diluted (5-fold), and plated on either 'permissive' SC(-Leu, -Trp) (left column) or SC(-Leu, -Trp, -Ade, -His) medium (right column). pDHB1 and pPR3-N are the initial (vector) plasmids. pPR3-N* contained a stop codon

immediately after the ORF encoding the mutant N-terminal half of Ub (NUb) in pPR3-N. (e) The UBR box, the BRR region, the RING domain, and the AI (autoinhibitory) domain of the *S. cerevisiae* Ubr1 N-recognin (11, 17, 23). Fragments of Ubr1 employed to map its Ufd4-interacting region are below the diagram. (f) Extracts from JD52 *S. cerevisiae* that expressed ^{ha}Ufd4 and either full-length ^{f}Ubr1 or its flag-tagged fragments were incubated with antibody-lacking beads (lanes 2, 5, 8, 11 and 14) or with anti-ha pre-bound to beads (lanes 3, 6, 9, 12 and 15). Bound proteins were eluted from washed beads, followed by SDS-PAGE and immunoblotting with anti-flag. Input lanes, samples of extracts that corresponded to 1% of initial extracts. (g) Coimmunoprecipitation of ^{f}Ubr1$^{454\text{-}795}$ and ^{ha}Ufd4 with anti-ha. Lane 1, 1% input of the initial extract. Lane 2, extracts from cells that expressed the ^{f}Ubr1$^{454\text{-}795}$ fragment and full-length ^{ha}Ufd4 were incubated with antibody-free beads (lanes 2). Bound proteins were eluted from washed beads and fractionated by SDS-PAGE, followed by immunoblotting with anti-flag. Lane 3, same as lane 2 but immunoprecipitation with anti-ha pre-bound to beads. (h) Lanes 1-3, same as lanes 1-3 in g, but immunoprecipitation with anti-flag (instead of anti-ha), followed by immunoblotting with anti-ha.

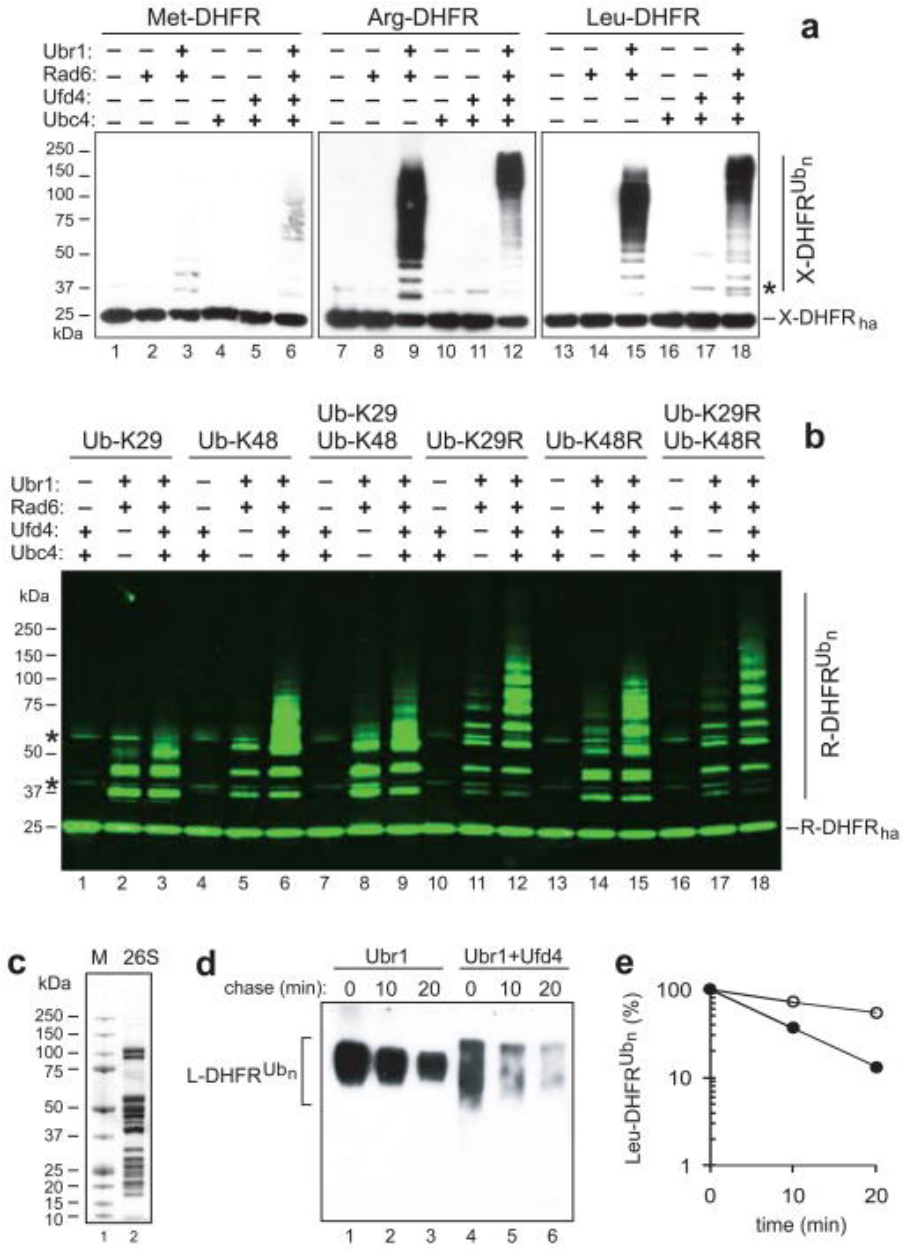

Figure 2.3. Enhancement of ubiquitylation and degradation of Arg/N-end rule substrates by Ufd4. (a) X-e^{K}-DHFR$_{ha}$ (X=Met, Arg, Leu), denoted as X-DHFR$_{ha}$, are C-terminally ha-tagged Arg/N-end rule reporters (54) produced from Ub-X-DHFR$_{ha}$ using in vitro deubiquitylation (55) (Fig. S1b). X-DHFR$_{ha}$ contained the mouse dihydrofolate reductase (DHFR) moiety and the ~40-residue N-terminal extension called e^{K} [extension (e) containing lysine (K)] (18). Purified X-DHFR$_{ha}$ (X=Met, Arg,

Leu) (1.25 μM; 2 μl) were incubated in 20 μl of a ubiquitylation assay (12) for 15 min at 30° C, followed by SDS-PAGE and immunoblotting with anti-ha. Lanes 1, 7, 13: X-DHFR$_{ha}$ in the absence of indicated assay's components. Lanes 2, 8, 14: same as lanes l, 7, 13 but with Rad6 E2. Lane 3, 9, 15, same as lanes 1, 7, 13 but with Ubr1 and Rad6. Lanes 4, 10, 16 same as lanes 1, 7, 13 but with Ubc4 E2. Lane 5, 11, 17 same as lane 1, 7, 13 but with Ufd4 and Ubc4. Lane 6, 12, 18 same as lane 1 but with Ubr1, Rad6, Ufd4 and Ubc4. Asterisk on the right denotes a protein that crossreacted with anti-ha antibody. (b) Same as in a but the assay was carried out with Arg-DHFR$_{ha}$ and indicated Ub mutants. Detection of immunoblotted proteins in this experiment was performed using Odyssey (Li-Cor, Lincoln, NE, USA). Asterisks on the left indicate two bands of proteins (e.g., lanes 1, 4) that crossreacted with anti-ha, and were also present in samples lacking E2s and E3s. Lanes 1, 4, 7, 10, 13, 16, ubiquitylation of Arg-DHFR$_{ha}$ with Ufd4/Ubc4 in the presence of either Ub^{K29} (lane 1), Ub^{K48} (lane 4), a 50-50 mixture of Ub^{K29} and Ub^{K48} (lane 7), Ub^{K29R} (lane 10), Ub^{K48R} (lane 13), or a 50-50 mixture of Ub^{K29R} and Ub^{K48R} (lane 16). Lanes 2, 5, 8, 11, 14, 17, same as lanes 1, 4, 7, 10, 13, 16, respectively, but with Ubr1/Rad6 instead of Ufd4/Ubc4. Lanes 3, 6, 9, 12, 15, 18, same as lanes 1, 4, 7, 10, 13, 16, respectively, but with Ubr1/Rad6 plus Ufd4/Ubc4. (c) Lanes 1 and 2, molecular mass markers and Coomassie-stained proteins of the affinity-purified *S. cerevisiae* 26S proteasome, respectively. (d) Lanes 1–3, assay with 26S proteasome and polyubiquitylated Leu-DHFR$_{ha}$ that had been prepared using Ubr1/Rad6 alone, with chase times of 10 and 20 min. Lanes 4–6, same as lanes 1–3, but with polyubiquitylated Leu-DHFR$_{ha}$ that had been prepared with Ubr1/Rad6 plus and Ufd4/Ubc4. (e) Quantitation of data in

d, using ImageJ (http://rsb.info.nih.gov/ij/index.html). In plotting the levels of Leu-$DHFR_{ha}$ for each data set (lanes 1–3 and 4–6 in d), the levels at time zero were taken as 100%. Open and closed circles, Leu-$DHFR_{ha}$ that had been ubiquitylated by Ubr1/Rad6 and by Ubr1/Rad6 plus Ufd4/Ubc4, respectively.

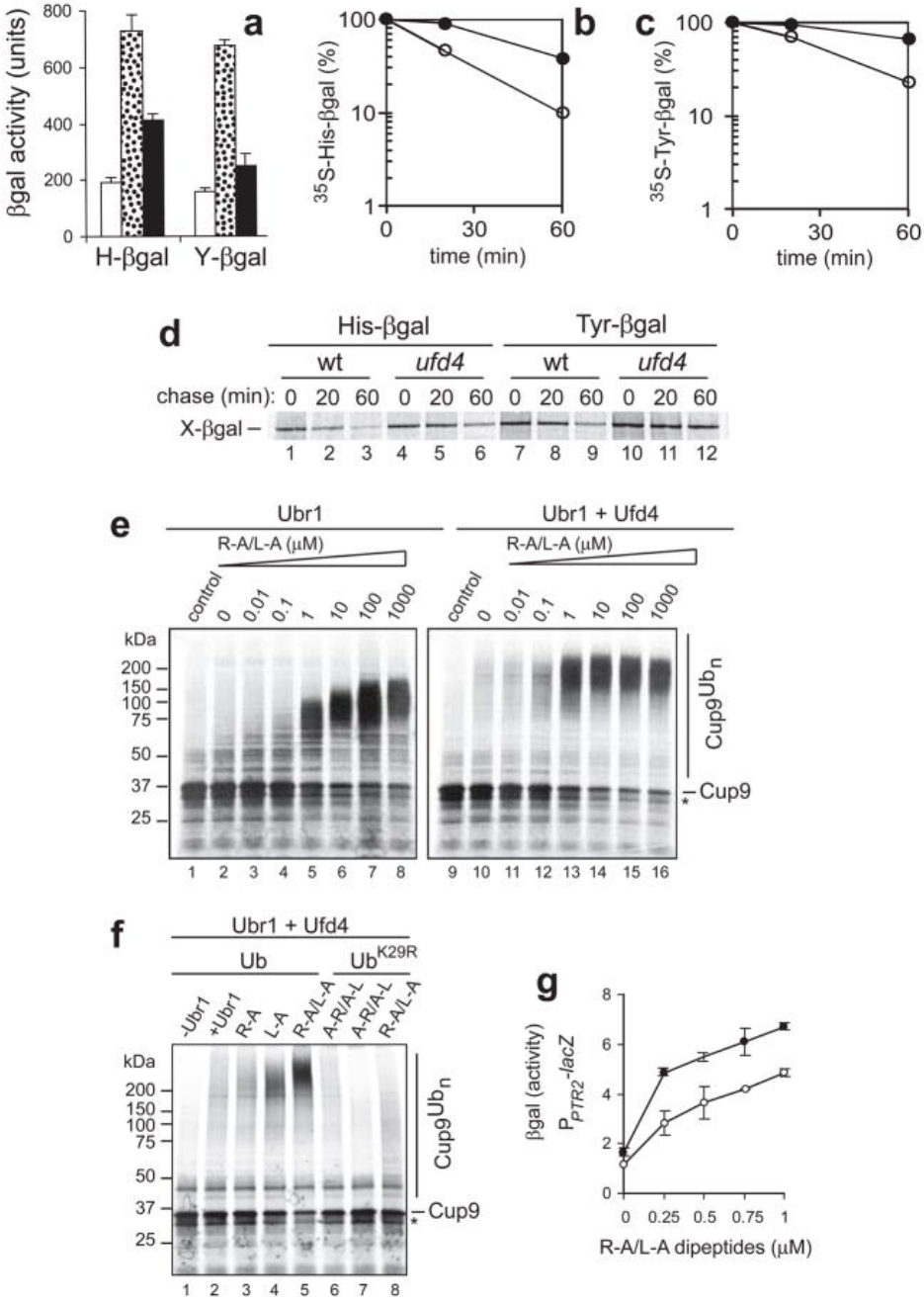

Figure 2.4. Ufd4 augments the Arg/N-end rule pathway. (a) β gal activity in extracts from *S. cerevisiae* RJD347 (wild-type; white bars), AVY26 (*ubr1Δ*; dotted bars), and CHY251 (*ufd4Δ*; black bars) that expressed His-β gal or Tyr-β gal. (b ,c) Quantitation of data (using PhosphorImager) in a pulse-chase assay (d) for His-β gal (b) and Tyr-β gal (c). Open and closed circles, wild-type (RJD347) and *ufd4Δ* (CHY251) cells,

respectively. In d, *S. cerevisiae* expressing Ub-His-β gal or Ub-Tyr-β gal were labeled for 5 min with 35S-methionine/cysteine, followed by a chase for 20 and 60 min, immunoprecipitation with anti-β gal, SDS-PAGE and autoradiography (1, 54). Lanes 1–3, His-β gal in wild-type cells. Lanes 4–6, His-β gal in ufd4Δ cells. Lanes 7–9, Tyr-β gal in wild-type cells. Lanes 10–12, Tyr-β gal in *ufd4Δ* cells. (e) Ubr1/Rad6-mediated polyubiquitylation of Cup9. *In vitro* ubiquitylation assay (12) was performed with ^{35}S-labeled Cup9$_{NSF}$ (see Methods). Lane 1, ^{35}S-Cup9 in an otherwise complete assay but without E3s. Lanes 2–8, same as lane 1 but with Ubr1/Rad6, in the presence of Arg-Ala (R-A)/Leu-Ala (L-A). Lane 9, same as lane 1 but a separate assay. Lanes 10–16, same as lanes 2–8, but with Ubr1 plus Ufd4. (f) Maximal stimulation of Cup9 ubiquitylation by Ubr1-Ufd4 requires both type-1 and type-2 dipeptides. Lane 1, ^{35}S-Cup9, with Ufd4 and wild-type Ub, but in the absence of both Ubr1 and type-1/2 dipeptides. Lane 2, same as lane 1 but with Ubr1. Lane 3, same as lane 2, but with 1 μM R-A. Lane 4, same as lane 2 but in the presence of 1 μM L-A. Lane 5, same as lane 2, but in the presence of R-A and L-A, each at 1 μM. Lane 6, same as lane 2 but in the presence of Ala-Arg/Ala-Leu, each at 1 μM. Lanes 7, same as lane 6, but with Ub^{K29R}, instead of wild-type Ub. Lane 8, same as lane 7, but in the presence of R-A/L-A, each at 1 μM. (g) Dipeptide-mediated induction of the PTR2 transporter in the absence or presence of Ufd4. *S. cerevisiae* RJD347 (wild-type; closed circles) and CHY251 (*ufd4Δ*; open circles) expressed *E. coli* lacZ (β-galactosidase) from the P$_{PTR2}$ promoter. Cells were grown to A600 of ~0.8 in the SHM medium at 30° C in the presence of indicated concentrations of R-A/L-A, followed by measurements in triplicate, of β gal activity in cell extracts, with standard deviations shown.

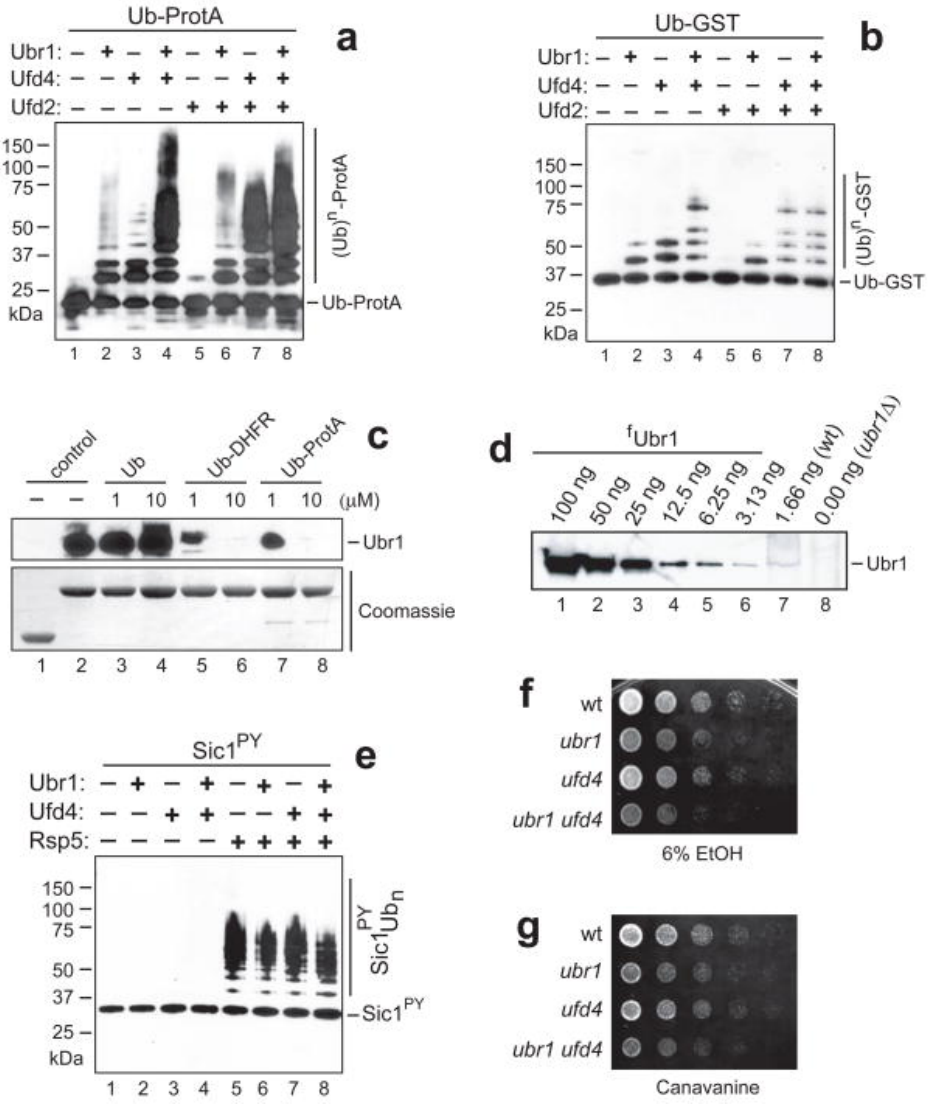
Ub-ProtA
a
Ubr1:
Ufd4:
Ufd2:
150
100
75
50
37
25
kDa
(Ub)n-ProtA
Ub-ProtA
1 2 3 4 5 6 7 8
Ub-GST
b
(Ub)n-GST
Ub-GST
control
Ub
Ub-DHFR
Ub-ProtA
c
(μM)
Ubr1
Coomassie
fUbr1
d
100 ng
50 ng
25 ng
12.5 ng
6.25 ng
3.13 ng
1.66 ng (wt)
0.00 ng (ubr1Δ)
Sic1PY
e
Rsp5:
Sic1PYUbn
Sic1PY
f
wt
ubr1
ufd4
ubr1 ufd4
6% EtOH
g
Canavanine

Figure 2.5. Recognition and synergistic polyubiquitylation of UFD substrates by Ufd4 and Ubr1. (a) Ubiquitylation assay12, for 15 min at 30° C, with Ub-ProtA, a UFD substrate (0.125 μM) (Fig. S1c), followed by SDS-PAGE and immunoblotting with anti-ProtA antibody. Lane 1, without E3s. Lane 2, same as lane 1 but with Ubr1/Rad6. Lane 3, same as lane 1 but with Ufd4/Ubc4. Lane 4, same as lane 1 but with Ubr1/Rad6 plus Ufd4/Ubc4. Lane 6, same as lane 1 but with Ufd2/Ubc4 plus Ubr1/Rad6. Lane 7, same as lane 1 but with Ufd2/Ubc4 plus Ufd4/Ubc4. Lane 8, same as lane 1 but with Ufd2/Ubc4, Ubr1/Rad6 and Ufd4/Ubc4. (b) Ubiquitylation assay with Ub-GST (0.125 μM). Lane 1, Ub-GST without E3s. Lane 2, same as lane 1 but with Ubr1/Rad6. Lane 3, same as lane 1 but with Ufd4/Ubc4. Lane 4, same as lane 1 but with Ubr1/Rad6 plus Ufd4/Ubc4. Lane 5, same as lane 1 but with Ufd2/Ubc4. Lane 6, same as lane 1 but with Ufd2/Ubc4 plus Ubr1/Rad6. Lane 7, same as lane 1 but with Ufd2/Ubc4 plus Ufd4/Ubc4. Lane 8, same as lane 1 but with Ufd2/Ubc4, Ubr1/Rad6 and Ufd4/Ubc4. (c) Interaction of Ubr1 with immobilized UFD substrates could be competed out by UFD substrates but not by free Ub. Equal amounts of purified ^{f}Ubr1 (1 μg) were incubated (in either the presence or absence of free Ub, Ub-DHFR$_{ha}$ (Ub-Met-DHFR$_{ha}$) or Ub-ProtA, each of them at 1 or 10 μM)) with GST alone or Ub-GST (~5 μg) that had been linked to glutathione-Sepharose beads. Bound proteins were eluted from the beads, followed by SDS-PAGE and immunoblotting with anti-flag (upper panel), with subsequent Coomassie staining of the blotted PVDF membrane (lower panel). Lane 1, GST alone. Lane 2, Ub-GST. Lane 3, same as lane 2 but in the presence of 1 μM free Ub. Lane 4, same as lane 2

but with 10 μM free Ub. Lane 5, same as lane 2 but in with 1 μM Ub-$DHFR_{ha}$. Lane 6, same as lane 2 but with 10 μM Ub-$DHFR_{ha}$. Lane 7, same as lane 2 but with 1 μM Ub-ProtA. Lane 8, same as lane 2 but with 10 μM Ub-ProtA. (d) *In vivo* levels of endogenous Ubr1. Lanes 1–6, a dilution series with the indicated amounts of purified ^{f}Ubr1 was fractionated by SDS-PAGE, followed by immunoblotting with affinity-purified anti-Ubr1 antibody (11). Lane 7, extract (50 μg) from wild-type *S. cerevisiae* (JD52) that grew exponentially (A_{600} of ~1) in YPD medium. Lane 8, same as lane 7 but extract from *ubr1Δ* cells (JD55). These data and straightforward calculations indicated that 'wild-type', haploid, exponentially growing *S. cerevisiae* contained 500 to 1000 Ubr1 molecules per cell. (e)Ubr1 and Ufd4 did not affect the Rsp5-mediated polyubiquitylation of T7 epitope-tagged $Sic1^{PY}$. The PY motif is the sequence Pro-Pro-X-Tyr, which binds to the WW domain of Rsp5 (see Methods). Purified $Sic1^{PY}$ (Fig. S1c) was incubated in the above ubiquitylation assay, followed by SDS-PAGE and immunoblotting with anti-T7 antibody. Lane 1, $Sic1^{PY}$ without E3s. Lane 2, same as lane 1 but with Ubr1/Rad6. Lane 3, same as lane 1 but with Ufd4/Ubc4. Lane 4, same as lane 1 but with Ubr1/rad6 plus Ufd4/Ubc4. Lane 5, same as lane 1 but with Rsp5/Ubc4. Lane 6, same as lane 1 but with Rsp5/Ubc4 and Ubr1/Rad6. Lane 7, same as lane 1 but with Rsp5/Ubc4 plus Ufd4/Ubc4. Lane 8, same as lane 1 but with Rsp5/Ubc4, Ubr1/Rad6 and Ufd4/Ubc4. (f, g) Equal amounts of cells from wild-type (JD52), *ubr1Δ* (JD55), *ufd4Δ* (CHY194) or *ubr1Δufd4Δ* (CHY195) strains were 5-fold serially diluted, plated on YPD plates containing 6% ethanol (6%) (f) or canavanine at 0.4 mg/ml (g), and incubated at 30° C for 3 days and 1 day, respectively.

References

1. Bachmair A, Finley D, Varshavsky A. In vivo half-life of a protein is a function of its amino-terminal residue. Science. 1986;234:179–186.

2. Varshavsky A. The N-end rule: functions, mysteries, uses. Proc Natl Acad Sci USA. 1996;93 :12142–12149.

3. Varshavsky A. Discovery of cellular regulation by protein degradation. J Biol Chem. 2008;283:34469–34489.

4. Ravid T, Hochstrasser M. Diversity of degradation signals in the ubiquitin-proteasome system. Nat Rev Mol Cell Biol. 2008;9:679–689.

5. Turner GC, Du F, Varshavsky A. Peptides accelerate their uptake by activating a ubiquitin-dependent proteolytic pathway. Nature. 2000;405:579–583.

6. Rao H, Uhlmann F, Nasmyth K, Varshavsky A. Degradation of a cohesin subunit by the N-end rule pathway is essential for chromosome stability. Nature. 2001;410:955–960.

7. Hu RG, et al. The N-end rule pathway as a nitric oxide sensor controlling the levels of multiple regulators. Nature. 2005;437:981–986.

8. Tasaki T, Kwon YT. The mammalian N-end rule pathway: new insights into its components and physiological roles. Trends Biochem Sci. 2007;32:520–528.

9. Mogk A, Schmidt R, Bukau B. The N-end rule pathway of regulated proteolysis: prokaryotic and eukaryotic strategies. Trends Cell Biol.

2007;17:165–172.

10. Hu R-G, Wang H, Xia Z, Varshavsky A. The N-end rule pathway is a sensor of heme. Proc Natl Acad Sci USA. 2008;105:76–81.

11. Hwang C-S, Varshavsky A. Regulation of peptide import through phosphorylation of Ubr1, the ubiquitin ligase of the N-end rule pathway. Proc Natl Acad Sci USA. 2008;105:19188–19193.

12. Hwang C-S, Shemorry A, Varshavsky A. Two proteolytic pathways regulate DNA repair by co-targeting the Mgt1 alkyguanine transferase. Proc Natl Acad Sci USA. 2009;106:2142–2147.

13. Schmidt R, Zahn R, Bukau B, Mogk A. ClpS is the recognition component for Escherichia coli substrates of the N-end rule degradation pathway. Mol Microbiol. 2009;72:506–517.

14. Román-Hernández G, Grant RA, Sauer RT, Baker TA. Molecular basis of substrate selection by the N-end rule adaptor protein ClpS. Proc Natl Acad Sci USA. 2009;106:8888–8893.

15. Wang H, Piatkov KI, Brower CS, Varshavsky A. Glutamine-specific N-terminal amidase, a component of the N-end rule pathway. Mol Cell. 2009;34:686–695.

16. Brower CS, Varshavsky A. Ablation of arginylation in the mouse N-end rule pathway: loss of fat, higher metabolic rate, damaged spermatogenesis, and neurological perturbations. PLoS ONE. 2009;4:e7757.

17. Tasaki T, et al. The substrate recognition domains of the N-end rule pathway. J Biol Chem. 2009;284:1884–1895.

18. Hwang CS, Shemorry A, Varshavsky A. N-terminal acetylation of cellular proteins creates specific degradation signals. Science. 2010;327:973–977.

19. Liu F, Walters KJ. Multitasking with ubiquitin through multivalent interactions. Trends Biochem Sci. 2010;35:352–360.

20. Hochstrasser M. Origin and function of ubiquitin-like proteins. Nature. 2009;458:422–429.

21. Dye BT, Schulman BA. Structural mechanisms underlying posttranslational modification by ubiquitin-like proteins. Annu Rev Biophys Biomol Struct. 2007;36:131–150.

22. Du F, Navarro-Garcia F, Xia Z, Tasaki T, Varshavsky A. Pairs of dipeptides synergistically activate the binding of substrate by ubiquitin ligase through dissociation of its autoinhibitory domain. Proc Natl Acad Sci USA. 2002;99:14110–14115.

23. Xia Z, et al. Substrate-binding sites of UBR1, the ubiquitin ligase of the N-end rule pathway. J Biol Chem. 2008;283:24011–24028.

24. Choi WS, et al. Structural basis for the recognition of N-end rule substrates by the UBR box of ubiquitin ligases. Nat Struct Mol Biol. 2010;17:1175–1182.

25. Matta-Camacho E, Kozlov G, Li FF, Gehring K. Structural basis of substrate recognition and specificity in the N-end rule pathway. Nat Struct Mol Biol.

2010;17:1182–1188.

26. Sriram SM, Kwon YT. The structural basis of N-end rule recognition. Nat Struct Mol Biol. 2010;17:1164–1165.

27. Xia Z, Turner GC, Hwang C-S, Byrd C, Varshavsky A. Amino acids induce peptide uptake via accelerated degradation of CUP9, the transcriptional repressor of the PTR2 peptide transporter. J Biol Chem. 2008;283:28958–28968.

28. Heck JW, Cheung SK, Hampton RY. Cytoplasmic protein quality control degradation mediated by parallel actions of the E3 ubiquitin ligases Ubr1 and San1. Proc Natl Acad Sci USA. 2010;107:1106–1111.

29. Eisele F, Wolf DH. Degradation of misfolded proteins in the cytoplasm by the ubiquitin ligase Ubr1. FEBS Lett. 2008;582:4143–4146.

30. Prasad R, Kawaguchi S, Ng DTW. A nucleus-based quality control mechanism for cytosolic proteins. Mol Biol Cell. 2010;21:2117–2127.

31. Nillegoda NB, et al. Ubr1 and Ubr2 function in a quality control pathway for degradation of unfolded cytosolic proteins. Mol Biol Cell. 2010;21:2102–2116.

32. Kwon YT, et al. An essential role of N-terminal arginylation in cardiovascular development. Science. 2002;297:96–99.

33. Cai H, Kauffman S, Naider F, Becker JM. Genomewide screen reveals a wide regulatory network for di/tripeptide utilization in Saccharomyces cerevisiae.

Genetics. 2006;172:1459–1476.

34. Graciet E, Wellmer F. The plant N-end rule pathway: structure and functions. Trends Plant Sci. 2010;15:447–453.

35. Kurosaka S, et al. Arginylation-dependent neural crest cell migration is essential for mouse development. PLoS Genet. 2010;6:e1000878.

36. Karakozova M, et al. Arginylation of beta-actin regulates actin cytoskeleton and cell motility. Science. 2006;313:192–196.

37. Caprio MA, Sambrooks CL, Durand ES, Hallak M. The arginylation-dependent association of calreticulin with stress granules is regulated by calcium. Biochem J. 2010;429:63–72.

38. Johnson ES, Ma PC, Ota IM, Varshavsky A. A proteolytic pathway that recognizes ubiquitin as a degradation signal. J Biol Chem. 1995;270:17442–17456.

39. Ravid T, Hochstrasser M. Autoregulation of an E2 enzyme by ubiquitin-chain assembly on its catalytic residue. Nat Cell Biol. 2007;9:422–427.

40. Ju D, Wang X, Xu H, Xie Y. The armadillo repeats of the Ufd4 ubiquitin ligase recognize ubiquitin-fusion proteins. FEBS Lett. 2007;581:265–270.

41. Xie Y, Varshavsky A. Physical association of ubiquitin ligases and the 26S proteasome. Proc Natl Acad Sci USA. 2000;97:2497–2502.

42. Xie Y, Varshavsky A. UFD4 lacking the proteasome-binding region catalyses

ubiquitination but is impaired in proteolysis. Nature Cell Biol. 2002;4:1003–1007.

43. Kee Y, Huibregtse JM. Regulation of catalytic activities of HECT ubiquitin ligases. Biochem Biophys Res Commun. 2007;354:329–333.

44. Johnson ES, Bartel BW, Varshavsky A. Ubiquitin as a degradation signal. EMBO J. 1992;11:497–505.

45. Koegl M, et al. A novel ubiquitination factor, E4, is involved in multiubiquitin chain assembly. Cell. 1999;96:635–644.

46. Xu P, et al. Quantitative proteomics reveals the function of unconventional ubiquitin chains in proteasomal degradation. Cell. 2009;137:133–145.

47. Hochstrasser M. Lingering mysteries of ubiquitin-chain assembly. Cell. 2006;124:27–34.

48. Chau V, et al. A multiubiquitin chain is confined to specific lysine in a targeted short-lived protein. Science. 1989;243:1576–1583.

49. Rodrigo-Brenni MC, Morgan DO. Sequential E2s drive polyubiquitin chain assembly on APC targets. Cell. 2007;130:127–139.

50. Hoppe T. Multiubiquitylation by E4 enzymes: 'one size' doesn't fit all. Trends Biochem Sci. 2005;30:183–187.

51. Scott DC, et al. A dual mechanism for Rub1 ligation to Cdc53. Mol Cell. 2010;39:784–796.

52. Johnsson N, Varshavsky A. Split ubiquitin as a sensor of protein interactions in vivo. Proc Natl Acad Sci USA. 1994;91:10340–10344.

53. Möckli N, et al. Yeast split-ubiquitin-based cytosolic screening system to detect interactions between transcriptionally active proteins. BioTechniques. 2007;42:725–729.

54. Varshavsky A. Ubiquitin fusion technique and related methods. Meth Enzymol. 2005;399:777–799.

55. Catanzariti AM, Soboleva TA, Jans DA, Board PG, Baker RT. An efficient system for high-level expression and easy purification of authentic recombinant proteins. Protein Sci. 2004;13:1331–1339.

56. Saeki Y, Isono E, Toh EA. Preparation of ubiquitinated substrates by the PY motif-insertion method for monitoring 26S proteasome activity. Meth Enzymol. 2005;399:215–227.

57. Turner GC, Varshavsky A. Detecting and measuring cotranslational protein degradation in vivo. Science. 2000;289:2117–2120.

58. Liu C, et al. Ubiquitin chain elongation enzyme Ufd2 regulates a subset of Doa10 substrates. J Biol Chem. 2010;285:10265–10272.

59. Tu D, Li W, Ye Y, Brunger AT. Structure and function of the yeast U-box-containing ubiquitin ligase Ufd2p. Proc Natl Acad Sci USA. 2007;104:15599–15606.

60. Ghaemmaghami S, et al. Global analysis of protein expression in yeast.

Nature. 2003;425:737–741.

61. Courbard JR, et al. Interaction between two ubiquitin-protein isopeptide ligases of different classes, CBLC and AIP4/ITCH. J Biol Chem. 2002;277:45267–45275.

62. Chen C, et al. The WW domain-containing E3 ubiquitin protein ligase 1 upregulates ErbB2 and EGFR through RING finger protein 11. Oncogene. 2008;27:6845–6855.

63. Magnifico A, et al. WW domain HECT E3s target Cbl RING finger E3s for proteasomal degradation. J Biol Chem. 2003;278:43169–43177.

64. Zaaroor-Regev D, et al. Regulation of the polycomb protein Ring1B by self-ubiquitination or by E6-AP may have implications to the pathogenesis of Angelman syndrome. Proc Natl Acad Sci USA. 2010;107:6788–6793.

65. Varshavsky A. Spalog and sequelog: neutral terms for spatial and sequence similarity. Curr Biol. 2004;14:R181–R183.

66. Park Y, Yoon SK, Yoon JB. The HECT domain of TRIP12 ubiquitinates substrates of the ubiquitin fusion degradation pathway. J Biol Chem. 2009;284:1540–1549.

67. Gardner RG, Nelson ZW, Gottschling DE. Degradation-mediated protein quality control in the nucleus. Cell. 2005;120:803–815.

68. Longtine MS, et al. Additional modules for versatile and economical PCR-based gene deletion and modification in Saccharomyces cerevisiae. Yeast.

1998;14:953–961.

69. Ausubel FM, et al. Current Protocols in Molecular Biology. Wiley-Interscience; New York: 2006.

70. Kushnirov VV. Rapid and reliable protein extraction from yeast. Yeast. 2000;16:857–860.

CHAPTER 3:

CHARACTERIZATION OF THE UBR1-UFD4 E3-E3 COMPLEX

(Unpublished data in follow-up to Chapter 2)

Abstract

This chapter describes unpublished follow-up experiments for our paper entitled "*The N-End Rule Pathway is Mediated by a Complex of the RING-type Ubr1 and HECT-type Ufd4 Ubiquitin Ligases*" (1). These previously published results (see Chapter 2) demonstrate that the RING-type Ubr1 E3 and the HECT-type Ufd4 E3 interact, both physically and functionally. The experiments in this chapter address the interaction of the Ubr1-Ufd4 complex with Mgt1 (a DNA repair protein) and the formation of the E3-E3 complex itself. We found that the presence of MNNG, an alkylating agent that causes DNA damage, in the yeast growth media contributes to the formation of a complex of Ubr1-Ufd4 with Mgt1 and also, remarkably, to the formation of the Ubr1-Ufd4 complex itself. Conversely, type-1 and type-2 dipeptides apparently interfere with the complex formation.

Introduction and Results

In *S. cerevisiae,* the Arg/N-end rule pathway is mediated by a physical complex of the RING-type Ubr1 E3 (N-recognin) and the HECT-type Ufd4 E3, in association with their cognate E2s Rad6 and Ubc4/Ubc5, respectively (1) (Chapter 2). The physical interaction between Ufd4 and Ubr1 was previously demonstrated both in vitro and in vivo (Fig. 2.2). We further characterized this interaction using gel filtration of purified N-terminally flag-tagged Ufd4 (^{f}Ufd4) and Ubr1 (^{f}Ubr1). We showed that purified ^{f}Ubr1 and ^{f}Ufd4 elute differently when the proteins were preincubated together (Fig. 3.1 lower panel) rather than separately run on the

column (Fig. 3.1 upper panel). When Ubr1 and Ufd4 are incubated together before running on the column, the two proteins elute in the same fractions (fractions 20-22). According to molecular weight standards, the size of the Ubr1-Ufd4 complex is 400-500 kDa, which would indicate a 1:1 stoichiometry of Ubr1 to Ufd4. Although Ubr1 is larger than Ufd4, 225 kDa versus 168 kDa, Ufd4 alone eluted earlier (fractions 17-18) than Ubr1 (fractions 22-23), suggesting that Ufd4 forms a homo-oligomer complex in the absence of Ubr1.

In contrast to Ubr1, Ufd4 is not an N-recognin, that is, it does not, by itself, recognize N-degrons. However, through its physical interaction with the Ubr1 E3, the Ufd4 E3 functions as a novel component of the Arg/N-end rule pathway that increases the overall efficacy of degradation of Arg/N-end rule substrates, at least in part by augmenting the processivity of their polyubiquitylation by the Ubr1/Rad6-Ufd4/Ubc4 double E3-E2 complex. Interestingly, the function of Ufd4 in the Arg/N-end rule pathway is not confined to processivity of polyubiquitylation, as Ufd4 was also shown to recognize the internal degron of the Mgt1 DNA repair protein (a substrate of the Arg/N-end rule pathway targeted through an internal degron) even in the absence of Ubr1, i.e., ubr1Δ cells, that is, in the absence of Ubr1. Thus, the sets of internal degrons recognized by Ubr1 and Ufd4 are at least partially overlapping. In a coimmunoprecipitation experiment, we found that Ubr1 and Ufd4 compete for binding to Mgt1. Specifically, we overexpressed ^{f}Ufd4 alone from the P_{CUP1} promoter, untagged Ubr1 alone from the P_{GAL1} promoter or ^{f}Ufd4 and Ubr1 together. We used purified N-terminally GST-tagged Mgt1 to pull down proteins that interacted with this fusion from a protein extract. We found that when both Ufd4 and Ubr1 were

overexpressed together, the amount of the target protein (i.e. Ubr1 or Ufd4) pulled down was less than when either was expressed alone (Fig. 3.2 compare lanes 3 and 9 for Ubr1; lanes 3 and 6 for Ufd4). A parsimonious interpretation of this result is that Ubr1 and Ufd4 each contain a substrate binding site specific for Mgt1. It is also possible but less likely (this ambiguity can be experimentally resolved) that the interaction between Ubr1 and Ufd4 weakens or abrogates their affinity for Mgt1, at least in vitro.

Earlier studies introduced the operationally defined concept of an E4 as an E3-like enzyme that cooperates with substrate-specific ubiquitylation machinery to increase the efficacy (including processivity) of polyubiquitylation. Ufd2, an E4-type enzyme of the UFD pathway, increased the processivity of ubiquitylation of the Ufd4 E3 (1). In contrast to Ufd4, Ufd2 had only a weak effect on ubiquitylation by Ubr1 (Fig. 2.4). Owing to these results, we also tested the in vivo stability of Mgt1 in the absence of Ufd2. MNNG, a DNA alkylating agent, was previously shown to accelerate the degradation of Mgt1 (4). Using a cycloheximide chase (CHX) experiment, we found that both in the presence and absence of the MNNG, Mgt1 became more unstable in ufd2Δ cells (lacking Ufd2) (Fig. 3.3). Similar results were observed with ubr2Δ mutants, cells lacking Ubr2, an E3 and sequelog of Ubr1 that does not function as an N-recognin (Fig. A1.2D). Ramifications of these results remain to be understood.

Since the DNA damaging agent MNNG accelerates the degradation of Mgt1, we decided to test how the presence of MNNG in the growth media affects the

interaction of the Ubr1-Ufd4 complex with Mgt1 and the interaction between Ufd4 and Ubr1. The presence of MNNG in the media had no effect on the binding of Ubr1 and Ufd4 to Mgt1 when they were expressed independently (Fig. 3.4A compare lanes 3 and 6). However, if Ubr1 and Ufd4 were co-overexpressed, the presence of MNNG in the growth media decreased the binding of either Ubr1 or Ufd4 to Mgt1 (Fig. 3.4B compare lanes 3 and 6). We also found that when cells overexpressing both Ubr1 and Ufd4 were grown in the presence of MNNG, the in vitro interaction observed between Ubr1 and Ufd4 became stronger (Fig. 3.5A and B compare lanes 3 and 6 in the top panel). It is possible (these issues remain to be addressed experimentally) that the formation of the Ubr1-Ufd4 complex inhibits the binding of its components to Mgt1. It is also possible that in vivo, MNNG might be a signal for Ubr1 to initiate the binding and ubiquitylation of Mgt1, followed by the binding of Ufd4 that increases the processivity of polyubiquitylation. This circuit, interesting both functionally and mechanistically, remains to be deciphered in detail.

The binding of short peptides with destabilizing N-terminal residues to the type-1/2 sites of Ubr1 allosterically activates the third substrate-binding site of Ubr1 that recognizes an internal degron of Cup9, a transcriptional repressor (5). The in vitro binding of ^{f}Ubr1 to GST-Cup9 required the presence of cognate dipeptides such as Arg-Ala (type-1 dipeptide) and Leu-Ala (type-2 dipeptide) (Fig. A2.S4B, lanes 11 and 12). Interestingly, however, the interaction between ^{f}Ubr1 and GST-Mgt1 was inhibited by the type 1/2 dipeptides (Fig. A2.S4B, lanes 3-8). On the other hand, the binding of ^{ha}Ufd4 to GST-Mgt1 occurred irrespective of the presence or absence of type-1/2 or other tested dipeptides (Fig. A2.S4C). Given these results,

we decided to examine the effect of type-1/2 dipeptides (Arg/Ala and Leu/Ala) on the interaction between Ubr1 and Ufd4 as assayed by gel filtration. In the control experiment, with dipeptides Ala-Leu and Ala-Arg, the elution of both Ubr1 and Ufd4 was unchanged from the elution pattern observed in the absence of dipeptides (compare Fig. 3.1 and 3.5 top panel). However, when Ubr1 and Ufd4 were separately incubated with type-1/2 dipeptides (Arg-Ala and Leu-Ala) and ran independently on the gel filtration column, Ubr1 and Ufd4 eluted differently. Specifically, an increased signal for Ubr1 was observed in the same fractions as with non-type-1/2 dipeptides, whereas Ufd4 eluted later when there were no dipeptides present or non-type-1/2 dipeptides. We also examined gel-filtration properties of the Ubr1-Ufd4 complex in the presence of type-1/2 dipeptides. Remarkably, the Ubr1-Ufd4 complex apparently dissociates in the presence of Arg-Ala and Leu-Ala, the complex of Ubr1 and Ufd4 dissociates, with Ubr1 eluting later and Ufd4 eluting earlier than in the presence of the control dipeptides Ala-Arg and Ala-Leu. As mentioned above, these results are fascinating in more ways than one but remain to be made more detailed and interpretable more unambiguously through additional experimentation.

Discussion

In this chapter, the previously discovered Ubr1-Ufd4 complex was explored further. Our previous studies showed that Ufd4 and Ubr1 interact, both physically and functionally. We employed both in vivo and in vitro methods to begin examining conditions for the formation of this complex. Gel filtration was used to examine the

complex using purified Ufd4 and Ubr1. Interestingly, when Ufd4 was present by itself, its elution patterns suggested that Ufd4 formed a homo-oligomer complex. When Ufd4 and Ubr1 were preincubated together, gel filtration patterns indicated that the two proteins formed what appeared to be a 1:1 complex (Fig. 3.1). Our previous study found that Ufd4 binds to a short segment of Ubr1 (Fig. 2.2). However, the Ubr1-binding site of Ufd4 remains unknown, and the interaction itself (let alone the crystal structures of these full-length E3s) remains to be studied in greater detail. (The crystal structure of the 80-residue UBR box of the 225 kDa Ubr1 was solved in 2010 (6, 7)). It is possible that difficulties in crystallizing Ubr1, experienced over many years by more than one group, might stem, in part, from a higher flexibility of Ubr1 in the absence of Ufd4, implying that the Ubr1-Ufd4 complex might be prove easier to crystallize.

Ufd4 and Ubr1 apparently compete for their binding to Mgt1 (Fig. 3.2), suggesting that in the Mgt1-bound Ubr1-Ufd4 complex, only one of these E3s occupies the degron of Mgt1 at a time. We also found that the presence of the MNNG alkylating agent in the growth media facilitates the formation of the Ufd4-Ubr1 complex (Fig. 3.5). Thus, there might be an intracellular signal, elicited by MNNG, that induces this complex to form, either through a structural change or a posttranslational modification. (Another, less likely but not precluded possibility is that the cell-penetrating MNNG might alkylate either Ubr1 or Ufd4, or both of them, thereby altering their interactions.) Previous work has shown that Ubr1 is allosterically activated to bind the internal degron of Cup9 by the presence of type-1/2 dipeptides. In the previous study, we found that Ufd4, in the presence of type-

1/2 dipeptides, enhances the processivity of ubiquitylation of Cup9 (Fig. 2.4). Interestingly, we found, in this follow-up study, that the presence of type-1/2 dipeptides inhibits the formation of the Ubr1-Ufd4 complex (Fig. 3.6). Thus, the binding of type-1/2 dipeptides may cause a structural change in Ubr1 that prevents Ufd4 from binding. In sum, the results in Figs. 3.2, 5, and 6, while technically clear, are conceptually incomplete in that further studies will be required to decipher the Mgt1-Ubr1/Rad6-Ufd4/Ubc4/5 circuit comprehensively, both in vitro and in vivo.

When cells are exposed to the DNA-alkylating agent MNNG, Mgt1 becomes particularly unstable. We found that also found that Mgt1 is made more unstable (in the absence of MNNG) by the absence of Ufd2, a previously identified E4-type enhancer of poly-ubiquitylation (Fig. 3.3). This destabilizing effect on Mgt1 was also observed in the absence of Ubr2, a sequelog of Ubr1 that does not function as an N-recognin (Fig. 2.2). Possible explanations of this effect (which suggests the involvement of Ufd2 and Ubr2 in processes under discussion) include upregulation of Ubr1 or the proteasome. Again, given the complexity of new phenomena revealed by experiments in this chapter, the operation of the recently discovered Mgt1-Ubr1-Ufd4 circuit remains to be investigated more comprehensively.

REFERENCES

1. Hwang, C. S., Shemorry, A., Auerbach, D., and Varshavsky, A. (2010) *Nature cell biology* **12**, 1177-1185

2. Bartel, B., Wunning, I., and Varshavsky, A. (1990) *The EMBO journal* **9**, 3179-3189

3. Hanzelmann, P., Stingele, J., Hofmann, K., Schindelin, H., and Raasi, S. (2010) *The Journal of biological chemistry* **285**, 20390-20398

4. Hwang, C. S., Shemorry, A., and Varshavsky, A. (2009) *Proceedings of the National Academy of Sciences of the United States of America* **106**, 2142-2147

5. Xia, Z., Turner, G. C., Hwang, C. S., Byrd, C., and Varshavsky, A. (2008) *The Journal of biological chemistry* **283**, 28958-28968

6. Choi, W. S., Jeong, B. C., Joo, Y. J., Lee, M. R., Kim, J., Eck, M. J., and Song, H. K. (2010) *Nature structural & molecular biology* **17**, 1175-1181

7. Matta-Camacho, E., Kozlov, G., Li, F. F., and Gehring, K. (2010) *Nature structural & molecular biology* **17**, 1182-1187

FIGURES

A. fUbr1 and fUfd4 independently fractionated

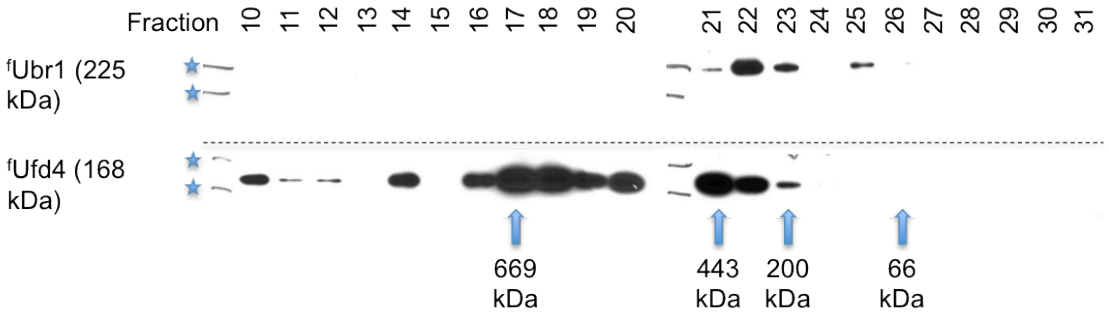

B. fUbr1 and fUfd4 preincubated together

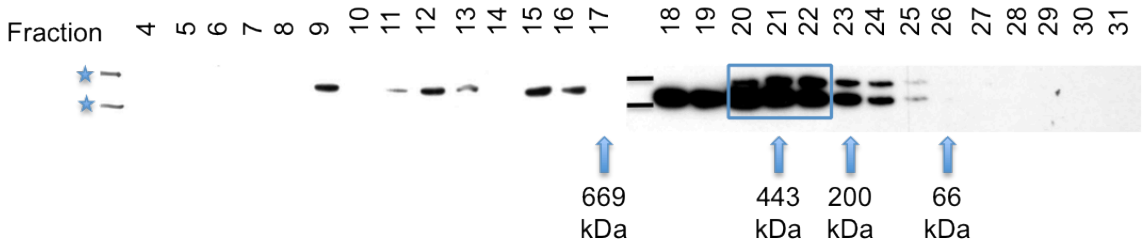

Figure 3.1. Gel-filtration of purified flag-Ubr1 (fUbr1) and flag-Ufd4 (fUfd4).

A. fUbr1 and fUfd4 were run independently on the gel filtration column, using an equal molar amount for each protein. The bulk of fUbr1 eluted in fraction 22, which corresponds to about 300 kDa, according to molecular weight standards run on the same column. fUfd4 eluted earlier, at fractions 17 and 18, which is about 600 kDa. Since Ufd4 is smaller than Ubr1, this shift in elution (i.e. fUfd4 eluting earlier than fUbr1) indicated the formation of a Ufd4 homo-oligomer complex.

B. fUbr1 and fUfd4 were preincubated together and fractionated over the column at the same time. fUfd4 and fUbr1 eluted in the same fractions, 20 through 22, as

indicated by the box. This elution range would suggest a complex size between 400 and 500 kDa, which would be equivalent to a 1:1 complex of Ubr1 to Ufd4. The elution patterns of the molecular weight standards are indicated beneath the panels. The two stars on the right of each panel-denote molecular mass markers of 250 kDa and 150 kDa.

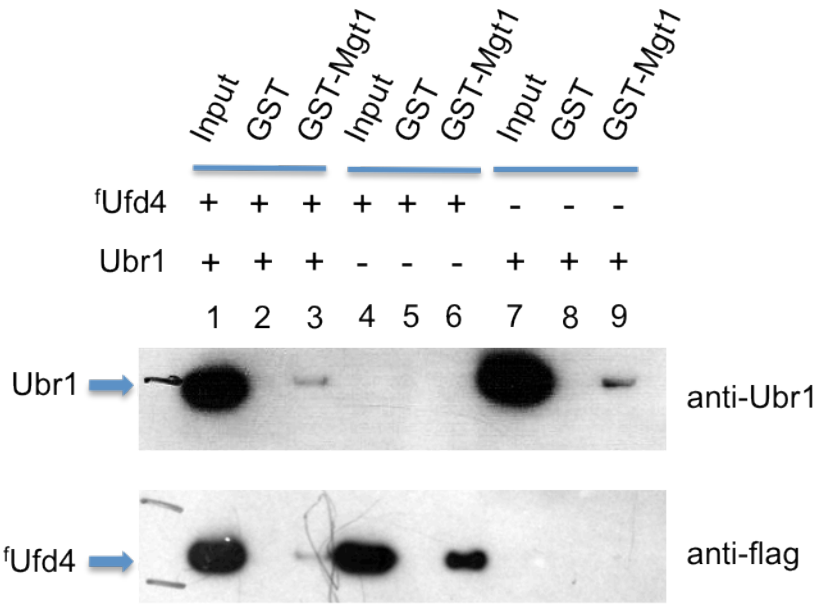

Figure 3.2. Ubr1 and Ufd4 compete for binding to Mgt1. Ubr1 is overexpressed from the integrated P_{GAL1} promoter at the UBR1 locus. ^{f}Ufd4 is overexpressed on a plasmid from the P_{CUP1} promoter. Cells either overexpressing Ubr1 alone, ^{f}Ufd4 alone or both Ubr1 and ^{f}Ufd4 were grown to an A_{600} of ~1.0. 5 µg of purified GST-Mgt1 was incubated with extracts from cells expressing Ubr1 and/or Ufd4. Mgt1 was pulled down with glutathione agarose and the interacting proteins were detected by immunoblotting with either anti-Ubr1 (top panel) or anti-flag (bottom panel) antibodies. As a control, protein extracts were incubated with purified GST (2.5 µg). The co-expression of Ubr1 and Ufd4 decreased each of their binding to Mgt1 (compare lanes 3 and 9 for Ubr1 and lanes 3 and 6 for Ufd4).

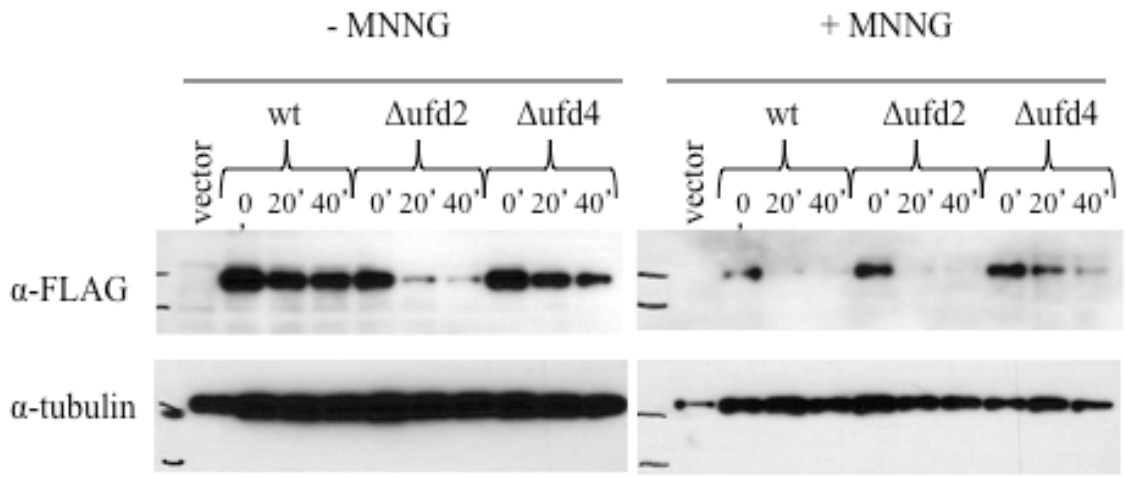

Figure 3.3. Deletion of Ufd2 destabilizes Mgt1. ^{f}Mgt1 was expressed from the P_{CUP1} promoter in wildtype (wt), in cells lacking Ufd2 (Δufd2), or in cells lacking Ufd4 (Δufd4). Cells were grown either in the presence or absence of MNNG. Cycloheximide (CHX) was added to the cells and chased for the indicated times. Protein extracts were fractionated by SDS-PAGE and then immunoblotted with either anti-flag or anti-tubulin antibodies.

A. Ubr1 and ^{f}Ufd4 overexpressed independently

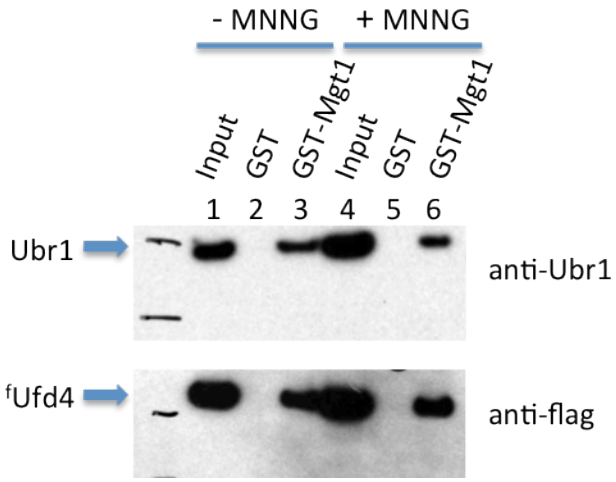

Figure 3.4A. Expression of Ubr1 or Ufd4 independently in the presence or absence of MNNG does not affect binding to Mgt1. Ubr1 was expressed from the P_{GAL1} promoter in the absence of overexpressed Ufd4. ^{f}Ufd4 was overexpressed from the P_{CUP1} promoter in the absence of Ubr1 (Δubr1). Cells were grown either in the presence or absence of MNNG. Proteins extracs were made and incubated with purified GST-Mgt1 or GST alone. Mgt1 was pulled down with glutathione sepharose and the coprecipitated proteins were fractionated by SDS-PAGE, followed by immunoblotting with either anti-Ubr1 (top panel) or anti-flag antibodies (bottom panel). The relative amounts of Ubr1 or Ufd4 pulled down with Mgt1 did not change with the addition of MNNG.

B. Ubr1 and ^{f}Ufd4 overexpressed together

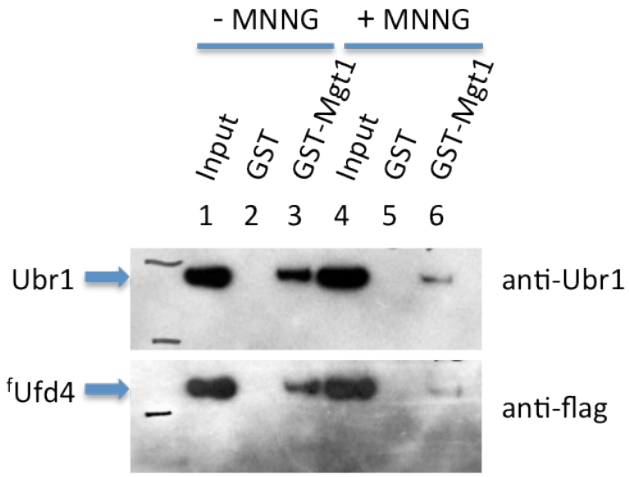

Figure 3.4B. Coexpression of Ubr1 and Ufd4 in the presence of MNNG decreases their binding to Mgt1. Ubr1 was overexpressed from the P_{GAL1} promoter and ^{f}Ufd4 was overexpressed in the same cells from the P_{CUP1} promoter. Cells coexpressing both proteins were grown either in the presence or absence of MNNG. Protein extracts were incubated with either purified GST-Mgt1 or GST alone. Coprecipitated proteins were eluted and fractionated by SDS-PAGE, followed by immunoblotting with either anti-Ubr1 (top panel) or anti-Flag (bottom panel) antibodies. The amount of Ubr1 and Ufd4 pulled down with Mgt1 decreased when the cells were grown in the presence of MNNG (compare lanes 3 and 6).

A. IP with anti-flag

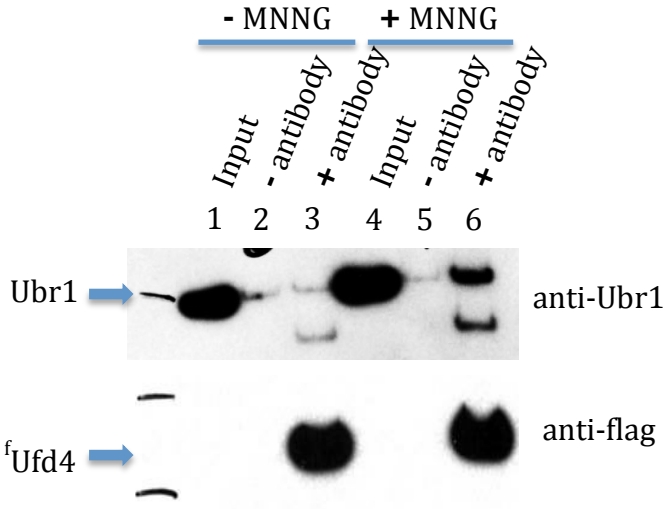

B. IP with anti-Ubr1

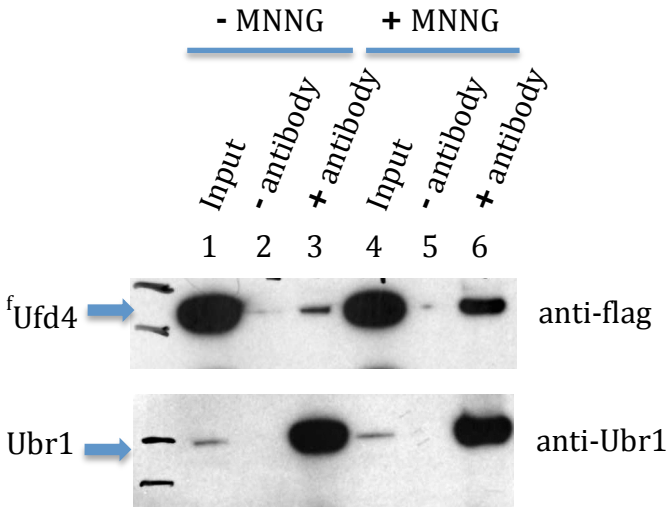

Figure 3.5. The presence of MNNG in the growth media augments the formation of the Ubr1-Ufd4 complex. Ubr1 was overexpressed from the P_{GAL1} promoter and ^{f}Ufd4 was overexpressed from the P_{CUP1} promoter. Cells overexpressing both proteins

either in the presence or absence of MNNG were grown to an A_{600} of ~1.0. Protein extracts were either immunoprecipitated with anti-flag (A) or anti-Ubr1 (B) antibodies. The antibodies were either bound to IgG or Ig magnetic beads. The coimmunoprecipitated proteins were eluted and fractionated by SDS-PAGE, followed by immunoblotting with either anti-Ubr1 or anti-flag antibodies. The amounts of coimmunoprecipitated proteins increased in the presence of MNNG in the growth media (compare lanes 3 and 6, top panels in A and B).

A. fUbr1 and fUbr1 independently fractionated with dipeptides

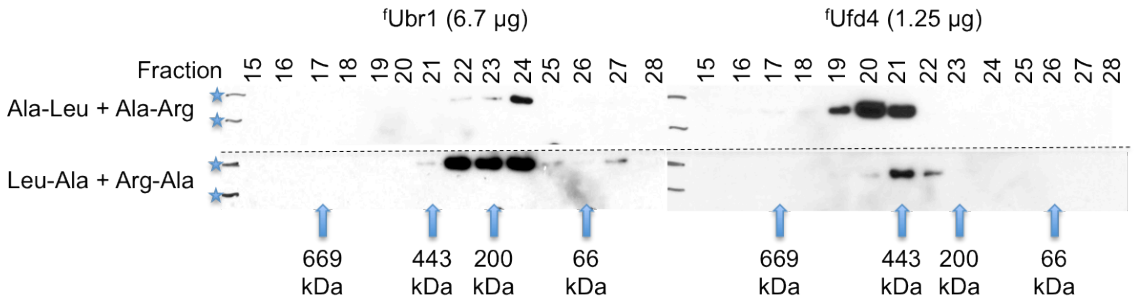

B. fUbr1 and fUbr1 preincubated together with dipeptides

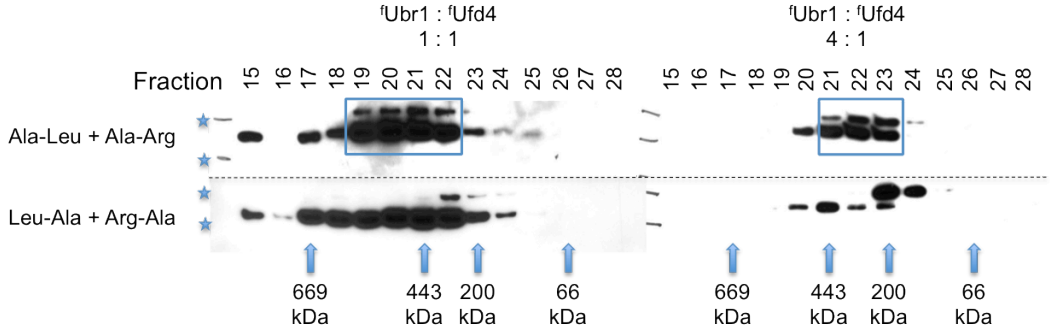

Figure 3.6. The presence of type-1/2 dipeptides decreases the formation of the Ubr1-Ufd4 complex.

A. Purified fUbr1 or purified fUdf4 were fractionated separately by gel filtration in the presence of either 1mM Ala/Leu and Ala/Arg (control dipeptides; top panel) or 1 mM Leu/Ala and Arg/Ala (type-1/2 dipeptides; lower panel). Protein was precipitated by trichloroacetic acid (TCA), fractionated by SDS-PAGE, and immunoblotted with anti-flag.

B. Purified fUbr1 and fUfd4 were preincubated together in a 1:1 molar ratio (left panels) or 4:1 molar ratio, with Ubr1 in excess (right panels). The Ubr1-Ufd4

complex in the top panel is indicated by the box (upper panels). The Ubr1-Ufd4 complex apparently dissociated in the presence of type-1/2 dipeptides, as indicated by the absence of overlapping Ubr1 and Ufd4 bands in the elution profile (lower panels). The elution patterns of the molecular weight standards are indicated beneath the panels. The two stars on the left of each panel denote the molecular weight ladder at 250 kDa and 150 kDa.

TABLES

Yeast strains used in this study

Strain	Relevant Genotype	Source
JD52	*MATa trp1- 63 ura3-52 his3- 200 leu2-3112. lys2-801*	Lab collection
JD54	P_{GAL1}::UBR1 in JD52	Lab Collection
JD55	Δubr1::HIS3 in JD52	Lab Collection
BY4741	MATa his3Δ1 leu2Δ0 met15Δ0 ura3Δ0	Open Biosystems
BY4425	Δufd2::KANMX6 in BY4741	Open Biosystems
BY3216	Δufd4::KANMX6 in BY4741	Open Biosystems

Plasmids used in this study

Plasmid	Description	Source
p314CUP1FlagUfd4	Ufd4 with N-terminal Flag tag in pRS314 with P_{CUP1} promoter	Lab Collection
pCH285	pGEX4T3 $Mgt1_{HIS10}$	ref. (4)
pFlagUbr1SBX	^{f}Ubr1 in YEplac181, with P_{ADH1} promoter	ref. (4)

MATERIALS AND METHODS

Purification of Ufd4 and Ubr1

N-terminally flag-tagged Ubr1 (^{f}Ubr1) was overexpressed in *S. cerevisiae* SC295 and purified by fractionation over anti-flag M2 antibody agarose resin as described in Chapter 2 and Appendix 1. The *S. cerevisiae* JD52 that carried p314CUP1FlagUFD4 and expressed the N-terminally flag-tagged Ufd4 (^{f}Ufd4). ^{f}Ufd4 was purified using anti-flag M2 antibody agarose as described in (4).

Gel-filtration

Samples were run on a Superose 6, 10/300 column connected to an FPLC system. Fractions were collected at 0.25 ml/min. The gel-filtration buffer was 0.1 M NaCl, 25 mM Na-HEPES pH 7.5. Samples were incubated at room temperature for 30 min, centrifuged at 10,000g and then loaded onto the column. If dipeptides were used, they were incubated with the sample at a concentration of 1 mM at this time. In these experiments, the gel-filtration buffer also contained the appropriate dipeptides. Ovalbumin at a concentration of 0.1 mg/ml was used in the sample buffer to stabilize the proteins and prevent aggregation. 0.5 mL fractions were collected and the proteins were precipitated with trichloroacetic acid (TCA). The proteins were fractionated by SDS-PAGE, followed by immunoblotting with anti-flag antibody (Stratagene). Molecular weight markers (Sigma) were run on the column as described by the manufacturer's instructions.

GST Pulldowns

GST-Mgt1-His_{10} was purified from BL21-Codon Plus (DE3)-RIL *E. coli* strain (Stratagene), as described previously in Appendix 1 using Ni-NTA resin (Qiagen). The *S. cerevisiae* strain JD54 (JD52 background strain overexpressing Ubr1 from the P_{GAL1} promoter) was transformed with either pRS313Cup1FlagUfd4 or the empty pRS313Cup1 vector. The *S. cerevisiae* yeast strain JD55 (JD52 background with a deletion of the UBR1 coding region) was also transformed with the pRS313Cup1FlagUfd4 vector. A 50 mL culture was grown to an A_{600} of ~1 in SC (-His) medium containing 0.2 M $CuSO_4$ (to induce the P_{CUP1} promoter) and either in 2% glucose or galactose (to induce the P_{GAL1} promoter). Cells were then grown either in the presence or absence of 68 μM MNNG for 1 h. The cells were spun down, washed once with PBS and stored at -80°C. Cells were thawed and lysed by bead beating in GST binding buffer (10% glycerol, 0.05% Nonidet P-40, 50 mM NaCl, 50 mM Na-HEPES, pH 7.8). Purified GST-Mgt1 or GST alone was bound to GST-sepharose and GST pulldowns were performed as described previously, using equal amounts of protein extracts, followed by SDS-PAGE and immunoblotting with either anti-Ubr1 or anti-flag antibodies.

Co-immunoprecipitation Assay

Cells overexpressing ^{f}Ufd4 and/or untagged Ubr1 were grown as described in the section describing the GST-pulldown assay. The coimmunoprecipitation experiments were performed as described previously, except that the previously described, affinity purified anti-Ubr1 antibody was used to immunoprecipitate Ubr1

and anti-flag antibody was used immunoprecipitate Ufd4. These antibodies were also used for immunoblotting.

Cycloheximide Chase Experiment

S. cerevisiae were grown to A_{600} of 0.8 to 1.0 in selective (plasmid-maintaining) liquid media at 30°C, followed by treatment with cycloheximide (CHX), at the final concentration of 0.1 mg/ml. At indicated times, cell samples (corresponding to 1 ml of cell suspension at A_{600} of 1) were harvested by centrifugation for 1 min at 11,200*g*, and resuspended in 1 ml of 0.2 M NaOH. The samples were incubated for 20 min on ice, or for 5 min at room temperature, followed by centrifugation for 1 min at 11,200*g*. Pelleted cells were resuspended in 50 µl of 1X LDS buffer (Invitrogen, Carlsbad, CA) containing 1X reducing agent and 1X protease inhibitor cocktail "for use with fungal and yeast extracts" (Sigma), and heated for 10 min at 70°C. After centrifugation at 5 min at 11,200g, 10 µl of supernatant was fractionated by SDS-4-12% NuPAGE, followed by immunoblotting with the appropriate antibody.

CHAPTER 4:

N-TERMINAL ACETYLATION OF CELLULAR PROTEINS CREATES SPECIFIC DEGRADATION SIGNALS

From Hwang, C. S., Shemorry, A., and Varshavsky, A. (2010) *Science* 327, 973-977

Abstract

The retained N-terminal methionine (Met) residue of a nascent protein is often N-terminally acetylated (Nt-acetylated). Removal of N-terminal Met by Met-aminopeptidases frequently leads to Nt-acetylation of the resulting N-terminal alanine (Ala), valine (Val), serine (Ser), threonine (Thr), and cysteine (Cys) residues. Although a majority of eukaryotic proteins (for example, more than 80% of human proteins) are cotranslationally Nt-acetylated, the function of this extensively studied modification is largely unknown. Using the yeast *Saccharomyces cerevisiae*, we found that the Nt-acetylated Met residue could act as a degradation signal (degron), targeted by the Doa10 ubiquitin ligase. Moreover, Doa10 also recognized the Nt-acetylated Ala, Val, Ser, Thr, and Cys residues. Several examined proteins of diverse functions contained these N-terminal degrons, termed ^{Ac}N-degrons, which are a prevalent class of degradation signals in cellular proteins.

Introduction and Results

Many eukaryotic proteins are acetylated at the α-amino group of their N-terminal residues (fig. S1A) (1). Previous studies of N$^{\alpha}$-terminal acetylation (Nt-acetylation) have characterized Nt-acetylated proteins and Nα-terminal acetyltransferases (Nt-acetylases) that catalyze this cotranslational modification (2–7). Owing to the design of the genetic code, nascent proteins contain N-terminal Met. A retained N-terminal Met that is followed by “acetylation-permissive” residues is usually Nt-acetylated (fig. S1A) (5–7). Met-aminopeptidases cleave off the N-terminal Met if the residue at position 2 has a small enough side chain, resulting in N-terminal Ala, Val, Ser, Thr,

Cys, Gly, or Pro (fig. S1B) (8). With the near-exception of Gly and Pro, these N-terminal residues are often Nt-acetylated, similarly to N-terminal Met (5–7). In cell extracts, some Nt-acetylated proteins can be degraded by the ubiquitin (Ub) system (9). However, no cognate Ub ligases have been identified, and it has been assumed that the relevant degradation signals were internal (not N-terminal) (9). Currently, the prevalent view of Nt-acetylation is that this modification protects proteins from degradation. To the contrary, we report here that Nt-acetylation creates specific degradation signals (degrons) that are targeted by a branch of the Ub-dependent N-end rule pathway.

Destabilizing N-terminal sequences. The N-end rule relates the *in vivo* half-life of a protein to the identity of its N-terminal residue (10–20). N-terminal degradation signals of the N-end–rule pathway are called N-degrons. Their main determinant is a destabilizing N-terminal residue of a protein (fig. S1C). Recognition components of the N-end–rule pathway are called N-recognins. An N-recognin is an E3 Ub ligase that can target for polyubiquitylation at least a subset of N-degrons (13, 15, 18, 19). The N-end rule of the yeast *S. cerevisiae* comprises 12 destabilizing, unacetylated N-terminal residues (out of the fundamental set of 20 amino acids) (12–15, 18, 19). Among these residues, eight are primary destabilizing residues; that is, recognized directly by the Ubr1 N-recognin, whereas the other four N-terminal residues, called secondary or tertiary destabilizing residues, must be modified through deamidation and/or arginylation before the corresponding proteins can be targeted by Ubr1 (fig. S1C).

In mammalian cells, the N-terminal Cys of N-end–rule substrates can be oxidized, by nitric oxide (NO) and oxygen, and thereafter arginylated by an arginyl-transferase. The resulting N-terminal Arg is recognized by Ubr1-type N-recognins (15, 16). In contrast, N-terminal Cys appeared to be a stabilizing residue in *S. cerevisiae*, which lacks NO synthases (11). That study also classified N-terminal Met, Ala, Val, Ser, and Thr as stabilizing residues in *S. cerevisiae* (11). One caveat in these assignments is the possible influence of sequences downstream of the reporter's N terminus. To determine whether N-terminal Cys can be destabilizing in yeast, we performed a screen in ura3 S. cerevisiae with Cys-Z-e^K-Ura3 reporters, produced by deubiquitylation (10, 21) of Ub-Cys-Z-e^K-Ura3. Z denotes a varied residue at position 2, and e^K [extension (e) containing lysine (K)] denotes a ~40-residue sequence upstream of Ura3. The e^K extension (fig. S1D) has the technically valuable property of lacking internal degrons while containing "ubiquitylatable" Lys residues (10–12). This screen identified Cys-Z-e^K-Ura3 fusions (Z = Leu, Val, or Pro) with low Ura3 activity. We examined these fusions using a cycloheximide (CHX)–chase assay, in which a protein is analyzed by immunoblotting as a function of time after the inhibition of translation by CHX (18, 19). The above three reporters were short-lived in vivo [half-life ($t_{1/2}$) < 1 hour], in contrast to GL-e^K-Ura3 (N-terminal Gly) and CK-e^K-Ura3 (Lys at position 2), which were long-lived (Fig. 1, A, B, and D; fig. S2B; and fig. S3, A and D). Other nonbasic residues at position 2 also yielded short-lived CZ- e^K -Ura3 (Z = Trp, Glu, Gly, or Ile) (Fig. 1B and fig. S3A).

Several other XL-e^K-Ura3 reporters (X = Met, Ser, Val, Ala, or Thr) were also short-lived *in vivo*, like CL-e^K-Ura3 and in contrast to long-lived MK-e^K-Ura3 (Lys at

position 2), MR-e^K-Ura3 (Arg at position 2), GL-e^K-Ura3 (N-terminal Gly), and PL-e^K-Ura3 (N-terminal Pro) (Fig. 1, A to D; fig. S2, A and B; and fig. S3, B, C, and E). We also performed ^{35}S-pulse chases (18, 19) with CL-e^K-Ura3 and ML-e^K-Ura3 versus CK-e^K-Ura3 and MK-e^K-Ura3 (fig. S4, A to C). The techniques of CHX chases and ^{35}S-pulse chases are complementary, because the former method monitors the degradation of all molecules of a specific protein, whereas the latter assay measures the degradation of newly formed (pulse-labeled) molecules. ^{35}S-pulse chases confirmed the instability of XL-e^K-Ura3 (X = Cys or Met) and stability of XK-e^K-Ura3 (X = Cys or Met) (Fig. 1, A and C; fig. S2, A and B; and fig. S4, A to C). The degradation of ML-e^K-Ura3 was proteasome-dependent, because the MG132 proteasome inhibitor significantly increased the level of the normally short-lived ML-e^K-Ura3 but not of the long-lived MK-e^K-Ura3, whose levels were high both in the presence and absence of MG132 (Fig. 1G).

The Doa10 ubiquitin ligase recognizes acetylated N-terminal residues. To search for a Ub ligase or ligases that mediate the degradation of XL- e^K -Ura3 (X = Met, Ala, Val, Ser, Thr, or Cys), we expressed CL- e^K -Ura3 in *S. cerevisiae* mutants that lacked specific E3 or E2 enzymes (fig. S4D). CL- e^K -Ura3 became long-lived in the absence of Doa10 (Fig. 1E and fig. S4, D and E). Moreover, other short-lived XL-e^K -Ura3 proteins (Z = Met, Ser, or Val) were also stable in *doa10Δ* cells (Fig. 1F and fig. S4, F and G). Doa10 is a transmembrane E3 Ub ligase that functions with the Ubc6/Ubc7 E2s and resides in the endoplasmic reticulum (ER) and inner nuclear membrane (INM) (22–24). To address the above results, we focused on MATα2, a physiological substrate of Doa10.

The 24-kD MATα2 contains more than one degradation signal and has an in vivo half-life of 5 to 10 min (13, 25, 26). MATα2 represses transcription of a-specific genes in α-cells, whereas in a/α diploids the MATα2-MATa1 complex represses haploid-specific genes (27, 28). The 67-residue N-terminal region of MATα2, termed Deg1, has been shown to harbor a Doa10-dependent degron (22–24). MATα2 is absent from databases of Nt-acetylated proteins (5, 6), possibly because of its short in vivo half-life. We expressed full-length MATα2 in *doa10Δ ubc4Δ* yeast and analyzed purified MATα2 using liquid chromatography–tandem mass spectrometry (LC-MS/MS). The results (fig. S5A) indicated virtually complete Nt-acetylation of MATα2 (no MATα2 that lacked Nt-acetylation could be detected), in agreement with Nt-acetylation of other proteins containing the N-terminal Met-Asn (5–7). Similar LC-MS/MS of the Doa10-targeted, purified ML- e^K -Ura3 (fig. S5, B and C) indicated the Nt-acetylation of this reporter, in agreement with Nt-acetylation of other proteins containing the N-terminal Met-Leu (5–7). We also observed Nt-acetylation of a Deg1-bearing reporter that was purified from *E. coli* and incubated with *S. cerevisiae* extracts (fig. S6A).

In addition, we produced an antibody, termed anti-^{AcNt}MATα2, that recognized the Nt-acetylated N-terminal sequence of MATα2 (Fig. 2C) and was specific for the Nt-acetylated, hemagglutinin (HA)–tagged, MATα2-derived, MN-$\alpha^{23\text{-}67}$- e^K -Ura3 reporter, denoted MNα2 (Fig. 2, A and B). Anti-^{AcNt}MATα2 and anti-Ha (the latter antibody recognized both Nt-acetylated and unacetylated MNα2) were used to immunoblot extracts of cells that expressed MNα2. Wild-type cells contained barely detectable steady-state levels of either total or Nt-acetylated MNα2 (Fig. 2A),

owing to its rapid degradation. In contrast, nat3Δ cells, which lacked the cognate NatB Nt-acetylase, contained high levels of unacetylated MNα2 (detected by anti-Ha) and almost no Nt-acetylated MNα2 (Fig. 2A). Similar patterns were observed in wild-type cells that expressed MKα2 (Lys at position 2) or GNα2 (N-terminal Gly) (Fig. 2A). As shown by proteome-scale analyses, S. cerevisiae proteins containing Lys at position 2 are virtually never Nt-acetylated, and few proteins that bear N-terminal Gly are Nt-acetylated (5–7). Most importantly, high levels of Nt-acetylated MNα2 were present in *doa10Δ* cells (Fig. 2A), owing to metabolic stabilization of Nt-acetylated MNα2 in the absence of Doa10. These data (Fig. 2A) were in agreement with the LC-MS/MS results showing that MATα2 was Nt-acetylated (fig. S5A).

To determine whether the Doa10 Ub ligase recognizes the Nt-acetylated Met (^{AcNt}Met), we used the X-peptide assay (15) with synthetic peptides XNKIPIKDLLNC (X = Met, ^{Ac}Met, or Gly) (29). Except for C-terminal Cys and the varied N-terminal residues, these peptides were identical to the N-terminal region of MATα2. Immobilized peptides were incubated with extract from yeast that expressed myc13-tagged Doa10, followed by elution of the bound proteins and immunoblotting with antibody to myc. $Doa10_{myc13}$ bound to the MATα2 peptide with N-terminal AcNtMet but not to the otherwise identical peptides with unmodified N-terminal Met or with N-terminal Gly (Fig. 2D). Additional controls, which did not bind to $Doa10_{myc13}$, were peptides XIFSTDTGPGGC (X = Gly, Met, Arg, or Phe) derived from the N terminus of nsP4, a Sindbis viral protein (13) (Fig. 2D). Thus, Doa10 recognizes the ^{AcNt}Met residue and does not have a significant affinity for downstream sequences of MATα2 or nsP4.

Doa10 specificity was also analyzed with the synthetic peptide arrays on membrane support (SPOT) technique, in which synthetic XZ- $e^{K(3-11)}$ peptides and their Nt-acetylated ^{Ac}XZ- $e^{K(3-11)}$ counterparts were C-terminally linked to a membrane as "dots" in equal molar amounts. SPOT peptides were identical to the N-terminal region of e^{K} (fig. S1D), with varied residues at positions 1 and 2. A SPOT assay with C-terminally flag-tagged $Doa10_{f}$ indicated the recognition of ^{AcNt}Met by Doa10, in agreement with the results of the X-peptide assay (Fig. 2, D and E). SPOT also indicated a highly preferential binding of Doa10f to other Nt-acetylated (versus unacetylated) ^{Ac}XZ- $e^{K(3-11)}$ peptides (X = Gly, Ala, Val, Pro, Ser, Thr, or Cys), including Nt-acetylated Gly and Pro (Fig. 2E). Thus, Gly and Pro are (largely) stabilizing in the N-end rule (Fig. 1D and fig. S3E) because N-terminal Gly and Pro are Nt-acetylated in relatively few proteins (5–7). Doa10 did not bind to N-terminal ^{AcNt}Met if it was followed by Lys at position 2 (Fig. 2E). Thus, the metabolic stability of XK- e^{K} -Ura3 (X = Met or Cys) containing Lys at position 2 (Fig. 1, A and C) stems not only from the absence of Nt-acetylation (5–7) but also from the rejection, by Doa10, of Lys at position 2 (Fig. 2E).

The Doa10-dependent ^{Ac}N-degron of MATα2. Taking advantage of the specificity of anti-^{AcNt}MATα2 for Nt-acetylated MNα2, we performed CHX chases as well, in addition to steady-state assays (Fig. 2, A and B). MNα2 was short-lived in wild-type cells. Even "time-zero" samples, at the time of addition of CHX, contained barely detectable levels of either Nt-acetylated or total MNα2 (Fig. 2B). In contrast, MNα2 was a long-lived protein in *doa10Δ* and *nat3Δ* cells, but for different reasons: In *doa10Δ* cells, which lacked the cognate Ub ligase, MNα2 was long-lived despite its

Nt-acetylation; whereas in *nat3Δ* cells, which lacked the cognate Nt-acetylase, the largely unacetylated MNα2 was long-lived because the targeting by Doa10 required Nt-acetylation (Fig. 2B).

MATα2 contains yet another degradation signal, targeted by an unknown E3 in conjunction with the Ubc4 and (to a minor extent) Ubc5 E2s (25, 26). This degron is nearly inactive in *ubc4Δ* cells (23, 26). In contrast, the Doa10 Ub ligase functions with the Ubc6/Ubc7 E2s and remains active in *ubc4Δ* cells (22). In ^{35}S-pulse chases with C-terminally flag-tagged full-length MATα2f, the rapid degradation of wild-type MNMATα2f in ubc4Δ cells ($t_{1/2} \approx 9$ min) was substantially decreased in *doa10Δ* ubc4Δ cells (t1/2 ≈ 35 min) (Fig. 2F and fig. S6, B and C). A Lys residue at position 2 in a polypeptide chain is known to preclude Nt-acetylation in *S. cerevisiae*, and few proteins that bear N-terminal Gly are Nt-acetylated (5, 6). The absence of Nt-acetylation in ^{MK}MATα2$_f$ (Lys at position 2) or ^{GN}MATα2$_f$ (Gly at position 1) decreased the rate of MATα2 degradation in wild-type cells (Fig. 2F and fig. S6, B and C). The extent of this decrease, in comparison to degradation of Nt-acetylated ^{MN}MATα2$_f$ in wild-type cells, was indistinguishable from the decrease of ^{MN}MATα2$_f$ degradation in *doa10Δ* cells, which lacked the Doa10 Ub ligase (Fig. 2F and fig. S6, B to E). In addition to indicating that the sole degron targeted by Doa10 in MATα2 is its ^{Ac}N-degron, these results were also in agreement with technically independent evidence that used the anti-^{AcNt}MATα2 to prove that the Nt-acetylation of MNα2 was required for its targeting by Doa10 (Fig. 2, A to C).

^{Ac}N-degrons in cellular proteins. As expected, given the presence of the ^{Ac}N-degron in MATα2, both full-length MATα2$_f$ and MNα2 were strongly stabilized in

nat3Δ cells, which lacked the cognate NatB Nt-acetylase (Fig. 2, A and B, and fig. S6, D and E). Besides MATα2, our survey of *S. cerevisiae* proteins has encompassed, thus far, Tbf1, a regulator of telomeres; Slk19, a regulator of chromosome segregation; Ymr090w, a cytosolic protein of unknown function; His3, an enzyme of histidine biosynthesis; Pop2, a subunit of mRNA-deadenylating complexes; Hsp104, a chaperone; Tho1, an RNA-binding regulator; Ubp6, a deubiquitylating enzyme; and Aro8, an aromatic aminotransferase (Fig. 3; fig. S2, C and D; and fig. S7) (30).

Wild-type Tbf1, Slk19, Pop2, Hsp104, Tho1, Ubp6, and Aro8 are known to be Nt-acetylated (5, 6). In contrast, the testing of His3 and Ymr090w stemmed from our two-dimensional electrophoretic analyses, including ^{35}S-pulse chases. The resulting patterns contained a number of protein spots with significantly higher levels of ^{35}S in samples from *doa10Δ* versus wild-type cells (fig. S8). We examined three of these spots using matrix-assisted laser desorption/ionization–MS fingerprinting techniques and identified His3, Ymr090w, and Aro8 as putative substrates of Doa10 (fig. S8). The testing for AcN-degrons in Tbf1, Slk19, Ymr090w, His3, Pop2, Hsp104, Tho1, Ubp6, and Aro8 (this analysis included second-residue mutants of some of these proteins) involved CHX chases in the presence or absence of a cognate Nt-acetylase or the Doa10 Ub ligase. As shown in Fig. 3; fig. S2, C and D; and fig. S7, we identified ^{Ac}N-degrons in all of these proteins (in addition to MATα2), except Pop2 and Tho1 [see also (30)].

Discussion

Our results, summarized in Fig. 4, revealed the function of Nt-acetylation, producing the largest increase in the scope of the N-end–rule pathway since its

discovery more than two decades ago (10–13). At present, only ~10 proteins in all eukaryotes have been identified that require, or are inferred to require, Nt-acetylation for their in vivo roles, which are unrelated to protein degradation [(30) and references therein]. In contrast, the creation of degradation signals by Nt-acetylation (Fig. 4) is relevant, in principle, to all Nt-acetylated proteins. N-terminal Met, Ala, Val, Ser, Thr, and Cys are shown here to function as secondary destabilizing residues in the N-end rule pathway, in that they must be Nt-acetylated before their recognition by the S. cerevisiae Doa10 Ub ligase as N-degrons, termed ^{Ac}N-degrons, that require Nt-acetylation (Fig. 4). Out of 20 amino acids in the genetic code, 18 are now known to function as destabilizing N-terminal residues in the N-end rule pathway (Fig. 4 and fig. S1C). More than 50% of proteins in *S. cerevisiae* and more than 80% of proteins in human cells are Nt-acetylated (5–7). Thus, remarkably, the majority of eukaryotic proteins harbor a specific degradation signal from the moment of their birth. Putative metazoan counterparts of the yeast Doa10 Ub ligase (22–24) include human TEB4 (31), indicating the likely relevance of our results to all eukaryotes.

The Nt-acetylation is largely cotranslational, apparently irreversible, and involves a majority of cellular proteins. What functions are subserved by such a massive production of degradation signals (^{Ac}N-degrons) in nascent proteins if many of these proteins are destined for long half-lives? We suggest that a major role of these degradation signals involves quality-control mechanisms and the regulation of protein stoichiometries in a cell. A key feature of such mechanisms would be conditionality of ^{Ac}N-degrons. If a nascent Nt-acetylated protein can fold its N-

terminal domain rapidly enough, or if this protein either interacts with a "protective" chaperone such as Hsp90 or becomes assembled into a cognate multisubunit complex, the cotranslationally created ^{Ac}N-degron of this protein may become inaccessible to the Doa10 Ub ligase. Consequently, the degradation of this protein would be decreased or precluded. In contrast, delayed or defective folding of a protein's N-terminal domain (because of oxidative, heat, or other stresses; or a conformation-perturbing mutation; or nonstoichiometric levels of cognate protein ligands) would keep an ^{Ac}N-degron exposed (active) and thereby increase the probability of the protein's destruction.

The discovery that Nt-acetylation is a part of the N-end rule pathway (Fig. 4) has also revealed the physiological functions of Nt-acetylases and Met-aminopeptidases. Nt-acetylases produce AcN-degrons, whereas the upstream Met-aminopeptidases make possible these degradation signals, all of them except the one mediated by Nt-acetylated Met (Fig. 4). Nt-acetylases and Met-aminopeptidases are universally present, extensively characterized, and essential enzymes whose physiological roles were largely unknown. These enzymes are now functionally understood components of the N-end rule pathway (Fig. 4 and fig. S1C).

Although the bulk of Nt-acetylation is cotranslational (4), posttranslational Nt-acetylation is likely to be extensive as well. A number of proteases can specifically cleave a variety of intracellular proteins, resulting in C-terminal fragments that often bear destabilizing N-terminal residues of the Ubr1-mediated branch of the N-end–rule pathway (fig. S1C). Such fragments are often short-lived in vivo, thereby regulating specific circuits [reviewed in (13)]. Given the major

expansion of the N-end rule in the present work (Fig. 4), most in vivo produced C-terminal fragments of intracellular proteins should now be viewed, a priori, as putative targets of the Doa10 or Ubr1 branches of the N-end rule pathway.

The topologically unique location of N-terminal residues, their massive involvement in proteolysis, and their extensive modifications make N-degrons a particularly striking example of the scope and subtlety of regulated protein degradation (Fig. 4 and fig. S1C).

Materials and Methods

Yeast strains, media and genetic techniques

S. cerevisiae strains used in this study are described in Table S1. Standard techniques (1, *2)* were employed for strain construction and transformation. The strains CHY248, CHY223, or CHY229 were produced using PCR-derived KanMX6 modules (3). The strains CH287 and CHY288 were constructed by disrupting *UBC4* in BY4742 and BY17299 (Table S1) through a PCR-mediated gene targeting that employed the pRS315 plasmid (4), similarly to a previously described procedure (5). E2, E3 and N-acetyltransferase (Nt-acetylase) mutant strains used in this study were from the Varshavsky laboratory's strain collection or from Open Biosystems (Huntsville, AL). *S. cerevisiae* media included YPD (1% yeast extract, 2% peptone, 2% glucose; only most relevant components are cited); SD medium (0.17% yeast nitrogen base, 0.5% ammonium sulfate, 2% glucose); and synthetic complete (SC) medium (0.17% yeast nitrogen base, 0.5% ammonium sulfate, 2% glucose), plus a drop-out mixture of compounds required by a given auxotrophic strain.

Test proteins and construction of plasmids

The plasmids used in this study are described in Table S2. The low copy (CEN) plasmid pCH178, which expressed Ub-CK- e^K -Ura3 (Ub-Cys-Lys- e^K -ha-Ura3) from the P_{CUP1} promoter was derived from the pRS314 vector (4). To construct pCH178, a ubiquitin (Ub)-gene fragment from the pMET416FUPRCUP9$_{NSF}$ plasmid (6) was PCR-amplified (using primers OCH201 and OCH214 (Table S3)), digested with *EcoRI/BamHI* and thereafter subcloned into *EcoRI/BamHI-cut* pBAM (Table S2). pCH669, pCH508 or pCH509 were constructed by subcloning relevant DNA fragments from *SacI/XhoI-cut* pCH504, pCH505 or pCH506 that expressed ML- e^K -Ura3, SL- e^K -Ura3 or TL- e^K -Ura3, respectively, into *SacI/XhoI-cut* pRS313 vector (4). To produce other plasmids that expressed XZ- e^K-Ura3 proteins, the corresponding *EcoRI/BamHI-digested* PCR-produced fragments encoding Ub-XZ- e^K-Ura3 (X and **Z** denote varied residues) were subcloned into *EcoRI/BamHI-cut* pBAM vector or pCH508 (Table S2). *S. cerevisiae* Tbf1 is a 63 kDa (N-terminal Met-Asp) transcriptional activator and regulator of telomere length (refs. (7-9) and refs. therein). The 95 kDa Slk19 (N-terminal Met-Asn) is a kinetochore-associated regulator of chromosome segregation (10, *11).* The 25 kDa Ymr090w (N-terminal Ser-Pro) is a cytosolic protein of unknown function, with sequence similarities to DTDP-glucose 4,6-dehydratases. The 24 kDa His3 (N-terminal Thr-Glu) is imidazole glycerol-phosphate dehydratase (IGPD), an enzyme of histidine biosynthesis (12, *13).* The 50 kDa Pop2 (N-terminal Met-Gln) is a subunit of a complex that deadenylates mRNAs (14). The 102-kDa Hsp104 (N-terminal Met-Asn) is a chaperone and heat stress protein (refs. (15, *16)* and refs. therein). The 56 kDa Aro8 (N-terminal Thr-Leu) is an aromatic aminotransferase that participates in

particular, in the biosynthesis of phenylalanine (17). The 57 kDa Ubp6 (N-terminal Ser-Gly) is a deubiquitylating enzyme associated with the 26S proteasome (18-20). The 24 kDa Tho1 (N-terminal Ala-Asp) is a nuclear RNA-binding protein (21). The open reading frame (ORF) encoding $TBF1_{ha}$ with a C-terminal ha tag was subcloned into the low-copy (CEN) pRS316 vector (4), and was expressed from the vector's P_{CUP1} promoter. The $TBF1_{ha}$ ORF was produced by PCR, using *S. cerevisiae* genomic DNA and specific primers for DNA fragments encoding wild-type $^{MD}Tbf1_{ha}$ (with N-terminal Met-Asp), the mutant $^{MK}Tbf1_{ha}$, (with Lys at position 2), and the mutant $^{MG}Tbf1_{ha}$ (with N-terminal Gly, after removal of N-terminal Met by MetAPs). Similar procedures were used to construct and amplify DNA fragments encoding wild-type $^{MN}Slk19_{ha}$ (with N-terminal Met-Asn); mutant $^{MK}Slk19_{ha}$ (with Lys at position 2); mutant $^{MG}Slk19_{ha}$ (with N-terminal Gly); wild-type $^{MS}Ymr090w_{ha}$ (with N-terminal Met-Ser); mutant $^{MK}Ymr090w_{ha}$ (with Lys at position 2); mutant $^{MG}Ymr090w_{ha}$ (with N-terminal Gly); wild-type $^{MT}His3_{ha}$ (with N-terminal Met-Thr); wild-type $^{MQ}Pop2_{ha}$ (with N-terminal Met-Gln); wild-type $^{MN}Hsp104_{ha}$ (with N-terminal Met-Asn); mutant $^{MK}Hsp104_{ha}$ (with Lys at position 2); and also wild-type $Aro8_{ha}$, $Ubp6_{ha}$, and $Tho1_{ha}$. These DNA fragments were digested with *BamHI/NotI* or *EcoRI/XhoI* and subcloned into *BamHI/NotI-cut* pRS316-CUP1 or *EcoRI/XhoI-cut* pCH508. To construct a library of plasmids encoding Ub-CZ- e^{K}-Ura3 (Z=any residue except Trp, Gln, Glu, Lys), *EcoRI/BamHI-digested,* PCR-amplified Ub gene fragment from pBAM (Table S2) were subcloned into *EcoRI/BamHI-cut* pCH178 (Table S2), followed by transformation of *E. coli* DH5α. PCR primers used for the above amplification were OCH201 (GGG GAA TTC ATG CAG ATT TTC GTC AAG ACT TTG GTC, *EcoRI* site

underlined) and OCH202 (AAA GGA TCC RNN ACA ACC ACC TCT TAG CCT TAG CAC AAG, R=A, G; N=A, C, G, T; *BamHI* site underlined). *EcoRI/BamHI-digestion* of 20 randomly retrieved plasmids from transformants suggested correct insertions in more than 90% of plasmids in this library. After pooling ~1,000 *E. coli* transformants, a plasmid DNA preparation was made and thereafter used as the CZ-e^K-Ura3 library. pCH535, which expressed ^{MN}MATα$^{23-67}$- e^K-Ura3, was constructed by subcloning a *SacII/BamHI-digested* DNA fragment (produced by PCR from *S. cerevisiae* genomic DNA and the primer pairs OCH817 and OCH833 (Table S3)) into *SacII/BamHI-cut* pCH178. pCH641 (Table S2) was produced by inserting *SacI/XhoI-cut* pCH535 into *SacI/XhoI-cut* p416MET25. To construct pCH645, *SacII/KpnI-digested* pCH535 (Table S2) was subcloned into *SacII/KpnI-cut* pH10UE, yielding pCH622. Thereafter *BamHI/HindIII-cut* pEJJ-M was subcloned into pCH622 (Table S2), yielding pCH645. To construct pCH595, a DNA fragment containing a 5'-proximal part of the *S. cerevisiae DOA10* ORF, a *SmaI* site and a 3-proximal part of the *DOA10$_f$* fragment was PCR-amplified using the primers OCH901 and OCH902 (Table S3). The resulting DNA fragment was subcloned into *BamHI/XhoI-cut* p425GAL1 vector (22), yielding pCH581. That plasmid was digested with *SmaI* and transformed into the SC295 *S. cerevisiae* strain to clone C-terminally flag-tagged *DOA10* using gap repair. The resulting pCH595 plasmid (Table S2) expressed Doa10$_f$ from the P_{GAL1} promoter of the high copy pRS425GAL1 plasmid. pCH704, pCH705, or pCH706, which expressed XZ-MATα$^{23-210_f}$ from the P_{MET25} promoter on a low copy plasmid, were constructed by inserting the *BamHI/XhoI-digested,* C-terminally flag-tagged *MATα2$_f$* ORF (produced by PCR from *S. cerevisiae* genomic DNA and the

primer pairs OCH989/OCH819, OCH990/OCH819 or OCH991/OCH819 (Table S3)) into the p416MET25 vector (Table S2). pCH719, expressing MATα2_f as Ub-reference fusions (see fig. S5D, E), were constructed by subcloning *SacII/XhoI-cut MATα2f* ORF (PCR-produced using the primer pairs OCH817/OCH819 (Table S3)) into *SacII/XhoI-cut* pMET416$_F$UPRCUP9$_{NSF}$ (Table S2). Construction details for other plasmids (Table S2) are available upon request. All final constructs were verified by DNA sequencing.

Screening a library of CZ-e^K-Ura3 fusions

CZ-e^K-Ura3 library plasmids were transformed into *S. cerevisiae* JD52 (Table S1) and thereafter plated on SC(-Trp; -Ura; +FOA (1 mg/ml); +CuSO4 (10 μM)). Among ~6,200 transformants, ~165 colonies were formed on these FOA-based plates, with selection for low levels of Ura3. After streaking and re-growing FOA-resistant transformants on the same medium for 2 days at 30°C, 80 colonies were re-isolated. Plasmids were retrieved from these colonies and initially analyzed using *BamHI/EcoRI* digestion and gel electrophoresis, followed by a partial sequencing of 51 plasmids. Although most CZ-e^K-Ura3 fusions that yielded low levels of Ura3 activity resulted from truncating mutations in the Ub or Ura3 moieties, three low-Ura3 isolates (Z=Leu, Val, Pro) encoded intact Ub and Ura3. These fusions were analyzed using degradation assays (see the main text).

Purification of Ub-XZ-MATα23-67-eK-DHFRha and in vitro deubiquitylation

The plasmids pCH645, pCH646, pCH647, and pCH648, which encoded His$_{10}$Ub-XZ-α$^{23-67}$-e^K-DHFR$_{ha}$ (X=Met, Gly, Arg; Z=Asn, Lys), were transformed into BL21(DE3) CodonPlus *E. coli* cells (Stratagene, La Jolla, CA). 50-ml overnight culture

of transformed cells was inoculated into 800 ml of LB medium containing 100 μg/ml ampicilin and 34 μg/ml chloramphenicol, followed by growth at 37°C to A_{600} of ~0.6. Expression of His_{10}Ub-XZ-Matα$^{23-67}$-e^{K}-$DHFR_{ha}$ was induced with isopropyl β-D-thiogalactoside (IPTG) at 0.2 mM for 4 hr at 30°C. His_{10}Ub-XZ-Matα$^{23-67}$-e^{K}-$DHFR_{ha}$ fusion proteins were purified by affinity chromatography with Ni-NTA resin (Qiagen, Valencia, CA). Briefly, *E. coli* cells were harvested by centrifugation and frozen at -80°C. Cell pellets were thawed and resuspended in Ni-NTA binding buffer (10% glycerol, 20 mM imidazole, 0.3 M NaCl, 10 mM β-mercaptoethanol, 1 mM PMSF, 50 mM NaH_2PO_4/Na_2HPO_4 (pH 7.5)) containing 1x Protease Inhibitor Cocktail "for *use in purification of histidine-tagged proteins"* (Sigma-Aldrich, St. Louis, MO). Cells were disrupted by sonication, 5 times for 1 min each at 1-min intervals, followed by the addition of NP40 to the final concentration of 0.1%. After centrifugation of the extract at 11,200*g* for 30 min, the supernatant was added to 2 ml of Ni-NTA resin (Qiagen, 50% slurry), and incubated for 2 hr at 4°C. The resin was transferred to a 10-ml column and washed 4 times with 50 ml of washing buffer (10% glycerol, 50 mM imidazole, 0.3 M NaCl, 10 mM β-mercaptoethanol, 50 mM NaH_2PO_4/Na_2HPO_4, pH 7.5). His_{10}Ub-XZ-Matα$^{23-67}$-e^{K}-$DHFR_{ha}$ proteins were then stepwise eluted using 2-ml samples of the binding buffer that contained increasing concentrations of imidazole (100, 150, 200, 250, 300 mM). Pooled eluted samples were dialyzed overnight at 4°C against storage buffer (10% glycerol, 0.15 M NaCl, 10 mM β-mercaptoethanol, 50 mM NaH_2PO_4/Na_2HPO_4, pH 7.5). Thus purified His_{10}Ub-X-e^{K}-$DHFR_{ha}$ proteins (~1 mg) were digested with purified Usp2-cc deubiquitylating enzyme(23, *24)* (0.1 mg overnight at 4°C in 1 ml of cleavage buffer (10% glycerol,

0.3 M NaCl, 2 mM β-mercaptoethanol 50 mM NaH_2PO_4/Na_2HPO_4, pH 7.5). His_{10}-tagged ubiquitin and His6- tagged Usp2-cc were removed by incubation with Ni-NTA (0.5 ml) for 1 h at 4°C. The unbound proteins were dialyzed against second storage buffer (10% glycerol, 0.15 M NaCl, 5 mM β-mercaptoethanol, 50 mM HEPES, pH 7.5) and frozen at -80°C.

In vitro acetylation assay

A sample of purified XZ-Matα^{3-67}-e^{K}-$DHFR_{ha}$s (~15 µg) was incubated in 20 µl of anti-ha agarose (50% slurry) (Sigma-Aldrich) on ice for 30 min, was further washed in 0.25 ml of lysis buffer (10% glycerol, 0.15 M NaCl, 1 mM PMSF, 50 mM HEPES (pH 7.5)) containing 1x protease inhibitor cocktail *"for use with fungal and yeast extracts"* (Sigma-Aldrich). Whole-cell extracts from wild-type (BY4742; Table S1) *S. cerevisiae* were passed through the Protein Desalting Spin columns (Thermo Scientific, Rockford, IL). Samples of XZ-α^{3-67}-e^{K}-$DHFR_{ha}$ bound to anti-ha-agarose beads were incubated in 0.1 ml of a reaction mixture (0.1 mg crude extract, 5 mM Na-butyrate (Sigma-Aldrich), 0.2 µCi C14-Acetyl-Coenzyme A (Ac-CoA) (1.85 Mbq) (Perkin-Elmer, Fremont, CA) for 1 hr at 30°C. After washing the beads 3 times with 0.4 ml of lysis buffer, the bound proteins were eluted and fractionated by SDS-12% PAGE (Tris-glycine), followed by autoradiography with X-ray films, at -80°C for 30 days.

Antibody specific for Nt-acetylated N-terminal sequence of MATα2

The Nt-acetylated synthetic peptide ^{Ac}MNKIPIKDLLNC and its unacetylated counterpart MNKIPIKDLLNC were produced and purified by Abgent (San Diego, CA). Except for C-terminal Cys (used for conjugation of peptides to keyhole limpet

hemocyanin), the amino acid sequence of these peptides was identical to the N-terminal region of MATα2. Standard procedures (2) were employed by Abgent to produce rabbit antisera to ^{Ac}MNKIPIKDLLNC. Antibodies that bound to ^{Ac}MNKIPIKDLLNC were selected from immune sera by affinity chromatography on a resin derivatized with this Nt-acetylated peptide. The resulting samples were then "negatively" selected by passing them through a resin derivatized with MNKIPIKDLLNC, the unacetylated counterpart of ^{Ac}MNKIPIKDLLNC. The resulting antibody, termed anti-^{AcNt}MATα2, was highly specific for Nt-acetylated Matα2, and was employed to directly detect Nt-acetylated species of a Matα2-derived reporter in *S. cerevisiae* extracts (see Results). Immunoblotting with anti-^{AcNt}MATα2 (0.5 μg/ml) were carried out for 4 h at room temperature (RT) in 5% skin milk in PBST (PBS containing 0.5% Tween-20). The bound anti-^{AcNt}MATα2 was detected using the Odyssey Imaging System (Li-Cor, Lincoln, NE) and a goat anti-rabbit antibody (at 1:5,000 dilutions) that was conjugated to IRDye-680 (Li-Cor).

Cycloheximide-chase degradation assay

S. cerevisiae were grown to A600 of 0.8 to 1.0 in plasmid-maintaining (selective) liquid media at 30°C, followed by treatment with cycloheximide (CHX), at the final concentration of 0.1 mg/ml). At indicated times, cell samples (corresponding to 1 ml of cell suspension at A600 of 1) were harvested by centrifugation for 30 sec at 11,200*g*, and resuspended in 1 ml of 0.2 M NaOH, for 20 min on ice, or for 5 min at room temperature, followed by centrifugation for 30 sec at 11,200*g*. Pelleted cells were resuspended in 50 μl of HU buffer (8 M urea, 5% SDS, 1 mM EDTA, 0.1 M dithiothreitol (DTT), 0.005% bromophenol blue, 0.2 M Tris-HCl,

pH 6.8) containing 1x protease inhibitor cocktail *"for use with fungal and yeast extracts"* (Sigma-Aldrich), and heated for 10 min at 70°C. After centrifugation at 5 min at 11,200*g*, 10 µl of supernatant was fractionated by SDS-4-12% NuPAGE (Invitrogen, Carlsbad, CA), followed by immunoblotting with anti-ha (1:2,000) and anti-tubulin (1:4,000) antibodies (Sigma-Aldrich). Quantitations of CHX-chase immunoblotting patterns (see fig. S2) were carried out using the ImageJ software (http://rsb.info.nih.gov/ij/index.html).

^{35}S-pulse-chase degradation assays

^{35}S-pulse-chase experiments were performed essentially as described (5, *6, 25),* with slight modifications. *S. cerevisiae* BY4742 (wild type), BY17299 (*doa10Δ*) , BY15546 (*nat3Δ*), and CHY287 (*ubc4Δ*), or CHY288 (*ubc4Δ doa10Δ)* that carried either p416MET25, pCH704, pCH705, pCH706 or pCH719 were grown at 30°C to A_{600} of ~1 in 10 ml of SD medium with required amino acids for auxotrophic growth. Cells were pelleted by centrifugation and washed with 0.8 ml of SD medium with required amino acids. Cell pellets were gently resuspended in 0.4 ml of the same medium and labeled for 5 min at 30°C with 0.16 mCi of ^{35}S-EXPRESS (Perkin-Elmer). Cells were pelleted again and resuspended in 0.3 ml of SD medium containing cold 10 mM methionine and 5 mM cysteine and required amino acids. Samples (0.1 ml) were taken at the indicated time points, followed by preparation of extracts, immunoprecipitation with anti-flag agarose, SDS-4-12% NuPAGE, and autoradiography. In other, similar ^{35}S-pulse-chase experiments, *S. cerevisiae* JD53 expressing either pCH178, pCH195, pCH504 or pCH547 were grown at 30°C to A_{600} of ~1 in 10 ml of SC(-Trp) medium containing 10 µM $CuSO_4$ and required amino

acids. Pulse-chases were then preformed as described above, in SD medium with 10 μM $CuSO_4$ and required amino acids.

For ^{35}S-pulse-chase assays that involved 2-D electrophoresis (fig. S8 and data not shown), *S. cerevisiae* BY4742 (wild type) or BY17299 (*doa10Δ*) that carried pCH641 (Table S2) were grown at 30°C to A_{600} of ~0.8 in 200 ml of SD medium with required amino acids and 0.1 mM $CuSO_4$. Cells were pelleted by centrifugation and washed with 10 ml of SD medium with required amino acids and 0.1 mM $CuSO_4$, followed by incubation for 30 min at 30°C in the same medium that lacked methionine and cysteine. Cells were harvested by centrifugation. The pellets were gently resuspended in 20 ml of the same medium and labeled for 15 min at 30°C with 2 mCi of ^{35}S-EXPRESS (Perkin-Elmer). Cells were pelleted again and resuspended in 20 ml of SD medium containing unlabeled 10 mM methionine and 5 mM cysteine, required amino acids, and 0.1 mM $CuSO_4$. Samples (10 ml) were taken at 0 and 3-hr time points, followed by preparation of extracts, using the Sample Buffer Mailing kit (Kendrick laboratories, Madison, WI). 2D-electrophoretic analyses and autoradiography of our samples were carried out by Kendrick Laboratories, Inc. The first-dimension isoelectric focusing was performed using IEF tube gel containing 2% pH 4-8 mixed ampholines. The second dimension fractionation was by SDS-10% PAGE, using 22-cm long slab gels. The latter were stained with Coomassie, vacuum-dried, and subjected to autoradiography with Kodak BioMax X-ray film for 6 hr at RT. Image matching of the autoradiograms to Coomassie- stained gels was carried out manually. The relevant spots were excised from the gel, followed by their processing for in-gel digestion with trypsin and mass

spectrometry (MALDI-TOF), which were performed by the Protein Analysis Facility at the Columbia University (New York, NY).

Analysis of Nα-terminal acetylation by mass spectrometry

CHY288 (*doa10Δ ubc4Δ) S. cerevisiae* expressing the C-terminally flag-tagged full-length Matα2$_f$ from the P_{GAL1} promoter were grown to A_{600} of~ 0.6 in 2 l of SC(-Ura) medium containing 0.1% glucose (instead of usual 2%), and were incubated for a further 24 hr after the addition of 30% galactose to the final concentration of 2%. Cells were harvested by centrifugation at 5,000*g* for 5 min, washed in phosphate-buffered saline (PBS) and stored at -80°C. The pellets were resuspended in 10 ml of lysis buffer (10% glycerol 0.1% NP40, 0.2 M KCl, 1 mM EDTA, 5 mM β-mercaptoethanol, 1 mM PMSF, 50 mM HEPES (pH 7.5)) containing 1x protease inhibitor cocktail *"for use with fungal and yeast extracts"* (Sigma-Aldrich). Cells were then disrupted using a FastPrep-24 instrument (MP Biomedicals, Solon OH) at the speed setting of 6.5, at 20 sec/cycle, for 10 cycles. After removal of glass beads, the extracts were clarified by centrifugation at 11,2000*g* for 30 min and incubated with 0.2 ml of anti-flag M2 agarose beads (50% slurry, Sigma-Aldrich) for 2 hr at 4°C. Beads were washed once in 10 ml of lysis buffer, then in 10 ml of the washing buffer (lysis buffer containing 0.5 M KCl) and finally in 10 ml of elution buffer (lysis buffer without NP40). Matα2$_f$ was eluted with 0.2 mg/ml of the flag peptide (Sigma-Aldrich) in elution buffer. The eluted Matα2$_f$ was precipitated by 20% CCl_3COOH (TCA) (final concentration), and washed twice with cold acetone at -20°C. Thus precipitated sample was solubilized in SDS-sample buffer, heated at 95°C for 5 min, and fractionated by SDS-4-12% NuPAGE. Proteins were stained with Novex

Colloidal Blue Staining kit (Invitrogen). The band of Matα2_f (~1 μg) was excised and transferred to 0.65 ml of SafeSeal Microcentrifuge tube (Sorenson, Salk Lake City, UT). Gel slices were incubated 2 times for 30 min at 37°C by shaking in 0.2 ml of destaining solution (25 mM NH_4HCO_3 in 50% acetonitrile, pH 8.0). After removing destaining solution, the samples were incubated at 60°C for 10 min in 30 μl of reducing buffer (50 mM Tris[2-carboxyethyl]phosphine (TCEP) (Thermo Scientific) in 25 mM NH4HCO3, pH 8.0). After cooling the sample to RT and removing the reducing buffer, gel slices were incubated in the dark at RT for 1 hr in 30 μl of alkylation buffer (0.1 M iodoacetamide, 25 mM NH_4HCO_3, pH 8.0). After removing the alkylation buffer, gel slices were shrank by incubating them twice for 15 min at 37°C (with shaking) in 50 μl of acetonitrile at RT. After removing acetonitrile, gel slices were air-dried for 10 min and swelled in 25 μl of 25 mM NH_4HCO_3, pH 8.0. Thereafter Matα2_f in gel slices was digested *in situ* with 100 ng of Asp-N endoprotease (Roche, Indianapolis, IN) overnight at 37°C, whereas ML-e^K-Ura3 (see below) was digested identically but with 100 ng of activated trypsin (Thermo Scientific). Nt-acetylated peptides in the resulting samples were analyzed by nanoscale-microcapillary reversed phase liquid chromatography and tandem mass spectrometry (cLC-MS/MS), using the QSTAR XL quadrupole time of flight mass spectrometer (Applied Biosystems, Foster City, CA). Acetylation sites were assigned by manual inspection of MS/MS spectra and also by using the Mascot search engine (Matrix Science, Boston, MA).

Similar procedures were used to analyze N^α-terminal acetylation of the short-lived ML-e^K-Ura3 (ML-e^K-ha-Ura3) (fig. S5B, C) and SL-e^K-Ura3 (SL-e^K-ha-Ura3). CHY223

(*doa10Δ*) *S. cerevisiae* expressing pCH504 or pCH505 (Table S1) were grown to A_{600} of 3 to 4 in 1 liter of SC(-Trp) medium containing 0.1 mM $CuSO_4$. The cells were harvested by centrifugation at 5,000*g* for 5 min, washed in PBS, stored at -80°C, and were processed for isolation of ML-e^K-Ura3 and SL-e^K-Ura3 identically to the steps above for Matα2_f, except that a cell extract was incubated with 0.4 ml of anti-ha agarose beads (50% slurry) for 2 hr at 4°C. Beads were washed in 50 ml of the lysis buffer and thereafter in 10 ml of the elution buffer (lysis buffer without NP40). ML-e^K-Ura3 and SL-e^K-Ura3 were eluted with 1 ml of the ha peptide (0.25 mg/ml; Sigma-Aldrich) in the elution buffer, and thereafter by 2 ml of 0.1 M glycine (pH 3.0). The eluted proteins were precipitated by 20% TCA. The rest of the procedure was identical to the one with Matα2_f, except that ML-e^K-Ura3 and SL-e^K-Ura3 were digested *in situ* with trypsin, without reduction/alkylation steps.

X-peptide pulldown assay with Doa10myc13

The previously characterized X-peptide pulldown assay (26, *27)* utilized, in the present study, a set of 12-residue synthetic peptides XNKIPIKDLLNC (X=Met, ^{Ac}Met, Gly). Except for C-terminal Cys (added for crosslinking to beads) and the varied identity of N-terminal residue, these peptides were identical to the 11-residue N-terminal region of MATα2. We also employed 12- residue peptides XIFSTDTGPGGC (X=Gly, Met, Arg, Phe). Except for C-terminal Gly-Gly-Cys and the varied identity of N-terminal residue, these peptides were identical to the 9-residue N-terminal region of Sindbis virus RNA polymerase (nsP4) (refs. (26, *28),* and refs. therein). Each peptide, synthesized by Abgent (San Diego, CA), was purified by HPLC to greater than 95% purity, and verified by mass spectrometry. A peptide (1 mg)

was crosslinked, via its C-terminal Cys residue, to 2 ml (50% slurry) of SulfoLink Immobilization Kit for Peptides (Thermo Scientific), as described in the manufacturer's protocol. Extract from *S. cerevisiae* CHY248 cells (Table S1) containing full-length, C-terminally myc13-tagged $Doa10_{myc13}$, was diluted by lysis buffer (10% glycerol, 1% Triton X100, 0.15 M NaCl, 5 mM β-mercaptoethanol, 1 mM PMSF, 50 mM HEPES, (pH 7.5) containing 1x protease inhibitor cocktail *"for use with fungal and yeast extracts"* (Sigma- Aldrich)) to 1 mg/ml of total protein. These samples also contained 50 μM bestatin (Sigma- Aldrich), an aminopeptidase inhibitor. A sample (1 ml) was transferred to a tube containing 20 μl (packed volume) of a carrier-linked 12-residue peptide, followed by gentle mixing for 2 hr at 4°C. Beads were pelleted by a brief centrifugation in a microcentrifuge, followed by three washes, for 5 min each, with lysis buffer. The beads were then suspended in 20 μl of SDS/PAGE loading buffer, and heated at 65°C for 10 min, followed by a brief spin in a microcentrifuge, SDS-4-12% NuPAGE, and detection of $Doa10_{myc13}$ by immunoblotting with anti-myc antibody.

Purification of $Doa10_f$ for SPOT binding assay

S. cerevisiae SC295 that carried pCH595 and expressed the C-terminally flag-tagged Doa10 ($Doa10_f$) from the P_{GAL1} promoter and the high copy plasmid pRS425 was grown at 30°C to A_{600} of ~1 in 4 liters of SC(-Leu) medium containing 1% glucose and 2% galactose. Cells were harvested by centrifugation, washed once with ice-cold PBS, quick-frozen in liquid nitrogen, and stored at -80°C. Frozen pellets were resuspended in 50 ml of lysis buffer (0.1 M sorbitol 50 mM K-acetate, 2 mM EDTA, 1 mM DTT, 1 mM PMSF, 20 mM HEPES (pH 7.5) plus 1x protease inhibitor

cocktail *"for use with fungal and yeast extracts"* (Sigma-Aldrich). Cells were then disrupted using a FastPrep-24 instrument (MP Biomedicals, Solon OH) at the speed setting of 6.5, at 20 sec/cycle, for 6 cycles. After removal of the glass beads, unbroken cells were removed by two rounds of centrifugation in the Sorvall RT-600B centrifuge at 3,000 rpm for 5 min at 4°C. The resulting supernatant was centrifuged at 11,200*g* for 10 min at 4°C. The pellets, which contained membrane-embedded $Doa10_f$, were washed twice in 25 ml of buffer 88 (0.25 M sorbitol, 0.15 M K-acetate, 5 mM Mg-acetate, 20 mM HEPES (pH 6.8)) containing 1x protease inhibitor cocktail *"for use with fungal and yeast extracts"* (Sigma-Aldrich), using centrifugation at 11,200g for 10 min. The resulting microsomes were resuspended and solubilized by incubating in 20 ml of extraction buffer (10% glycerol, 1% Triton X-100, 0.2 M KCl, 1 mM EDTA, 5 mM β-mercaptoethanol, 1 mM PMSF, 50 mM HEPES (pH 7.5)) containing 1x protease inhibitor cocktail *"for use with fungal and yeast extracts"* (Sigma-Aldrich) for 2 hr at 4°C. The resulting suspension was centrifuged at 11,200g for 30 min, and the supernatant was gently mixed with 2 ml of anti-flag M2 affinity beads (50% slurry) (Sigma-Aldrich) for 2 h at 4°C. The beads were then collected by centrifugation in the Sorvall RT-600B centrifuge at 1,000 rpm for 5 min at 4°C, and were washed, repeatedly, with 100 ml of extraction buffer. The anti-flag antibody-bound $Doa10_f$ was eluted with 5 ml of extraction buffer containing 0.5 mg/ml of the flag peptide (Sigma-Aldrich), followed by dialysis at 4°C overnight against storage buffer (10% glycerol, 1% Triton X-100, 0.15 M NaCl, 5 mM β-mercaptoethanol, 50 mM HEPES, pH 7.5).

SPOT binding assay

These experiments employed synthetic XZ-$e^{K(3-11)}$ peptides and their Nt-acetylated ^{Ac}XZ-$e^{K(3-11)}$ counterparts that were C-terminally linked to a cellulose-PEG membrane as "dots", in equal molar amounts. Except for varied residues XZ at positions 1 and 2 (including Nt-acetylated versus unacetylated residues at position 1), the sequences of the 11-residue SPOT-arrayed peptides were identical to the N-terminal sequence of e^K (fig. S1D). These PepSpot (PEG) peptides were synthesized using JPT Peptide Technology, GmbH (JPT) (Berlin, Germany) (29). Each peptide "spot" contained approximately 5 nmoles of identical peptides covalently conjugated, C-terminally, to a cellulose-PEG-membrane. Before the binding assay, dry membranes were washed in methanol for 10 min, and 3 times for 20 min each in Tris-buffered saline (TBS) (170 mM NaCl, 6.4 mM KCl, 31 mM Tris-HCl, pH 7.6) at RT, and thereafter blocked by incubation in buffer A (10% glycerol, 50 μM bestatine, 0.1 M NaCl, 5 mM β-mercaptoethanol, 50 mM HEPES, pH 7.5) for 30 min at RT. Thereafter a SPOT membrane was incubated with 2.5 ml of the purified $Doa10_f$ (0.1 mg/ml) in the storage buffer (10% glycerol, 1% Triton X-100, 0.15 M NaCl, 5 mM β-mercaptoethanol, 50 mM HEPES, pH 7.5) at RT for 2 hr. The membrane was then washed twice in buffer A for 15 min. The bound $Doa10_f$ was electroblotted onto polyvinylene difluoride (PVDF) membranes (Millipore) using a semi-dry blotter (Bio-Rad, Hercules, CA). During the transfer, PVDF membranes were sandwiched between blotting paper soaked with cathode buffer (25 mM Tris-base, 40 mM 6-aminohexane acid, 0.01% SDS, 20% MeOH) and one of the anode buffers (AI: 30 mM Tris base, 20% MeOH; AII: 300 mM Tris base, 20% MeOH). Electroblotting was performed twice for 30 min at the constant current of 0.8 mA per cm^2 of cellulose

membrane. The transferred $Doa10_f$ were detected by immunoblotting with anti-flag antibody, using a SuperSignal West Pico Chemiluminescent Substrate (Thermo Scientific).

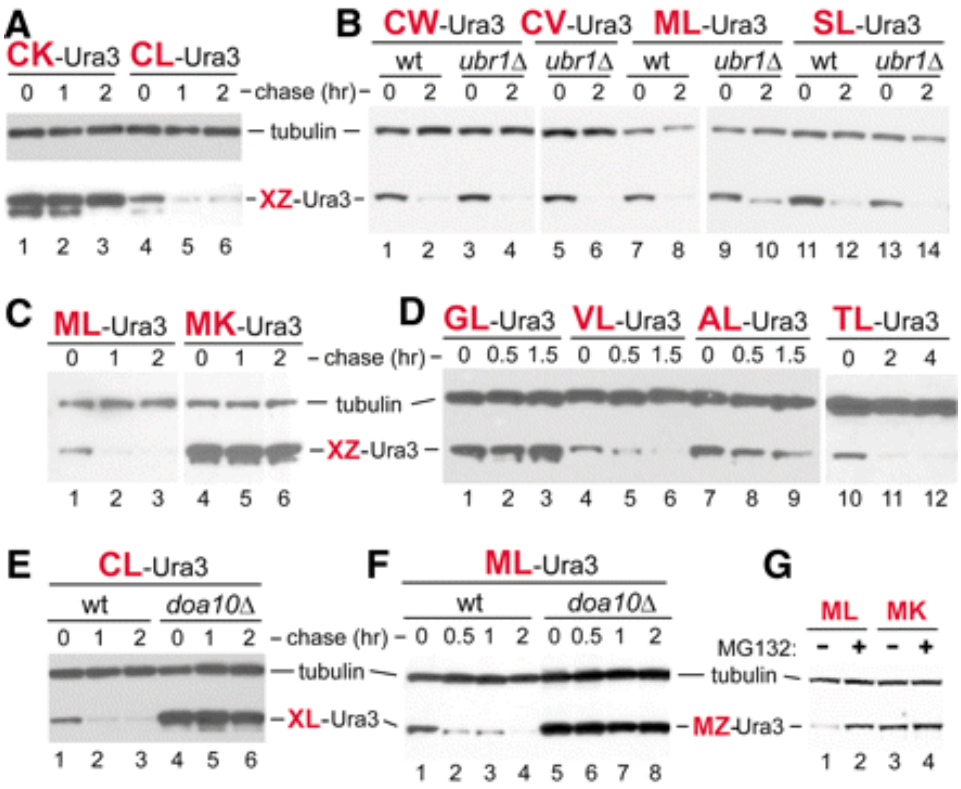

Figure 4.1. Destabilizing N-terminal residues. (A) CHX chases, for 0, 1, and 2 hours in wild-type S. cerevisiae expressing CK-e^{K}-Ura3 (lanes 1 to 3) or CL-e^{K}-Ura3 (lanes 4 to 6). Cell extracts were fractionated by SDS–polyacrylamide gel electrophoresis, followed by immunoblotting with anti-Ha and anti-tubulin, the latter a loading control. (B) As in (A) but chases for 0 and 2 hours with XZ-e^{K}-Ura3 (X = Cys, Met, or Ser; Z = Trp, Val, or Leu) in wild-type versus *ubr1Δ* cells. (C) As in (A) but with MZ-e^{K}-Ura3 (Z = Leu or Lys) in wild-type cells. (D) As in (A) but chases for 0, 0.5, and 1.5 hours with XL-e^{K}-Ura3 (X = Gly, Val, Ala, or Thr) in wild-type cells. (E) As in (A) but with CL-e^{K}-Ura3 in wild-type cells (lanes 1 to 3) versus *doa10Δ* cells (lanes 4 to 6). (F) As in (E) but chases for 0, 0.5, 1, and 2 hours with ML-e^{K}-Ura3. (G) Lanes 1 and 2, short-lived ML-e^{K}-Ura in the MG132-sensitive *pdr5Δ* S. cerevisiae, in the absence

and presence of MG132, respectively. Lanes 3 and 4, same as lanes 1 and 2 but with long-lived MK-e^{K}-Ura3.

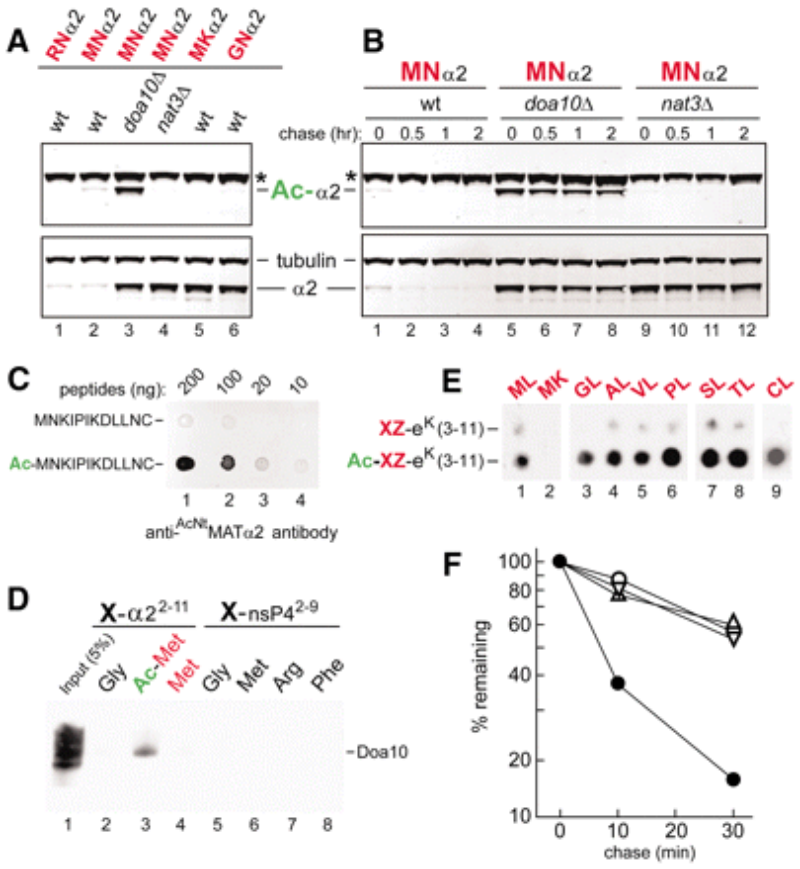

Figure 4.2. Doa10 as an N-recognin. (A) Extracts from wild-type, *doa10Δ*, and *nat3Δ* *S. cerevisiae* that expressed XZ-α^{23-67}-e^{K}-Ura3 (XZα2) (X = Met, Arg, or Gly; Z = Asn or Lys) were immunoblotted with anti-^{AcNt}MATα2 (which selectively recognized Nt-acetylated MNα2) or (separately) with anti-Ha, which recognized both Nt-acetylated and unacetylated MNα2, or with anti-tubulin. XZα2 ("α2"), Nt-acetylated XZα2 ("Ac-α2"), and tubulin are indicated. Asterisks denote a protein cross-reacting with anti-^{AcNt}MATα2. (B) As in (A) but CHX chases for 0, 0.5, 1, and 2 hours with MNα2, in wild-type, *doa10Δ*, and *nat3Δ* cells. (C) Indicated amounts of the Nt-acetylated Ac-MNKIPIKDLLNC peptide versus its unacetylated counterpart were spotted onto membrane and assayed for their binding to anti-^{AcNt}MATα2. (D) X-peptide pulldown with peptides XNKIPIKDLLNC (X = Met, AcMet, or Gly) (lanes 2 to 4) or

XIFSTDTGPGGC (X = Gly, Met, Arg, or Phe) (lanes 5 to 8) and extract of *S. cerevisiae* that expressed $Doa10_{myc13}$. Lane 1, input extract (5%). (E) SPOT assay with purified, flag-tagged $Doa10_f$ and spot-arrayed synthetic peptides XZ-$e^{K(3\text{-}11)}$ (X = Gly, Ala, Val, Pro, Ser, Thr, or Cys; Z = Leu or Lys) and their Nt-acetylated XZ-$e^{K(3\text{-}11)}$ counterparts. XZ residues are indicated at the top of the membrane. (F) Quantitation, using a PhosphorImager, of ^{35}S-pulse chases with $MAT\alpha2_f$ and its mutant derivatives (fig. S6, B and C). Solid circles, $^{MN}MAT\alpha2_f$; open circles, $^{MK}MAT\alpha2_f$; upright triangles, $^{GN}MAT\alpha2_f$ (initially $^{MGN}MAT\alpha2_f$) in *ubc4Δ* cells; inverted triangles, $^{MN}MAT\alpha2_f$ in *ubc4Δ doa10Δ* cells.

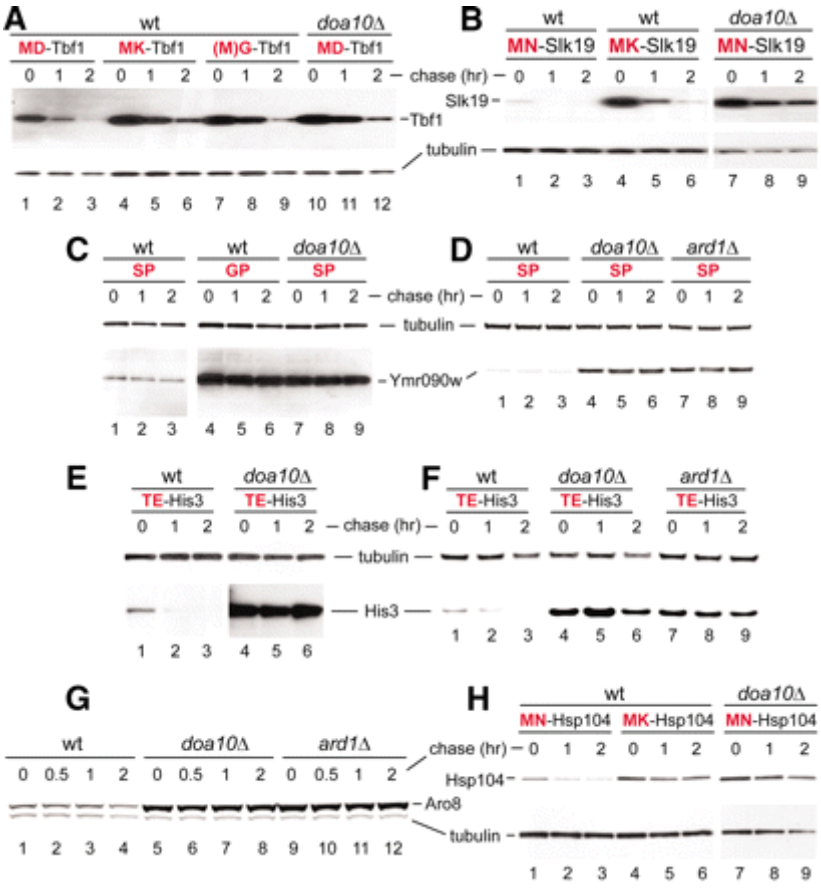

Figure 4.3. ^{Ac}N-degrons in yeast proteins. (A) Lanes 1 to 3, CHX chase for 0, 1, and 2 hours in wild-type *S. cerevisiae* expressing $Tbf1_{ha}$. Lanes 4 to 6, 7 to 9, and 10 to 12, analogous patterns but in *doa10Δ* cells with $^{MK}Tbf1_{ha}$ (Lys at position 2), $^{G}Tbf1_{ha}$ (initially $^{MG}Tbf1_{ha}$), and wild-type Tbf1ha, respectively. (B) As in (A) but with wild-type $Slk19_{ha}$ and its mutant derivatives in wild-type versus *doa10Δ* cells. (C) As in (A) but with wild-type $Ymr090w_{ha}$ and its mutant derivatives in wild-type versus *doa10Δ* cells. (D) As in (C) but with wild-type $Ymr090w_{ha}$ in wild-type versus *doa10Δ* and *ard1Δ* cells. (E) As in (A) but with wild-type $His3_{ha}$ in wild-type versus *doa10Δ* cells. (F) As in (E), with wild-type $His3_{ha}$ in wild-type versus *doa10Δ* and *ard1Δ* cells. (G) As in (A) but CHX chases for 0, 0.5, 1, and 2 hours with wild-type

Aro8$_{ha}$ in wild-type versus *doa10Δ* and *ard1Δ* cells. (H) As in (A) but with wild-type Hsp104$_{ha}$ and its mutant derivatives in wild-type versus *doa10Δ* cells.

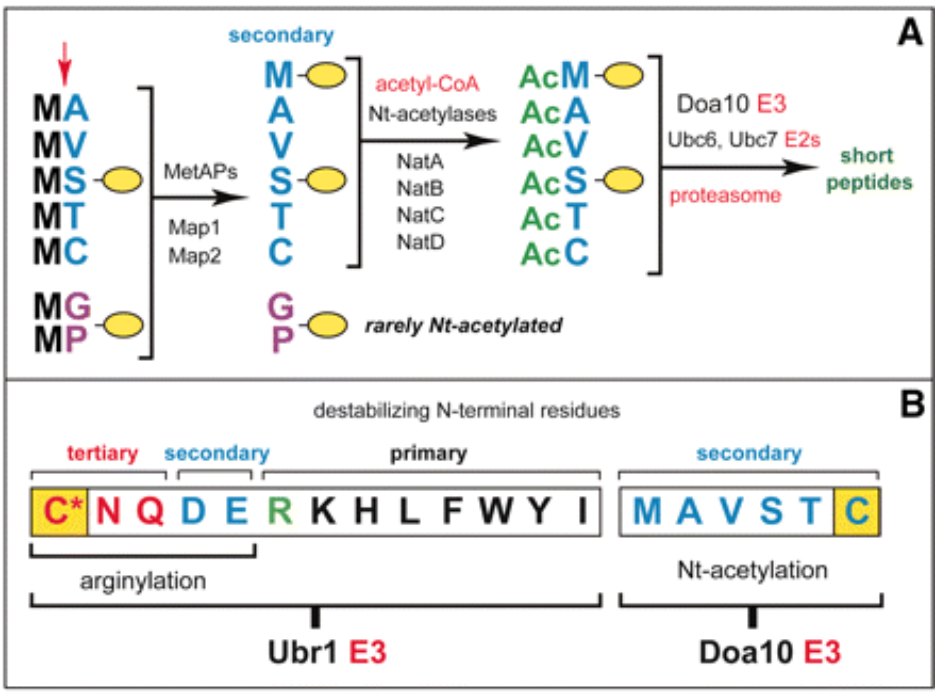

Figure 4.4. N$^{\alpha}$-terminal acetylases, Met-aminopeptidases, and the Doa10 branch of the N-end rule pathway. (A) The Doa10-mediated branch of the *S. cerevisiae* N-end rule pathway (see fig. S1C for the Ubr1-mediated branch of this pathway). The red arrow on the left indicates the MetAP-mediated removal of N-terminal Met. This Met is retained if a residue at position 2 is nonpermissive (too large) for MetAPs. If the retained N-terminal Met or N-terminal Ala, Val, Ser, Thr, and Cys are followed by acetylation-permissive residues, the above N-terminal residues are usually Nt-acetylated (5–7). The resulting N-degrons are termed ^{Ac}N-degrons. The term "secondary" refers to the necessity of modification (Nt-acetylation) of a destabilizing N-terminal residue before a protein can be recognized by a cognate Ub ligase (fig. S1C). Proteins containing ^{Ac}N-degrons are targeted for ubiquitylation (and proteasome-mediated degradation) by the Doa10 E3 Ub ligase. Although Gly or Pro can be made N-terminal by MetAPs, and although Doa10 can recognize Nt-

acetylated Gly and Pro (Fig. 2E), few proteins with N-terminal Gly or Pro are Nt-acetylated (5–7). (B) The Ubr1 and Doa10 branches of the N-end rule pathway. Both branches target, through different mechanisms, the N-terminal Cys residue (yellow rectangles), with oxidized Cys marked by an asterisk.

References and Notes

1. H. Jörnvall, Acetylation of Protein N-terminal amino groups structural observations on alpha-amino acetylated proteins. J. Theor. Biol. 55, 1 (1975).
2. J. R. Mullenet al., Identification and characterization of genes and mutants for an N-terminal acetyltransferase from yeast. EMBO J. 8, 2067 (1989).
3. E. C. Park, J. W. Szostak, ARD1 and NAT1 proteins form a complex that has N-terminal acetyltransferase activity. EMBO J. 11, 2087 (1992).
4. M. Gautschiet al., The yeast N(alpha)-acetyltransferase NatA is quantitatively anchored to the ribosome and interacts with nascent polypeptides. Mol. Cell. Biol. 23, 7403 (2003).
5. B. Polevoda, F. Sherman, N-terminal acetyltransferases and sequence requirements for N-terminal acetylation of eukaryotic proteins. J. Mol. Biol. 325, 595 (2003).
6. T. Arnesenet al., Proteomics analyses reveal the evolutionary conservation and divergence of N-terminal acetyltransferases from yeast and humans. Proc. Natl. Acad. Sci. U.S.A. 106, 8157 (2009).
7. S. Goetzeet al., Identification and functional characterization of N-terminally acetylated proteins in Drosophila melanogaster. PLoS Biol. 7, e1000236 (2009).
8. F. Frottinet al., The proteomics of N-terminal methionine cleavage. Mol. Cell. Proteomics 5, 2336 (2006).

9. A. Mayer, N. R. Siegel, A. L. Schwartz, A. Ciechanover, Degradation of proteins with acetylated amino termini by the ubiquitin system. Science 244, 1480 (1989).

10. A. Bachmair, D. Finley, A. Varshavsky, In vivo half-life of a protein is a function of its amino-terminal residue. Science 234, 179 (1986).

11. A. Bachmair, A. Varshavsky, The degradation signal in a short-lived protein. Cell 56, 1019 (1989).

12. A. Varshavsky, The N-end rule: Functions, mysteries, uses. Proc. Natl. Acad. Sci. U.S.A. 93, 12142 (1996).

13. A. Varshavsky, Discovery of cellular regulation by protein degradation. J. Biol. Chem. 283, 34469 (2008).

14. A. Mogk, R. Schmidt, B. Bukau, The N-end rule pathway for regulated proteolysis: Prokaryotic and eukaryotic strategies. Trends Cell Biol. 17, 165 (2007).

15. T. Tasaki, Y. T. Kwon, The mammalian N-end rule pathway: New insights into its components and physiological roles. Trends Biochem. Sci. 32, 520 (2007).

16. R.-G. Huet al., The N-end rule pathway as a nitric oxide sensor controlling the levels of multiple regulators. Nature 437, 981 (2005).

17. R.-G. Hu, H. Wang, Z. Xia, A. Varshavsky, The N-end rule pathway is a sensor of heme. Proc. Natl. Acad. Sci. U.S.A. 105, 76 (2008).

18. C.-S. Hwang, A. Varshavsky, Regulation of peptide import through phosphorylation of Ubr1, the ubiquitin ligase of the N-end rule pathway. Proc. Natl. Acad. Sci. U.S.A. 105, 19188 (2008).

19. C.-S. Hwang, A. Shemorry, A. Varshavsky, Two proteolytic pathways regulate DNA repair by cotargeting the Mgt1 alkylguanine transferase. Proc. Natl. Acad. Sci. U.S.A. 106, 2142 (2009).

20. H. Wang, K. I. Piatkov, C. S. Brower, A. Varshavsky, Glutamine-specific N-terminal amidase, a component of the N-end rule pathway. Mol. Cell 34, 686 (2009).

21. A. Varshavsky, Ubiquitin fusion technique and related methods. Methods Enzymol. 399, 777 (2005).

22. R. Swanson, M. Locher, M. Hochstrasser, A conserved ubiquitin ligase of the nuclear envelope/endoplasmic reticulum that functions in both ER-associated and Matalpha2 repressor degradation. Genes Dev. 15, 2660 (2001).

23. M. Deng, M. Hochstrasser, Spatially regulated ubiquitin ligation by an ER/nuclear membrane ligase. Nature 443, 827 (2006). Caltech

24. T. Ravid, S. G. Kreft, M. Hochstrasser, Membrane and soluble substrates of the Doa10 ubiquitin ligase are degraded by distinct pathways. EMBO J. 25, 533 (2006).

25. M. Hochstrasser, A. Varshavsky, In vivo degradation of a transcriptional regulator: The yeast alpha 2 repressor. Cell 61, 697 (1990).

26. P. Chen, P. Johnson, T. Sommer, S. Jentsch, M. Hochstrasser, Multiple ubiquitin-conjugating enzymes participate in the in vivo degradation of the yeast MAT alpha 2 repressor. Cell 74, 357 (1993).

27. A. D. Johnson, Molecular mechanisms of cell-type determination in budding yeast. Curr. Opin. Genet. Dev. 5, 552 (1995).

28. O. A. Zill, J. Rine, Interspecies variation reveals a conserved repressor of alpha-specific genes in Saccharomyces yeasts. Genes Dev. 22, 1704 (2008).

29. Single-letter abbreviations for the amino acid residues are as follows: A, Ala; C, Cys; D, Asp; E, Glu; F, Phe; G, Gly; H, His; I, Ile; K, Lys; L, Leu; M, Met; N, Asn; P, Pro; Q, Gln; R, Arg; S, Ser; T, Thr; V, Val; W, Trp; and Y, Tyr.

30. Materials and methods are available as supporting material on Science Online.

31. G. Hassinket al., TEB4 is a C4HC3 RING finger-containing ubiquitin ligase of the endoplasmic reticulum. Biochem. J. 388, 647 (2005).

32. We thank J. Zhou (Caltech) for MS analyses and C. Brower for comments on the paper. We are grateful to members of the Varshavsky laboratory for their advice in the course of this study and particularly thank O. Batygin for her technical assistance. This work was supported by grants from NIH and the March of Dimes Foundation to A.V.

CHAPTER 5:

CONTROL OF PROTEIN QUALITY AND STOICHIOMETRIES BY N-TERMINAL ACETYLATION AND THE N-END RULE PATHWAY

Anna Shemorry, Cheol-Sang Hwang, Alexander Varshavsky

SUMMARY

N^{α}-terminal acetylation of cellular proteins was recently discovered to create specific degradation signals, termed Ac/N-degrons and targeted by the Ac/N-end rule pathway. We show that Hcn1, a subunit of the APC/C ubiquitin ligase, contains an Ac/N-degron that is repressed by Cut9, another APC/C subunit and the ligand of Hcn1. Cog1, a subunit of the Golgi-associated COG complex, is also shown to contain an Ac/N-degron. Cog2 and Cog3, direct ligands of Cog1, can repress this degron. Furthermore, the subunit decoy technique was developed and used to show that the endogenous, long-lived Cog1 is destabilized and destroyed via its Ac/N-degron if the total level of Cog1 is increased in a cell. Hcn1 and Cog1 are the first examples of regulation, through physiologically relevant steric shielding, of natural Ac/N-degrons. This mechanistically straightforward circuit can employ the exceptional pervasiveness and conditionality of Ac/N-degrons to regulate subunit stoichiometries and other aspects of protein quality control.

INTRODUCTION

Nearly 90% of human proteins are N^{α}-terminally acetylated (Nt-acetylated) (86-90). There is no evidence for Nt-deacetylases, i.e., Nt-acetylation is apparently irreversible, in contrast to the dynamic acetylation-deacetylation of internal lysines in cellular proteins (91). Nt-acetylation can occur posttranslationally but the bulk of it is cotranslational, being mediated by ribosome-associated Nt-acetylases (92-94). We discovered that a major biological function of Nt-acetylation is the creation of specific degradation signals (degrons) in cellular proteins (95). These degrons, implemented by a novel branch of the N-end rule pathway, are the largest class of degradation signals in the proteome, as Nt-acetylation involves the majority of eukaryotic proteins (95,96).

The N-end rule pathway targets proteins containing N-terminal degradation signals called N-degrons, polyubiquitylates these proteins and thereby causes their processive degradation by the proteasome (Figure S1A, B). The main determinant of an N-degron is a destabilizing N-terminal residue of a protein. Recognition components of the N-end rule pathway are called N-recognins. In eukaryotes, N-recognins are E3 ubiquitin (Ub) ligases that can target N-degrons. Regulated destruction of specific proteins by the N-end rule pathway mediates a strikingly broad range of biological functions, cited in the legend to Figure S1 (96-101).

In eukaryotes, the N-end rule pathway comprises two branches, the Arg/N-end rule pathway and the Ac/N-end rule pathway (Figure S1A, B). The Arg/N-end rule pathway recognizes specific unacetylated N-terminal residues. N-terminal Arg, Lys, His, Leu, Phe, Tyr, Trp, and Ile are directly recognized by E3 N-recognins. In

contrast, N-terminal Asn, Gln, Asp, and Glu (as well as Cys, under some metabolic conditions) are destabilizing owing to their preliminary enzymatic modifications, which include Nt-deamidation and Nt-arginylation (Figure S1B) (96,102-105).

In contrast to the Arg/N-end rule pathway, the Ac/N-end rule pathway targets proteins through their Nt-acetylated residues, largely Nt-acetylated Met, Ala, Val, Ser, Thr, or Cys. These N-terminal degradation signals are called Ac/N-degrons, to distinguish them from other N-degrons. In the yeast *Saccharomyces cerevisiae*, the Ac/N-end rule pathway is mediated by the Doa10 E3 Ub ligase and possibly by other N-recognins as well (Figure S1A) (95,96).

Nt-acetylation is largely cotranslational, apparently irreversible, and involves a large majority of proteins. What functions are subserved by such a massive production of specific degradation signals, if proteins bearing Ac/N-degrons are often destined for in vivo half-lives of many hours or days? We suggested that the biological roles of Ac/N-degrons include protein quality control, including the regulation of input stoichiometries of subunits in oligomeric proteins (95,96). In the latter process, a free subunit of a protein complex is short-lived until the subunit becomes a part of the complex.

Consider a multisubunit protein that sterically shields a cognate subunit's Nt-acetylated residue. The initial destruction, through an Ac/N-degron, of some of this subunit's newly formed molecules would be halted by the formation of the complex and the resulting sequestration of the Ac/N-degron. If the shielding occurs through intramolecular folding or through homo-oligomeric interactions, this Ac/N-degron would be self-regulated by default. If the shielding involves hetero-oligomeric

interactions, there is an upper boundary on the level of subunit expression that is compatible with self-regulation. Above that boundary, some subunit molecules would remain short-lived, owing to titration of protein ligands that would normally sequester the subunit's Ac/N-degron.

In this model, the regulation of input stoichiometries of subunits in protein complexes involves the degradation of uncomplexed, e.g., overproduced proteins in, for example, aneuploid cells. The same mechanism can mediate the degradation of misfolded or otherwise abnormal proteins that cannot sequester their Ac/N-degrons through protein interactions. Because most Ac/N-degrons are formed cotranslationally, the processive proteolysis of a protein by the Ac/N-end rule pathway would occur, in part, concurrently with the synthesis of a nascent polypeptide or shortly after its completion, for example during the cotranslational assembly of protein complexes, or in the context of a polypeptide's interaction with chaperones (106-109).

The same logic applies to any conditional degradation signal. In fact, specific internal degrons participate in degradation-mediated protein homeostasis, including the destruction of abnormal proteins (96,110-116). Note, however, that compared to other characterized degradation signals, Ac/N-degrons are unique in their prevalence and mechanistic uniformity, as nearly 90% of human proteins are Nt-acetylated and Ac/N-degrons are the earliest degradation signals to form in nascent polypeptide chains. Physiological functions of Ac/N-degrons were suggested to involve the metabolic fates of most cellular proteins, from Nt-

acetylated subunits of protein dimers to Nt-acetylated subunits of the largest intracellular complexes such as the proteasome and the ribosome (95,96).

To begin addressing this model and the new field of the Ac/N-end rule pathway, we focused on Cog1 and Hcn1. *S. cerevisiae* Cog1 is a 48 kDa subunit of the Conserved Oligomeric Golgi (COG) complex, which comprises the subunits Cog1-Cog8, resides in the cytosol, associates with membranes, and participates in Golgi transport (117,118). Cog1 is a bridging subunit between the lobes of the COG complex (119,120). Hcn1 (Cdc26) is a 9 kDa subunit of the Anaphase-Promoting Complex/Cyclosome (APC/C) Ub ligase, which mediates the degradation of mitotic regulators and other proteins (121-123).

We show here that both Cog1 and Hcn1 contain Ac/N-degrons. We also show, using the subunit decoy technique, that the Ac/N-degrons of Cog1 and Hcn1 are regulated through the formation of complexes between these proteins and their cognate protein ligands. These results constitute the first evidence for the physiologically relevant conditionality of Ac/N-degrons and for the steric shielding basis of this conditionality. In addition, these advances clarify, in hindsight, the cause of the long-held assumption (before the discovery of Ac/N-degrons) that Nt-acetylation protects intracellular proteins from degradation. Specifically, many Nt-acetylated proteins appeared to be long-lived, a correct but incomplete conclusion. The new understanding is two-fold. First, the Nt-acetylation of a protein creates an Ac/N-degron while precluding the targeting of this protein by proteolytic systems (e.g., the Arg/N-end rule pathway) that require the unmodified N-terminus. Second,

those Nt-acetylated proteins that become long-lived enter this state after cessation of their initial degradation by the Ac/N-end rule pathway.

RESULTS

The Ac/N-Degron of Cog1, a Subunit of the COG Complex

S. cerevisiae Cog1 is Nt-acetylated (86). Independent evidence for Nt-acetylation of Cog1 is described below. The encoded Met-Asp (MD) N-terminal sequence of wild-type (wt) Cog1, termed MD-Cog1^{wt}, implied that its (retained) N-terminal Met is Nt-acetylated by the NatB Nt-acetylase (Figure S2B-D). MD-Cog1^{wt} was expressed in *S. cerevisiae* using low copy plasmids, the P_{CUP1} promoter, and C-terminal epitope tagging.

Cycloheximide (CHX)-chases showed that MD-Cog1^{wt} was short-lived in wt cells ($t_{1/2}$ << 1 hr) (Figure 1A, lanes 1-3). MD-Cog1^{wt} remained short-lived in *doa10Δ* cells lacking the Doa10 E3 Ub ligase, one of the E3s (see below) that target Ac/N-degrons (Figure 1A, lanes 1-3, 7-9, Figure S3A, and Figure S5D, E). In agreement with the presence of an Ac/N-degron in MD-Cog1^{wt}, it was stabilized, including its increased levels at time zero (the beginning of the chase) in *naa20Δ* (*nat3Δ*) cells, which lacked the catalytic subunit of the cognate NatB Nt-acetylase (Figures S2D and S3A, lanes 7-9 vs. lanes 1-3; Figure S3C, lanes 7-9 vs. lanes 1-6, 10-15; and Figure S3G, lanes 4-6 vs. lanes 1-3). In contrast, the instability of MD-Cog1^{wt} did not require the non-cognate Nt-acetylases NatA, NatC or NatD (Figures S2C, D and S3C, lanes 7-9 vs. lanes 1-6, 10-15).

A CHX-chase monitors the degradation of both “young” and “old” protein molecules. ^{35}S-pulse-chases were used to analyze newly formed Cog1. In agreement with CHX-chases, MD-Cog1^{wt} was short-lived in wt and *doa10Δ* cells ($t_{1/2} \approx 10$ min) but was nearly completely stabilized in *naa20Δ* cells lacking the NatB Nt-acetylase (Figures S2D and 1B, lanes 1-3, 7-9; Figure 1C, lanes 1-4 vs. lanes 9-12; and Figure 1D).

We also constructed the MK-Cog1^{D2K} and P-Cog1 mutants. In MK-Cog1^{D2K}, wt Asp^2 (Figure S2B) was replaced by Lys. In P-Cog1, the Pro residue was inserted before Asp^2. The N-terminal sequences of mutant proteins were Met-Lys (MK) and Pro-Asp (PD), respectively, the latter after the cotranslational removal of N-terminal Met. It has been shown that either N-terminal Pro followed by any residue or N-terminal Met followed by a basic residue are not Nt-acetylated in *S. cerevisiae* (Figure S2C) (86,124). In agreement with the presence of an Ac/N-degron in MD-Cog1^{wt}, the non-Nt-acetylatable MK-Cog1^{D2K} and P-Cog1^{D2P} were stabilized in CHX-chases compared to MD-Cog1^{wt}, including their increased levels at time zero (the beginning of the chase) (Figure 1A, lanes 4-6 vs. lanes 1-3; and Figure S3B, lanes 4-6 vs. lanes 1-3). The non-Nt-acetylatable P-Cog1^{D2P} was also stabilized in ^{35}S-pulse-chases, in comparison to MD-Cog1^{wt} (Figure 1B, lanes 4-6 vs. lanes 1-3, Figure 1C, lanes 5-8, vs. lanes 1-4, and Figure 1D).

The bulk of MD-Cog1^{wt} degradation was mediated by the proteasome, as shown using either *pdr5Δ S. cerevisiae*, which allowed for the intracellular retention of MG132, a proteasome inhibitor (Figure S3D, lanes 1 vs. 2, and Figure S3E), or through a CHX-chase of MD-Cog1^{wt} in wt cells made permeable to MG132 by low

levels of SDS (Figure S3G). In contrast, phenylmethanesulfonyl fluoride (PMSF), a serine protease inhibitor, had no significant effect on the levels of MD-Cog1^{wt} (Figure S3D, lanes 3 vs. 4, and Figure S3F).

MD-Cog1^{wt} was also examined using the temperature-sensitive *uba1-204* allele of the Uba1 Ub-activating (E1) enzyme (125). MD-Cog1^{wt} was short-lived in wt and *uba1-204* cells at 30°C and remained short-lived in wt cells at the nonpermissive temperature of 37°C (Figure S3H, lanes 1-9). In contrast, MD-Cog1^{wt} was stabilized at 37°C in *uba1-204* cells, including its increased levels at time zero (Figure S3H, lanes 10-12 vs. lanes 1-9). Thus, the degradation of MD-Cog1^{wt} requires ubiquitylation, most likely of MD-Cog1^{wt} itself.

Antibody Specific for Nt-Acetylated Cog1

Ac-MDEVLPLFRDS, the Nt-acetylated N-terminal peptide of MD-Cog1^{wt}, was used to produce a rabbit antibody, termed anti-Cog1^{AcNt}, that recognized Ac-MDEVLPLFRDS but not the unacetylated peptide (Figure S4A-C). This antibody detected Nt-acetylated MD-Cog1^{wt} in extracts from wt cells either at the beginning of the CHX-chase (Figure 1E, lane 1) or under steady-state conditions (Figure S4B, lane 1). In contrast, anti-Cog1^{AcNt} detected, at most, trace amounts of MD-Cog1^{wt} in otherwise identical extracts from *naa20Δ* (*nat3Δ*) cells lacking the cognate NatB Nt-acetylase (Figure 1E, lane 1 vs. lane 7), thereby providing independent (immunological) confirmation of the earlier mass spectrometric evidence (86) for Nt-acetylation of MD-Cog1^{wt} in wt cells. The same immunoblot re-probed with anti-flag antibody revealed comparable levels of MD-Cog1^{wt} (C-terminally tagged with 3

flag epitopes) in both wt and *naa20Δ* cells at the beginning of CHX-chase, thereby confirming the specificity of anti-Cog1^{AcNt} for Nt-acetylated MD-Cog1^{wt} (Figure 1F, lanes 1, 7 vs. Figure 1E, lanes 1, 7). In agreement with previously cited chases (Figures 1A-D and S3A-C), MD-Cog1^{wt} was short-lived in wt cells but was stabilized in *naa20Δ* cells (Figure 1E, F, lanes 1-3 vs. lanes 7-9, and Figure 1G, H), whereas P-Cog1 was almost completely stable under all conditions (Figure 1E, F, lanes 4-6 vs. lanes 1-3, and Figure 1H).

Together, CHX-chases, ^{35}S-pulse-chases, and anti-Cog1^{AcNt} results with wt versus mutant *S. cerevisiae* and with mutants of MD-Cog1^{wt} (Figures 1, S3, and S4A-C) identified this subunit of the COG complex as a short-lived substrate of the Ac/N-end rule pathway, which targets the Ac/N-degron of MD-Cog1^{wt}.

Cog1 Interactions with Other COG Subunits and Membranes In the Absence of Nt-Acetylation

The targeting of some cytosolic proteins, such as Arl3, to the Golgi membrane requires their Nt-acetyl group (126). Cog1 contributes to interactions of the COG complex with the Golgi membrane (117,118). In a test that did not distinguish between Golgi and other membranes, cell extracts were fractionated into soluble ("cytosol") and insoluble ("membrane") parts. The absence of Nt-acetylation of MD-Cog1^{wt} in *naa20Δ* cells did not affect its partitioning between membrane and soluble fractions (Figure S4D-E).

Schulman and colleagues showed that the Nt-acetyl moiety can significantly contribute to the affinity between an Nt-acetylated protein and its protein ligand

(90,127). We used anti-flag to immunoprecipitate the C-terminally triple-flagged MD-Cog1^{wt} from extracts of cells that co-expressed the C-terminally ha-tagged Cog3$_{ha}$ or Cog4$_{ha}$. Both Cog3$_{ha}$ and Cog4$_{ha}$ were coimmunoprecipitated with MD-Cog1^{wt} from wt and *naa20Δ* extracts (Figure S4G, H). We conclude that Nt-acetylation of MD-Cog1^{wt} is not strictly required for its direct or indirect interactions with Cog3 and Cog4, i.e., a possibly lower affinity of unacetylated MD-Cog1^{wt} (in *naa20Δ* cells) for its protein ligands was still sufficient for coimmunoprecipitation.

Interestingly, the apparent M_r of the 93-kDa Cog3 was increased by ~8 kDa either in *naa20Δ* cells lacking the NatB Nt-acetylase or in the absence of overexpressed MD-Cog1^{wt}. The upshifted Cog3 also coimmunoprecipitated with MD-Cog1^{wt} (Figure S4G, lane 1 vs. lane 2, lane 5 vs. lane 6). This increase in M_r is consistent with, e.g., monoubiquitylation of Cog3 under the above conditions. There are no data about Nt-acetylation of COG subunits other than MD-Cog1^{wt}. All of these subunits, save for Cog3, are expected to be Nt-acetylated in wt cells (Figure S2B, C).

Ac/N-Degrons Are Recognized by More Than One Ubiquitin Ligase

MD-Cog1^{wt}, whose degradation is Ub-dependent (Figure S3H), was not stabilized in cells lacking the Doa10 E3, an N-recognin of the Ac/N-end rule pathway (Figure 1A, lanes 1-3, 7-9; Figure 1B, lanes 1-3, 7-9; Figure S1A; Figure S3A, lanes 1-6; and Figure S5D, lanes 1-6). In agreement with these results, MD-Cog1^{wt} was also not stabilized in the *ubc6Δ ubc7Δ* double-mutant cells lacking cognate E2s of the Doa10 E3 (Figure S5F, G). In addition, MD-Cog1^{wt} was not stabilized in null mutants

of nine other E2s (Figure S5A-C). Examination of *ubr1Δ* and *san1Δ* cells lacking, respectively, the E3 N-recognin of the Arg/N-end rule pathway (Figure S1B) and a nuclear E3 mediating the degradation of misfolded proteins (113), yielded similar results (Figure S5D, E).

The affinity of the Doa10 N-recognin for Nt-acetylated peptides involves largely their Nt-acetyl moiety and is less dependent on the side chain of the N-terminal residue (95). Therefore it is likely that Doa10 can recognize Nt-acetylated MD-Cog1^{wt} but may not be able to efficaciously target its Ac/N-degron. Similarly to other N-degrons, an Ac/N-degron of a protein is expected to be at least tripartite, with its other determinants being a "ubiquitylatable" internal lysine and a disordered chain segment (96). In sum, an unknown E3 N-recognin (*S. cerevisiae* genome encodes more than 150 E3s) targets the Ac/N-degron of MD-Cog1^{wt} either by itself or redundantly with Doa10.

Endogenous Cog1 Is Long-Lived

In experiments described so far, MD-Cog1^{wt} was moderately overexpressed from a low copy plasmid and the P_{CUP1} promoter (Figures 1 and S3-S5). We also replaced, through in vivo recombination, the chromosomal *COG1* with an otherwise identical DNA segment that expressed the C-terminally triply ha-tagged MD-Cog1^{wt} (MD-Cog1$^{wt}_{3ha}$) from the endogenous P_{COG1} promoter. Remarkably, in cells expressing solely the endogenous MD-Cog1$^{wt}_{3ha}$ at its wt levels, it was much more stable than the triply flag-tagged MD-Cog1$^{wt}_{3f}$ overexpressed from the P_{CUP1} promoter. Specifically, less than 10% of the endogenous MD-Cog1$^{wt}_{3ha}$ was degraded during 2 hrs of CHX-

chase, in contrast to degradation of nearly all overexpressed MD-Cog1$^{wt}_{3f}$ (Figure 2A vs., for example, Figure 1A, lanes 1-3, or Figure 1F, lanes 1-3). In addition, the metabolic stability of endogenous MD-Cog1$^{wt}_{3ha}$ remained unaltered in *naa20Δ* cells lacking the cognate NatB Nt-acetylase, in contrast to a strong stabilization of the (short-lived) overexpressed MD-Cog1$^{wt}_{3f}$ in the absence of NatB (Figure 2A vs. Figures 1C, S3A, and S3C).

Short-Lived Cog1 Is Stabilized by Coexpression of Cog2-Cog4

Both the conjectured conditionality of Ac/N-degrons (95) and electron microscopy of the yeast Cog1-Cog4 subcomplex (Figure S1D) (120) suggested that the Ac/N-degron of MD-Cog1^{wt} may be at least partially sequestered in the subcomplex. In agreement with this possibility, the striking dichotomy between the Ac/N-degron-mediated degradation of overexpressed MD-Cog1^{wt} and the stability of non-overexpressed, endogenous MD-Cog1^{wt} (Figures 1 and S2A-C vs. Figure 2A) suggested an involvement, in the latter case, of other COG subunits.

Cog2 and Cog3 are direct binding ligands of MD-Cog1^{wt} (117). We asked whether the short-lived, moderately overexpressed (from the P$_{CUP1}$ promoter on a low copy plasmid) MD-Cog1$^{wt}_{3f}$ could be stabilized by expressing, from the galactose-inducible P$_{GAL1\text{-}10}$ promoter on a high copy plasmid, the COG subunits Cog2, Cog3 and Cog4. Indeed, the short-lived MD-Cog1$^{wt}_{3f}$ was strongly stabilized by coexpression of either Cog2 and Cog3 or of Cog2, Cog3 and Cog4 (Figure 2B, lanes 1-3 vs. lanes 4-6; Figure 2C, lanes 1-3 vs. lanes 4-6; and Figure 2D, E). We conclude

that the Ac/N-degron of MD-Cog1^{wt} is conditional in a physiologically relevant manner (see Discussion).

Subunit Decoy Technique Reveals the Cause of Stability of Endogenous Cog1

The above results suggested that the stability of endogenous MD-Cog1^{wt} (Figure 2A) stems from sequestration of its Ac/N-degron by other COG subunits during the assembly of the degradation-resistant COG complex. We addressed this possibility by an approach termed the subunit decoy technique. First, a C-terminally epitope-tagged protein of interest is expressed at its endogenous level from its native chromosomal location and transcriptional promoter. Second, the same protein but C-terminally tagged with an alternative epitope is also expressed in these cells (Figure 3A).

In one design of the subunit decoy experiment, cells expressing wt levels of MD-Cog1$^{wt}_{13myc}$ (C-terminally tagged with 13 myc epitopes) from the chromosomal *COG1* locus were transformed either with a vector alone or with a plasmid expressing the otherwise identical MD-Cog1$^{wt}_{3f}$ (C-terminally tagged with 3 flag epitopes) from the constitutive P$_{ADH1}$ promoter (Figure 3A). Remarkably, whereas the endogenous MD-Cog1$^{wt}_{13myc}$ was stable in the absence of ectopically expressed MD-Cog1$^{wt}_{3f}$, the same endogenous MD-Cog1$^{wt}_{13myc}$ became a short-lived protein in the presence of the (also short-lived) MD-Cog1$^{wt}_{3f}$ (Figure 3A, B). In a different design of the subunit decoy experiment, cells expressing wt levels of MD-Cog1$^{wt}_{3ha}$ (C-terminally tagged with 3 ha epitopes) from the chromosomal *COG1* locus were transformed with a plasmid expressing the otherwise identical MD-Cog1$^{wt}_{3f}$ from the

galactose-inducible P_{GAL1} promoter. In glucose medium, where MD-Cog1$^{wt}_{3f}$ was not expressed, the endogenous MD-Cog1$^{wt}_{3ha}$ was long-lived ($t_{1/2}$ >> 1 hr), as evidenced by its stability in a CHX-chase and the absence of a significant change in *naa20Δ* cells lacking the cognate NatB Nt-acetylase (Figure 3C, F). In striking contrast, the same endogenous MD-Cog1$^{wt}_{3ha}$ became short-lived ($t_{1/2}$ << 30 min) in the presence of galactose, which induced MD-Cog1$^{wt}_{3f}$ (Figure 3C-F). The conditional sequestration model of Ac/N-degrons predicts the observed destabilization of endogenous MD-Cog1^{wt} under these conditions (see Discussion).

The Ac/N-Degron of Hcn1, a Subunit of the APC/C Ubiquitin Ligase

In the crystal structure, by Barford and colleagues, of the complex between the APC/C subunits Hcn1 and Cut9 of the yeast *Schizosaccharomyces pombe* (128), the Nt-acetylated Met residue of Hcn1 was found to be enclosed within a chamber of the folded Cut9 subunit (Figure S1C). (128) interpreted this result as a possible example of the sequestration of Ac/N-degrons proposed by (95).

The encoded Met-Leu (ML) N-terminal sequence of the 9-kDa wt Hcn1, termed ML-Hcn1^{wt}, implied that its (retained) N-terminal Met was Nt-acetylated by the NatC Nt-acetylase (Figure S2C). ML-Hcn1^{wt} was C-terminally tagged with 3 flag epitopes and expressed in *S. cerevisiae* from the P_{CUP1} promoter. As determined using both CHX-chases and ^{35}S-pulse-chases, ML-Hcn1^{wt} was indeed short-lived in wt cells, with $t_{1/2}$ < 40 min in the CHX-chase (Figure 4A, lanes 1-3) and $t_{1/2}$ of ~10 min in the ^{35}S-pulse-chase (Figure 4C, lanes 1-3, and Figure 4D). In contrast, ML-Hcn1^{wt} was virtually completely stabilized in *naa30Δ* (*mak3Δ*) cells lacking the

catalytic subunit of the cognate NatC Nt-acetylase (Figure 4A, lanes 1-3 vs. lanes 4-6; Figure 4C, lanes 1-3 vs. lanes 4-6; and Figure 4D). We conclude that the degradation of ML-Hcn1^{wt} is mediated by its Ac/N-degron.

We also asked whether Cdc26, the *S. cerevisiae* counterpart of *S. pombe* Hcn1, contained an Ac/N-degron. Its N-terminal sequence being Met-Ile, Cdc26 is a substrate of the NatC Nt-acetylase (Figure S2C). Cdc26 was indeed unstable in wt cells but was nearly completely stabilized in *naa30Δ* (*mak3Δ*) cells, in addition to an increase of its zero-time level (Figure 4B, lanes 1-3 vs. lanes 4-6).

Coexpression of Cut9 with Hcn1 Represses the Ac/N-degron of Hcn1

Given the sequestration of the Nt-acetylated Met of ML-Hcn1^{wt} in a cleft of Cut9 (Figure S1C), and the demonstrated degradation of ML-Hcn1^{wt} (in the absence of Cut9) by the Ac/N-end rule pathway (Figure 4), we asked whether coexpression of Cut9 would inhibit the degradation of ML-Hcn1^{wt}. Several independent CHX-chase assays have shown that the short-lived ML-Hcn1^{wt} was virtually completely stabilized by Cut9 upon its overexpression from the galactose-inducible P_{GAL1} promoter (Figure 4E, F). These results were analogous to the metabolic stabilization of the short-lived MD-Cog1^{wt} by its coexpressed ligands Cog2-Cog4 (Figure 2A-E), except that the inhibition of the degradation of ML-Hcn1^{wt} by Cut9 (Figure 4E, F) can now be understood at near-atomic resolution, owing to the crystal structure of the Hcn1-Cut9 complex (Figure S1C) (128).

DISCUSSION

The discovery of the Ac/N-end rule pathway and Ac/N-degrons (Figure S1A) (95) has revealed the largest class of degradation signals in the proteome, as nearly 90% of human proteins are Nt-acetylated. Because most proteins acquire Ac/N-degrons cotranslationally, the bulk of these degradation signals would be expected to be rapidly (and reversibly) repressed, as many proteins are long-lived in vivo. Given the exceptional prevalence of Ac/N-degrons, they would be likely to underlie processes that encompass the bulk of the proteome, for example, the control of protein quality, including the regulation of input stoichiometries of subunits in oligomeric proteins. Until now, these were merely suggestions about possible biological roles of Ac/N-degrons, made upon the discovery of the Ac/N-end rule pathway (95).

To address the functions of Ac/N-degrons, we chose two unrelated natural Nt-acetylated proteins, Cog1 (MD-Cog1^{wt}) and Hcn1 (ML-Hcn1^{wt}), described in Introduction. CHX-chases and ^{35}S-pulse-chases with MD-Cog1^{wt} and its site-directed mutants expressed in wt or mutant *S. cerevisiae*, as well as the development of an antibody, anti-Cog1^{AcNt}, that selectively recognized Nt-acetylated MD-Cog1^{wt}, identified this subunit of the COG complex as a short-lived substrate of the Ac/N-end rule pathway (Figures 1 and S3-S5). Analogous experiments with ML-Hcn1^{wt} also showed it to be an unstable protein targeted through its Ac/N-degron (Figure 4). As discussed below, further analyses of MD-Cog1^{wt} and ML-Hcn1^{wt} showed that their Ac/N-degrons are regulated through the formation of complexes between these proteins and their cognate protein ligands. These mechanistically unambiguous

results (Figures 2-5) constitute the first evidence for the physiologically relevant conditionality of Ac/N-degrons and for the steric sequestration basis of this conditionality.

Being an *S. pombe* protein, ML-Hcn1^{wt} was not expected to have ligands in *S. cerevisiae* that might shield its Nt-acetylated Met and thereby repress its Ac/N-degron. The disposition was different with *S. cerevisiae* MD-Cog1^{wt}, in that some newly formed molecules of overexpressed MD-Cog1^{wt} were expected to associate with Cog1-binding subunits of the COG complex and thereby possibly repress, through steric shielding, the Ac/N-degron of MD-Cog1^{wt}. However, a majority of newly formed molecules of overexpressed MD-Cog1^{wt} would be unable to experience such a fate, as they would "run out" of cognate COG protein ligands to bind to. If so, overexpressed MD-Cog1^{wt} and ML-Hcn1^{wt} would be expected to be stabilized by coexpression of their cognate protein ligands.

Indeed, a short-lived, overexpressed MD-Cog1^{wt} became a long-lived protein when Cog2 and Cog3 (direct ligands of Cog1) or Cog2, Cog3 and Cog4 were coexpressed (Figure 2B-E). Analogously, the short-lived ML-Hcn1^{wt} was stabilized upon coexpression of its cognate ligand Cut9 (Figure 4E, F). Thus, the Ac/N-degrons of MD-Cog1^{wt} and ML-Hcn1^{wt} are conditional in a physiologically relevant manner, as they can be repressed through the availability of the previously demonstrated physical interactions between these proteins and their protein ligands.

When MD-Cog1^{wt} was expressed at wt levels and in the absence of other versions of Cog1 in the cell, it was found to be long-lived, in striking contrast to overexpressed MD-Cog1^{wt}, the bulk of which was degraded through the Ac/N-

degron (Figure 1A, lanes 1-3 vs. Figure 2A). This finding, one of several key insights of the present work, provided a new explanation for earlier observations, by a number of studies over many years (for example, (129)), that most Nt-acetylated proteins appeared to be long-lived. These – correct but incomplete – observations were a major cause of the long-held assumption (before the discovery of Ac/N-degrons) that Nt-acetylation protects intracellular proteins from degradation. To the contrary, the clear-cut existence of Ac/N-degrons, their exceptionally high prevalence in the proteome (95), and the results of this study (Figures 1-5, S1-S5) indicated a different view of the observed stability of Nt-acetylated proteins. Specifically, those Nt-acetylated proteins that become long-lived do so after cessation of their initial degradation by the Ac/N-end rule pathway. The initial destruction of a fraction of a newly formed protein containing an Ac/N-degron, before this degron is repressed through protein interactions, can be transient enough to be overlooked in conventional degradation assays.

This understanding was further advanced by an approach we termed the subunit decoy technique, in which a C-terminally epitope-tagged protein is expressed at its wt level in the absence or presence of the same protein that is alternatively tagged and overexpressed (Figure 3). A subunit decoy assay is employed when, for example, an epitope-tagged protein is overexpressed in the presence of an endogenous (and experimentally distinguishable) version of the same protein. Over the last two decades, it was occasionally reported that an overexpressed protein diminishes the expression of its endogenous counterpart,

and that this repression is often posttranscriptional, i.e., it can involve protein degradation, through unknown degrons (e.g., (130)).

Our subunit decoy experiments provided a direct, mechanistically explicit explanation of this phenomenon in the context of Ac/N-degrons and thereby completed the explanation of why a protein (e.g., MD-Cog1^{wt}) expressed at wt levels can be long-lived while the same but overexpressed protein is metabolically unstable (Figure 1A, lanes 1-3 vs. Figure 2A). Specifically, when the C-terminally ha-tagged, long-lived endogenous MD-Cog1$^{wt}_{3ha}$ was expressed in the presence of the otherwise identical but flag-tagged and overexpressed MD-Cog1$^{wt}_{3f}$ decoy, the previously stable MD-Cog1$^{wt}_{3ha}$ became short-lived (Figure 3). The conditional sequestration model of Ac/N-degrons predicts this outcome. Specifically, endogenous (i.e., sufficiently low) expression levels of MD-Cog1$^{wt}_{3ha}$ would be comparable to the endogenous levels of protective subunits of the COG complex such as Cog2 and Cog3. As a result, most (though not necessarily all) molecules of newly formed MD-Cog1$^{wt}_{3ha}$ escape the degradation by the Ac/N-end rule pathway through the formation of complexes with other COG subunits that shield the Ac/N-degron of MD-Cog1$^{wt}_{3ha}$. In contrast, the "additional" expression of the MD-Cog1$^{wt}_{3f}$ decoy results in total levels of MD-Cog1^{wt} that outstrip the supply of endogenous Cog1-binding subunits of the COG complex. Consequently, most newly formed molecules of MD-Cog1$^{wt}_{3ha}$ are no longer forming protected COG-based complexes and therefore remain short-lived, alongside the also short-lived molecules of the MD-Cog1$^{wt}_{3f}$ decoy (Figure 3).

The subunit decoy experiments produced yet another insight. Specifically, it was the bulk (not just a small subset) of the endogenous MD-Cog1$^{wt}_{3ha}$ that was destabilized by the coexpression of the MD-Cog1$^{wt}_{3f}$ decoy (Figure 3). In other words, this destabilization of MD-Cog1$^{wt}_{3ha}$ included its older molecules that were the long-lived components of the COG complex, before the expression of the MD-Cog1$^{wt}_{3f}$ decoy. While a detailed understanding of this effect must await further studies, these findings implied that the COG complex is dynamic in vivo, with dissociations-reassociations of COG subunits (on the scale of minutes or less) that repeatedly "expose" the Ac/N-degron of MD-Cog1$^{wt}_{3ha}$. The fact that endogenous MD-Cog1$^{wt}_{3ha}$ is relatively long-lived in the absence of the MD-Cog1$^{wt}_{3f}$ decoy (Figure 3) implies a physiologically significant but low (in absolute terms) probability of destruction of MD-Cog1$^{wt}_{3ha}$ upon a single cycle of its transient (and rapidly reversed) dissociation from the COG complex. In contrast, dissociation of the COG complex in the presence of the coexpressed MD-Cog1$^{wt}_{3f}$ decoy would prevent, through competition, an efficacious re-incorporation of MD-Cog1$^{wt}_{3ha}$ into the reassembled COG complex, thereby greatly increasing the probability of destruction of the "orphaned" (competed out) MD-Cog1$^{wt}_{3ha}$ by the Ac/N-end rule pathway (Figure 3).

Expression levels of subunits that comprise a protein complex are adjusted, on evolutionary timescales, to be roughly stoichiometric. The additional, fine-tuning and homeostatic control of subunit stoichiometries is mediated by selective and conditional protein degradation of the kind dissected in the present study using MD-Cog1^{wt} and ML-Hcn1^{wt}. For example, we showed that the Ac/N-degron of ML-Hcn1^{wt}, a subunit of the APC/C Ub ligase, is repressed by Cut9, another subunit of

APC/C that binds to ML-Hcn1^{wt} and sterically shields its Nt-acetylated Met residue (Figures 4 and S1C) (128). The resulting regulatory circuit, summarized in Figure 5 and mediated by Ac/N-degrons, is mechanistically straightforward. As discussed above in the context of Cog1 and Hcn1, this mechanism can underlie the degradation-mediated control of input stoichiometries of subunits in oligomeric proteins. This mechanism can also mediate the destruction of misfolded or otherwise abnormal proteins whose cotranslationally formed Ac/N-degrons do not become shielded soon enough.

One setting in which the control, by the Ac/N-end rule pathway and Ac/N-degrons, of the input stoichiometries of protein subunits may prove to be particularly significant physiologically is aneuploidy, in which the chromosome number in a cell is not an exact multiple of the haploid number. Aneuploidy is often encountered in natural cell populations, from *S. cerevisiae* to human cells, including human cancers and birth defects such as the Down syndrome. Physiological defects in aneuploid cells are caused, at least in part, by maladaptive molar ratios of newly formed proteins in such cells, given their deviations from normal gene dosages. Homeostatic responses in aneuploid cells would have to destroy a higher than normal load of unassembled protein subunits. This may account for the known hypersensitivity of these cells to proteasome inhibitors (131). Now that the conditionality of Ac/N-degrons (Figure 5) is no longer a conjecture, it should be possible to determine, using, for example, the in vivo dynamics of Cog1 and other subunits of the COG complex as reporter proteins (Figures 1-3), whether the Ac/N-

end rule pathway plays a major role in homeostatic responses that compensate, through selective proteolysis, for protein subunit misbalances in aneuploid cells.

The Nt-acetyl group at protein N-termini contributes to the physical affinities between specific subunits in oligomeric proteins (90,127,128). It would be important to determine, therefore, whether the striking prevalence of Ac/N-degrons (nearly 90% of human proteins are Nt-acetylated (see Introduction)) has resulted, on evolutionary timescales, largely from adaptive (fitness-increasing) effects of these degrons, as distinguished, for example, from adaptive effects of Nt-acetylation on the strengthening of specific protein-protein interactions, irrespective of proteolysis. The function of the Nt-acetyl group as a key determinant of Ac/N-degrons is compatible with other aspects of Nt-acetylation, including its contributions to protein-membrane interactions, to physical affinities between specific proteins, and to the negative regulation of protein translocation into the endoplasmic reticulum ((90,126,132) and references therein).

Some protein complexes are formed cotranslationally, i.e., a specific subunit of a (future) complex can interact with its protein ligands while being a ribosome-associated nascent polypeptide chain ((106,107), and references therein). The metabolic stability of such a subunit is strongly decreased in the absence of its protein ligand (106). Because most proteins acquire their Ac/N-degrons cotranslationally (95), the conditional degradation of subunits in cotranslationally assembling complexes may involve Ac/N-degrons. This proposition can now be addressed experimentally, either though analyses of Ac/N-degrons in previously

characterized complexes of this class (106) or by determining whether the assembly of the COG complex of the present work occurs cotranslationally.

Either “soluble” or transmembrane proteins that enter the endoplasmic reticulum (ER) can be retrotranslocated to the cytosol and destroyed if these proteins are recognized as abnormal and acted upon by a quality control system termed the ER-associated degradation (ERAD) (110,111). The ER-embedded transmembrane Doa10 E3 Ub ligase is one N-recognin of the Ac/N-end rule pathway and also, at the same time, an E3 that mediates ERAD. Given this remarkable dichotomy, it is possible and indeed likely that Ac/N-degrons and the Ac/N-end rule pathway are a part of ERAD as well, a verifiable proposition. In conjunction with the initial discovery of the Ac/N-degrons (95), the present study of Cog1 and Hcn1 opened up a number of experimental strategies for further advances in the functional understanding of the Ac/N-end rule pathway.

EXPERIMENTAL PROCEDURES

Yeast Strains, Plasmids, and Genetic Techniques

Tables S1 and S2 describe *S. cerevisiae* strains and plasmids used in this study. Standard techniques were employed for strain and plasmid construction.

Cycloheximide-Chase and ^{35}S-Pulse-Chase Degradation Assays

These assays were carried out largely as described (95,133). The Odyssey near-infrared scanner (Li-Cor) was used for visualizing secondary antibodies and for quantifying specific protein bands. Quantification of ^{35}S-pulse-chases was carried out using Storm PhosphorImager and ImageQuant (GE Healthcare).

Antibody Specific for N-Terminally Acetylated Cog1

The Nt-acetylated synthetic peptide AcMDEVLPLFRDSC and its unacetylated counterpart MDEVLPLFRDSC were produced by Abgent (San Diego, CA). Details of the production and characterization of the anti-Cog1^{AcNt} antibody are described in the legend to Figure S4A-C and in Extended Experimental Procedures.

Coimmunoprecipitation of Cog1 with Cog2-Cog4

S. cerevisiae coexpressing flag-tagged MD-Cog1^{wt} and either Cog3 or Cog4 (ha-tagged) were lysed, and clarified extracts were subjected to immunoprecipitation using anti-flag magnetic beads. The immunoprecipitates were analyzed by SDS-PAGE and immunoblotting.

SUPPLEMENTAL INFORMATION

Supplemental Information includes Extended Experimental Procedures, five figures, and two tables.

ACKNOWLEDGMENTS

We thank R. Deshaies and K. Gould for gifts of plasmids. We are grateful to the present and former members of the Varshavsky laboratory for their assistance and advice. This work was supported by grants to C.-S.H. from the National Research Foundation of Korea (NRF-2011-0021975) and the Korea Healthcare technology R&D Project (A111324), and to A.V. from the National Institutes of Health (DK039520, GM031530 and GM085371).

REFERENCES

1. Varshavsky, A. (2011) *Protein science : a publication of the Protein Society*
2. Ang, X. L., and Wade Harper, J. (2005) *Oncogene* **24**, 2860-2870
3. Finley, D., Ulrich, H. D., Sommer, T., and Kaiser, P. (2012) *Genetics* **192**, 319-360
4. Varshavsky, A. (2006) *Protein science : a publication of the Protein Society* **15**, 647-654
5. Varshavsky, A. (1991) *Cell* **64**, 13-15
6. Finley, D. (2009) *Annual review of biochemistry* **78**, 477-513
7. Kravtsova-Ivantsiv, Y., and Ciechanover, A. (2012) *Journal of cell science* **125**, 539-548
8. Hochstrasser, M. (2006) *Cell* **124**, 27-34
9. Kulathu, Y., and Komander, D. (2012) *Nature reviews. Molecular cell biology* **13**, 508-523
10. Behrends, C., and Harper, J. W. (2011) *Nature structural & molecular biology* **18**, 520-528
11. Gallastegui, N., and Groll, M. (2010) *Trends in biochemical sciences* **35**, 634-642
12. Marques, A. J., Palanimurugan, R., Matias, A. C., Ramos, P. C., and Dohmen, R. J. (2009) *Chemical reviews* **109**, 1509-1536
13. Xie, Y., and Varshavsky, A. (2000) *Proceedings of the National Academy of Sciences of the United States of America* **97**, 2497-2502

14. Metzger, M. B., Hristova, V. A., and Weissman, A. M. (2012) *Journal of cell science* **125**, 531-537

15. Deshaies, R. J., and Joazeiro, C. A. (2009) *Annual review of biochemistry* **78**, 399-434

16. Rotin, D., and Kumar, S. (2009) *Nature reviews. Molecular cell biology* **10**, 398-409

17. Bachmair, A., Finley, D., and Varshavsky, A. (1986) *Science* **234**, 179-186

18. Bachmair, A., and Varshavsky, A. (1989) *Cell* **56**, 1019-1032

19. Varshavsky, A., Bachmair, A., and Finley, D. (1987) *Biochemical Society transactions* **15**, 815-816

20. Varshavsky, A., Bachmair, A., Finley, D., Gonda, D. K., and Wunning, I. (1989) *Biotechnology* **13**, 109-143

21. Varshavsky, A. (2004) *Current biology : CB* **14**, R181-183

22. Choi, W. S., Jeong, B. C., Joo, Y. J., Lee, M. R., Kim, J., Eck, M. J., and Song, H. K. (2010) *Nature structural & molecular biology* **17**, 1175-1181

23. Matta-Camacho, E., Kozlov, G., Li, F. F., and Gehring, K. (2010) *Nature structural & molecular biology* **17**, 1182-1187

24. Tasaki, T., and Kwon, Y. T. (2007) *Trends in biochemical sciences* **32**, 520-528

25. Xia, Z., Webster, A., Du, F., Piatkov, K., Ghislain, M., and Varshavsky, A. (2008) *The Journal of biological chemistry* **283**, 24011-24028

26. Hu, R. G., Brower, C. S., Wang, H., Davydov, I. V., Sheng, J., Zhou, J., Kwon, Y. T., and Varshavsky, A. (2006) *The Journal of biological chemistry* **281**, 32559-32573

27. Wang, H., Piatkov, K. I., Brower, C. S., and Varshavsky, A. (2009) *Molecular cell* **34**, 686-695

28. Hu, R. G., Sheng, J., Qi, X., Xu, Z., Takahashi, T. T., and Varshavsky, A. (2005) *Nature* **437**, 981-986

29. Xia, Z., Turner, G. C., Hwang, C. S., Byrd, C., and Varshavsky, A. (2008) *The Journal of biological chemistry* **283**, 28958-28968

30. Du, F., Navarro-Garcia, F., Xia, Z., Tasaki, T., and Varshavsky, A. (2002) *Proceedings of the National Academy of Sciences of the United States of America* **99**, 14110-14115

31. Dohmen, R. J., Madura, K., Bartel, B., and Varshavsky, A. (1991) *Proceedings of the National Academy of Sciences of the United States of America* **88**, 7351-7355

32. Hwang, C. S., Shemorry, A., Auerbach, D., and Varshavsky, A. (2010) *Nature cell biology* **12**, 1177-1185

33. Hwang, C. S., Shemorry, A., and Varshavsky, A. (2009) *Proceedings of the National Academy of Sciences of the United States of America* **106**, 2142-2147

34. Johnson, E. S., Ma, P. C., Ota, I. M., and Varshavsky, A. (1995) *The Journal of biological chemistry* **270**, 17442-17456

35. Johnson, E. S., Bartel, B., Seufert, W., and Varshavsky, A. (1992) *The EMBO journal* **11**, 497-505

36. Park, Y., Yoon, S. K., and Yoon, J. B. (2009) *The Journal of biological chemistry* **284**, 1540-1549

37. Park, Y., Yoon, S. K., and Yoon, J. B. (2008) *Biochemical and biophysical research communications* **374**, 294-298

38. Hu, R. G., Wang, H., Xia, Z., and Varshavsky, A. (2008) *Proceedings of the National Academy of Sciences of the United States of America* **105**, 76-81

39. Varshavsky, A. (2008) *The Journal of biological chemistry* **283**, 34469-34489

40. Mogk, A., Schmidt, R., and Bukau, B. (2007) *Trends in cell biology* **17**, 165-172

41. Graciet, E., and Wellmer, F. (2010) *Trends in plant science* **15**, 447-453

42. An, J. Y., Seo, J. W., Tasaki, T., Lee, M. J., Varshavsky, A., and Kwon, Y. T. (2006) *Proceedings of the National Academy of Sciences of the United States of America* **103**, 6212-6217

43. Kwon, Y. T., Xia, Z., An, J. Y., Tasaki, T., Davydov, I. V., Seo, J. W., Sheng, J., Xie, Y., and Varshavsky, A. (2003) *Molecular and cellular biology* **23**, 8255-8271

44. Kwon, Y. T., Kashina, A. S., Davydov, I. V., Hu, R. G., An, J. Y., Seo, J. W., Du, F., and Varshavsky, A. (2002) *Science* **297**, 96-99

45. Kwon, Y. T., Xia, Z., Davydov, I. V., Lecker, S. H., and Varshavsky, A. (2001) *Molecular and cellular biology* **21**, 8007-8021

46. Kwon, Y. T., Balogh, S. A., Davydov, I. V., Kashina, A. S., Yoon, J. K., Xie, Y., Gaur, A., Hyde, L., Denenberg, V. H., and Varshavsky, A. (2000) *Molecular and cellular biology* **20**, 4135-4148

47. Hwang, C. S., and Varshavsky, A. (2008) *Proceedings of the National Academy of Sciences of the United States of America* **105**, 19188-19193

48. Brower, C. S., and Varshavsky, A. (2009) *PloS one* **4**, e7757

49. Graciet, E., Walter, F., Maoileidigh, D. O., Pollmann, S., Meyerowitz, E. M., Varshavsky, A., and Wellmer, F. (2009) *Proceedings of the National Academy of Sciences of the United States of America* **106**, 13618-13623

50. Eisele, F., and Wolf, D. H. (2008) *FEBS letters* **582**, 4143-4146

51. Heck, J. W., Cheung, S. K., and Hampton, R. Y. (2010) *Proceedings of the National Academy of Sciences of the United States of America* **107**, 1106-1111

52. Prasad, R., Kawaguchi, S., and Ng, D. T. (2010) *Molecular biology of the cell* **21**, 2117-2127

53. Nillegoda, N. B., Theodoraki, M. A., Mandal, A. K., Mayo, K. J., Ren, H. Y., Sultana, R., Wu, K., Johnson, J., Cyr, D. M., and Caplan, A. J. (2010) *Molecular biology of the cell* **21**, 2102-2116

54. Ouyang, Y., Kwon, Y. T., An, J. Y., Eller, D., Tsai, S. C., Diaz-Perez, S., Troke, J. J., Teitell, M. A., and Marahrens, Y. (2006) *Mutation research* **596**, 64-75

55. Yoshida, S., Ito, M., Callis, J., Nishida, I., and Watanabe, A. (2002) *The Plant journal : for cell and molecular biology* **32**, 129-137

56. Holman, T. J., Jones, P. D., Russell, L., Medhurst, A., Ubeda Tomas, S., Talloji, P., Marquez, J., Schmuths, H., Tung, S. A., Taylor, I., Footitt, S., Bachmair, A., Theodoulou, F. L., and Holdsworth, M. J. (2009) *Proceedings of the National Academy of Sciences of the United States of America* **106**, 4549-4554

57. Rai, R., Wong, C. C., Xu, T., Leu, N. A., Dong, D. W., Guo, C., McLaughlin, K. J., Yates, J. R., 3rd, and Kashina, A. (2008) *Development* **135**, 3881-3889

58. Zhang, F., Saha, S., Shabalina, S. A., and Kashina, A. (2010) *Science* **329**, 1534-1537

59. Kurosaka, S., Leu, N. A., Zhang, F., Bunte, R., Saha, S., Wang, J., Guo, C., He, W., and Kashina, A. (2010) *PLoS genetics* **6**, e1000878

60. Saha, S., Mundia, M. M., Zhang, F., Demers, R. W., Korobova, F., Svitkina, T., Perieteanu, A. A., Dawson, J. F., and Kashina, A. (2010) *Molecular biology of the cell* **21**, 1350-1361

61. de Groot, R. J., Rumenapf, T., Kuhn, R. J., Strauss, E. G., and Strauss, J. H. (1991) *Proceedings of the National Academy of Sciences of the United States of America* **88**, 8967-8971

62. Lloyd, A. G., Ng, Y. S., Muesing, M. A., Simon, V., and Mulder, L. C. (2007) *Virology* **360**, 129-135

63. Mulder, L. C., and Muesing, M. A. (2000) *The Journal of biological chemistry* **275**, 29749-29753

64. Lecker, S. H., Solomon, V., Price, S. R., Kwon, Y. T., Mitch, W. E., and Goldberg, A. L. (1999) *The Journal of clinical investigation* **104**, 1411-1420

65. Lecker, S. H., Solomon, V., Mitch, W. E., and Goldberg, A. L. (1999) *The Journal of nutrition* **129**, 227S-237S

66. Carpio, M. A., Lopez Sambrooks, C., Durand, E. S., and Hallak, M. E. (2010) *The Biochemical journal* **429**, 63-72

67. Zenker, M., Mayerle, J., Lerch, M. M., Tagariello, A., Zerres, K., Durie, P. R., Beier, M., Hulskamp, G., Guzman, C., Rehder, H., Beemer, F. A., Hamel, B., Vanlieferinghen, P., Gershoni-Baruch, R., Vieira, M. W., Dumic, M., Auslender, R., Gil-da-Silva-Lopes, V. L., Steinlicht, S., Rauh, M., Shalev, S. A., Thiel, C., Ekici,

A. B., Winterpacht, A., Kwon, Y. T., Varshavsky, A., and Reis, A. (2005) *Nature genetics* **37**, 1345-1350

68. Hwang, C. S., Shemorry, A., and Varshavsky, A. (2010) *Science* **327**, 973-977
69. Moerschell, R. P., Hosokawa, Y., Tsunasawa, S., and Sherman, F. (1990) *The Journal of biological chemistry* **265**, 19638-19643
70. Li, X., and Chang, Y. H. (1995) *Proceedings of the National Academy of Sciences of the United States of America* **92**, 12357-12361
71. Van Damme, P., Lasa, M., Polevoda, B., Gazquez, C., Elosegui-Artola, A., Kim, D. S., De Juan-Pardo, E., Demeyer, K., Hole, K., Larrea, E., Timmerman, E., Prieto, J., Arnesen, T., Sherman, F., Gevaert, K., and Aldabe, R. (2012) *Proceedings of the National Academy of Sciences of the United States of America* **109**, 12449-12454
72. Starheim, K. K., Gevaert, K., and Arnesen, T. (2012) *Trends in biochemical sciences* **37**, 152-161
73. Van Damme, P., Arnesen, T., and Gevaert, K. (2011) *The FEBS journal* **278**, 3822-3834
74. Helsens, K., Van Damme, P., Degroeve, S., Martens, L., Arnesen, T., Vandekerckhove, J., and Gevaert, K. (2011) *Journal of proteome research* **10**, 3578-3589
75. Arnesen, T., Van Damme, P., Polevoda, B., Helsens, K., Evjenth, R., Colaert, N., Varhaug, J. E., Vandekerckhove, J., Lillehaug, J. R., Sherman, F., and Gevaert, K. (2009) *Proceedings of the National Academy of Sciences of the United States of America* **106**, 8157-8162

76. Polevoda, B., Brown, S., Cardillo, T. S., Rigby, S., and Sherman, F. (2008) *Journal of cellular biochemistry* **103**, 492-508

77. Kreft, S. G., and Hochstrasser, M. (2011) *The Journal of biological chemistry* **286**, 20163-20174

78. Ravid, T., Kreft, S. G., and Hochstrasser, M. (2006) *The EMBO journal* **25**, 533-543

79. Kreft, S. G., Wang, L., and Hochstrasser, M. (2006) *The Journal of biological chemistry* **281**, 4646-4653

80. Behnia, R., Panic, B., Whyte, J. R., and Munro, S. (2004) *Nature cell biology* **6**, 405-413

81. Setty, S. R., Strochlic, T. I., Tong, A. H., Boone, C., and Burd, C. G. (2004) *Nature cell biology* **6**, 414-419

82. Jackson, C. L. (2004) *Nature cell biology* **6**, 379-380

83. Hofmann, I., and Munro, S. (2006) *Journal of cell science* **119**, 1494-1503

84. Graham, T. R. (2004) *Current biology : CB* **14**, R483-485

85. Coulton, A. T., East, D. A., Galinska-Rakoczy, A., Lehman, W., and Mulvihill, D. P. (2010) *Journal of cell science* **123**, 3235-3243

86. Hanzelmann, P., Stingele, J., Hofmann, K., Schindelin, H., and Raasi, S. (2010) *The Journal of biological chemistry* **285**, 20390-20398

87. Arnesen, T., Van Damme, P., Polevoda, B., Helsens, K., Evjenth, R., Colaert, N., Varhaug, J. E., Vandekerckhove, J., Lillehaug, J. R., Sherman, F., and Gevaert, K. (2009) *Proc. Natl. Acad. Sci. USA* **106**, 8157-8162

88. Starheim, K. K., Gevaert, K., and Arnesen, T. (2012) *Trends Biochem. Sci.* **37**, 152-161

89. Polevoda, B., and Sherman, F. (2003) *J. Mol. Biol.* **325**, 595-622

90. Van Damme, P., Lasac, M., Polevoda, B., Gazquezc, C., Elosegui-Artolae, A., Kim, D. S., De Juan-Pardoe, E., Demeyera, K., Holef, K., Larreac, E., Timmermana, E., Prietoc, J., Arnesenf, T., Shermand, F., Gevaerta, K., and Aldabec, R. (2012) *Proc. Natl. Acad. Sci. USA* **109**, 12449-12454

91. Scott, D. C., Monda, J. K., Bennett, E. J., Harper, J. W., and Schulman, B. A. (2011) *Science* **334**, 674-678

92. Choudhary, C., Kumar, C., Gnad, F., Nielsen, M. L., Rehman, M., Walther, T. C., Olsen, J. V., and Mann, M. (2009) *Science* **325**, 834-840

93. Gautschi, M., Just, S., Mun, A., Ross, S., Rücknagel, P., Dubaquié, Y., Ehrenhofer-Murray, A., and Rospert, S. (2003) *Mol. Cell. Biol.* **23**, 7403-7414

94. Mullen, J. R., Kayne, P. S., Moerschell, R. P., Tsunasawa, S., Gribskov, M., Colavito-Shepanski, M., Grunstein, M., Sherman, F., and Sternglanz, R. (1989) *EMBO J.* **8**, 2067-2075

95. Park, E. C., and Szostak, J. W. (1992) *EMBO J.* **11**, 2087-2093

96. Hwang, C.-S., Shemorry, A., and Varshavsky, A. (2010) *Science* **327**, 973-977

97. Varshavsky, A. (2011) *Prot. Sci.* **20**, 1298-1345

98. Piatkov, K. I., Brower, C. S., and Varshavsky, A. (2012) *Proc. Natl. Acad. Sci. USA* **109**, E1839-E1847

99. Tasaki, T. S., Sriram, S. M., Park, K. S., and Kwon, Y. T. (2012) *Annu. Rev. Biochem.* **81**, 261-289

100. Dougan, D. A., Micevski, D., and Truscott, K. N. (2011) *Biochim. Biophys. Acta* **1823**, 83-91

101. Mogk, A., Schmidt, R., and Bukau, B. (2007) *Trends Cell Biol.* **17**, 165-172

102. Varshavsky, A. (2008) *J. Biol. Chem.* **283**, 34469-34489

103. Hwang, C.-S., Shemorry, A., and Varshavsky, A. (2010) *Nat. Cell Biol.* **12**, 1177-1185

104. Wang, H., Piatkov, K. I., Brower, C. S., and Varshavsky, A. (2009) *Mol. Cell* **34**, 686-695

105. Brower, C. S., and Varshavsky, A. (2009) *PLoS ONE* **4**, e7757

106. Piatkov, P. I., Colnaghi, L., Bekes, M., Varshavsky, A., and Huang, T. T. (2012) *(submitted for publication)*

107. Halbach, A., Zhang, H., Wengi, A., Jablonska, Z., Gruber, I. M., Halbeisen, R. E., Dehé, P. M., Kemmeren, P., Holstege, F., Géli, V., Gerber, A. P., and Dichtl, B. (2009) *EMBO J.* **28**, 2959-2570

108. Duncan, C. D., and Mata, J. (2011) *PLoS Genet.* **7**, e1002398

109. Brandman, O., Stewart-Ornstein, J., Wong, D., Larson, A., Williams, C. C., Li, G. W., Zhou, S., King, D., Shen, P. S., Weibezahn, J., Dunn, J. G., Rouskin, S., Inada, T., Frost, A., and Weissman, J. S. (2012) *Cell* **151**, 1042-1054

110. Hartl, F. U., Bracher, A., and Hayer-Hartl, M. (2011) *Nature* **475**, 324-332

111. Wolf, D. H., and Stolz, A. (2012) *Biochim. Biophys. Acta* **1823**, 117-124

112. Guerriero, C. J., and Brodsky, J. L. (2012) *Physiol Rev.* **92**

113. Ravid, T., and Hochstrasser, M. (2008) *Nat. Rev. Mol. Cell Biol.* **9**, 679-689

114. Fredrickson, E. K., and Gardner, R. G. (2012) *Semin. Cell Dev. Biol.* **23**, 530-537

115. Varshavsky, A. (2012) *Annu. Rev. Biochem.* **81**, 167-176

116. Finley, D., Ulrich, H. D., Sommer, T., and Kaiser, P. (2012) *Genetics* **192**, 319-360

117. Smith, M. H., Ploegh, H. L., and Weissman, J. S. (2011) *Science* **334**, 1086-1090

118. Sztul, E., and Lupashin, V. (2009) *FEBS Lett.* **583**, 3770-3783

119. Miller, V. J., and Ungar, D. (2012) *Traffic* **13**, 891-897

120. Fotso, P., Koryakina, Y., Pavliv, O., Tsiomenko, A. B., and Lupashin, V. V. (2005) *J. Biol. Chem.* **280**, 27613-27623

121. Lees, J. A., Yip, C. K., Walz, T., and Houghton, F. M. (2010) *Nat. Struct. Mol. Biol.* **11**, 1292-1298

122. Barford, D. (2011) *Q. Rev. Biophys.* **44**, 153-190

123. Hershko, A. (2010) *Mol. Biol. Cell* **15**, 1645-1647

124. Pines, J. (2011) *Nat. Rev. Mol. Cell Biol.* **12**, 427-438

125. Goetze, S., Qeli, E., Mosimann, C., Staes, A., Gerrits, B., Roschitzki, B., Mohanty, S., Niederer, E. M., Laczko, E., Timmerman, E., Lange, V., Hafen, E., Aebersold, R., Vandekerckhove, J., Basler, K., Ahrens, C. H., Gevaert, K., and Brunner, E. (2009) *PLoS Biol.* **7**, e1000236

126. Ghaboosi, N., and Deshaies, R. J. (2007) *Mol. Biol. Cell.* **18**, 1953-1963

127. Setty, S. R. G., Strochlic, T. I., Tong, A. H. Y., Boone, C., and Burd, C. G. (2004) *Nat. Cell Biol.* **6**, 414-419

128. Monda, J. K., Scott, D. C., Miller, D. J., Lydeard, J., King, D., Harper, J. W., Bennett, E. J., and Schulman, B. A. (2012) *Structure* **21**, 1-12

129. Zhang, Z., Kulkarni, K., Hanrahan, S. J., Thompson, A. J., and Barford, D. (2010) *EMBO J.* **29**, 3733-3744

130. Helbig, A. O., Gauci, S., Raijmakers, R., van Breukelen, B., Slijper, M., Mohammed, S., and Heck, A. J. R. (2010) *Mol Cell Proteom.* **9**, 928-939

131. Chen, J., and Archer, T. (2005) *Mol. Cell. Biol.* **25**, 9016-9027

132. Siegel, J. J., and Amon, A. (2012) *Annu. Rev. Cell. Dev Biol.* **28**, 189-214

133. Forte, G. M. A., Pool, M. R., and Stirling, C. J. (2011) *PLoS Biol.* **9**, e1001073

134. Hwang, C.-S., Shemorry, A., and Varshavsky, A. (2009) *Proc. Natl. Acad. Sci. USA* **106**, 2142-2147

135. Hwang, C.-S., and Varshavsky, A. (2008) *Proc. Natl. Acad. Sci. USA* **105**, 19188-19193

136. Xia, Z., Webster, A., Du, F., Piatkov, K., Ghislain, M., and Varshavsky, A. (2008) *J. Biol. Chem.* **283**, 24011-24028

137. Xia, Z., Turner, G. C., Hwang, C.-S., Byrd, C., and Varshavsky, A. (2008) *J. Biol. Chem.* **283**, 28958-28968

138. Turner, G. C., Du, F., and Varshavsky, A. (2000) *Nature* **405**, 579-583

139. Byrd, C., Turner, G. C., and Varshavsky, A. (1998) *EMBO J.* **17**, 269-277

140. Hu, R.-G., Wang, H., Xia, Z., and Varshavsky, A. (2008) *Proc. Natl. Acad. Sci. USA* **105**, 76-81

141. Eisele, F., and Wolf, D. H. (2008) *FEBS Lett.* **582**, 4143-4146

142. Heck, J. W., Cheung, S. K., and Hampton, R. Y. (2010) *Proc. Natl. Acad. Sci. USA* **107**, 1106-1111

143. Graciet, E., and Wellmer, F. (2010) *Trends Plant Sci.* **15**, 447-453

144. Varshavsky, A. (1996) *Proc. Natl. Acad. Sci. USA* **93**, 12142-12149

145. Hu, R.-G., Sheng, J., Xin, Q., Xu, Z., Takahashi, T. T., and Varshavsky, A. (2005) *Nature* **437**, 981-986

146. Hwang, C.-S., Sukalo, M., Batygin, O., Addor, M. C., Brunner, H., Aytes, A. P., Mayerle, J., Song, H. K., Varshavsky, A., and Zenker, M. (2011) *PLoS One* **6**, e24925

147. Zenker, M., Mayerle, J., Lerch, M. M., Tagariello, A., Zerres, K., Durie, P. R., Beier, M., Hülskamp, G., Guzman, C., Rehder, H., Beemer, F. A., Hamel, B., Vanlieferinghen, P., Gershoni-Baruch, R., Vieira, M. W., Dumic, M., Auslender, R., Gil-da-Silva-Lopes, V. L., Steinlicht, S., Rauh, R., Shalev, S. A., Thiel, C., Winterpacht, A., Kwon, Y. T., Varshavsky, A., and Reis, A. (2005) *Nat. Genet.* **37**, 1345-1350

148. Prasad, R., Kawaguchi, S., and Ng, D. T. W. (2010) *Mol. Biol. Cell* **21**, 2117-2127

149. Kurosaka, S., Leu, N. A., Zhang, F., Bunte, R., Saha, S., Wang, J., Guo, C., He, W., and Kashina, A. (2010) *PLoS Genet.* **6**, e1000878

150. Zhang, F., Saha, S., Shabalina, S. A., and Kashina, A. (2010) *Science* **329**, 1534-1537

151. Lee, M. J., Tasaki, T., Moroi, K., An, J. Y., Kimura, S., Davydov, I. V., and Kwon, Y. T. (2005) *Proc. Natl. Acad. Sci. USA* **102**, 15030-15035

152. Piatkov, K. I., Colnaghi, L., Bekes, M., Varshavsky, A., and Huang, T. T. (2012) *Mol. Cell* **(in press)**

153. Kwon, Y. T., Kashina, A. S., Davydov, I. V., Hu, R.-G., An, J. Y., Seo, J. W., Du, F., and Varshavsky, A. (2002) *Science* **297**, 96-99

154. Lee, M. J., Kim, D. E., Zakrzewska, A., Yoo, Y. D., Kim, S. H., Kim, S. T., Seo, J. W., Lee, Y. S., Dorn, G. W., 2nd, Oh, U., Kim, B. Y., and Kwon, Y. T. (2012) *J. Biol. Chem.* **287**, 24043-24052

155. Polevoda, B., Arnesen, T., and Sherman, F. (2009) *BMC Proceedings* **3**, S2

156. Ausubel, F. M., Brent, R., Kingston, R. E., Moore, D. D., Smith, J. A., Seidman, J. G., and Struhl, K. (2010) *Current Protocols in Molecular Biology.*, Wiley-Interscience, New York

157. Sherman, F. (1991) *Meth. Enzymol.* **194**, 3-21

158. Longtine, M. S., McKenzie, A., 3rd., Demarini, D. J., Shah, N. G., Wach, A., Brachat, A., Philippsen, P., and Pringle, J. R. (1998) *Yeast* **14**, 953-961

159. Dohmen, R. J., Stappen, R., McGrath, J. P., Forrová, H., Goffeau, A., and Varshavsky, A. (1995) *J. Biol. Chem.* **270**, 18099-18109

160. Mumberg, D., Muller, R., and Funk, M. (1994) *Nucleic Acids Res.* **22**, 5767-5768

Figure 5.1

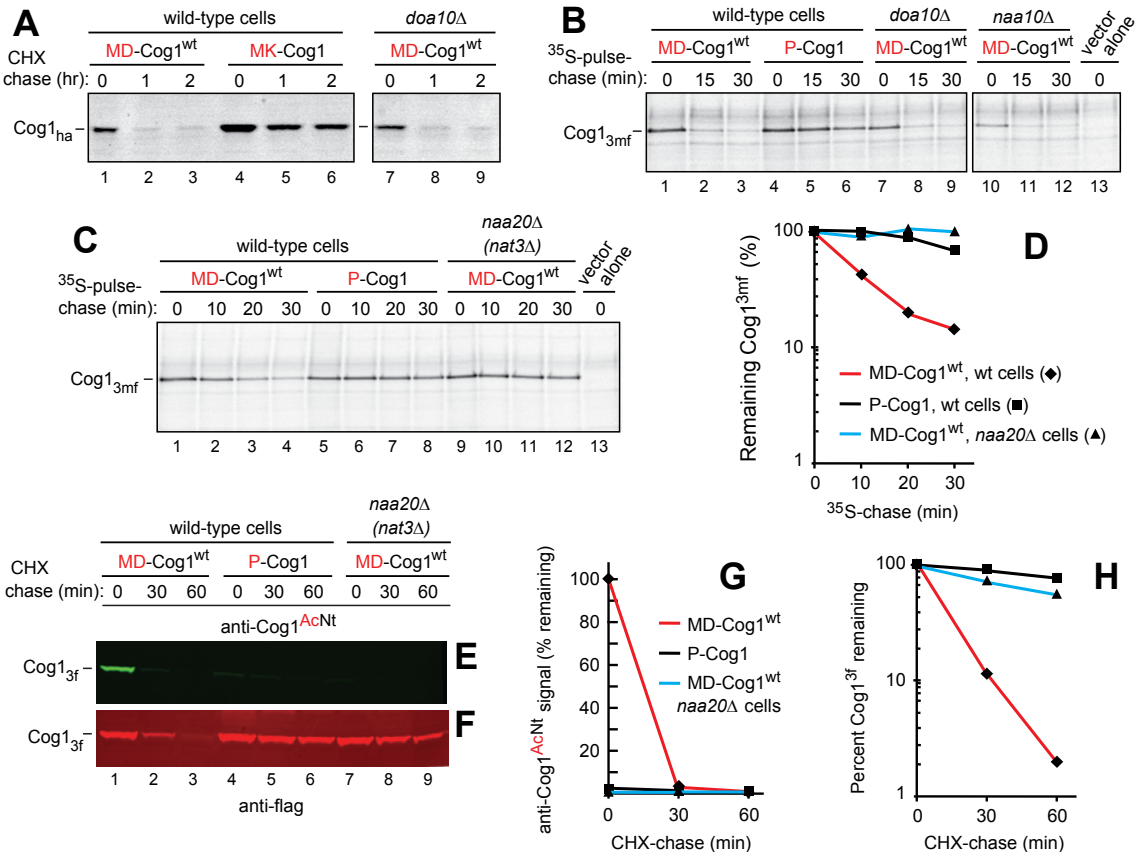

Figure 5.1. The Ac/N-degron of Cog1.

(A) Cycloheximide (CHX)-chases were carried out at 30°C with wild-type (wt) or *doa10Δ S. cerevisiae* that expressed either wt Cog1, termed MD-Cog1^{wt}, or its MK-Cog1 derivative in which Asp^2 was replaced with Lys^2. Both proteins were C-terminally ha-tagged. At the indicated times of chase, proteins in cell extracts were fractionated by SDS-PAGE and assayed by immunoblotting with anti-ha antibody.

(B) ^{35}S-pulse-chase with MD-Cog1^{wt} or P-Cog1 in wt, *doa10Δ*, or *naa10Δ* (*ard1Δ*) *S. cerevisiae*, the latter lacking the catalytic subunit of the non-cognate (for MD-Cog1^{wt}) NatA Nt-acetylase (Figure S2). Cog1 proteins were C-terminally tagged

with 3 flag epitopes modified to contain a Met residue in each epitope, to increase ^{35}S-Met in Cog1.

(C) Same as in B but another ^{35}S-pulse-chase. It included *naa20Δ* (*nat3Δ*) *S. cerevisiae* lacking the catalytic subunit of the cognate (for MD-Cog1^{wt}) NatB Nt-acetylase (Figure S2).

(D) Quantification of data in C. ◆, MD-Cog1^{wt} in wt cells. ▲, MD-Cog1^{wt} in *naa20Δ* cells. ■, P-Cog1 in wt cells.

(E) Anti-Cog1^{AcNt} antibody specific for Nt-acetylated MD-Cog1^{wt} (see Figure S4A-C) was used for immunoblotting in CHX-chase assays with MD-Cog1^{wt} and P-Cog1 (C-terminally tagged with 3 flag epitopes) in either wt or *naa20Δ* (*nat3Δ*) *S. cerevisiae* (see the main text).

(F) Same as in E, except that the same membrane was reprobed with anti-flag antibody.

(G) Quantification of anti-Cog1^{AcNt}-specific immunoblotting patterns in E using Odyssey (Li-Cor) and a linear scale, with the level of MD-Cog1^{wt} at time zero in wt cells taken as 100%. ◆, MD-Cog1^{wt} in wt cells. ▲, MD-Cog1^{wt} in *naa20Δ* cells. ■, P-Cog1 in wt cells.

(H) Same as in G but quantification of the flag-specific Cog1 immunoblotting patterns in F. Same designations as in G.

Figure 5.2

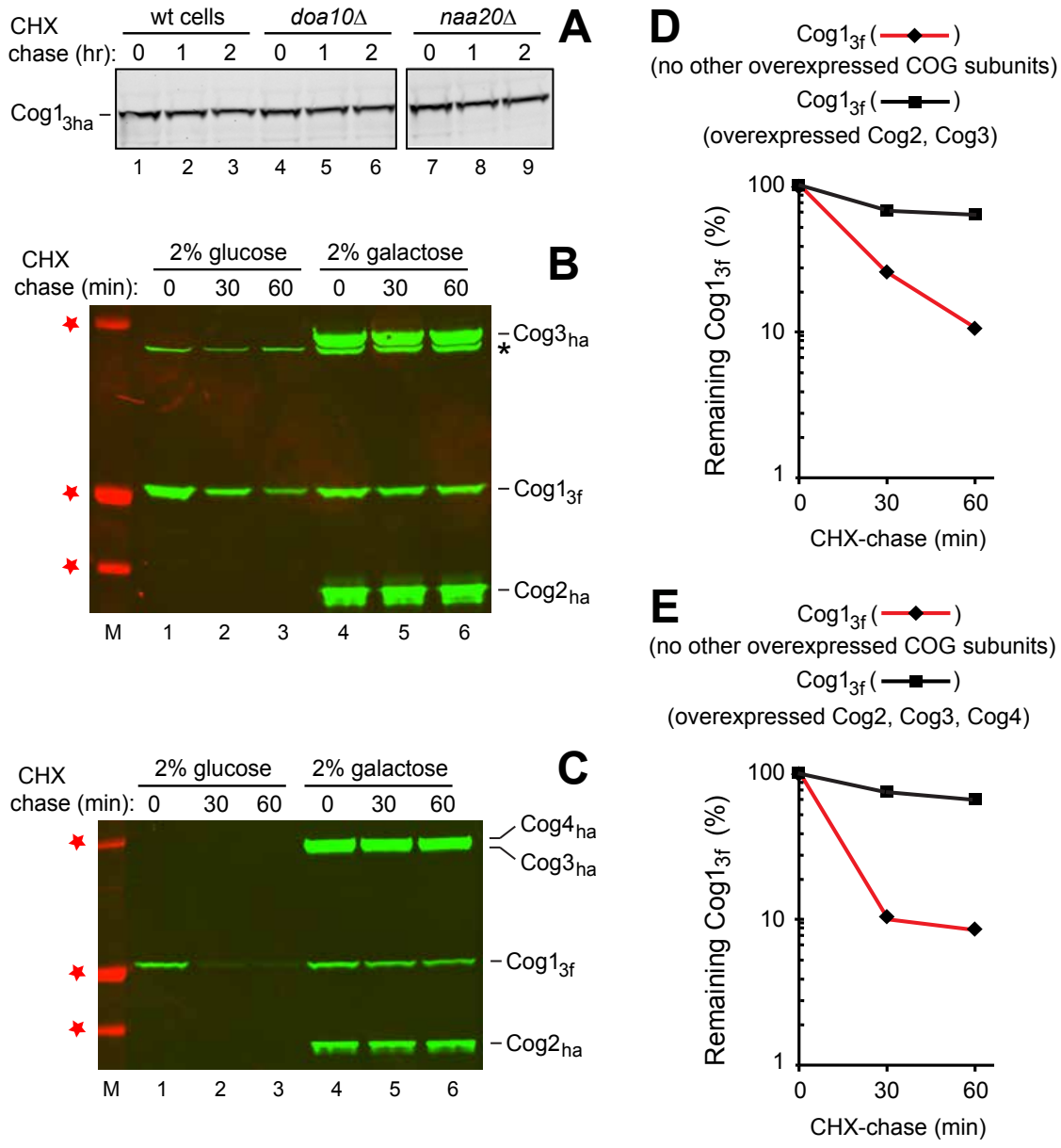

Figure 5.2. Metabolic Stability of Endogenous Cog1 and Stabilization of Overexpressed Cog1 by Coexpressed Cog2-Cog4.

(A) CHX-chases with MD-Cog1^{wt} (C-terminally tagged with 3 ha epitopes) expressed from the chromosomal *COG1* locus and the native P_{COG1} promoter in wt, *doa10Δ*, and *naa20Δ* (*nat3Δ*) cells.

(B) Stabilization of overexpressed MD-Cog1^{wt} by coexpressed Cog2 and Cog3. Lane M and red stars, molecular mass markers of 37, 50, and 100 kDa, respectively. Lanes 1-3, wt *S. cerevisiae* grown in 2% glucose, expressing MD-Cog1^{wt} (C-terminally tagged with 3 flag epitopes) from the P_{CUP1} promoter on a low copy plasmid, and carrying a high copy plasmid that expressed, only in galactose, both Cog2 and Cog3 (C-terminally tagged with ha) from the bidirectional $P_{GAL1/10}$ promoter. A CHX-chase was carried out for 30 and 60 min. Lanes 4-6, same as lanes 1-3 but with cells in 2% galactose. Asterisk on the right indicates a protein crossreacting with anti-ha.

(C) Same as in B but cells also carried a second high copy plasmid expressing Cog4 (C-terminally tagged with ha) from the $P_{GAL1/10}$ promoter.

(D) Quantification of data in B for MD-Cog1^{wt}. ◆, MD-Cog1^{wt} in cells that did not coexpress other COG subunits. ■, MD-Cog1^{wt} in cells that coexpressed (in galactose) Cog2 and Cog3.

(E) Quantification of data in C for MD-Cog1^{wt}. ◆, MD-Cog1^{wt} in cells that did not coexpress other COG subunits. ■, MD-Cog1^{wt} in cells that coexpressed (in galactose) Cog2-Cog4.

Figure 5.3

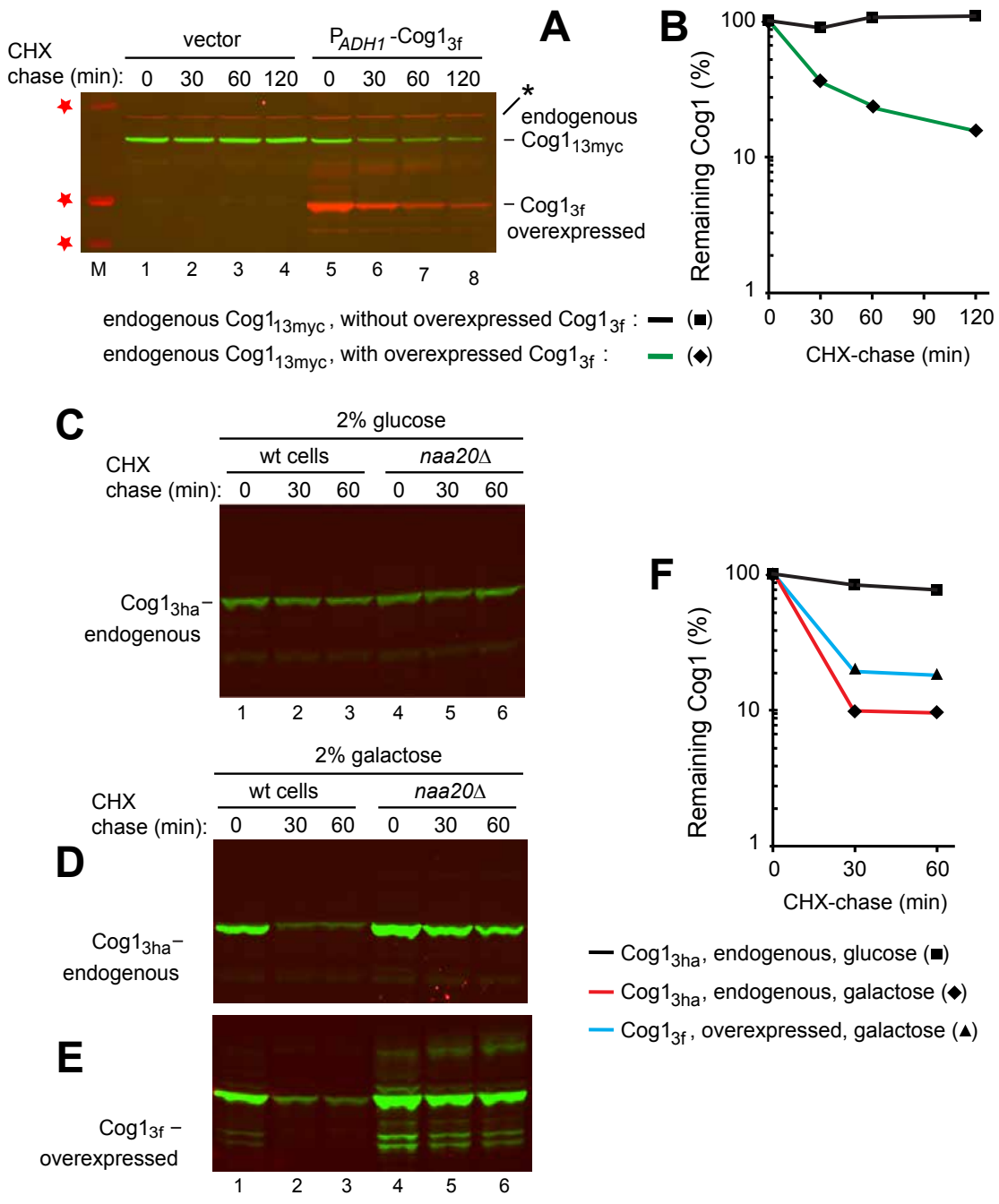

Figure 5.3. Subunit Decoy Technique and the Cause of Stability of Endogenous Cog1.

(A) Lane M and red stars, molecular mass markers of 37, 50, and 100 kDa, respectively. Lanes 1-4, stability of endogenous MD-Cog1$^{wt}_{13myc}$ (C-terminally tagged with 13 myc epitopes) in the absence of the MD-Cog1$^{wt}_{3f}$ decoy (C-terminally tagged with 3 flag epitopes). CHX-chase with MD-Cog1$^{wt}_{13myc}$ expressed from the chromosomal *COG1* locus and the native P$_{COG1}$ promoter in wt cells in the presence of a plasmid vector alone. Lanes 5-8, same as lanes 1-4 but cells carried a plasmid that expressed the MD-Cog1$^{wt}_{3f}$ decoy from the P$_{ADH1}$ promoter. An asterisk denotes a protein crossreacting with anti-flag antibody.

(B) Quantification of data in A. u, endogenous MD-Cog1$^{wt}_{13myc}$ in wt cells that did not express the MD-Cog1$^{wt}_{3f}$ decoy. n, endogenous MD-Cog1$^{wt}_{13myc}$ in wt cells that also expressed MD-Cog1$^{wt}_{3f}$.

(C) Lanes 1-3, stability of endogenous MD-Cog1$^{wt}_{3ha}$ (C-terminally tagged with 3 ha epitopes). CHX-chase with cells in 2% glucose expressing the endogenous MD-Cog1$^{wt}_{3ha}$ in the absence of the MD-Cog1$^{wt}_{3f}$ decoy. The latter was encoded by a plasmid that could express MD-Cog1$^{wt}_{3f}$ from the galactose-inducible P$_{GAL1}$ promoter. Lanes 4-6, same as lanes 1-3 but in *naa20Δ* cells.

(D) Same as in C but with wt and *naa20Δ* cells expressing the endogenous MD-Cog1$^{wt}_{3ha}$ in 2% galactose, i.e., in the presence of the coexpressed MD-Cog1$^{wt}_{3f}$ decoy. Immunoblotting was performed using anti-ha antibody, specific for MD-Cog1$^{wt}_{3ha}$.

(E) Same as in D but also probed (in a parallel immunoblot) with anti-flag antibody, specific for MD-Cog1$^{wt}_{3f}$.

(D) Quantification of data in C-E. ◆, endogenous MD-Cog1$^{wt}_{3ha}$ in wt cells growing in 2% glucose. ■, endogenous MD-Cog1$^{wt}_{3ha}$ in wt cells growing in 2% galactose, in the presence of the MD-Cog1$^{wt}_{3f}$ decoy. ▲, the MD-Cog1$^{wt}_{3f}$ decoy.

Figure 5.4

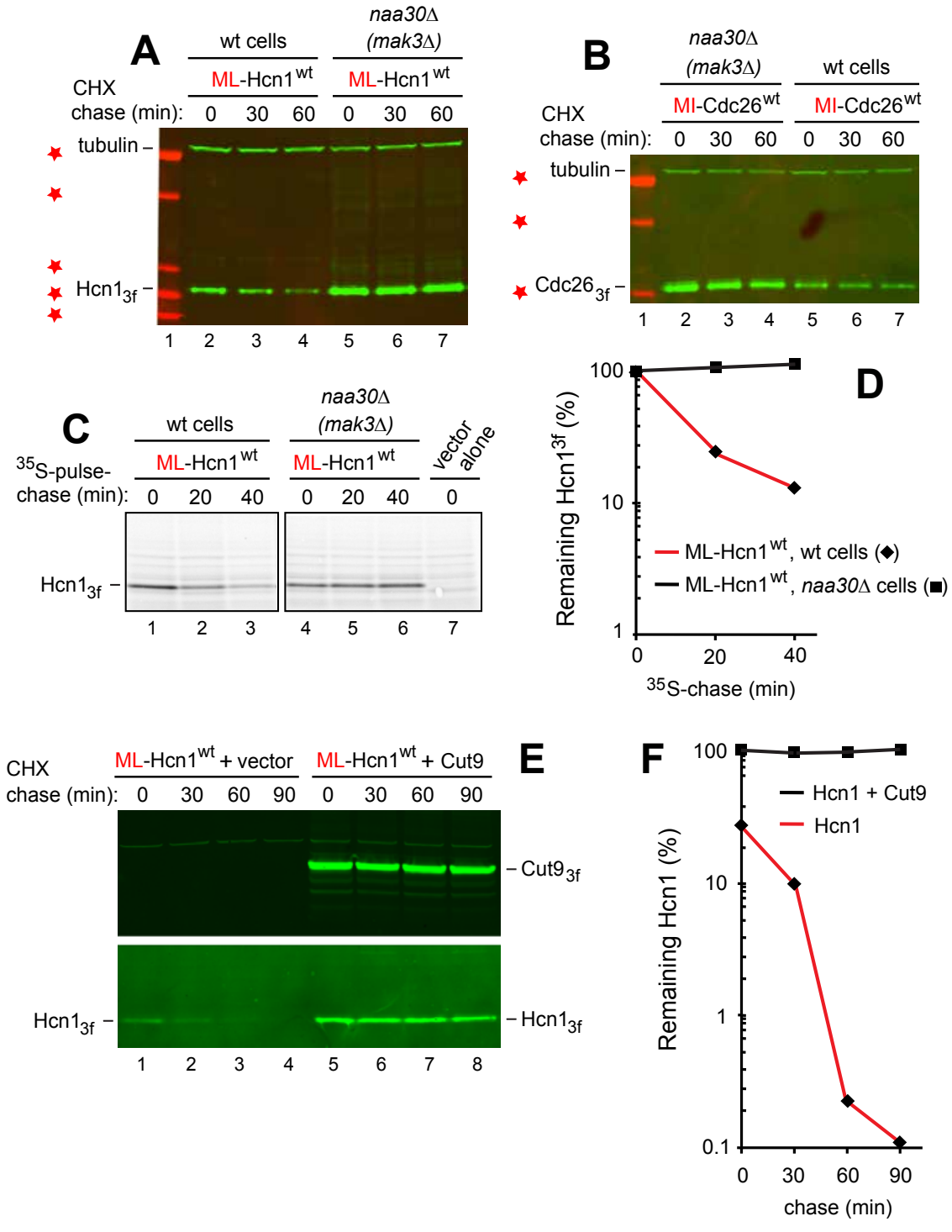
A
wt cells
naa30Δ (mak3Δ)
ML-Hcn1wt
CHX chase (min): 0 30 60 0 30 60
tubulin –
Hcn1 3f –
1 2 3 4 5 6 7
B
naa30Δ (mak3Δ)
wt cells
MI-Cdc26wt
CHX chase (min): 0 30 60 0 30 60
tubulin –
Cdc26 3f –
1 2 3 4 5 6 7
C
wt cells
naa30Δ (mak3Δ)
vector alone
ML-Hcn1wt
35S-pulse-chase (min): 0 20 40 0 20 40 0
Hcn1 3f –
1 2 3 4 5 6 7
D
Remaining Hcn1 3f (%)
100
10
1
0 20 40
35S-chase (min)
ML-Hcn1wt, wt cells (◆)
ML-Hcn1wt, naa30Δ cells (■)
E
CHX chase (min): 0 30 60 90 0 30 60 90
ML-Hcn1wt + vector
ML-Hcn1wt + Cut9
– Cut9 3f
Hcn1 3f –
– Hcn1 3f
1 2 3 4 5 6 7 8
F
Remaining Hcn1 (%)
100
10
1
0.1
0 30 60 90
chase (min)
Hcn1 + Cut9
Hcn1

Figure 5.4. The Ac/N-degron of Hcn1 and Repression of This Degron by Cut9.

(A) CHX-chases for 30 and 60 min in wt or *naa30Δ* (*mak3Δ*) *S. cerevisiae* that expressed the wt *S. pombe* Hcn1, termed ML-Hcn1^{wt}, C-terminally tagged with 3 flag epitopes. *naa30Δ* cells lack the catalytic subunit of the cognate NatC Nt-acetylase (Figure S2). Lane 1 and red stars, molecular mass markers of 10, 15, 20, 37, and 50 kDa, respectively.

(B) Same as in A but with Cdc26, termed MI-Cdc26^{wt}, the *S. cerevisiae* counterpart of *S. pombe* ML-Hcn1^{wt}. Lane 1 and red stars, molecular mass markers of 20, 37, and 50 kDa, respectively.

(C) ^{35}S-pulse-chase, for 20 and 40 min, of ML-Hcn1^{wt} in wt and *naa30Δ* (*mak3Δ*) *S. cerevisiae*. Lane 7, vector alone (negative control).

(D) Quantification of data in C. ◆, ML-Hcn1^{wt} in wt cells. ■, ML-Hcn1^{wt} in *naa30Δ* cells.

(E) Lanes 1-4, CHX-chases for 30, 60 and 90 min with wt cells in 2% galactose (and without methionine) that expressed ML-Hcn1^{wt} from the methionine-repressible P$_{MET25}$ promoter on a low copy plasmid and carried a vector alone (no Cut9 expression). Note the metabolic instability of ML-Hcn1^{wt} (lower panel). Lanes 5-8, same as lanes 1-4 but with a low copy plasmid (instead of control vector) expressing Cut9 from the galactose-inducible P$_{GAL1}$ promoter, with both ML-Hcn1^{wt} and Cut9 C-terminally tagged with 3 flag epitopes. Note the metabolic stabilization of ML-Hcn1^{wt} (lower panel), including a strong increase of its level at the beginning of the chase.

(F) Quantification of data in E. ◆, ML-Hcn1^{wt} in the absence of co-expressed Cut9. ■, ML-Hcn1^{wt} in the presence of co-expressed Cut9.

Figure 5.5

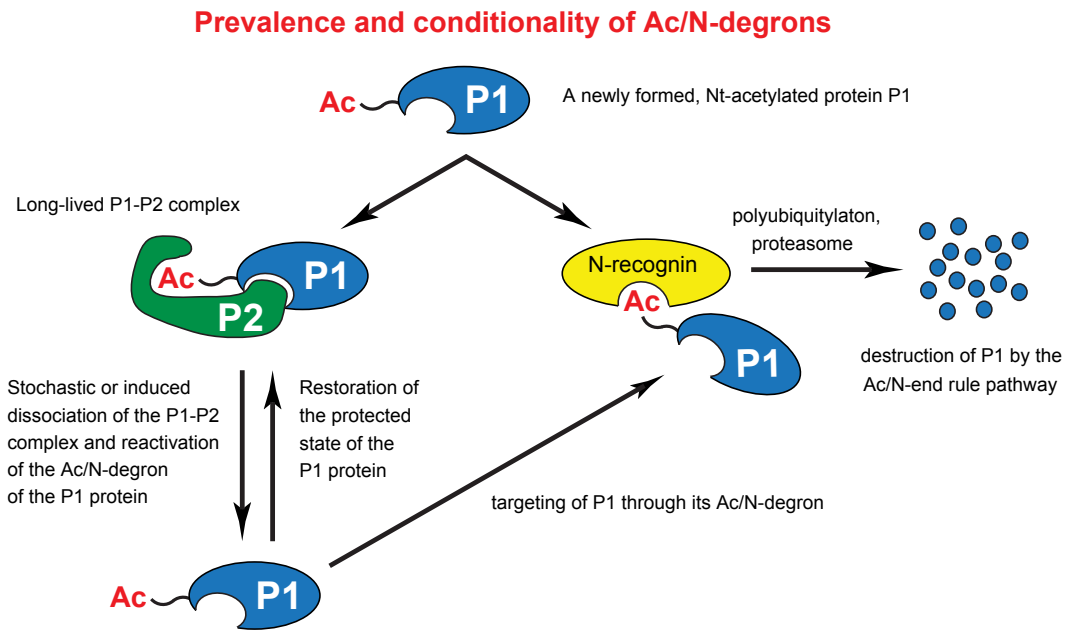

Figure 5.5. Prevalence and Conditionality of Ac/N-degrons As a Basis for the Control of Protein Quality and Stoichiometries.

This diagram summarizes the understanding of the functional dynamics of Nt-acetylated proteins vis-à-vis the Ac/N-end rule pathway that was attained by the present study, in conjunction with results that initially revealed the Ac/N-end rule pathway (95). See Introduction and Discussion.

APPENDIX 1:

TWO PROTEOLYTIC PATHWAYS REGULATE DNA REPAIR BY COTARGETING THE MGT1 ALKYLGUANINE TRANSFERASE

From Hwang, C. S., Shemorry, A., and Varshavsky, A. (2009) *Proceedings of the National Academy of Sciences of the United States of America* **106**, 2142-2147

Abstract

O^6-methylguanine (O^6meG) and related modifications of guanine in double-stranded DNA are functionally severe lesions that can be produced by many alkylating agents, including N-methyl-N-nitro-N-nitrosoguanidine (MNNG), a potent carcinogen. O^6meG is repaired through its demethylation by the O^6-alkylguanine-DNA alkyltransferase (AGT). This protein is called Mgmt (or MGMT) in mammals and Mgt1 in the yeast *Saccharomyces cerevisiae*. AGT proteins remove methyl and other alkyl groups from an alkylated O^6 in guanine by transferring the adduct to an active-site cysteine residue. The resulting S-alkyl-Cys of AGT is not restored back to Cys, so repair proteins of this kind can act only once. We report here that S. cerevisiae Mgt1 is cotargeted for degradation, through a degron near its N terminus, by 2 ubiquitin-mediated proteolytic systems, the Ubr1/Rad6-dependent N-end rule pathway and the Ufd4/Ubc4-dependent ubiquitin fusion degradation (UFD) pathway. The cotargeting of Mgt1 by these pathways is synergistic, in that it increases not only the yield of polyubiquitylated Mgt1, but also the processivity of polyubiquitylation. The N-end rule and UFD pathways comediate both the constitutive and MNNG-accelerated degradation of Mgt1. Yeast cells lacking the Ubr1 and Ufd4 ubiquitin ligases were hyperresistant to MNNG but hypersensitive to the toxicity of overexpressed Mgt1. We consider ramifications of this discovery for the control of DNA repair and mechanisms of substrate targeting by the ubiquitin system.

Introduction

Since the 1987 discovery that a key DNA repair protein, Rad6, was a ubiquitin (Ub)-conjugating enzyme (1, 2), there have been great strides in understanding the

massive, multilevel involvement of the Ub–proteasome system in the DNA damage response (reviewed in refs. 3 and 4). A major aspect of this response is the repair of damage caused by alkylating agents such as N-methyl-N'-nitro-N-nitrosoguanidine (MNNG) and methyl methane sulfonate (MMS), which produce both mutagenic and cytotoxic lesions in DNA (4, 5). One functionally severe lesion in double-stranded DNA is O^6-methylguanine (O^6meG), which is demethylated by the O^6-alkylguanine-DNA alkyltransferase (AGT). This protein is called Mgmt (or MGMT) in mammals and Mgt1 in the yeast Saccharomyces cerevisiae (5–8). Compounds that produce O^6meG in DNA are common environmental carcinogens. Some of these compounds are also formed as a part of normal cellular metabolism. The repair of O^6meG in DNA is down-regulated in many cancers, usually because of lower than normal levels of Mgmt in cancer cells. Consequently, some anticancer drugs are DNA alkylating agents whose targets include O^6 in guanine. An acquired or preexisting resistance of cancer cells to such drugs often involves an up-regulation of Mgmt (4, 5). AGT proteins remove methyl and other alkyl groups from alkylated O^6 in guanine by transferring an adduct to an active-site Cys residue (5, 6). The resulting S-alkyl-Cys residue of AGT is not restored back to Cys, so repair proteins of this kind can act only once. In mammals, the alkylated (inactive) Mgmt and possibly the unmodified Mgmt are short-lived proteins, degraded by an unknown pathway (9). In human cells that express the E6 protein of the human papilloma virus (HPV), MGMT is also targeted for degradation by a complex of the viral E6 protein and E6AP, one of mammalian HECT-domain E3 Ub ligases (8, 10).

In this study, we discovered that Mgt1, the O^6meG-DNA alkyltransferase of S. cerevisiae, is a physiological substrate of both the Ubr1-dependent N-end rule pathway and the Ufd4-dependent Ub fusion degradation (UFD) pathway (Fig. 1). S. cerevisiae Mgt1 is a 188-residue protein that is sequelogous (similar in sequence) (11) to mammalian Mgmt (7, 12, 13). The N-end rule relates the in vivo half-life of a protein to the identity of its N-terminal residue (2, 14–17). Degradation signals (degrons) that are targeted by the N-end rule pathway include a set called N-degrons (2, 15). The main determinant of an N-degron is a destabilizing N-terminal residue of a substrate protein. The N-end rule has a hierarchic structure that involves the primary, secondary, and tertiary destabilizing N-terminal residues (Fig. 1A). Destabilizing activities of these residues differ by their requirements for a preliminary enzymatic modification (refs. 2 and 15–18 and references therein). E3 Ub ligases of the N-end rule pathway are called N-recognins (15, 17, 19–21). They bind to primary destabilizing N-terminal residues of N-end rule substrates. The *S. cerevisiae* N-end rule pathway contains a single N-recognin, Ubr1, a 225-kDa sequelog (11) of mammalian Ubr1 and Ubr2 (Fig. 1A) (19–23). The functions of the N-end rule pathway (Fig. 1A) include the sensing of nitric oxide (NO), oxygen, heme, and short peptides; the maintenance of the high fidelity of chromosome segregation; the control of peptide import; regulation of signaling by transmembrane receptors, through the NO/O_2-dependent degradation of regulators of G protein signaling (RGS) proteins that downregulate G proteins; specific functions of the pancreas; regulation of apoptosis, meiosis, spermatogenesis, neurogenesis, and cardiovascular development in mammals; and regulation of leaf senescence in plants (refs. 2, 17,

18, and 21–25 and references therein). The UFD pathway was discovered through the use of engineered Ub fusions in which the structure of either the N-terminal Ub moiety or its junction with a downstream polypeptide inhibited the cleavage of a Ub fusion by deubiquitylating enzymes (DUBs) (14, 26, 27). Genetic dissection of the UFD pathway in *S. cerevisiae* identified Ufd1–Ufd5 as proteins that were required, either strictly or in part, for the degradation of engineered UFD substrates (27, 28). Ufd4 is the 168-kDa HECT-domain E3 enzyme of the UFD pathway, which functions together with the E2 enzymes Ubc4 or Ubc5. Distinct domains of Ufd4 were shown to recognize the N-terminal Ub moiety of UFD substrates (29) and also specific subunits of the 26S proteasome (30, 31). Ufd4 plays a role in the conditional autoubiquitylation and degradation of the Ubc7 E2 enzyme (32). Rad4, a nucleotide excision repair protein, is partially stabilized in *ufd4Δ* cells, suggesting that Rad4 may be a substrate of the UFD pathway (33).

Besides its relevance to DNA repair, the identification of *S. cerevisiae* Mgt1 DNA alkyltransferase as a physiological substrate of both the N-end rule and UFD pathways (Fig. 1) brings together 2 mechanistically distinct targeting systems, in that Ubr1 is a RING-type E3, whereas Ufd4 is a HECT-type E3. The N-end rule and UFD pathways were the first specific pathways of the Ub system to be discovered (14). Studies of these pathways have been proceeding largely in parallel (2, 14, 15, 26–29, 31, 33), until the present discovery of their functional and mechanistic connection, as described below.

Results and Discussion

N-End Rule Pathway Targets Mgt1 for Degradation

Large-scale identification of *S. cerevisiae* protein complexes through coimmunoprecipitation and other assays suggested that the 225-kDa Ubr1 E3 Ub ligase (Fig. 1A) may physically interact with Ygl081w, Pex7, Yak1, Mgt1, Ccr4, Gal80, and Srs2 [see supporting information (SI) Materials and Methods and the legend to Fig. S1]. We asked whether any of these putative Ubr1 ligands were short-lived in vivo, and, if so, whether they were degraded at least in part by the N-end rule pathway. We used a ''cycloheximide-chase'' assay with wild type (wt) versus *ubr1Δ S. cerevisiae.* In this method, the in vivo levels of a protein of interest are determined by SDS/PAGE and immunoblotting (IB) of cell extracts as a function of time after the inhibition of translation by cycloheximide. A majority of the above proteins were found to metabolically unstable. However, the absence of Ubr1 stabilized just one of these proteins, Mgt1 (Fig. S1A), the sole O^6-methylguanine DNA-alkyltransferase in S. cerevisiae (see Introduction). Although the inferred ORF of *S. cerevisiae* Mgt1 contains 2 in-frame start codons, 18 codons apart (7), only the smaller, 188-residue Mgt1 is produced in vivo (13). We replaced the chromosomal MGT1 gene with an otherwise identical ORF expressing $Mgt1_{m13}$ (C-terminally tagged with 13 copies of the 10-residue myc epitope) from the endogenous P_{MGT1} promoter. $Mgt1_{m13}$ was indistinguishable from wt MGT1 in its ability to protect cells from MNNG, a DNA-alkylating agent (Fig. S1C). The instability of $Mgt1_{m13}$ could be restored by reintroducing UBR1 into *ubr1Δ* cells (Fig. 2A). Importantly, this rescue did not occur with $Ubr1^{C1220S}$, an inactive Ubr1 mutant (20) (Fig. 2A).

A cycloheximide-chase assay monitors the in vivo decay of both ‘‘young’’ and ‘‘old’’ molecules of a test protein. To assess the metabolic fate of newly formed Mgt1, we carried out pulse–chase assays with ^{f}DHFR-Ub^{K48R}-Mgt1^{f} [‘‘f’’ denotes the flag epitope linked to the N terminus and C terminus of the dihydrofolate reductase (DHFR) and Mgt1 moieties, respectively]. DUBs cotranslationally cleave this Ub fusion at the Ub^{K48R}-Mgt1^{f} junction, yielding the long-lived reference ^{f}DHFR-Ub^{K48R} and the test protein Mgt1^{f}. In this Ub-reference technique (refs. 23 and 25 and references therein), the free ^{f}DHFR-Ub^{K48R} serves as a ‘‘built-in’’ reference protein to compensate for scatter of expression levels and immunoprecipitation efficiency, thereby increasing the accuracy of pulse–chase assays. The in vivo half-life ($t_{1/2}$) of Mgt1^{f} at 30 °C was 19 min in wt cells and 32 min in *ubr1Δ* cells (Fig. S2A), consistent with the results of cycloheximide-chase assays (Fig. S1A), including the residual instability of Mgt1 in *ubr1Δ* cells. We also used the *pdr5Δ* S. cerevisiae strain, in which the absence of the Pdr5 transporter allows the intracellular accumulation of MG132, a proteasome inhibitor. No Mgt1$_{m13}$-linked polyUb ‘‘ladders’’ were detected in wt cells in the absence of MG132 (Fig. S1B, lanes 1 and 2), suggesting that polyubiquitylation of Mgt1 (in contrast to its subsequent destruction by the proteasome) was rate-limiting under these conditions. Consistent with this interpretation, larger, presumably polyubiquitylated forms of Mgt1$_{m13}$ appeared after the treatment of cells for 1 h with MG132 (Fig. S1B, lanes 1 and 2 versus lanes 3 and 4). The levels of MG132-induced Mgt1$_{m13}$ derivatives were much lower in *ubr1Δ* cells but were still detectable (Fig. S1B, lane 4 versus lane 6), suggesting that another Ub ligase may also target Mgt1. In a different assay, Mgt1$_{ha}$

(C-terminally ha-tagged) was coexpressed in wt S. cerevisiae with His_6-tagged $Ub^{K48R,G76A}$, a double-mutant Ub that can become a part of polyUb chains but would inhibit their disassembly by DUBs (ref. 2 and references therein). *S. cerevisiae* was treated with MNNG, and polyubiquitylated proteins were isolated from cell extracts by using His_6-specific chromatography, followed by SDS/PAGE and IB with anti-ha antibody. A smear of high-Mr, $Mgt1_{ha}$ containing proteins was observed near the top of the gel, whereas such proteins were virtually absent in a test with His_6-lacking $Ub^{K48R,G76A}$ (Fig. 2B).

The Ub ligase holoenzyme of the N-end rule pathway is Ubr1-Rad6, in which the 20-kDa Rad6 is the Ub-conjugating enzyme (E2) (15, 20). To determine whether other E2s might also play a role, we carried out cycloheximide-chase assays with a collection of E2-null mutants that expressed $Mgt1_{f3}$ (wt Mgt1 C-terminally tagged with 3 copies of the flag epitope). $Mgt1_{f3}$ was strongly stabilized only in rad6Δ cells (Fig. S1D, lanes 5 and 6). In addition to being the E2 of the Ubr1 E3, Rad6 also functions as a part of Ub ligases that contain, in particular, the Bre1, Ubr2, or Rad18 E3s (34). In cycloheximide-chase assays with null mutants in these E3s, Mgt1 was significantly stabilized only in *ubr1Δ* cells (Fig. 2D). Interestingly, the degradation of Mgt1 was accelerated in a *ubr2Δ* strain, compared with its wt counterpart (Fig. 2D, lanes 5 and 6; compare with lanes 1 and 2). Ubr2 is a sequelog of Ubr1 that also functions in a complex with Rad6. However, in contrast to Ubr1, Ubr2 does not recognize N-degrons (35). The enhancement of Mgt1 degradation in *ubr2Δ*

cells (Fig. 2D and Fig. S2B) could be caused by an increased level of Ubr1-accessible Rad6, and also, nonalternatively, by an up-regulation of the proteasome, owing to an increase in Rpn4, which is partially stabilized in *ubr2Δ* cells (35, 36).

Either MNNG or High Temperature Accelerate Mgt1 Degradation

At approximately 200 molecules per haploid cell in exponential cultures, the endogenous Mgt1 is a scarce protein in *S. cerevisiae* (12). Mgt1-dependent DNA-alkyltransferase activity in *S. cerevisiae* extracts was strongly decreased after a treatment of cells with MNNG or shifting them from 30°C to 37°C (12). Our results account for these effects, as the in vivo degradation of Mgt1 was accelerated by these treatments (Fig. 2E and Fig. S2C). Strong effects of increased temperature on Mgt1 degradation could be detected by either cycloheximide-chase or conventional pulse–chase assays (Fig. 2 C and F and Figs. S1E and S2C). In contrast, oxidizing agents such as H_2O_2 (Fig. S2C) or t-butyl hydroxide (data not shown) did not increase the rate of Mgt1 degradation. The acceleration of yeast Mgt1 degradation by MNNG (Fig. 2E) was analogous to the previously observed effects of either MNNG or O^6-benzylguanine (the latter alkylates the active-site Cys of Mgmt) on the degradation, by an unknown pathway, of Mgmt, the mammalian counterpart of Mgt1 (9). We also examined *mgt1Δ* cells that expressed either $Mgt1_{f3}$, $Mgt1^{C151M,f3}$, or $Mgt1^{C151S,f3}$. In the latter derivatives of Mgt1, the active-site Cys151 was replaced either by Met, a mimic of methylated Cys, or by Ser, a substitution that also inactivates Mgt1. *S. cerevisiae* expressing $Mgt1^{C151M,f3}$ or $Mgt1^{C151S,f3}$ were hypersensitive to MNNG (Fig. 2G). In the absence of MNNG, $Mgt1^{C151M,f3}$ was much shorter-lived than wt $Mgt1_{f3}$ (data not shown). By contrast, and in agreement with

the inability of the Ser-mutant $Mgt1^{C151S,f3}$ to be alkylated at position 151, this mutant was longer-lived than wt $Mgt1_{f3}$ in cells that were treated with MNNG (Fig. 3A).

The 3D structure of the 22-kDa human MGMT (6), a counterpart of the 21-kDa *S. cerevisiae* Mgt1, showed that MGMT consists of a ''ribonuclease-like'' N-terminal domain (residues 6–92) and a C-terminal DNA-binding domain (residues 96–176) (Fig. S3 A, B, and D). A putative 3D structure of S. cerevisiae Mgt1 was modeled on human MGMT and took into account its sequelogy to Mgt1 (Fig. S4C). The active-site Cys of human MGMT resides between the C-terminal DNA-binding domain and the N-terminal lobe that faces away from DNA (6) (Fig. S3B). Our findings (see Fig. S4A) indicate that the degron of S. cerevisiae Mgt1 is close to its N terminus. Thus, the active-site Cys151 of Mgt1 is not a part of its degron per se. Instead, the alkylation of Cys151 that accompanies the repair of alkylated DNA by Mgt1 may change its conformation and/or conformational mobility and thereby increase the accessibility of its degron (which would be expected to ''face away'' from DNA) to cognate Ub ligases. This model is consistent with the above-mentioned faster degradation of $Mgt1^{C151M,f3}$, which contains Met151, a mimic of methylated Cys, instead of wt Cys151. The absence of Ubr1 made S. cerevisiae 10-fold more resistant to MNNG, compared with wt cells (Fig. 2H and Fig. S2E). These results suggested that Ubr1 targets not only alkylated (inactive) Mgt1 but also unmodified Mgt1. This interpretation would account for the higher MNNG resistance of ubr1Δ cells, as the absence of degradation of unmodified Mgt1 would result in more of it available for DNA repair. In agreement with the hyperresistance

of ubr1Δ cells to MNNG, they were also found to exhibit a lower frequency of MNNG-induced mutations (Fig. S2D).

Ubr1 Targets Mgt1 Via a Degron Near Its N Terminus.

C-terminally truncated fragments of $Mgt1_{f3}$ were expressed in either *ubr1Δ* or wt *S. cerevisiae*, followed by SDS/PAGE of cell extracts and IB with anti-flag antibody (Fig. S4A). $Mgt1^{1–100,f3}$, which contained the ribonuclease-like N-terminal domain of Mgt1 but lacked the activesite Cys151, was undetectable in wt cells but readily detectable in *ubr1Δ* cells (Fig. S4A, lanes 5 and 6), indicating the presence of a Ubr1-specific degron in the N-terminal half of Mgt1. The results with $Mgt1^{1–144,f3}$ (Fig. S4A, lanes 3 and 4) were similar to those with $Mgt1^{1–100,f3}$. $Mgt1^{84–188,f3}$, an N-terminally truncated Mgt1, could not be expressed at detectable levels in either wt or *ubr1Δ* cells (Fig. S4A, lanes 7 and 8).

UFD and N-End Rule Pathways Cotarget Mgt1 for Degradation

Given the residual instability of Mgt1 in the absence of Ubr1 (Fig. 2 A, D, and E), we attempted to identify another E3 that may target Mgt1. This search involved expression of the $Mgt1^{1–100,f3}$ fragment from the P_{MGT1} promoter (Fig. S4A) and a set of *S. cerevisiae* mutants in several E3s (*ubr1Δ, ubr2Δ, hrd1Δ, hrd3Δ, doa10Δ, ufd2Δ, tul1Δ, hul4Δ, hul5Δ, ufd4Δ, tom1Δ, rps5-1^{ts}*). Among these mutants, the $Mgt1^{1–100,f3}$ fragment was significantly stabilized in ubr1Δ cells (as expected), and also, remarkably, in *ufd4Δ* cells (Fig. 3B, lane 3). Ufd4 is a 168-kDa HECT-domain E3 Ub ligase that mediates the UFD pathway (see Introduction and Fig. 1B). Given this result, we carried out cycloheximide chase assays with wt, *ubr1Δ*, and *ubr1Δufd4Δ* double-mutant *S. cerevisiae* strains that expressed full-length $Mgt1_{m13}$. The absence

of both Ubr1 and Ufd4 stabilized Mgt1 much more than the absence of Ubr1 alone (Fig. 3C and Fig. S2F). The synergistically enhanced stabilization of $Mgt1_{m13}$ in *ubr1Δufd4Δ* cells was observed either at 37°C (Fig. S2F) or upon a treatment with MNNG (Fig. 3C). Moreover, a conventional pulse–chase assay at 37°C with $Mgt1_{f3}$ and either wt, *ubr1Δ*, or *ubr1Δufd4Δ* cells has demonstrated a virtually complete stabilization of newly formed Mgt1 in *ubr1Δufd4Δ* cells (Fig. 3 D and E). As would be expected (given the results above), the absence of Ufd4 alone partially stabilized Mgt1, especially in *ufd4Δ* versus wt cells that were treated with MNNG (Fig. S2 G and H). *S. cerevisiae* lacking Ufd4 were 2.5-fold more resistant to MNNG than their wt counterparts (Fig. 3F and Fig. S4F). Double mutant *ubr1Δufd4Δ* cells, in which Mgt1 was particularly long-lived (Fig. 3 C–E), grew slightly slower than congenic wt cells (Fig. S4 F and G and data not shown). Moreover, overexpressing of $Mgt1_{f3}$ in either wt, *ubr1Δ*, or *ufd4Δ* cells did not significantly impair their growth (data not shown) but led to a severe growth defect in *ubr1Δufd4Δ* cells (Fig. S4 G and H). Thus, the inability to destroy Mgt1 is near-lethal upon overexpression of Mgt1 and is also likely to be deleterious, to a lower extent, at physiological levels of Mgt1.

In Vitro Binding of Ubr1 and Ufd4 to Mgt1 and Cup9

The type 1 and type 2 substrate-binding sites of Ubr1 are specific for basic N-terminal residues (Arg, Lys, His) and bulky hydrophobic N-terminal residues (Trp, Phe, Tyr, Leu, Ile), respectively. The third binding site of Ubr1 recognizes an internal (non-N-degron) degradation signal of Cup9, a transcriptional repressor of a regulon that includes the Ptr2 transporter of di- and tripeptides (19, 22, 25). This binding

site of Ubr1 is autoinhibited but can be allosterically activated by the binding of cognate peptides (including those imported into cells by Ptr2) to the type 1/2 sites of Ubr1. The resulting down-regulation of the Cup9 repressor, through its accelerated degradation by the N-end rule pathway, up-regulates the expression of the Ptr2 transporter. This positive-feedback circuit allows *S. cerevisiae* to detect the presence of extracellular peptides and to react by increasing their uptake (22, 23, 25). We used *cup9Δ*, *ubr1Δ*, and *cup9Δubr1Δ* mutants to determine whether the observed effect of Ubr1 on the *in vivo* degradation of Mgt1 (e.g., Fig. 2 A, B, D, and F) might be influenced by a circuit controlled by Cup9, and found no such influence (Fig. S4E). In agreement with previous work, which used GST-pulldown assays to demonstrate the dependence of interactions between Ubr1 and GST-Cup9 on the presence of cognate (type 1/2) dipeptides (19, 22), the in vitro binding of ^{f}Ubr1 to GST-Cup9 required the presence of cognate dipeptides such as Arg-Ala (type 1 dipeptide) and Leu-Ala (type 2 dipeptide) (Fig. S4B, lane 11; compare with lane 12). Analogous GST pulldowns were used to detect a specific interaction between ^{f}Ubr1 and GST-Mgt1 (Fig. S4B, lanes 3–9). Interestingly, this interaction did not require the presence of cognate dipeptides. Moreover, it was inhibited by the same (cognate) dipeptides at concentrations that activated the interaction of ^{f}Ubr1 with GST-Cup9 (Fig. S4B, lane 8, compare with lanes 3 and 9). The comparably robust but opposite effect of cognate peptides on the Ubr1-Mgt1 interaction remains to be understood in physiological terms. As would be expected from the Ufd4-dependent degradation of Mgt1 *in vivo* (Fig. 3 B–E and Fig. S2 G and H), a GST-Mgt1

pulldown with ^{ha}Ufd4 (instead of ^{f}Ubr1) confirmed the binding of Ufd4 to Mgt1 (Fig. S4C). In contrast to Mgt1-Ubr1 interactions, which were inhibited by cognate type 1/2 dipeptides (Fig. S4B), the binding of haUfd4 to GST-Mgt1 occurred irrespective of type 1/2 or other tested dipeptides (Fig. S4C). The same results were obtained with Mgt1-GST, in which the GST moiety was C-terminal rather than N-terminal (data not shown). The Ufd4-Mgt1interaction could also be detected by using a coimmunoprecipitation assay (Fig. S4D).

Synergistic Enhancement of the Extent and Processivity of Mgt1 Polyubiquitylation by Ubr1 and Ufd4

We developed an in vitro system that consisted of the following purified components: Ub; Uba1 (Ub-activating enzyme, E1); Rad6 and/or Ubc4 (E2 enzymes specific for Ubr1 and Ufd4, respectively); Ubr1 and/or Ufd4 (E3s that target Mgt1); and ATP. This system also contained ^{35}S-labeled Mgt1$_{f3}$, which was produced in reticulocyte lysate (see SI Materials and Methods). In the final reaction mix, 10% of the total volume was contributed by the ^{35}S-Mgt1-containing reticulocyte lysate. Either the Ubr1-Rad6 Ub ligase alone or the Ufd4-Ubc4 Ub ligase alone polyubiquitylated Mgt1 in vitro (Fig. 4, lanes 3 and 5; compare with lane 1). Whereas the yield of polyubiquitylated Mgt1 was higher with Ubr1-Rad6 alone than with Ufd4-Ubc4 alone, the latter Ub ligase was more processive. Specifically, Mgt1 that was polyubiquitylated by Ufd4-Ubc4 alone migrated as a set of derivatives in a relatively narrow size range, 180 kDa. This molecular mass implied the presence of a polyUb chain linked to the 21-kDa Mgt1 and containing 19 Ub moieties (Fig. 4, lane 5). In contrast, the polyubiquitylated Mgt1 produced by Ubr1-Rad6 alone migrated

as a more diffuse set of derivatives, and at a significantly lower size range, up to 150 kDa (Fig. 4, lanes 3 and 5; compare with lane 1). Strikingly, the polyubiquitylation of Mgt1 in the presence of Ubr1-Rad6 and Ufd4-Ubc4 together exhibited both a higher overall yield and higher processivity. Specifically, Mgt1 that was polyubiquitylated in the presence of both the N-end rule's and UFD's Ub ligases migrated as a set of higher-yield derivatives in a relatively narrow size range, 200 kDa on average (Fig. 4, lane 6; compare with lanes 3 and 5). This size was higher than the one with Mgt1 with Ufd4-Ubc4 alone (Fig. 4, lane 5) and much higher than the one with Mgt1 with Ubr1-Rad6 alone (Fig. 4, lane 3; compare with lane 1). This reproducible result (Fig. 4, lane 6, and data not shown) indicated that the targeting mechanisms of the N-end rule and UFD pathways are not simply ''additive'' in regard to Mgt1. Specifically, this cotargeting of Mgt1, reconstituted in the in vitro system, is synergistic both in regard to yields of polyubiquitylated Mgt1 and in regard to the processivity of polyubiquitylation (Fig. 4, lanes 1, 3, 5, and 6). Operationally, the Ufd4-Ubc4 Ub ligase appears to function, in part, as an enhancer of the processivity of Mgt1 polyubiquitylation by Ubr1-Rad6 (Fig. 4). Such a role of Ufd4-Ubc4 may be analogous to the function of Ufd2, a component of the UFD pathway that Jentsch and colleagues showed to act by increasing the processivity of polyubiquitylation of UFD substrates that contain the N-terminal Ub moiety (28).

Concluding Remarks

The discovery that Mgt1, the DNA alkyltransferase of *S. cerevisiae*, is a physiological substrate of both the N-end rule pathway and the UFD pathway (Fig.

1C) has ramifications for the control of DNA repair not only in fungi but in other eukaryotes as well. The AGT proteins (see Introduction), including yeast Mgt1 and mammalian Mgmt (MGMT), are highly sequelogous (Fig. S3D). In addition, the N-end rule and UFD pathways are present in all eukaryotes examined (2, 14, 26–29, 33). Using a split-Ub assay, we found that mouse Ubr1 and Ubr2, 2 sequelogous N-recognins of the mammalian N-end rule pathway, interact with mouse Mgmt in vivo (J. Sheng, C.-S. H., and A. V., unpublished data), strongly suggesting that (at least) the N-end rule pathway mediates the degradation of mammalian Mgmt. Mouse Ubr2/ fibroblasts, which lack Ubr2 and therefore contain a partially impaired N-end rule pathway, were found to be hypersensitive to mitomycin C, a DNA cross-linking agent (37). Melanoma cells that overexpress Mgmt are also hypersensitive to mitomycin C (38). Taken together with our results (Fig. 1C), these findings suggest that the degradation of mammalian Mgmt, presumably by both the N-end rule and UFD pathways, plays a role in determining the sensitivity of mammalian cells to alkylating agents, including some DNA crosslinking agents as well. The striking effect of simultaneous presence of the Ubr1-Rad6 and Ufd4-Ubc4 Ub ligases on both the yield and processivity of Mgt1 polyubiquitylation makes the *in vitro* system described in Fig. 4 a promising tool for further analyses of Mgt1 targeting. It should be possible to make this assay better defined through the provision of purified Mgt1, currently the system's sole unpurified component (Fig. 4). Questions that can be addressed by this approach include specific location(s) and topology of Mgt1-linked polyUb chains that are produced by the Ubr1-Rad6 versus Ufd4-Ubc4 Ub ligases.

The *in vivo* destruction of Mgt1 that had become alkylated (through the repair of alkylated DNA by Mgt1) may occur at or near the sites of repaired DNA lesions. A priori, it is likely (nothing is known about this at present) that Mgt1 functions as a part of chromosome-associated protein complexes. If so, the subunit selectivity of the N-end rule pathway, i.e., its ability to remodel a protein complex by destroying a subset of its subunits while sparing the rest of them (39), might play a role in the in vivo degradation of Mgt1. This process may be analogous to the previously discovered selective degradation, by the N-end rule pathway, of the separase-produced fragment of Scc1, a subunit of chromosome associated cohesin complexes (40). This degradation of the Scc1 fragment is essential for the high fidelity of chromosome segregation (40). Both the alkylated (inactive) Mgt1 protein (Fig. 1C) and the separase-produced fragment of the Scc1 cohesin subunit (40) are obligatory *in vivo* products of the corresponding circuits. These proteins are also ‘‘dead-end’’ structures. Under conditions where the Scc1 fragment cannot be eliminated by the N-end rule pathway, this protein can be shown to perturb chromosome mechanics (40). A chromosome-bound, alkylated but unremoved Mgt1 may present an analogous problem. Thus, the N-end rule and UFD pathways operate, in these contexts, as homeostasis-maintaining devices that employ their capacity for subunit-selective protein remodeling (39) to reset the states of relevant circuits. Because *ubr1Δ*, *ufd4Δ*, and particularly *ubr1Δufd4Δ* cells were hyperresistant (rather than hypersensitive) to the toxicity of MNNG (Fig. 3F), a precise role of the N-end rule and UFD pathways vis-a-vis DNA repair and other cellular functions remains to be understood. For example, a homeostatic role of these pathways in removing,

through degradation, the alkylated (chromosome-bound?) Mgt1 may be important not for the repair of alkylated DNA per se but for another chromosome-associated process(es) that would be either halted or function suboptimally in the presence of unremoved Mgt1. This interpretation is consistent with a strong toxicity of overexpressed Mgt1 in *ubr1Δufd4Δ* cells but not in wt cells (Fig. S4 G and H).

The discovery that Mgt1 is cotargeted by 2 otherwise dissimilar Ub-dependent pathways (Fig. 1) opens up new questions. For example: Might the cotargeting of Mgt1 by Ubr1 and Ufd4 (Fig. 1C) signify a physical interaction between these E3s? Our preliminary data suggest that Ubr1 and Ufd4 indeed interact, possibly in a conditional manner (unpublished data). Furthermore, previous work indicated that the both the Ubr1 and Ufd4 E3s interact with specific subunits of the 26S proteasome (30, 31). Thus, the demonstrated cotargeting of Mgt1 by the N-end rule and UFD pathways (Fig. 1C) may involve not only copolyubiquitylation of Mgt1 (Fig. 4) but proteasome-docking steps as well.

SI Materials and Methods

Yeast Strains, Media, and Genetic Techniques. The *S. cerevisiae* strains used in this work are described in Table S1. Standard techniques (1) were used for strain construction and transformation. The strains CHY107, CHY108, CHY115, CHY116, and CHY169 were produced by extending the endogenous MGT1 ORF in the *S. cerevisiae* strains JD52, JD55, CHY49, or CHY50 (Table S1) with a sequence encoding 13 head-to-tail repeats of the myc epitope tag (1). This was done using a PCR-mediated gene targeting that used pFA6a-13MYC-TRP1 (2), similarly to a previously

described procedure that was used for gene disruption (3). *S. cerevisiae* CHY121, CHY122, CHY169, CHY194, CHY195, and CHY219 were constructed through disruptions of MGT1 or UFD4 in JD52, JD55, and CHY108 strains (Table S1), using a PCR-mediated gene disruption that used pFA6aKanMX6 or pFA6a-TRP1 (2) similarly to a previously described procedure (3). *S. cerevisiae* that were null mutants in specific E2 or E3 genes were either from the Varshavsky laboratory's strain collection, or obtained from Dr. Youming Xie (Wayne State University, Detroit, MI), or purchased from Open Biosystems. *S. cerevisiae* media included YPD (1% yeast extract, 2% peptone, 2% glucose; only most relevant media components are cited); SD medium (0.17% yeast nitrogen base, 0.5% ammonium sulfate, 2% glucose); and synthetic complete (SC) medium (0.17% yeast nitrogen base, 0.5% ammonium sulfate, 2% glucose, plus a drop-out mixture of compounds required by a given auxotrophic strain).

Plasmids and Site-Directed Mutagenesis. The plasmids used in this study are cited in Table S2. The low copy (CEN-based) pCH336 plasmid expressed $Mgt1_{f3}$ (C-terminally tagged with flag3) from the native P_{MGT1} promoter. To construct pCH336, the promoter region and the MGT1 ORF were PCR-amplified from *S. cerevisiae* genomic DNA using OCH576/OCH450 and OCH492/OCH577 primers (Table S3). The resulting DNA fragments was digested with BamHI/HindIII and HindIII/XhoI, respectively, and triply ligated into BamHI/XhoI-cut pRS416 (4). Overlap extension PCR (5) was used to introduce codons encoding Ser^{151} or Met^{151} instead of wild-type (WT) active-site Cys^{151} into the ORF of MGT1. A pair of the above PCR primers (OCH576/OCH577) was used, in conjunction with primers OCH540/OCH541 or

OCH553/OCH554 (Table S3), for the cloning of pCH337or pCH338, respectively (Table S2). For example, to construct pCH337, which expressed Mgt1^{C151S}, two overlapping DNA fragments with a requisite missense mutation were produced initially, using PCR with the primer pairs OCH576/OCH541 and OCH540/OCH577 (Table S3). These fragments were then denatured and reannealed, so that they formed a partially duplex DNA that encompassed the site of mutation contained 3 overhangs that enabled another PCR, with the primers OCH576 and OCH577 (Table S3), that yielded both the MGT1^{C151S} ORF and its promoter. DNA fragments produced by this procedure (which encoded either Mgt1^{C151S} or Mgt1^{C151M}) were digested with BamHI/XhoI and subcloned into BamHI/XhoI-cut pRS416 vector, yielding, respectively, pCH337 and pCH338 (Table S2). The ubiquitin (Ub) reference (UR) (6) plasmids pCH280 and pCH281 were constructed by inserting the SacII/EcoRI-digested, PCR-amplified MGT1 ORF (using the primer pair OCH494/OCH495) into SacII/EcoR I-cut pMET416$_F$UPRCUP9$_{NSF}$ (7). To construct pCH285, which expressed GST-Mgt1-His$_{10}$, the MGT1-His$_{10}$ ORF, encoding also the C-terminal His$_{10}$ tag, was produced by PCR and the primer pair OCH492/OCH498 (Table S3). The resulting DNA fragment was cloned into BamHI/XhoI-cut pGEX-4T3 (GE Healthcare). Construction details for other plasmids (Table S2) are available upon request. All of the final plasmid constructs were verified by DNA sequencing.

Preparation of Cell Extracts for Immunoblot Analysis.

Yeast extracts were prepared using a modification of Kushnirov's method (8). After yeast cells were grown to exponential phase in selective medium, 1 mL of a culture with A_{600} of 1 was centrifuged for 30 sec at 11,200*g*. Cells were

resuspended in 1 mL of 0.2 M NaOH, and incubated for 20 min on ice or for 5 min at room temperature, followed by centrifugation for 30 sec at 11,200*g*. The pelleted cells were resuspended in 50 µL of HU buffer (8 M urea, 5% SDS, 1 mM EDTA, 100 mM DTT, 0.005% bromophenol blue, 0.2 M TrisHCl, pH 6.8) containing protease inhibitor mixture (Sigma–Aldrich), and heated for 10 min at 70°C. After centrifugation for 5 min at 11,200*g*, 10 µL of supernatant was subjected to SDS/4–12% NuPAGE (Invitrogen) and immunoblotted with either anti-flag (Stratagene), anti-myc, anti-ha, or anti-tubulin antibodies (Sigma–Aldrich). *In vivo* Mgt1 polyubiquitylation assays (Fig. 2B and the main text) used the plasmids pUB204 ($Ub^{K48R,G76A}$), pUB223 (His_6-^{UbK48R,G76A}), and pCH277 ($Mgt1_{ha}$) (Table S2). *S. cerevisiae* expressing $Mgt1_{ha}$ and overexpressing either $Ub^{K48R,G76A}$ (lane 1) or His_6-$Ub^{K48R,G76A}$ (lane 2) were grown to A_{600} of 0.5 in SD medium with required amino acids containing 0.2 mM $CuSO_4$ (to induce the P_{CUP1} promoter) for 3 h before the addition of MG132 to the final concentration of 50 µM for 30 min, followed by a further incubation in the presence of 68 µM MNNG for 1 h. Cell extracts were subjected to Ni-NTA chromatography under denaturing conditions; the retained proteins were fractionated by SDS/4–12% NuPAGE, followed by IB with anti-ha antibody (Fig. 2C and the main text).

GST Fusions and Pulldown Assay, and Purification of GST-Mgt1-His_{10} from *E. coli*. The plasmid pCH285 (Table S2), which encoded GST-Mgt1-His_{10}, was transformed into the *E. coli* BL21-Codon Plus (DE3)-RIL strain (Stratagene). A total of 50 mL of overnight culture of transformed cells was inoculated into 1 L of LB medium containing 0.1 mg/ml ampicilin and 34 g/ml chloramphenicol, followed by

growth at 37 °C for 1 h to A_{600} of 0.8. The expression of GST-Mgt1-His_{10} was induced with 0.2 mM isopropyl -D-thiogalactoside (IPTG) at 30 °C for 4 h. GST-Mgt1-His_{10}, was purified from cell extracts by affinity chromatography with Ni-NTA resin (Qiagen). Specifically, *E. coli* cells were harvested by centrifugation and frozen at -80 °C. Cell pellets were thawed and resuspended in the Ni-NTA binding buffer (0.3 M NaCl, 10 mM imidazole, 10 mM -mercaptoethanol, 50 mM NaH_2PO_4/Na_2HPO_4, pH 8.0) containing chicken egg white lysozyme (1 mg/ml; Sigma–Aldrich). The cells were incubated at 4 °C for 30 min and thereafter disrupted by sonication, 3 times for 1 min each at 1-min intervals, followed by the addition of Nonidet P-40 to the final concentration of 0.1%. After centrifugation at 11,200*g* for 30 min, the supernatant was added to a 2-ml Ni-NTA resin (Qiagen, 50% slurry), and incubated for 1 h at 4 °C. The resin was transferred to a 10-mL column and washed 4 times in 10 mL of washing buffer (0.5 M NaCl, 20 mM imidazole, 10 mM -mercaptoethanol, 0.1% Nonidet P-40, 50 mM NaH_2PO_4/Na_2HPO_4, pH 8.0). GST-Mgt1-His_{10} was then eluted with 1-mL samples of the binding buffer containing increasing levels of imidazole (25, 50, 100, 150, 200, 250, 300 mM), followed by overnight dialysis against storage buffer (10% glycerol, 0.15 M NaCl, 10 mM -mercaptoethanol, 50 mM Hepes, pH 7.5). GST-pulldown assays with extracts from *S. cerevisiae* containing ^{f}Ubr1 were carried out essentially as described in ref. 9, with a slight modification. Either a GST-fusion protein or GST alone (5 g) was incubated with 10 µL GST-Sepharose (50% slurry) in 50 µL of 50 mM NaH_2PO_4/Na_2HPO_4 (pH 8.0) for 20 min on ice. The beads were washed once with 0.5 mL of GST-loading buffer (10% glycerol, 1% Nonidet P-40, 0.5 M NaCl, 1 mM EDTA, 50 mM TrisHCl, pH 8.0) and once with 0.5 mL of GST-binding

buffer (10% glycerol, 0.05% Nonidet P-40, 50 mM NaCl, 50 mM Hepes, pH 7.8). Samples of washed beads in 0.1 mL of GST-binding buffer were incubated with 0.16-mL samples of yeast extracts containing ^{f}Ubr1 in the absence or presence of indicated dipeptides, at 1 mM each. The beads were washed 3 times with 0.25 mL of GST-binding buffer containing dipeptides at 1 mM, and the bound proteins were eluted by adding 12.5 μL of 2X SDS loading buffer and incubating the sample at 95 °C for 5 min, followed by SDS/4–12% NuPAGE and immunoblotting with anti-flag antibody.

Pulse–Chase Assays. Pulse–chase experiments were performed essentially as described (7, 10), with slight modifications. *S. cerevisiae* JD52 (WT), JD55 (*ubr1Δ*), and CHY195 (*ubr1Δufd4Δ*) (Table S1) that carried the plasmids pCH280, pCH437, pCH438, or pCH439 (Table S2) were grown at 30 °C to A600 of 1 in 10 mL of SD medium with required amino acids. Cells were pelleted by centrifugation and washed with 0.8 mL of the medium. Cell pellets were gently resuspended in 0.4 mL of the same medium and labeled for 5 or 10 min at 30 °C with 0.16 mCi of ^{35}S-EXPRESS (Perkin-Elmer). Cells were pelleted again and resuspended in 0.4 mL of SD medium containing unlabeled L-methionine (10 mM) and L-cysteine (5 mM), in addition to required amino acids. Samples (0.1 mL) were taken at the indicated time points, followed by preparation of extracts, immunoprecipitation with anti-flag antibody cross-linked to agarose beads (Sigma–Aldrich), SDS/4–12% NuPAGE in Mes buffer, and autoradiography.

Mutation Frequency and Sensitivity of Cells to MNNG Treatment. To measure increases in mutation rate that were caused by MNNG, the JD52 (UBR1), JD55

(*ubr1Δ*), CHY121 (*mgt1Δ*) or CHY122 (*mgt1Δubr1Δ*) *S. cerevisiae* were grown in YPD medium (from 200 cells per ml) for 2 days (38 h) to A_{600} of 5. The cells in YPD were incubated in the absence or presence of 34 μM MNNG for 30 min at 30 °C. Cells in 1 mL of culture (A_{600} of 5) were pelleted by centrifugation, then washed once in 1 mL of phosphate buffered saline (PBS), then pelleted again, and resuspended in 1 mL of PBS. To determine the frequency of mutations that conferred canavanine resistance, 0.1-mL samples of cells were spread onto SC-Arg plates containing canavanine (60 μg/ml) and incubated for 3 days at 30°C. To determine the fraction of viable cells, these cell suspensions were diluted 250,000-fold in PBS, and 0.1-mL samples were spread on YPD medium, followed by incubation for 3 days at 30 °C. To determine whether the C-terminal 13-myc epitope of $Mgt1_{m13}$ affects MNNG sensitivity of cells expressing $Mgt1_{m13}$ instead of WT Mgt1, the corresponding S. cerevisiae strains were grown to A_{600} of 0.5 in YPD medium, followed by the addition MNNG (to the final concentration of 30 M) for 3 h. The cultures were 5-fold serially diluted, spotted onto YPD medium, and incubated for 2 days at 30°C. To determine the fraction of surviving cells after treatments with MNNG, the YPH277 (UBR1) or YPH277 HR1 (*ubr1Δ*) *S. cerevisiae* strains (Table S1) were grown in YPD medium at 30°C to A_{600} of 1. Stock MNNG solution (6.8 mM in 50 mM Na-acetate, pH 5.0) was added to 1-ml cell suspensions, to the indicated final concentrations of MNNG. Samples were incubated with vigorous shaking for 1 h at 30 °C, followed by appropriate dilutions in PBS, spreading on YPD plates, incubation for 3 days at 30°C, and measurements of colony numbers.

In Vivo Ubiquitylation Assay. *S. cerevisiae* JD52 that expressed $Mgt1_{ha}$ (from pCH279) and overexpressed either $Ub^{K48R,G76A}$ (from pUB204) or His_6-$Ub^{K48R,G76A}$ (from pUB223) were grown at 30 °C to A_{600} of 0.4 in SC(-Trp, -Ura) medium. Cells were then treated with 0.2 mM $CuSO_4$ (to induce the expression of His_6-$Ub^{K48R,G76A}$) for 2.5 h at 30°C, and thereafter with 68 μM MNNG for 1 h. Pelleted and washed cells were resuspended and placed in the bead-beater in the denaturing lysis buffer [6 M guanidine hydrochloride, 1 mM PMSF, 0.1 M NaH2PO4, 10 mM N-ethylmaleimide, 20 mM TrisHCl (pH 8.0) and protease inhibitor mixture]. The suspension was centrifuged at 11,200g for 20 min, and the supernatant was incubated with Ni-NTA agarose beads (Qiagen) for 2 h at 4 °C. The beads were washed 4 times in denaturing lysis buffer, followed by 4 times in wash buffer (0.5 M NaCl 50 mM Tris, pH 8.0). Bound proteins were eluted in elution buffer (1% SDS, 0.1 M EDTA, 0.1 mM DTT, 0.1 M Tris, pH 6.8) and fractionated by SDS/4–12% NuPAGE, followed by immunoblotting with anti-ha antibody (Sigma–Aldrich).

Expression and Purification of Ufd4, Ubr1, Rad6 and Ubc4. The *S. cerevisiae* JD52 (Table S1) that carried p314CUP1FlagUFD4 (Table S2) and expressed the N-terminally flag-tagged Ufd4 (^{f}Ufd4) was grown at 30°C to A_{600} of 4 in 4-L of SC(-Trp) medium containing 0.2 mM $CuSO_4$. The cells were harvested by centrifugation, washed once with PBS, and frozen in liquid N_2. Cells in a frozen pellet (20 g) were broken using glass beads for 5 X40 sec at the power setting of 6.5 in FastPrep-24 (MP Biomedicals) in 40 mL of lysis buffer (10% glycerol, 0.5% Nonidet P-40, 0.2 M KCl, 1 mM PMSF, 5 mM -glycerol phosphate, 50 mM Hepes, pH 7.5) containing protease inhibitor mixture ‘‘for use with fungal and yeast extracts’’ (Sigma–Aldrich).

The suspension was centrifuged at 11,200*g* for 30 min, and the supernatant was mixed with 2 mL of anti-flag M2 affinity beads (Sigma–Aldrich) at 4 °C for 1 h. The beads were collected by centrifugation in Sorvall RT-600B at 1,000 rpm for 5 min at 4 °C, and were washed, sequentially, with 10 mL of lysis buffer, 10 mL of buffer A [10% glycerol, 0.5% Nonidet P-40, 1 M KCl, 1 mM EDTA, 50 mM Hepes (pH 7.5), 5 mM -mercaptoethanol], and 10 mL of buffer B (lysis buffer without Nonidet P-40). ^{f}Ufd4 that was bound by the anti-flag antibody was eluted from the beads with buffer C (buffer B containing flag peptide at 0.5 mg/ml), and thereafter dialyzed at 4 °C overnight against dialysis buffer (10% glycerol, 0.15 M NaCl, 5 mM -mercaptoethanol, 50 mM Hepes, pH 7.5). N-terminally flag-tagged Ubr1 (^{f}Ubr1) was overexpressed in *S. cerevisiae* SC295 (Table S1) and purified by fractionation over anti-flag M2 antibody agarose resin as described in ref. 3. *S. cerevisiae* Rad6 or Ubc4 were overexpressed in the *E. coli* BL21-Codon Plus (DE3)-RIL strain and purified as described previously (7, 9).

In Vitro Ubiquitylation Assay. Purified *S. cerevisiae* Uba1 (Ub activating enzyme, E1) and human Ub were from Boston Biochem. ^{35}S-labeled Mgt1$_{f3}$ was expressed in the reticulocytebased in vitro transcription/translation TNT T7 Quick for PCR DNA kit (Promega), using a PCR-derived DNA fragment that was produced with pCH437 (Table S2) as a template and the primer pair OCH834/OCH438 (Table S3). A total of 2 µl of ^{35}S-labeled Mgt1 was incubated with purified ^{f}Ubr1 (0.2 µM), ^{f}Ufd4 (0.2 µM), Rad6 (1 µM), and/or Ubc4 (1 µM) (see Fig. 4) at 30 °C for 15 min in 20 µL of reaction samples (4 mM ATP, 0.15 M NaCl, 5 mM $MgCl_2$, 1 mM DTT, 50 mM Hepes, pH 7.5) containing 100 nM Uba1 and 80 µM Ub. The reactions were

terminated by adding 8 μL of 4X SDS/PAGE loading buffer. Samples of 14 μL were heated at 95 °C for 5 min, followed by SDS/4–12% NuPAGE in Mops buffer, and autoradiography.

Table 2.S1 Some of the *S. cerevisiae* strains used in this study

Strains	Genotypes and characteristics	Source or ref.
JD52	*MATa trp1-Δ 63 ura3–52 his3-Δ 200 leu2–3112. lys2–801*	1
JD55	*ubr1Δ::HIS3* in JD52	1
SC295	*MATa ura3–52 leu2–3,112 regl-501 gal1 pep4–3*	2
AVY4	*ubr1Δ::LEU2* in JD52	Laboratory collection
AVY16	*leu2–3,112::LEU2* in JD52	Laboratory collection
AVY50	*cup9Δ::LEU2* in JD52	Laboratory collection
AVY51	*cup9Δ::LEU2* in JD55	Laboratory collection
AVY105	*ubr2Δ::HIS3* in JD52	Laboratory collection
CHY49	*pdr5Δ::KanMX6* in JD52	3
CHY50	*pdr5Δ::KanMX6* in JD55	3
CHY92	*GAL80::3HA::KanMX6* in JD52	This study
CHY93	*GAL80::3HA::KanMX6* in JD52	This study
CHY94	*KnaMX6::*P_{GAL1}*::3HA-SRS2*	This study
CHY95	*KnaMX6::*P_{GAL1}*::3HA-SRS2*	This study
CHY101	*SGS1::13MYC::TRP1* in JD52	This study
CHY102	*SGS::13MYC::TRP1* in JD55	This study
CHY107	*MGT1::13MYC::TRP1* in JD52	This study
CHY108	*MGT1::13MYC::TRP1* in JD55	This study
CHY109	*CCR4::3HA::TRP1* in JD52	This study
CHY110	*CCR4::3HA::TRP1* in JD55	This study
CHY115	*MGT1::13MYC::TRP1 pdr5Δ::KanMX6* in JD52	This study
CHY116	*MGT1::13MYC::TRP1 pdr5Δ::KanMX6* in JD55	This study
CHY121	*mgt1Δ::KanMX6* in JD52	This study
CHY122	*mgt1Δ::KanMX6* in JD55	This study
CHY134	*ubr1Δ::LEU2 ubr2Δ::HIS3* in JD52	This study
CHY161	*PEX7::3HA* in JD52	This study
CHY162	*PEX7::3HA::TRP1* in JD55	This study
CHY163	*YGL081W::13MYC::TRP1* in JD52	This study
CHY164	*YGL081W::13MYC::TRP1* in JD55	This study
CHY169	*MGT1::13MYC::TRP1 ufd4Δ::KanMX6* in JD55	This study
CHY107	*MGT1::13MYC::TRP1* in JD52	This study
CHY108	*MGT1::13MCY::TRP1* in JD55	This study
CHY194	*ufd4Δ::KanMX6* in JD52	This study
CHY195	*ubr1Δ::HIS3 ufd4Δ::KanMX6* in JD52	This study
CHY219	*ufd4Δ:: TRP1 MGT1–13MYC::KanMX6* in JD52	This study
YPH277	*MATa ura3–52 ade2–101 trp1-D1 leu2-D1 CFVII (RAD2.d) URA3 SUP11*	4
YPH277HR1	*ubr1Δ::LEU2* in YPH277	5
BY4425	*ubc2Δ:: KanMX4* in BY4741	Open Biosystems
BY3216	*ubc4Δ:: KanMX4* in BY4741	Open Biosystems
BY3994	*ubc5Δ::KanMX4* in BY4741	Open Biosystems
BBY67.3	*ubc6Δ::HIS3* in JD52	Laboratory collection
BY597	*ubc7Δ::KanMX4* in BY4741	Open Biosystems
BY6577	*ubc8Δ:: KanMX4* in BY4741	Open Biosystems
BY4763	*ubc10Δ:: KanMX4* in BY4741	Open Biosystems
BY1636	*ubc11Δ:: KanMX4* in BY4741	Open Biosystems
BY5214	*ubc12Δ:: KanMX4* in BY4741	Open Biosystems
BY4027	*ubc13Δ:: KanMX4* in BY4741	Open Biosystems
BY4454	*mms2Δ:: KanMX4* in BY4741	Open Biosystems
BY3771	*bre1Δ:: KanMX4* in BY4741	Open Biosystems
BY6430	*rad5Δ:: KanMX4* in BY4741	Open Biosystems
BY5787	*rad18Δ:: KanMX4* in BY4741	Open Biosystems
BY4425	*ufd2Δ:: KanMX4* in BY4741	Open Biosystems
BY3216	*ufd4Δ:: KanMX4* in BY4741	Open Biosystems
BY3994	*hul4Δ::KanMX4* in BY4741	Open Biosystems
BY597	*hul5Δ::KanMX4* in BY4741	Open Biosystems
BY6577	*tom1Δ:: KanMX4* in BY4741	Open Biosystems
BY4763	*hrd1Δ:: KanMX4* in BY4741	Open Biosystems
BY4156	*hrd3Δ:: KanMX4* in BY4741	Open Biosystems
BY4883	*tul1Δ:: KanMX4* in BY4741	Open Biosystems
BY7299	*doa10Δ::KanMX4* in BY4741	Open Biosystems
BY4814	*ubr1Δ:: KanMX4* in BY4741	Open Biosystems
BY1579	*ubr2Δ:: KanMX4* in BY4741	Open Biosystems
BY3771	*bre1Δ:: KanMX4* in BY4741	Open Biosystems
BY6430	*rad5Δ:: KanMX4* in BY4741	Open Biosystems
BY5787	*rad18Δ:: KanMX4* in BY4741	Open Biosystems
MGG15	*ura3–52 cdc34–2*	6
FW1808	*MAT Δhis4–912 R5 Δlys2–128 Δura3–52 rps5–1*	7

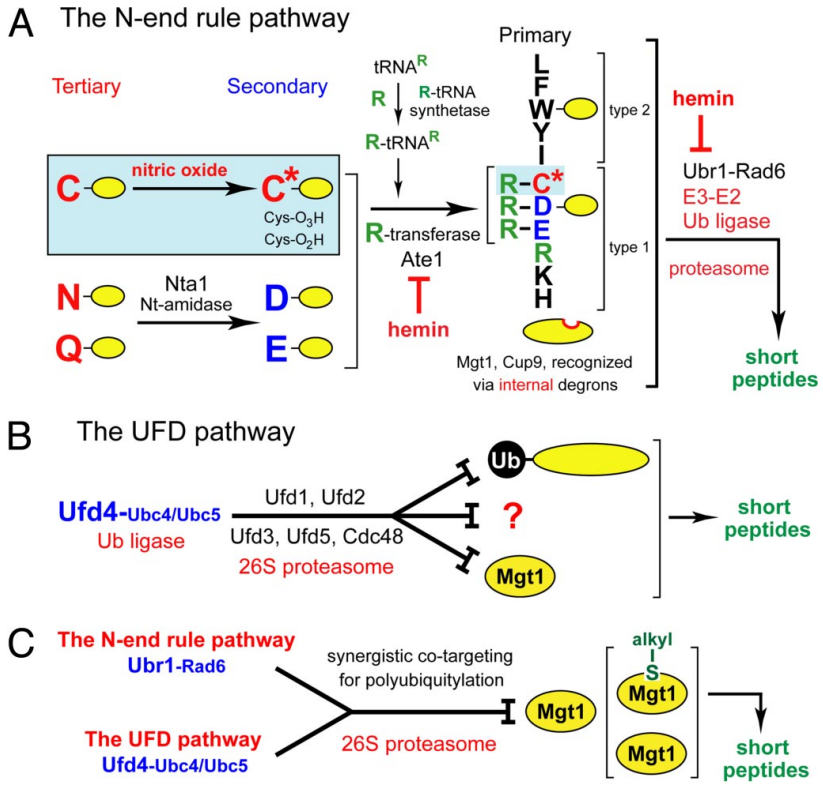

Figure A1.1. The N-end rule pathway, the UFD pathway, and cotargeting of the Mgt1 DNA alkyltransferase by these proteolytic systems. (A) The *S. cerevisiae* N-end rule pathway. N-terminal residues are indicated by single-letter abbreviations for amino acids. Yellow ovals denote the rest of a protein substrate. Primary, secondary, and tertiary denote mechanistically distinct subsets of destabilizing N-terminal residues. Hemin (Fe^{3+}-heme) inhibits the arginylation activity of the ATE1-encoded Arg-tRNA-protein transferase (R- transferase), and also inhibits a subset of Ubr1 functions (24). Reactions in the shaded rectangle are a part of the pathway that is active in multicellular eukaryotes, which produce NO (18), and is also relevant to eukaryotes such as *S. cerevisiae*, which lack NO synthases but can produce NO by other routes and can also be influenced by NO from extracellular sources. C*

denotes oxidized Cys, either Cys-sulfinate or Cys-sulfonate. (B) The S. cerevisiae UFD pathway. Previously known artificial (engineered) UFD substrates have in common a ‘‘nonremovable’’ N-terminal Ub moiety, which functions as a degron in the UFD pathway (14, 26, 27). Mgt1 is the first physiological UFD substrate that lacks an N-terminal Ub moiety and is not a component of the Ub system (see Introduction). A question mark denotes the expectation of other UFD substrates. (C) Cotargeting of Mgt1 by the N-end rule and UFD pathways.

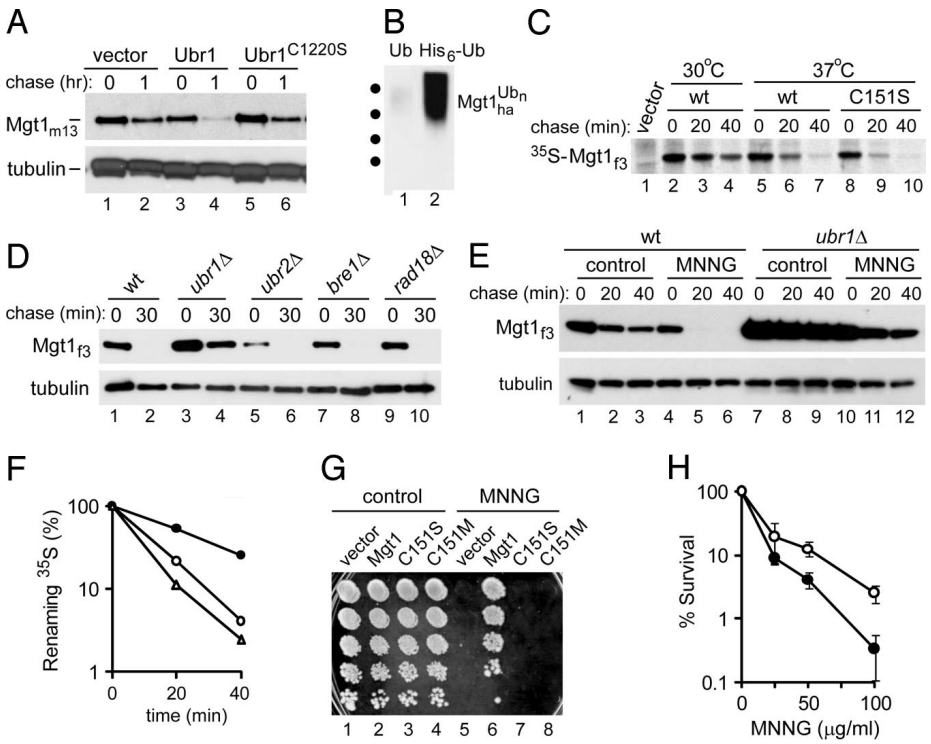

Figure A1.2. Mgt1 as a physiological substrate of the N-end rule pathway. (A) CHY108, a *ubr1Δ* strain of *S. cerevisiae* that expressed $Mgt1_{m13}$ (Mgt1 C-terminally tagged with 13 myc epitopes) (see *SI Materials and Methods* and Table S1) was transformed with pRS315 (vector alone), with pCH100 (expressing wt Ubr1), or with pCH159 (expressing inactive $Ubr1^{C1220S}$) (20). Cultures were grown to an A_{600} of ~1 in SD medium, followed by a ''chase'' with cycloheximide for 1 h and IB of cell extracts with either anti-myc or anti-tubulin antibodies (the latter antibody was used to verify the uniformity of total protein loads). (B) Polyubiquitylated $Mgt1_{ha}$, detected by IB with anti-ha antibody, in MNNG-treated cells that expressed untagged Ub (lane 1) or His_6-Ub (lane 2). Dots on the left refer to positions of molecular mass markers, at 75, 100, 150, and 250 kDa, respectively. (C) *S. cerevisiae* expressing $Mgt1_{f3}$ (pCH437) or $Mgt1^{C151S,f3}$ (pCH438) (Table S2) were grown in SD

medium to an A_{600} of ~0.8, then incubated further for 1 h at 30°C or 37°C and labeled with [^{35}S]methionine/cysteine for 5 min, followed by a chase for 0, 20, and 40 min at 30°C or 37°C, respectively. Cell extracts were precipitated with anti-flag antibody, followed by SDS–4–12% NuPAGE and autoradiography. (D) Cycloheximide ''chase'' assays with Mgt1 and *S. cerevisiae* null mutants in genes encoding the indicated E3 Ub ligases. (E) Wt and *ubr1Δ S. cerevisiae* expressing $Mgt1_{m13}$ ($Mgt1_{myc13}$) from the P_{MGT1} promoter were grown to an A_{600} of ~0.6 and incubated further in the presence of 68 μM MNNG for 1 h, followed by a ''chase'' with cycloheximide for 20 and 40 min, SDS– 4 –12% NuPAGE of cell extracts, and IB with anti-myc and anti-tubulin antibodies. (F) Quantitation of the data in *C,* using PhosphorImager. Open and solid circles indicate $Mgt1_{f3}$ at 37°C and at 30°C, respectively; open triangles indicate $Mgt1^{C151S,f3}$ at 37 °C. (G) CHY21 (*mgt1Δ*) *S. cerevisiae* expressing $Mgt1_{f3}$ (pCH336), $Mgt1^{C151S,f3}$ (pCH337), or $Mgt1^{C151M,f3}$ (pCH338) were grown to an A_{600} of ~0.8 at 30°C in SD medium, followed by a further incubation for 1 h, in either the presence or absence of 68 μM MNNG. The cultures were serially diluted, spotted on YPD plates, and incubated for 3 days at 30 °C. (H) Colony assay for MNNG toxicity. *S. cerevisiae* YPH277 (wt) (solid circles) and YPH277HR1 (*ubr1Δ*) (open circles) were grown in YPD medium at 30 °C to an A_{600} of ~1.0 and were further incubated for 1 h in the presence of MNNG at indicated concentrations. Cell suspensions were diluted in PBS, spread on YPD plates, and incubated for 3 days at 30 °C, followed by determination of colony numbers.

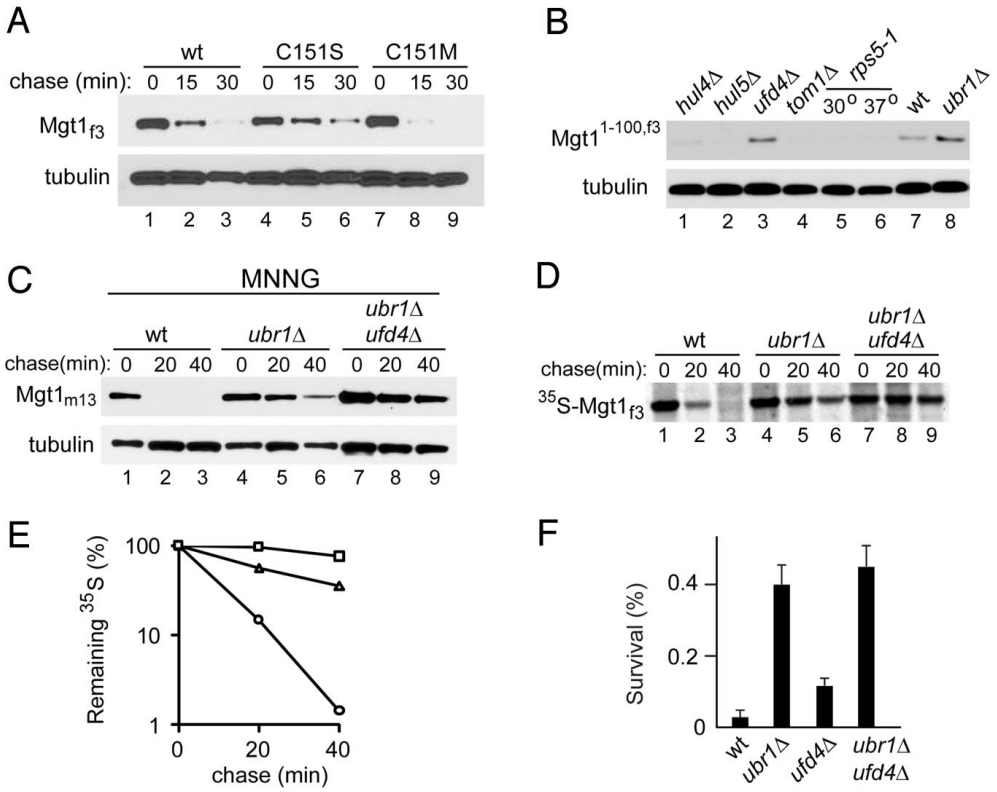

Figure A1.3. The UFD pathway plays a role in degradation of Mgt1. (A) CHY21 (*mgt1Δ*) *S. cerevisiae* expressing $Mgt1_{f3}$ (pCH336), $Mgt1^{C151S,f3}$ (pCH337), or $Mgt1^{C151M,f3}$ (pCH338) were grown to an A_{600} of ~0.8 at 30 °C, then incubated for 1 h with MNNG at 68 μM, followed by a ''chase'' with cycloheximide for 15 and 30 min, SDS–4– 12% NuPAGE of cell extracts, and IB with anti-flag and anti-tubulin antibodies. (B) The *in vivo* levels of $MGT1^{1-100,f3}$ (see Fig. S4A) were compared by IB, using anti-flag and anti-tubulin antibodies (the latter a loading control), with extracts from wt *S. cerevisiae* and its null mutants in either Ubr1 or several HECT-type E3 Ub ligases (a *ts* mutant in the case of Rps5). $MGT1^{1–100,f3}$ was expressed in these strains from pCH372 (Table S2). Cultures were grown at 30 °C to an A_{600} of ~0.8. Some IB assays (with *rps5-1* cells) were also carried out with extracts from cells that were incubated for 1 h at 37 °C. Note an increase of $MGT1^{1–100,f3}$ in *ufd4Δ*

cells, in addition to *ubr1Δ* cells. (C) Wt, *ubr1Δ,* and *ubr1Δufd4Δ S. cerevisiae* that expressed chromosomally integrated $MGT1_{m13}$ (see *SI Materials and Methods)* were grown at 30 °C to an A_{600} of ~0.8 and were further incubated in the presence of MNNG (68 μM) for 1 h, followed by a ''chase'' with cycloheximide for 20 and 40 min, SDS– 4 –12% NuPAGE of cell extracts, and IB with anti-myc and anti-tubulin antibodies. (D) Pulse–chase assays with $Mgt1_{f3}$ and wt (lanes 1–3), *ubr1Δ* (lanes 4–6), or *ubr1Δufd4Δ* (lanes 7–9) *S. cerevisiae.* Cells expressing $Mgt1_{f3}$ from the P_{MET25} promoter on a low copy plasmid were labeled for 5 min with [^{35}S]methionine/ cysteine and chased for 0, 20, or 40 min, followed by immunoprecipitation with anti-flag antibody, SDS/PAGE, and autoradiography (see *SI Materials and Methods).* (E) Quantitation of data in *D,* using PhosphorImager. Circles, wt cells; triangles, *ubr1Δ* cells; squares, *ubr1Δ ufd4Δ* cells. 100% refers to the relative amount of ^{35}S at time 0 (end of pulse) for each of 3 pulse–chases. (F) *S. cerevisiae* of the indicated genotypes were grown to an A_{600} of ~0.6 in YPD medium and were further incubated in either the presence or absence of MNNG (0.34 mM) for 1.5 h at 30 °C. Cell suspensions were diluted with PBS (PBS), spread on YPD plates, and incubated for 3 days at 30 °C. Survival refers to numbers of colonies in MNNG-treated samples as percentages of the corresponding numbers in untreated samples.

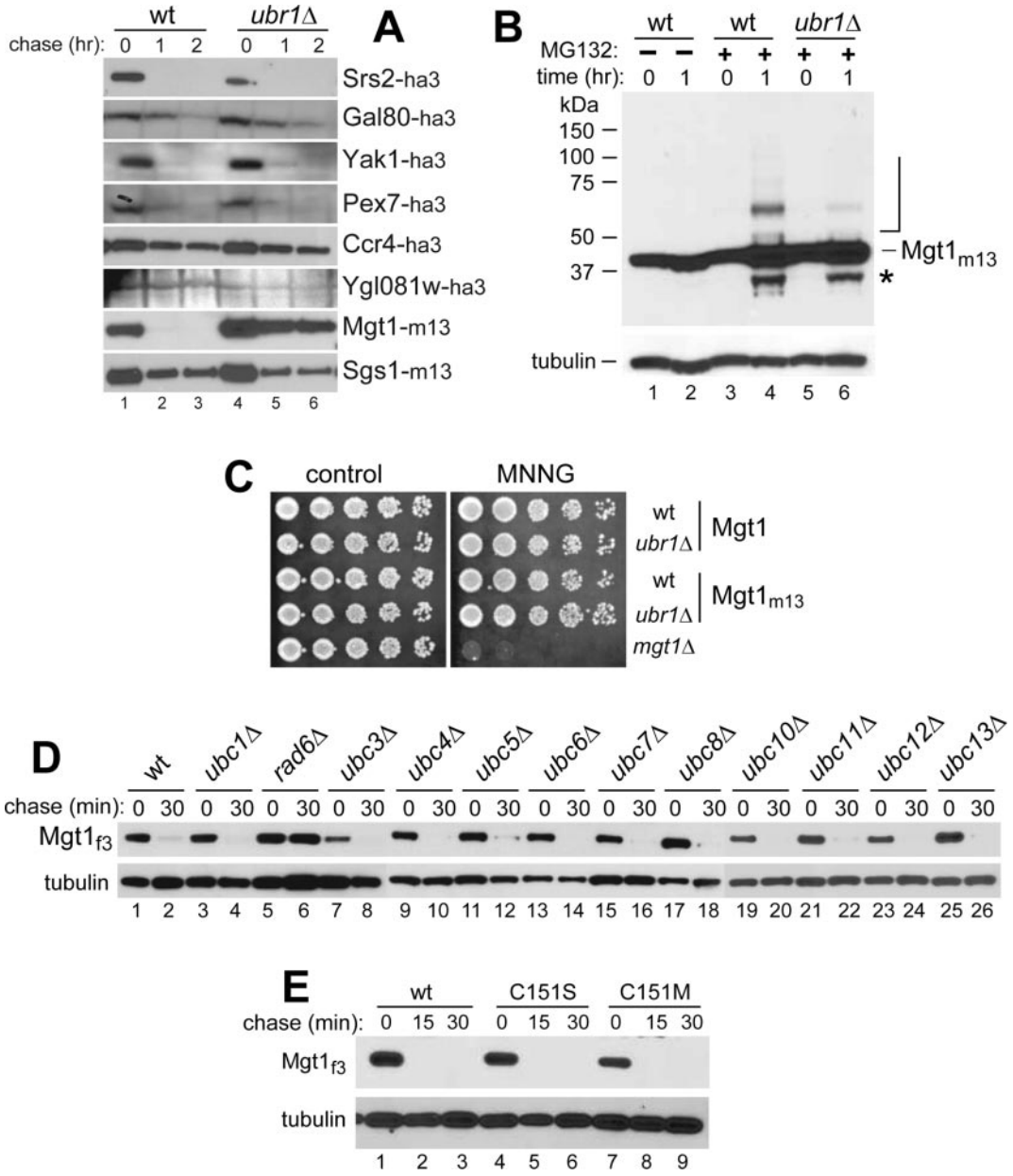

Figure A1.S1. (A) ‘‘Chases’’ with cycloheximide to test putative Ubr1-interacting proteins for their degradation by the N-end rule pathway *in vivo*. The *S. cerevisiae* proteins examined in these experiments were described as proteins that could be coimmunoprecipitated with *S. cerevisiae* Ubr1 in proteomic-scale experiments (1–3). JD52 (WT) and JD55 (*ubr1Δ*) *S. cerevisiae* carrying plasmids (Table S2) that expressed the indicated proteins were grown at 30 °C to A_{600} of ~1.0, followed by a

‘‘chase’’ with cycloheximide for 1 and 2 h, as described in *SI Materials and Methods,* using immunoblotting with anti-ha and anti-myc antibodies. Note that although most of the tested proteins were apparently short-lived *in vivo*, only Mgt1 was significantly stabilized in the absence of Ubr1. (B) Accumulation of ubiquitylated $Mgt1_{m13}$ (Mgt1myc13) in the presence of MG132, a proteasome inhibitor. MG132-sensitive *pdr5Δ S. cerevisiae* (4) CHY115 cells (MGT1myc13::TRP1 *pdr5Δ::KanMX6)* (Table S1) were grown to A_{600} of ∼1 and incubated further in the presence of either MG132 (50 μM) or dimethyl sulfoxide (an equivalent amount of solvent of the stock solution of MG132) for indicated times at 30 °C. Cell extracts were fractionated by SDS/4 –12% NuPAGE and immunoblotted with anti-myc and anti-tubulin antibodies. The (overexposed) band of full-length $Mgt1_{m13}$ and its ubiquitylated derivatives are denoted on the right. Overexposure was used to facilitate the detection of ubiquitylated $Mgt1_{m13}$. An asterisk denotes a (presumed) proteolytic fragment of $Mgt1_{m13}$. (C) WT *MGT1* was replaced by an ORF encoding $Mgt1_{m13}$, a derivative C-terminally tagged with the myc13 epitope and expressed from the native P_{MGT1} promoter. $Mgt1_{m13}$ was indistinguishable from WT Mgt1 in its ability to protect cells from MNNG. WT or *ubr1Δ* strains expressing either WT Mgt1 or $Mgt1_{m13}$, and a congenic WT strain lacking Mgt1 were grown to A_{600} of ∼0.5 in YPD medium and further grown either in the presence or absence of 30 μM MNNG for 3 h in the same medium. The cultures were serially diluted 5-fold, spotted on YPD plates, and incubated for 2 days at 30 °C. (D) The Rad6 E2 enzyme is required for Mgt1 degradation. A set of *S. cerevisiae* null mutants in genes encoding specific E2 (Ub-conjugating) enzymes carried pCH336, which expressed $Mgt1_{f3}$ from the P_{MGT1}

promoter. Cells were grown to A_{600} of ~0.8 at 30 °C, and thereafter incubated at 37 °C for 1 h (to increase the assay's sensitivity; see the main text), followed by a ''chase'' with cycloheximide (50 μg/ml) for 30 min. Cell extracts were fractionated by SDS/4 –12% NuPAGE, followed by IB with anti-flag and anti-tubulin antibodies. (E) Heat-induced degradation of $Mgt1_{f3}$ is apparently independent of the identity of its residue at position 151. The same strains and procedures as in *A,* except that cells were not treated with MNNG, and were incubated, instead, at 37 °C for 1 h, followed by a ''chase'' with cycloheximide, also at 37 °C.

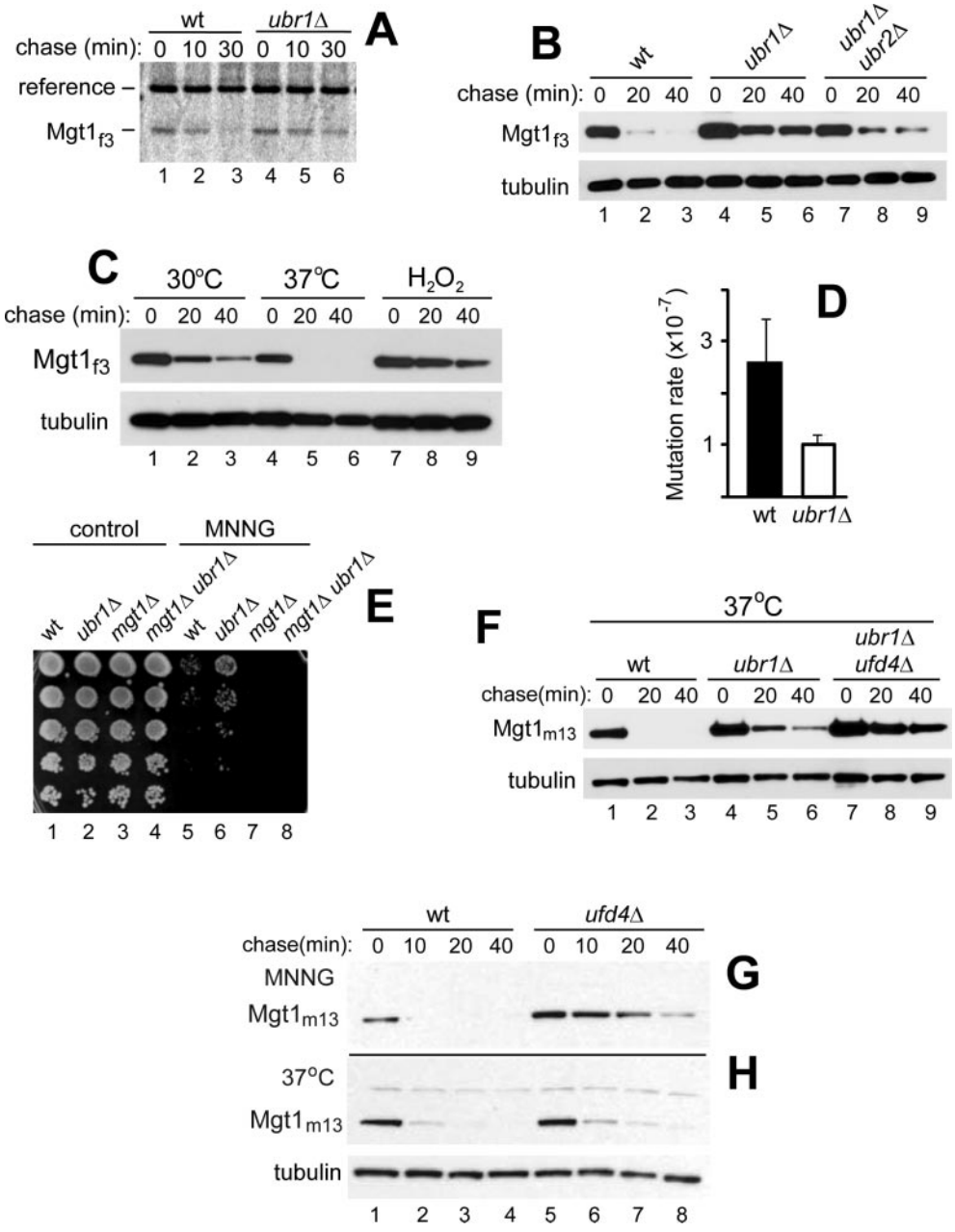

Figure A1.S2. (A) Pulse–chase analysis, using the Ub-reference (UR) technique, of flag-tagged $Mgt1_{f3}$. JD52 (WT) cells (lanes 1–3) and JD55 (*ubr1Δ*) cells (lanes 4 – 6) expressing $^{f}DHFR\text{-}Ub^{K48R}\text{-}Mgt1^{f}$ (pCH281) were grown at 30 °C to A_{600} of ~1, followed by labeling for 5 min with [^{35}S]methionine/cysteine and a chase (in the presence of cycloheximide) for 0, 10 or 30 min at 30 °C. Cell extracts were

precipitated with anti-flag antibody, followed by SDS/4 –12% NuPAGE and autoradiography. ‘‘Reference’’ on the left denotes the ^{f}DHFR-Ub^{K48R} moiety. (B) Cycloheximide ‘‘chase’’ assays with JD52 (WT), JD55 (*ubr1Δ*), or double-mutant CHY134 (*ubr1Δubr2Δ) S. cerevisiae* strains expressing $Mgt1_{f3}$. (C) WT *S. cerevisiae* expressing $Mgt1_{m13}$ ($Mgt1_{myc13}$) from the P_{MGT1} promoter were grown to A_{600} of ~0.6, and thereafter preincubated for 1 h at 30 °C (lanes 1–3), or at 37 °C (lanes 4 – 6), or at 30 °C but in the presence of 1 mM H_2O_2 (lanes 7–9), with the same (preincubation) conditions during cycloheximide ‘‘chases’’ for 20 and 40 min. Cell extracts were fractionated by SDS/4 –12% NuPAGE, followed by IB with anti-myc and anti-tubulin antibodies. (D) Ubr1-lacking *S. cerevisiae* are more resistant to MNNG-induced mutagenesis. JD52 (WT) (filled bar) and JD55 (*ubr1Δ*) (open bar) *S. cerevisiae* were seeded in YPD medium at ~200 cell/ml, and grown for ~38 h to A_{600} of ~5. Cell suspensions were incubated in the presence of 34 μM MNNG for 30 min at 30 °C, then diluted with PBS and spread onto either YPD plates or arginine-lacking SC(-Arg) plates containing canavanine (60 μg/ml), to select for canavanine-resistant cells. Plates were incubated for 3 days at 30 °C, and the resulting colonies were counted. (E) Cells of indicated genotypes (Table S1) were grown to A_{600} of ~0.6 in YPD medium at 30 °C, and were further incubated in the presence of 0.1 mM MNNG for 1 h. The cultures were serially diluted 5-fold, spotted on YPD plates, and incubated for 2 days at 30 °C. (F) WT, *ubr1Δ* and double-mutant *ubr1Δ ufd4Δ S. cerevisiae* that expressed chromosomally integrated $MGT1_{m13}$ (see *SI Materials and Methods)* were grown at 30 °C to A_{600} of ~0.8, and were further incubated for 1 h at 37 °C, followed by a ‘‘chase’’ with cycloheximide, also at 37 °C. SDS/4 –12% NuPAGE

of cell extracts was followed by IB with anti-myc and anti-tubulin antibodies. (G and *H)* WT and *ufd4Δ S. cerevisiae* with chromosomally integrated $MGT1_{m13}$ (see *SI Materials and Methods)* were grown in SC medium at 30 °C to A_{600} of ~0.8 and were further incubated in the presence of MNNG (68 μM) for 1 h (panel *G),* or at 37 °C (panel *H),* followed by a ‘‘chase’’ with cycloheximide for 10, 20, and 40 min, fractionation of cell extracts by SDS/4 –12% NuPAGE, and IB with anti-myc and anti-tubulin antibodies.

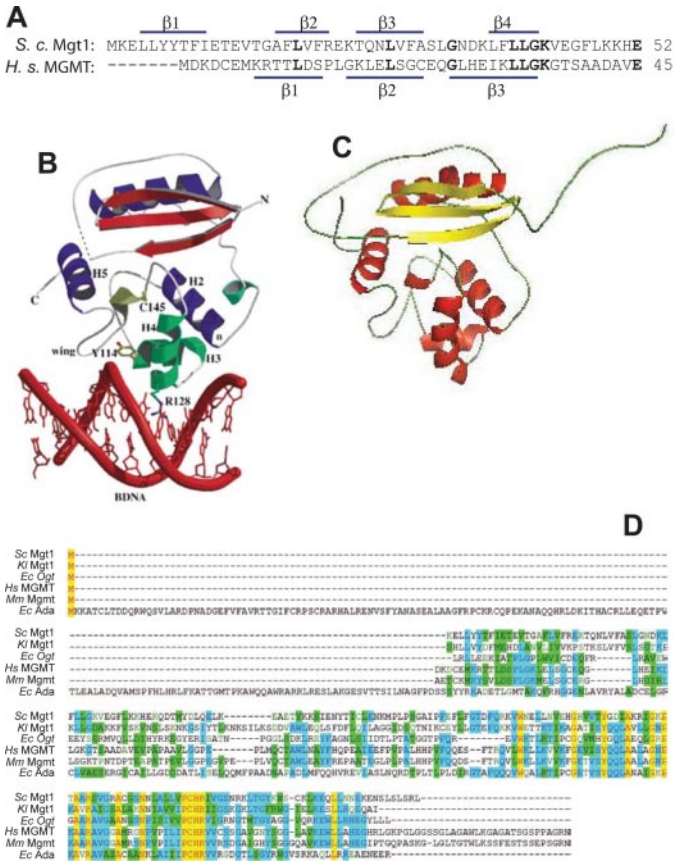

Figure A1.S3. (A) Four putative β-sheets in the N-terminal region of *S. cerevisiae* Mgt1 that are sequelogous (similar in sequence), and probably also spalogous (spatially similar) (1) to the corresponding regions of human Mgmt (MGMT), the structure of which was determined previously (2). Residues identical between *S. cerevisiae* Mgt1 and human MGMT are in bold. (B) The structure of human Mgmt and a model of its interaction with DNA (2). Alkyl lesions are removed by Mgt1 and Mgmt from DNA through a base-flipping mechanism (3). (C) The hypothetical 3D structure of *S. cerevisiae* Mgt1, produced by Modeller-9v1 (http://salilab.org/modeller/), using the structure of human Mgmt (1eh6.pdb) as its template, and displayed using PyMol (DeLano Scientific). (D) Sequence alignments among O^6-alkyguanine transferases of the yeasts (fungi) *S. cerevisiae* (Sc) and

Kluyveromyces lactis (Kl), the prokaryote *E. coli* (Ec), and the mammals *Homo sapiens* (Hs) and *Mus musculus* (Mm).

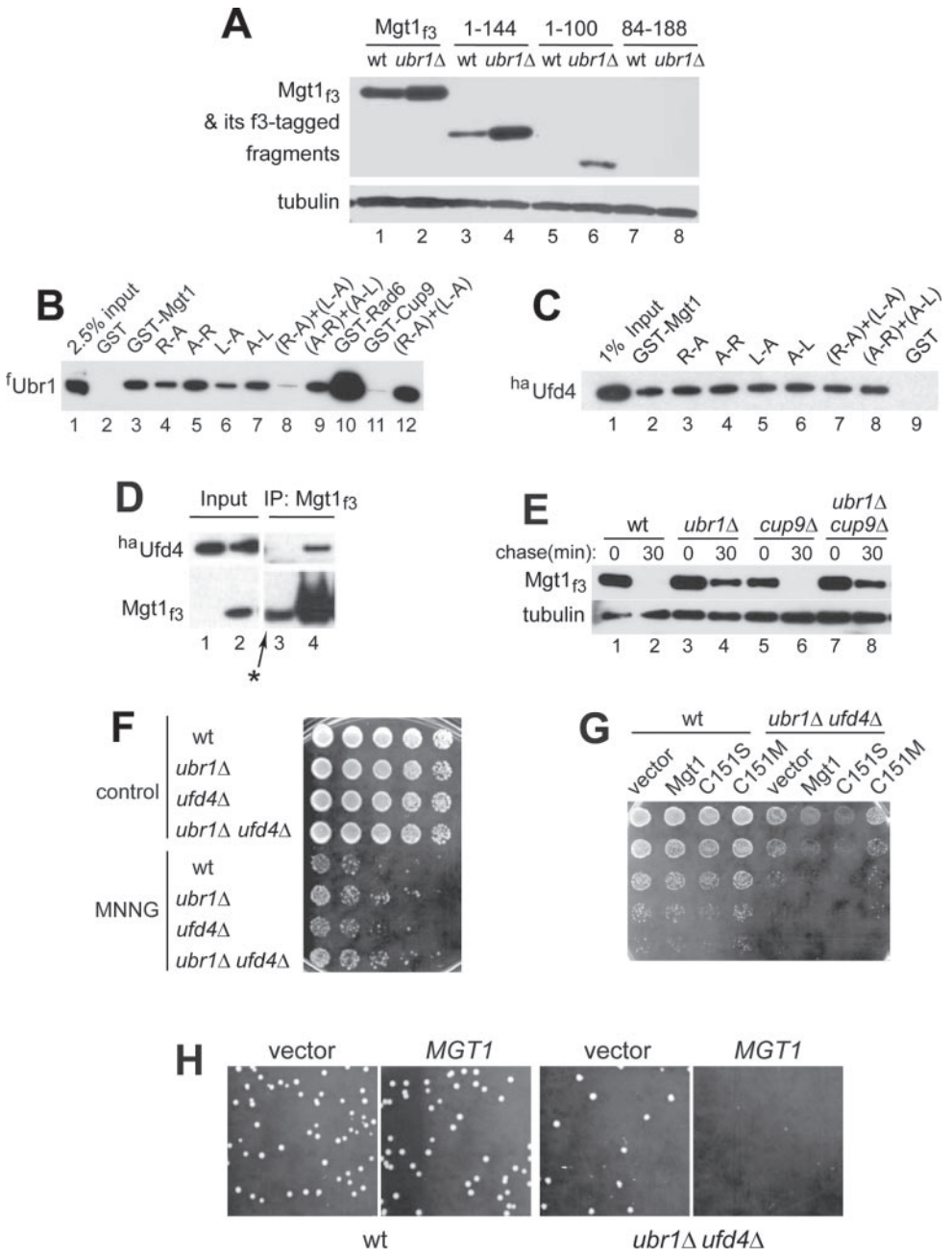

Fig. A1.S4. (A) JD52 (WT) and JD55 (*ubr1Δ*) *S. cerevisiae* expressing either full-length $Mgt1_{f3}$ (from the P_{MGT1} promoter on a low copy plasmid) or its C-terminally truncated derivatives were grown to A_{600} of ~0.8, followed by SDS/4 –12% NuPAGE of cell extracts and IB with anti-flag and anti-tubulin antibodies. Lanes 1 and 2, full-

length $Mgt1^{1–188,f3}$ in WT and *ubr1Δ* cells, respectively. Lanes 3 and 4, same as lanes 1 and 2, respectively, but with $Mgt1^{1–144,f3}$. Lanes 5 and 6, same but with $Mgt1^{1–100,f3}$. Lanes 7 and 8, same but with $Mgt1^{84–188,f3}$. (B) Equal amounts of extracts (50 μg) from *S. cerevisiae* that expressed the N-terminally flag-tagged Ubr1 (^{f}Ubr1) were incubated in either the presence or absence of specific dipeptides (each of them at 1 mM) with GST alone or specific GST fusions (~5 μg) that were linked to glutathione-Sepharose beads. Bound proteins were eluted from the beads and fractionated by SDS/4–12% NuPAGE, followed by IB with anti-flag antibody. Lane 1, 2.5% of the initial (total) input of ^{f}Ubr1. Lane 2, GST alone. Lane 3, GST-Mgt1. Lane 4, same as lane 3 but with Arg-Ala (R-A, 1 mM). Lane 5, same as lane 4 but with Ala-Arg (A-R, 1 mM). Lane 6, same as lane 3 but with Leu-Ala (L-A, 1 mM). Lane 7, same as lane 3 but with Ala-Leu (A-L, 1 mM). Lane 8, same as lane 3 but with both Arg-Ala and Leu-Ala (R-A and L-A, 1 mM each). Lane 9, same as lane 3 but with both Ala-Arg and Ala-Leu (A-R, A-L, 1 mM each). Lane 10, GST-Rad6. Lane 11, GST-Cup9. Lane 12, same as lane 11 but with both Arg-Ala and Leu-Ala (R-A and L-A, 1 mM each). (C) Equal amounts of extracts (0.2 mg) from *S. cerevisiae* that expressed the N-terminally ha-tagged Ufd4 (^{ha}Ufd4) were incubated with GST alone or specific GST fusions (~5 μg), and were processed as described in *B,* except that IB that ^{ha}Ufd4 was detected by was performed with anti-ha antibody. Lane 1, 1% of the initial (total) input of ^{ha}Ufd4. Lane 2, GST-Mgt1. Lane 3, same as lane 2 but with Arg-Ala (R-A, 1 mM). Lane 4, same as lane 2 but with Ala-Arg (A-R, 1 mM). Lane 5, same as lane 2 but with Leu-Ala (L-A, 1 mM). Lane 6, same as lane 2 but with Ala-Leu (A-L, 1 mM). Lane 7, same as lane 2 but with both Arg-Ala and Leu-Ala (R-A and L-A 1 mM each). Lane 8, same

as lane 2 but with both Ala-Arg and Ala-Leu (A-R and A-L, 1 mM each). Lane 9, GST alone. (D) Mgt1 interacts with Ufd4. Extracts (1 mg) from *S. cerevisiae* cells coexpressing ^{ha}Ufd4 (from the pRS313CUP1^{ha}UFD4 plasmid; Table S2) and either a vector alone or Mgt1$_{f3}$ (from the plasmid pCH437) were precipitated with anti-flag antibody, using protein G linked to magnetic beads. Immunoprecipitates were fractionated by SDS/4 –12% NuPAGE, followed by IB with anti-ha and anti-flag antibodies. Lane 1, input sample (0.25% of extract used in immunoprecipitation assays) from cells expressing ^{ha}Ufd4 and the (''empty'') vector p416MET25. Lane 2, same as lane 1 but from cells coexpressing ^{ha}Ufd4 and Mgt1$_{f3}$. Lane 3, haUfd4, immunoprecipitation with anti-flag antibody in the absence of coexpressed Mgt1$_{3f}$. Lane 4, same as lane 3 but ^{ha}Ufd4 was coexpressed with Mgt1$_{f3}$. The band detected in lane 3 with anti-flag antibody and marked by an arrow and asterisk, just below the position of Mgt1$_{f3}$ (see lane 4), is the light chain of anti-flag antibody that was used for immunoprecipitation as well (see above). Because of light-chain's abundance at that position on the IB membrane, this otherwise weak cross-reaction was detectable at the level of IB exposure shown (compare the level of the cross-reacting band with the levels of immunoprecipitated Mgt1 in lane 4). (E) Cup9-regulated circuits do not influence the Ubr1-mediated degradation of Mgt1. AVY16 (WT), AVY4 (*ubr1Δ*), AVY50 (*cup9Δ*), or AVY51 (*ubr1Δcup9Δ) S. cerevisiae* (Table S2) expressing Mgt1$_{f3}$ from the P_{MGT1} promoter on a low copy plasmid were grown to A_{600} of ~0.8 in SC(-Ura) medium at 30 °C, then incubated further at 37 °C for 1 h, followed by a 30-min ''chase'' with cycloheximide (at 50 μg/ml), fractionation of cell extracts by SDS/4 –12% NuPAGE and IB with anti-flag and anti-tubulin antibodies.

Note that $Mgt1_{f3}$ remained short-lived in *cup9Δ* cells (lanes 5, 6). (F) JD52 (WT), JD55 (*ubr1Δ*), CHY194 (*ufd4Δ*), or CHY195 (*ubr1Δufd4Δ) S. cerevisiae* (Table S1) were grown to A_{600} of ~0.6, and treated with MNNG (170 μM) for 1.5 h at 30 °C. The resulting cultures were serially diluted 5-fold, spotted on YPD plates, and incubated for 2 days at 30 °C. See also the main-text Fig. 3H. (G) A double-mutant *ubr1Δufd4Δ* strain of *S. cerevisiae* is hypersensitive to overexpression of Mgt1. JD52 (WT) and CHY195 (*ubr1Δufd4Δ)* cells carrying a vector alone (pRS426MET25), or expressing either $Mgt1_{f3}$ (pCH440), or $Mgt1^{C151S,f3}$ (pCH441), or Mgt1C151M,f3 (pCH442) were grown in SD medium (with essential amino acids) to A600 of ~0.8, serially diluted, and spotted on SD medium for 2 days at 30 °C. (H) Same as in *C* but single-colony growth assays with JD52 (WT) and CHY195 (*ubr1Δufd4Δ)* cells carrying either a vector alone or expressing $Mgt1_{f3}$ from the P_{MET25} promoter on a high copy plasmid.

REFERENCES

1. Jentsch S, McGrath JP, Varshavsky A (1987) The yeast DNA repair gene RAD6 encodes a ubiquitin-conjugating enzyme. *Nature* 329:131–134.

2. Varshavsky A (2008) Discovery of cellular regulation by protein degradation. *J Biol Chem* 283:34469 –34489.

3. Harper JW, Elledge SJ (2007) The DNA damage response: Ten years after. *Mol Cell* 28:739 –745.

4. Friedberg EC, *et al.* (2006) *DNA Repair and Mutagenesis* (ASM Press, Washington, DC).

5. Sedgwick B, Bates PA, Paik J, Jacobs SC, Lindahl T (2007) Repair of alkylated DNA: Recent advances. *DNA Repair* 6:429 – 442.

6. Wibley JEA, Pegg AE, Moody PCE (2000) Crystal structure of the human O6-alkylguanine-DNA alkyltransferase. *Nucl Acids Res* 28:393– 401.

7. Xiao W, Samson L (1992) The *Saccharomyces cerevisiae* MGT1 DNA repair methyltrans- ferase gene: Its promoter and entire coding sequence, regulation and in vivo biological functions. *Nucl Acids Res* 20:3599 –3606.

8. Srivenugopal KS, Ali-Osman F (2002) The DNA repair protein, O6-methylguanine-DNA methyltransferase is a proteolytic target for the E6 human papillomavirus oncoprotein. *Oncogene* 21:5940 –5945.

9. Srivenugopal KS, Yuan X-H, Friedman SH, Ali-Osman F (1996) Ubiquitination-dependent proteolysis of O6-methylguanine-DNA methyltransferase in

human and murine tumor cells following inactivation with O6-benzylguanine or 1,3-bis(2- chloroethyl)-1-nitrosourea. *Biochemistry* 35:1328 –1334.

10. Scheffner M, Staub O (2007) HECT E3s and human disease. *BMC Biochemistry* 8 (Suppl. I):S6.

11. Varshavsky A (2004) Spalog and sequelog: Neutral terms for spatial and sequence similarity. *Curr Biol* 14:R181–R183.

12. Sassanfar M, Samson L (1990) Identification and preliminary characterization of an O6-methylguanine DNA repair methyltransferase in the yeast Saccharomyces cerevisiae. *J Biol Chem* 265:20 –25.

13. Joo JH, *et al.* (1995) Expression of yeast O6-methylguanine-DNA methyltransferase (MGMT) gene. *Cell Mol Biol* 41:545–553.

14. Bachmair A, Finley D, Varshavsky A (1986) In vivo half-life of a protein is a function of its amino-terminal residue. *Science* 234:179 –186.

15. Varshavsky A (1996) The N-end rule: Functions, mysteries, uses. *Proc Natl Acad Sci USA* 93:12142–12149.

16. Mogk A, Schmidt R, Bukau B (2007) The N-end rule pathway of regulated proteolysis: Prokaryotic and eukaryotic strategies. *Trends Cell Biol* 17:165–172.

17. Tasaki T, Kwon YT (2007) The mammalian N-end rule pathway: New insights into its components and physiological roles. *Trends Biochem Sci* 32:520–528.

18. Hu R-G, *et al.* (2005) The N-end rule pathway as a nitric oxide sensor controlling the levels of multiple regulators. *Nature* 437:981–986.

19. Xia Z, Webster A, Du F, Piatkov K, Ghislain M, Varshavsky A (2008) Substrate-binding sites of UBR1, the ubiquitin ligase of the N-end rule pathway. *J Biol Chem* 283:24011– 24028.

20. Xie Y, Varshavsky A (1999) The E2–E3 interaction in the N-end rule pathway: The RING-H2 finger of E3 is required for the synthesis of multiubiquitin chain. *EMBO J* 18:6832– 6844

21. Hwang C-S, Varshavsky A (2008) Regulation of peptide import through phosphoryla- tion of Ubr1, the ubiquitin ligase of the N-end rule pathway. *Proc Natl Acad Sci USA* 105:19188 –19193.

22. Du F, Navarro-Garcia F, Xia Z, Tasaki T, Varshavsky A (2002) Pairs of dipeptides synergistically activate the binding of substrate by ubiquitin ligase through dissocia- tion of its autoinhibitory domain. *Proc Natl Acad Sci USA* 99:14110–14115.

23. Xia Z, Turner GC, Hwang C-S, Byrd C, Varshavsky A (2008) Amino acids induce peptide uptake via accelerated degradation of CUP9, the transcriptional repressor of the PTR2 peptide transporter. *J Biol Chem* 283:28958 –28968.

24. Hu R-G, Wang H, Xia Z, Varshavsky A (2008) The N-end rule pathway is a sensor of heme. *Proc Natl Acad Sci USA* 105:76 – 81.

25. Turner GC, Du F, Varshavsky A (2000) Peptides accelerate their uptake by activating a ubiquitin-dependent proteolytic pathway. *Nature* 405:579 –583.

26. Johnson ES, Bartel BW, Varshavsky A (1992) Ubiquitin as a degradation signal. *EMBO J* 11:497–505.

27. Johnson ES, Ma PC, Ota IM, Varshavsky A (1995) A proteolytic pathway that recognizes ubiquitin as a degradation signal. *J Biol Chem* 270:17442–17456.

28. Koegl M, *et al.* (1999) A novel ubiquitination factor, E4, is involved in multiubiquitin chain assembly. *Cell* 96:635– 644.

29. Ju D, Wang X, Xu H, Xie Y (2007) The armadillo repeats of the Ufd4 ubiquitin ligase recognize ubiquitin-fusion proteins. *FEBS Lett* 581:265–270.

30. Xie Y, Varshavsky A (2000) Physical association of ubiquitin ligases and the 26S proteasome. *Proc Natl Acad Sci USA* 97:2497–2502.

31. Xie Y, Varshavsky A (2002) UFD4 lacking the proteasome-binding region catalyses ubiquitination but is impaired in proteolysis. *Nat Cell Biol* 4:1003–1007.

32. Ravid T, Hochstrasser M (2007) Autoregulation of an E2 enzyme by ubiquitin-chain assembly on its catalytic residue. *Nat Cell Biol* 9:422–427.

33. Ju D, Xie Y (2006) A synthetic defect in protein degradation caused by loss of Ufd4 and Rad23. *Biochem Biophys Res Commun* 341:648 – 652.

34. Ullrich HD (2005) The RAD6 pathway: Control of DNA damage bypass and mutagenesis by ubiquitin and SUMO. *ChemBioChem* 6:1735–1743.

35. Wang L, Mao X, Ju D, Xie Y (2004) Rpn4 is a physiological substrate of the Ubr2 ubiquitin ligase. *J Biol Chem* 279:55218 –55223.

36. Xie Y, Varshavsky A (2001) RPN4 is a ligand, substrate, and transcriptional regulator of the 26S proteasome: A negative feedback circuit. *Proc Natl Acad Sci USA* 98:3056– 3061.

37. Ouyang Y, *et al.* (2006) Loss of Ubr2, an E3 ubiquitin ligase, leads to chromosome fragility and impaired homologous recombinational repair. *Mut Res* 596:64 –75.

38. Passagne I, *et al.* (2006) O6-methylguanine DNA-methyltransferase (MGMT) overexpression in melanoma cells induces resistance to nitrosoureas and temozolomide but sensitizes to mitomycin C. *Toxicol Appl Pharmacol* 211:97–105.

39. Johnson ES, Gonda DK, Varshavsky A (1990) Cis-trans recognition and subunit-specific degradation of short-lived proteins. *Nature* 346:287–291.

40. Rao H, Uhlmann F, Nasmyth K, Varshavsky A (2001) Degradation of a cohesin subunit by the N-end rule pathway is essential for chromosome stability. *Nature* 410:955–960.

APPENDIX 2:

SUPPLEMENTARY MATERIAL FOR CHAPTER 4

Supplementary Table S1. *S. cerevisiae* strains used in this study.

Strains	Relevant genotypes	Sources
SC295	*MAT***a** *ura3-52 leu2-3,112 regl-501 gall pep4-3*	ref. (*79*)
JD52	*MAT***a** *trp1- 63 ura3-52 his3- 200 leu2-3112. lys2-801*	ref. (*80*)
JD53	*MAT*α *trp1- 63 ura3-52 his3- 200 leu2-3112. lys2-801*	ref. (*81*)
JD55	*ubr1Δ::HIS3* in JD52	ref. (*80*)
JD83-1A	*ubr1Δ::HIS3* in JD53	ref. (*80*)
AVY105	*ubr2Δ::HIS3* in JD52	Lab collection
CHY49	*pdr5Δ::KanMX6* in JD52	This study
CHY134	*ubr1Δ::LEU2 ubr2Δ::HIS3* in JD52	This study
CHY194	*ufd4Δ::KanMX6* in JD52	This study
CHY195	*ubr1Δ::HIS3 ufd4Δ::KanMX6* in JD52	This study
CHY223	*doa10Δ::KanMX6* in JD53	This study
CHY229	*doa10Δ:KanMX6 ubr1Δ::HIS3* in JD53	This study
CHY248	*DOA10-13MYC:::KanMX6* in JD52	This study
CHY287	*ubc4Δ::LEU2* in BY4742	This study
CHY288	*ubc4Δ::LEU2 doa10Δ::KanMX6* in BY4742	This study
BY4742	*MAT*α *his3-1 leu2-0 lys2-0 ura3-0 can1-100,*	Open Biosystems
BY10976	*ard1Δ::KanMX6 in* BY4742	Open Biosystems
BY12509	*nat5Δ::KanMX6* in BY4742	Open Biosystems
BY15470	*mak3Δ::KanMX6 in* BY4742	Open Biosystems
BY15546	*nat3Δ::KanMX6 in* BY4742	Open Biosystems
BY16202	*nat4Δ::KanMX6* in BY4742	Open Biosystems
BY17299	*doa10Δ:KanMX6 in* BY4742	Open Biosystems
BY4741	*MAT***a** *his3-1 leu2-0 met15-0 ura3-0*	Open Biosystems
BY4425	*rad6Δ:: KanMX4* in BY4741	Open Biosystems
BY3771	*bre1Δ:: KanMX4* in BY4741	Open Biosystems
BY5787	*rad18Δ:: KanMX4* in BY4741	Open Biosystems
BY4425	*ufd2Δ:: KanMX4* in BY4741	Open Biosystems
BY3216	*ufd4Δ:: KanMX4* in BY4741	Open Biosystems
BY3994	*hul4Δ::KanMX4* in BY4741	Open Biosystems
BY597	*hul5Δ::KanMX4* in BY4741	Open Biosystems
BY4763	*hrd1Δ:: KanMX4* in BY4741	Open Biosystems
BY4156	*hrd3Δ:: KanMX4* in BY4741	Open Biosystems
BY4883	*tul1Δ:: KanMX4* in BY4741	Open Biosystems
BY7299	*doa10Δ::KanMX4* in BY4741	Open Biosystems
BY4814	*ubr1Δ:: KanMX4* in BY4741	Open Biosystems
BY1579	*ubr2Δ:: KanMX4* in BY4741	Open Biosystems
BY3771	*bre1Δ:: KanMX4* in BY4741	Open Biosystems
BY5787	*rad18Δ:: KanMX4* in BY4741	Open Biosystems
FW1808	*MAT*[illegible] *his4-912δR5 lys2-128δ ura3-52 rps5-1*	ref. (*82*)

Supplementary Table S2. Plasmids used in this study.

Plasmids	Descriptions	Sources
pBAM	Ub-MH-e^K-ha-Ura3 in p314CUP1	ref. (*41*)
pMET416$_F$UPR CUP9$_{NSF}$	^{f}DHFR-Ub^{K48R}-Cup9$_{NSF}$ in p416MET25	ref. (*83*)
pEJJ1-M	His$_6$Ub-Met-e^K-DHFR$_{ha}$ from the T7 promoter	ref. (*41*)
pCH178	Ub^{K48R}-CK-e^K-ha-Ura3 in p314CUP1	This study
pCH181	Ub-CZ-e^K-ha-Ura3 in p314CUP1	This study
pCH183	Ub^{K48R}-MK-e^K-ha-Ura3 in p314CUP1	This study
pCH194	Ub-CP-e^K-ha-Ura3 in p314CUP1	This study
pCH195	Ub^{Q49R}-CL-e^K-ha-Ura3 in p314CUP1	This study
pCH198	Ub-CV-e^K-ha-Ura3 in p314CUP1	This study
pCH499	Ub^{K48R}-CE-e^K-ha-Ura3 in p314CUP1	This study
pCH500	Ub^{K48R}-CG-e^K-ha-Ura3 in p314CUP1	This study
pCH501	Ub^{K48R}-CI-e^K-ha-Ura3 in p314CUP1	This study
pCH502	Ub^{K48R}-CL-e^K-ha-Ura3 in p314CUP1	This study
pCH503	Ub^{K48R}-CW-e^K-ha-Ura3 in p314CUP1	This study
pCH504	Ub^{K48R}-ML-e^K-ha-Ura3 in p314CUP1	This study
pCH505	Ub^{K48R}-SL-e^K-ha-Ura3 in p314CUP1	This study
pCH506	Ub^{K48R}-TL-e^K-ha-Ura3 in p314CUP1	This study
pCH507	Ub^{Q49R}-CL-e^K-ha-Ura3 in p313CUP1	This study
pCH508	Ub^{K48R}-SL-e^K-ha-Ura3 in p313CUP1	This study
pCH509	Ub^{K48R}-TL-e^K-ha-Ura3 in p313CUP1	This study
pCH535	Ub^{K48R}-MN-Mat$\alpha^{3\text{-}67}e^K$-ha-Ura3 in p314CUP1	This study
pCH547	Ub^{K48R}-MK-Mat$\alpha^{3\text{-}67}e^K$-ha-Ura3 in p314CUP1	This study
pCH548	Ub^{K48R}-ML-Mat$\alpha^{3\text{-}67}e^K$-ha-Ura3 in p314CUP1	This study
pCH549	Ub^{K48R}-MQ-Mat$\alpha^{3\text{-}67}e^K$-ha-Ura3 in p314CUP1	This study
pCH550	Ub^{K48R}-MD-Mat$\alpha^{3\text{-}67}e^K$-ha-Ura3 in p314CUP1	This study
pCH551	Ub^{K48R}-MA-Mat$\alpha^{3\text{-}67}e^K$-ha-Ura3 in p314CUP1	This study
pCH552	Ub^{K48R}-MP-Mat$\alpha^{3\text{-}67}e^K$-ha-Ura3 in pS314CUP1	This study
pCH553	Ub^{K48R}-RN-Mat$\alpha^{3\text{-}67}e^K$-ha-Ura3 in p314CUP1	This study
pCH554	Ub^{K48R}-LN-Mat$\alpha^{3\text{-}67}e^K$-ha-Ura3 in p314CUP1	This study
pCH555	Ub^{K48R}-NN-Mat$\alpha^{3\text{-}67}e^K$-ha-Ura3 in p314CUP1	This study
pCH556	Ub^{K48R}-DN-Mat$\alpha^{3\text{-}67}e^K$-ha-Ura3 in p314CUP1	This study
pCH581	Δdoa10 in p425GAL1	This study
pCH595	DOA10$_f$ in p425GAL1	This study
pCH604	Ub^{K48R}-MK-e^K-ha-Ura3-CL1 in p314CUP1	This study
pCH605	Ub^{K48R}-GK-e^K-ha-Ura3-CL1 in p314CUP1	This study
pH$_{10}$UE	His$_{10}$-Ub in pET15b	ref. (*23*)
pCH622	MN-Mat$\alpha^{3\text{-}67}e^K$-ha-Ura3 in pH$_{10}$UE	This study
pCH623	GN-Mat$\alpha^{3\text{-}67}e^K$-ha-Ura3 in pH$_{10}$UE	This study
pCH624	MK-Mat$\alpha^{3\text{-}67}e^K$-ha-Ura3 in pH$_{10}$UE	This study
pCH625	RN-Mat$\alpha^{3\text{-}67}e^K$-ha-Ura3 in pH$_{10}$UE	This study
pCH626	Ub^{K48R}-NN-Mat$\alpha^{3\text{-}67}e^K$-ha-Ura3 in p314CUP1	This study
pCH641	Ub^{K48R}-MN-Mat$\alpha^{3\text{-}67}e^K$-ha-Ura3 in p413CUP1	This study

pCH642	Ub^{K48R}-GN-Mat$\alpha^{3-67}e^{K}$-ha-Ura3 in p413CUP1	This study
pCH643	Ub^{K48R}-MK-Mat$\alpha^{3-67}e^{K}$-ha-Ura3 in p413CUP1	This study
pCH644	Ub^{K48R}-RN-Mat$\alpha^{3-67}e^{K}$-ha-Ura3 in p413CUP1	This study
pCH645	MN-Matα^{3-67}-e^{K}-$DHFR_{ha}$ in $pH_{10}UE$	This study
pCH646	GN-Matα^{3-67}-e^{K}-$DHFR_{ha}$ in $pH_{10}UE$	This study
pCH647	MK-Matα^{3-67}-e^{K}-$DHFR_{ha}$ in $pH_{10}UE$	This study
pCH648	RN-Matα^{3-67}-e^{K}-$DHFR_{ha}$ in $pH_{10}UE$	This study
pCH666	Ub^{K48R}-MK-Pca^{3-392}-e^{K}-ha-Ura3 in p413CUP1	This study
pCH667	Ub^{K48R}-GK-Pca^{3-392}-e^{K}-ha-Ura3 in p413CUP1	This study
pCH668	Ub^{K48R}-MK-e^{K}-ha-Ura3 in p313CUP1	This study
pCH669	Ub^{K48R}-ML-e^{K}-ha-Ura3 in p313CUP1	This study
pCH685	Ub^{K48R}-GL-e^{K}-ha-Ura3 in p313CUP1	This study
pCH686	Ub^{K48R}-AL-e^{K}-ha-Ura3 in p313CUP1	This study
pCH687	Ub^{K48R}-VL-e^{K}-ha-Ura3 in p313CUP1	This study
pCH688	Ub^{K48R}-MPL-e^{K}-ha-Ura3 in p313CUP1	This study
pCH689	Ub^{K48R}-CL-e^{K}-ha-Ura3 in p313CUP1	This study
pCH704	$Mat\alpha2_{flag}$ in p416MET25	This study
pCH705	MK-$Mat\alpha2^{3-210}{}_{f}$ in p416MET25	This study
pCH706	MG- $Mat\alpha2^{3-210}{}_{f}$ in p416MET25	This study
pCH707	$Mat\alpha2_{f}$ in p426GAL1	This study
pCH719	^{f}DHFR-Ub^{K48R}-MN-$Mat\alpha2_{f}$ in p416MET25	This study
pCH720	^{f}DHFR-Ub^{K48R}-MK-$Mat\alpha2_{f}$ in p416MET25	This study
pCH721	^{f}DHFR-Ub^{K48R}-GN-$Mat\alpha2_{f}$ in p416MET25	This study
pCH731	Ub^{K48R}-MD-e^{K}-ha-Ura3 in p313CUP1	This study
pCH732	Ub^{K48R}-ME-e^{K}-ha-Ura3 in p313CUP1	This study
pCH733	Ub^{K48R}-MQ-e^{K}-ha-Ura3 in p313CUP1	This study
pCH734	Ub^{K48R}-MN-e^{K}-ha-Ura3 in p313CUP1	This study
pCH735	Ub^{K48R}-MF-e^{K}-ha-Ura3 in p313CUP1	This study
pCH736	Ub^{K48R}-MY-e^{K}-ha-Ura3 in p313CUP1	This study
pCH737	Ub^{K48R}-MW-e^{K}-ha-Ura3 in p313CUP1	This study
pCH738	Ub^{K48R}-MI-e^{K}-ha-Ura3 in p313CUP1	This study

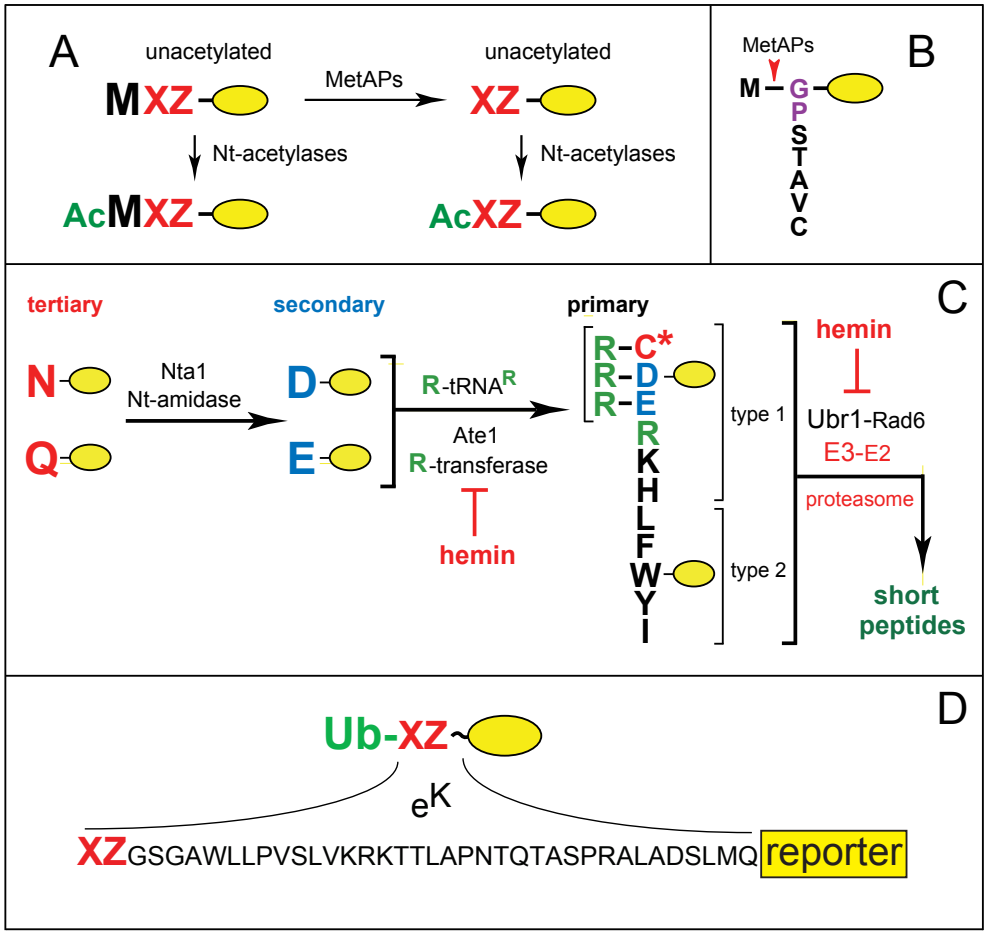

Figure A2.1. Nα-terminal acetylases, Met-aminopeptidases, and the Ubr1 branch of the N-end rule pathway. (A) N-terminal processing of nascent proteins by Nα-terminal acetylases (Nt-acetylases) and Met-aminopeptidases (MetAPs). "Ac" denotes the Nα-terminal acetyl moiety. M, Met. X and Z, single-letter abbreviations for any amino acid residue. Yellow ovals denote the rest of a protein. (B) MetAPs cleave off the N-terminal Met if a residue at position 2 belongs to the set of residues shown (ref. (73) and refs therein). (C) The Ubr1-mediated branch of the *S. cerevisiae* N-end rule pathway (5, 25-28, 30, 34, 48, 49, 74). See the main text for definitions of the "primary", "secondary" and "tertiary" destabilizing N-terminal residues. (D) A

diagram of ubiquitin (Ub) fusions employed as reporters. X and Z, varied residues; e^K is a previously described ~40-residue extension (30, 48-50) upstream of the ha-Ura3 reporter moiety.

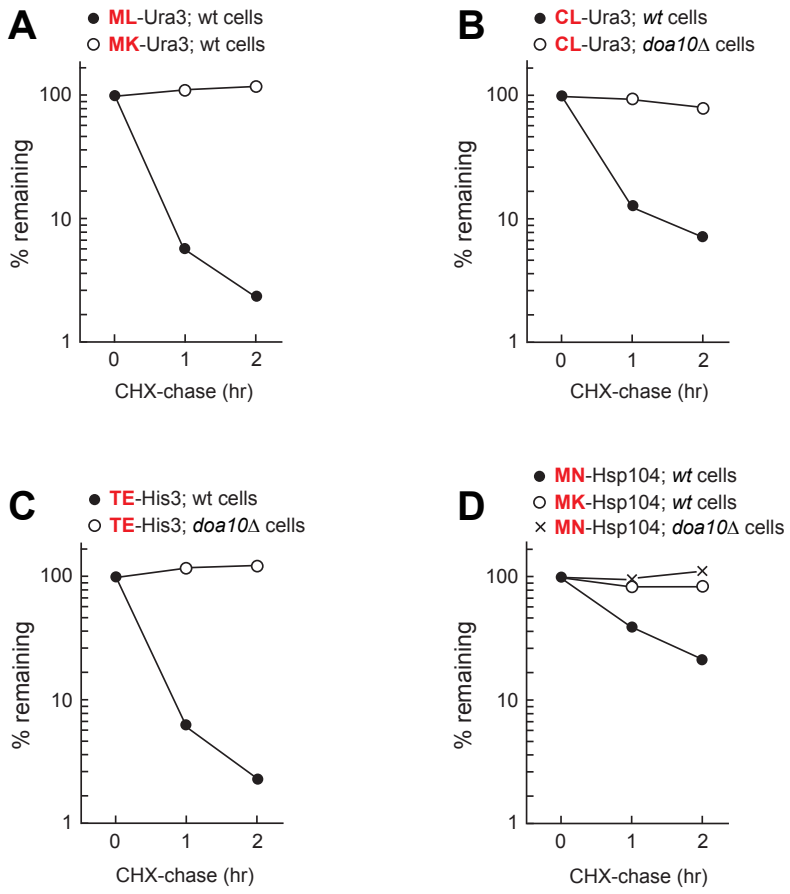

Figure A2.2. Quantitation of cycloheximide-chase assays. Cycloheximide (CHX)-chase assays (Fig. 1, Fig. 3, fig. S3, fig. S4D-G, and fig. S7) were carried out as described in Materials and Methods. Quantitations of the resulting immunoblots was performed using the ImageJ software (http://rsb.info.nih.gov/ij/index.html). For each time point, ImageJ was employed to determine the ratio of a test protein's band intensity to that of tubulin loading control in the same lane. The resulting value at time zero was taken as 100%. (A) ML-Ura3 and MK-Ura3 in wild-type S. cerevisiae (see Fig. 1C for corresponding immunoblots). (B) CL-Ura3 in wild-type and *doa10Δ S. cerevisiae* (see Fig. 1E for corresponding immunoblots). (C) His3 (TE-His3, with the wild-type Thr-Glu N-terminal sequence) in wild-type and *doa10Δ S.*

cerevisiae (see Fig. 3E for corresponding immunoblots). (D) Hsp104 (MN-Hsp104, with the wild-type Met-Asn N-terminal sequence, or MK-Hsp104, with the mutant Met-Lys N-terminal sequence) in wild-type and *doa10Δ S. cerevisiae* (see Fig. 3H for corresponding immunoblots.

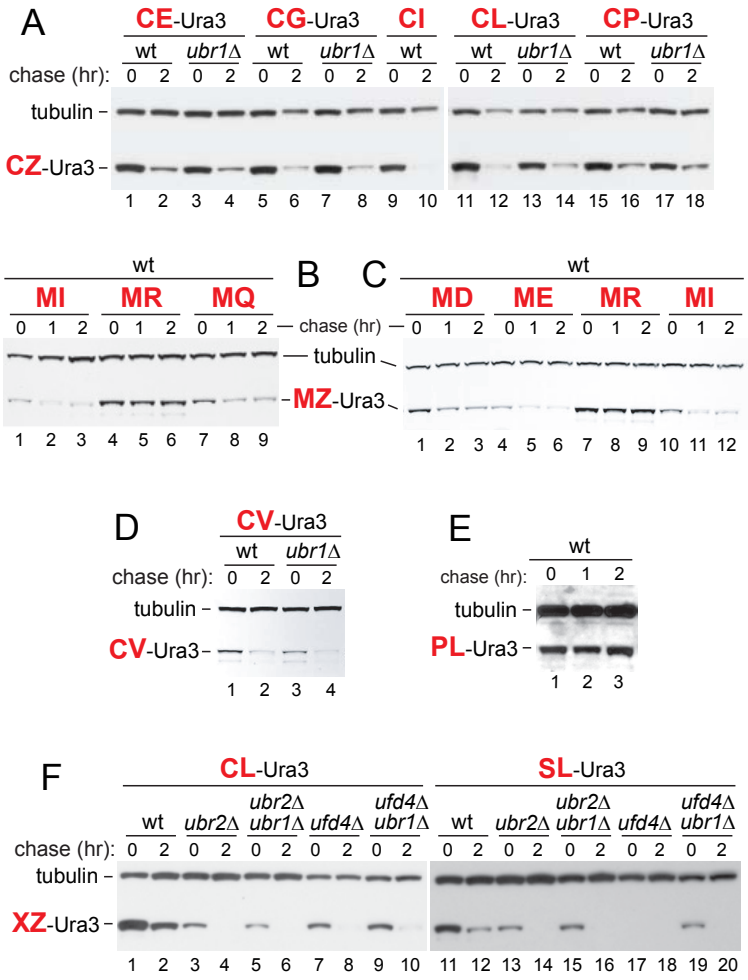

Figure A2.3. Cycloheximide-chase assays with Ura3-based reporters. (A) Cycloheximide (CHX)-chases, for 0 and 2 hr, with CZ-e^{K}-Ura3 (CZ-Ura3) (Z=Glu, Gly, Ile, Leu, Pro), in wild-type versus *ubr1Δ S. cerevisiae*. CZ-Ura3 proteins were produced using the Ub fusion technique as described in fig. S1D and Methods. Cell extracts were fractionated by SDS-PAGE, followed by immunoblotting with anti-ha antibody, and also with antibody to tubulin (loading controls). (B) As in A but CHX-chases for 0, 1 and 2 hr with MZ-Ura3 (Z=Ile, Arg, Gln) in wild-type *S. cerevisiae*. (C) As in B, with other MZ-Ura3 reporters (Z=Asp, Glu, Arg, Ile). (D) As in A, but with CV-Ura3. (E) As in C, but with PL-Ura3. (F) As in A, with CL-Ura3 (lanes 1-10) or SL-

Ura3 (lanes 11-20), in wild-type versus *ubr2Δ*, ufd4, and double-mutant *ubr2Δ ubr1Δ* and *ufd4Δ ubr1Δ* cells, as indicated.

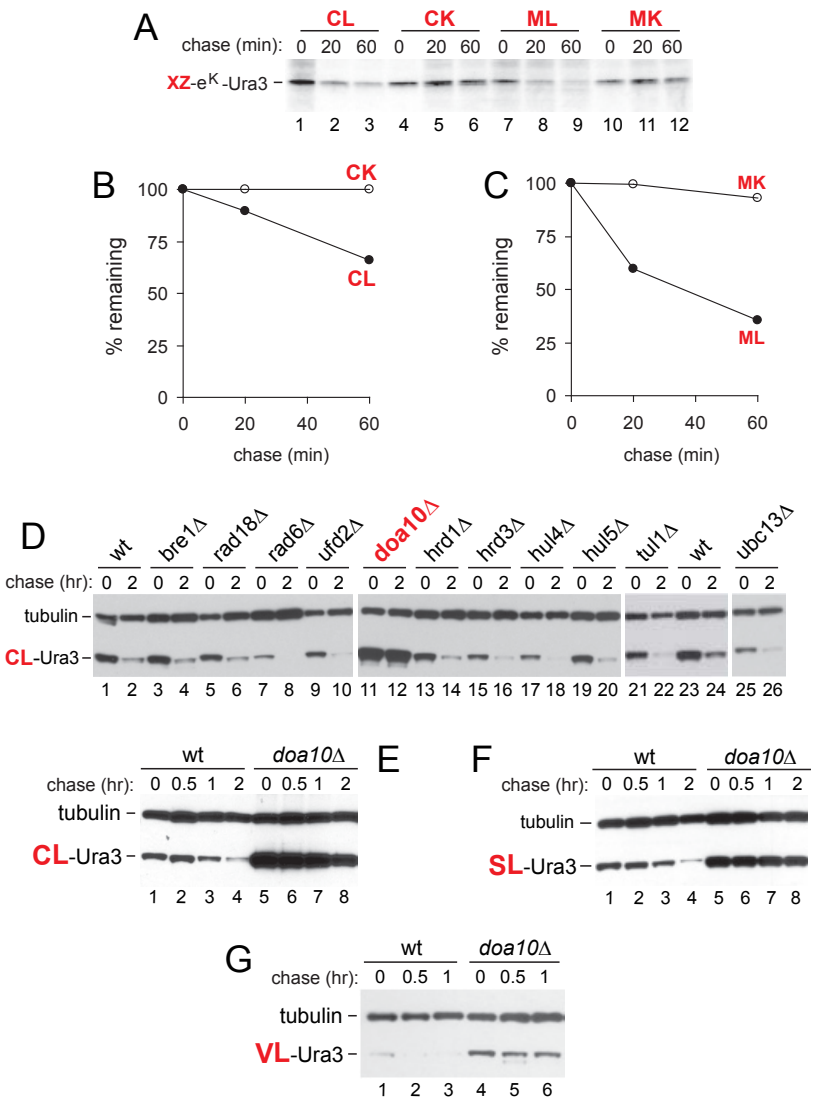

Figure A2.4. ^{35}S-pulse-chase assays with XZ-Ura3 reporters and identification of Doa10 as the cognate Ub ligase. (A)^{35}S-pulse-chase assay with XZ-Ura3 (X=Cys, Met; Z=Leu, Lys). Wild-type *S. cerevisiae* expressing XZ-Ura3 test proteins (produced using the Ub fusion technique as described in fig. S1D) were labeled for 5 min with [^{35}S]methionine/cysteine, followed by a chase for 20 and 60 min (see Methods). Lane 1-3, CL-Ura3. Lanes 4-6, CK-Ura3. Lanes 7-9, ML-Ura3. Lanes 10-12, MK-Ura3. (B) Quantitation of data in A, using PhosphorImager, for CL-Ura3 and CK-Ura3. (C) As in B, for ML-Ura3 and MK-Ura3. (D) CHX-chases for 0 and 2 hr with *S. cerevisiae*

null mutants in the indicated E2 or E3 enzymes that expressed CL-Ura3. Note the virtually complete stabilization of CL-Ura3 in *doa10Δ* cells, but not in other tested mutants or wild-type cells. (E) CHX-chase for 0, 0.5, 1 and 2 hr with CL-Ura3 in wild-type (lanes 1-4) versus *doa10Δ* cells (lanes 5-8). (F) As in E but with SL-Ura3. (G) As in **E** but CHX-chase for 0, 0.5 and 1 hr with VL-Ura3 in wild-type (lanes 1-3) and *doa10Δ* cells (lanes 4-6).

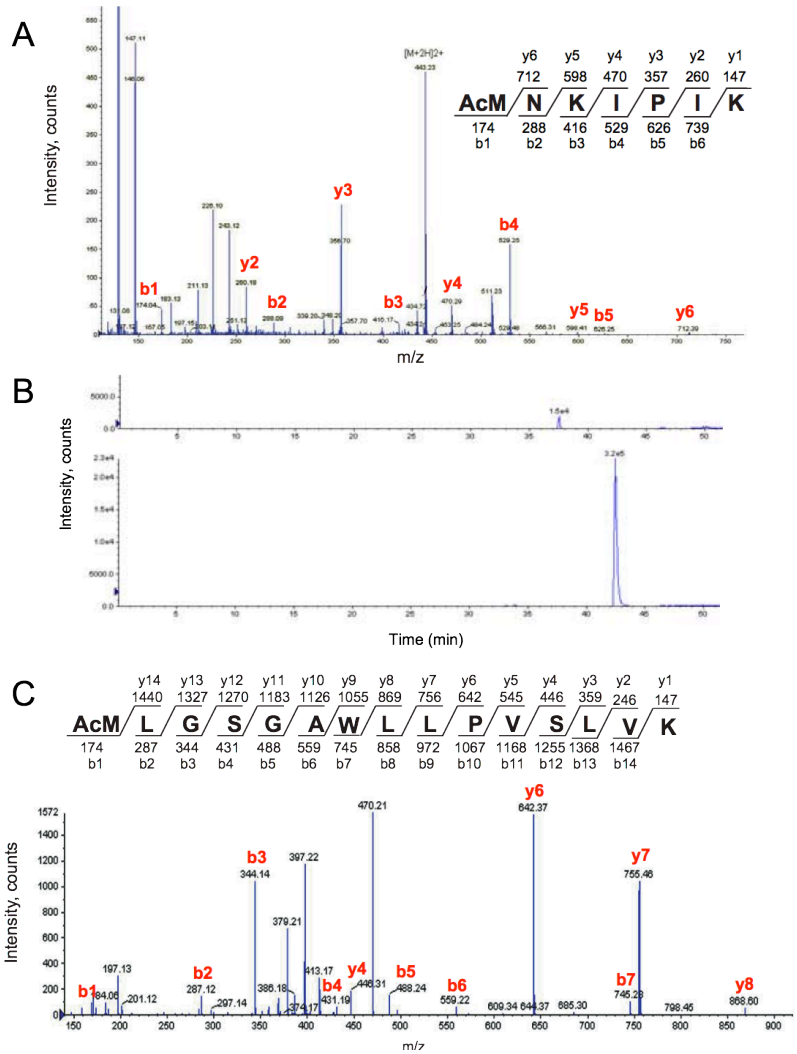

Figure A2.5. The MATα2 repressor and the ML-Ura3 reporter are Nt-acetylated in vivo. (A) Full-length, C-terminally flag-tagged MATα2$_f$ was produced in *doa10Δ ubc4Δ S. cerevisiae*, purified, and subjected to SDS-PAGE. The band of MATα2$_f$ was excised, followed by in-gel digestion with the Asp-N protease and analysis by LC-MS/MS (see Methods). Shown here, using standard MS notations, are both the Nt-acetylated peptide of MATα2$_f$ (a doubly-charged peptide ion, at 443 m/z; molecular mass 886 Da; see the diagram) and the MS/MS-derived fragment ion spectrum of

this peptide. The unacetylated counterpart of the Ac-MNKIPIK MATα2 peptide was not detected in two independent LC-MS/MS experiments. MATα2_f is thus nearly completely Nt-acetylated in vivo. (B) ML-Ura3 was produced in *doa10Δ S. cerevisiae* through the cotranslational deubiquitylation of Ub-ML-Ura3 (see fig. S1D), purified, and subjected to SDS-PAGE. The band of ML-Ura3 was excised, followed by in-gel digestion with trypsin and analysis by LC-MS/MS (see Methods). The small (upper panel) and large (lower panel) peaks on selective ion chromatograms represent the doubly charged unacetylated MLGSGAWLLPVSLVK peptide (m/z 785.97, 2+) for MLGSGAWLLPVSLVK (m/z 1571.96, 1+) (upper panel), and the doubly charged acetylated Ac-MLGSGAWLLPVSLVK peptide (m/z 807.00, 2+) for Ac-MLGSGAWLLPVSLVK (m/z 1613.96, 1+) (lower panel). According to the ratio of two species (the relative ion peak areas), more than 90% of ML-Ura3 was N-acetylated in vivo. (C) ML-Ura3, produced and analyzed by LC-MS/MS as described in B. Shown here is MS/MS-produced fragment ions spectrum of the doubly charged Nt-acetylated Ac-MLGSGAWLLPVSLVK peptide (m/z 806.99, 2+) sequenced through the identification of specific fragmentation ions (b1=174.06, b2=287.14, b3=344.16, b4=431.20, b5=488.22, b6=559.26, b7=745.33, y2=246.18, y3=359.27, y4=446.30, y6=642.42, y7=755.50, y8=868.50).

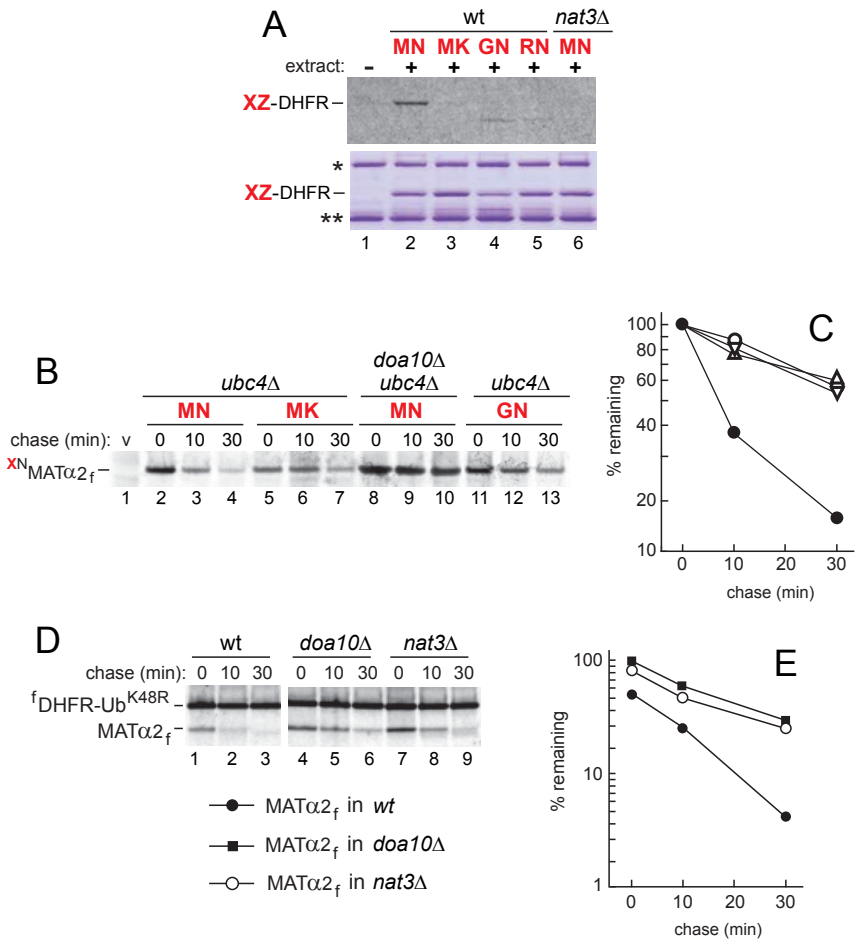

Figure A2.6. The ^{Ac}N-degron of the MATα2 repressor. (A) Upper panel: lane 1, Ub-MN-α2$^{3-67}$-e^{K}-DHFR$_{ha}$ was expressed in *E. coli,* purified, and deubiquitylated using a purified deubiquitylating enzyme. The resulting MN-α2$^{3-67}$-e^{K}-DHFR$_{ha}$ derived from the N-terminal Deg1 region of MATα2 (see the main text), was bound to agarose beads containing anti-ha antibody. Immobilized MN-α2$^{3-67}$-e^{K}-DHFR$_{ha}$ was incubated with buffer alone (negative control) in the presence of ^{14}C-labeled acetyl-CoA, followed by treatment of the beads with elution buffer, SDS-PAGE and autoradiography. Lane 2, same as lane 1 but incubation with extract from wild-type *S. cerevisiae.* Lanes 3-5, same as lane 2 but with MK-α2$^{3-67}$-eK-DHFR$_{ha}$, GN-α2$^{3-67}$-e^{K}-DHFR$_{ha}$ and RN-α2$^{3-67}$-e^{K}-DHFR$_{ha}$, respectively. Note the absence of Nt-acetylation of

these reporters, in contrast to MN-α2$^{3-67}$-e^{K}-DHFR$_{ha}$ (lane 2). Lane 6, same as lane 2 but with extract from *nat3Δ* cells, which lacked the cognate NatB Nt-acetylase. The lower panel shows a Coomassie-stained gel that yielded autoradiographic data in the upper panel. The bands of XZ-α2$^{3-67}$-e^{K}-DHFR$_{ha}$ (XZ-DHFR) reporters are indicated. Single and double asterisks denote an admixture of the light and heavy IgG chains, respectively, that partially leaked from agarose beads during the elution of reporters. (B) ^{35}S-pulse-chase assay with full-length, C-terminally flag-tagged MATα2$_f$. Lane 1, vector alone. Lanes 2-4, *ubc4Δ S. cerevisiae* expressing wild-type ^{MN}MATα2$_f$ were labeled for 5 min at 30°C with [^{35}S]methionine/cysteine, followed by a chase for 10 and 30 min. Cell extracts were precipitated with anti-flag antibody, followed by SDS-PAGE and autoradiography. Lanes 5-7, same as lanes 2-4 but with ^{MK}MATα2$_f$, containing Lys (instead of Asn) at position 2. Lanes 8-10, same as lanes 2-4 but in *ubc4Δ doa10Δ* cells. Lanes 11-13, same as lanes 1-4 but with ^{GN}MATα2$_f$ (expressed as ^{MGN}MATα2$_f$), containing N-terminal Gly. (C) Quantitation of the data in B, using PhosphorImager. Solid and open circles, upright and inverted triangles: ^{MN}MATα2$_f$, ^{MK}MATα2$_f$, ^{GN}MATα2$_f$ in *ubc4Δ* cells, and ^{MK}MATα2$_f$ in *ubc4Δ doa10Δ* cells, respectively (this is the same panel as Fig. 2F). (D) ^{35}S-pulse-chase assay with full-length, C-terminally flag-tagged MATα2$_f$ that differed from the assay in B, C by the utilization of a "built-in" reference protein. Specifically, wild-type MATα2$_f$ was expressed as a Ub fusion, ^{f}DHFR- Ub^{K48R}-MATα2$_f$. The cotranslational cleavage of this fusion at the Ub^{K48R}-MATα2$_f$ junction produced the long-lived ^{f}DHFR-Ub^{K48R} reference protein and the MATα2$_f$ test protein. For the Ub-reference technique, see Methods and refs. (75-78). The bands of MATα2$_f$ and ^{f}DHFR-Ub^{K48R} (the reference

protein) are indicated on the left. Lanes 1-3, wild-type cells. Lanes 4-6, *doa10Δ* cells. Lanes 7-9, *nat3Δ* cells (lacking the cognate NatB Nt-acetylase). (E) Quantitation of data in D, using PhosphorImager. Solid circles, solid squares, and open circles, MATα2$_f$ in wild-type cells, in *doa10Δ* cells, and in *nat3Δ* cells, respectively. In the Ub-reference technique (75-78), the presence of a "built-in" reference protein (^{f}DHFR-UbK48R) makes it possible to detect and measure the *initial* degradation of pulse-labeled MATα2$_f$ (i.e., its decay *during* the pulse). The degradation of MATα2$_f$ involved the targeting of AcN-degron, as a significant part of this degradation was found to require the presence of the Doa10 Ub ligase, and of the Nat3-containing NatB Nt-acetylase as well. Specifically, the level of MATα2$_f$ at 0 min (the end of pulse) in wild-type cells was 55% of the 0-min level of MATα2$_f$ in *doa10Δ* cells (the latter level was taken as 100%). The 0-min level of MATα2$_f$ in *nat3Δ* cells was 83%, *i.e.,* MATα2$_f$ was significantly stabilized in *nat3Δ* cells as well, though not as strongly as in *doa10Δ* cells. The reason for a significant residual degradation of the full-length MATα2$_f$ protein in *doa10Δ* cells is that MATα2$_f$ contains not only the Doa10-dependent ^{Ac}N-degron but at least two other, Doa10-independent degrons as well (see the main text).

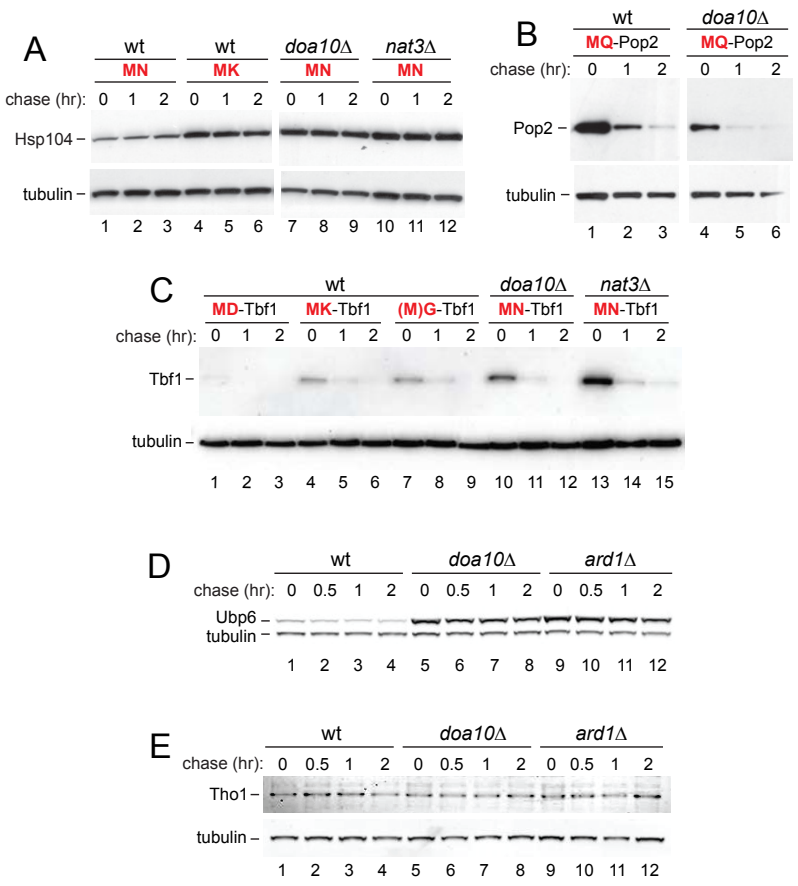

Figure A2.7. ^{Ac}N-degrons in *S. cerevisiae* proteins. (A) Lanes 1-3, CHX-chase, for 0, 1 and 2 hr, in wild-type cells expressing C-terminally ha-tagged $Hsp104_{ha}$ (N-terminal Met-Asn). Lanes 4-6, same as lanes 1-3 but with $^{MK}Hsp104_{ha}$, containing Lys (instead of Asn) at position 2. Lanes 7-9, same as lanes 1-3 but in *doa10Δ* cells. Lanes 10-12, same as lanes 1-3 but in *nat3Δ* cells, lacking the cognate NatB Nt-acetylase. (B) Lanes 1-3, CHX-chase, for 0, 1 and 2 hr, in wild-type cells expressing C-terminally ha-tagged $Pop2_{ha}$ (N-terminal Met-Gln). Lanes 4-6, same as lanes 1-3 but in *doa10Δ* cells. Note that $Pop2_{ha}$ remains short-lived in the absence of Doa10. (C) CHX-assays, for 0, 1 and 2 hr, with $Tbf1_{ha}$ (N-terminal Met-Asp), a set of experiments independent from that in Fig. 3A. Lanes 1-3, $Tbf1_{ha}$ in wild-type cells. At this level of sensitivity, to avoid overexposures of other lanes, the band of short-lived $Tbf1_{ha}$ is

nearly undetectable even at time 0. Lanes 4-6, same as lanes 1-3 but with $^{MK}Tbf1_{ha}$, containing Lys (instead of Asp) at position 2. Lanes 7-9, same as lanes 1-3 but with $^{G}Tbf1_{ha}$ ($^{MG}Tbf1_{ha}$), containing N-terminal Gly. Lanes 10-12, same as lanes 1-3 but in *doa10Δ* cells. Lanes 13-15, same as lanes 1-3 but in *nat3Δ* cells. (D) As in C, but CHX-assay for 0, 0.5, 1 and 2 hr with $Ubp6_{ha}$ (N-terminal Ser-Gly) in wild-type versus *doa10Δ* and *ard1Δ* cells, the latter lacking the cognate NatA Nt-acetylase. (E) As in D, but with $Tho1_{ha}$ (N-terminal Ala-Asp) in wild-type versus *doa10Δ* and *ard1Δ* cells. Note the metabolic stability of Tho1 and its essentially equal levels in different genetic backgrounds.

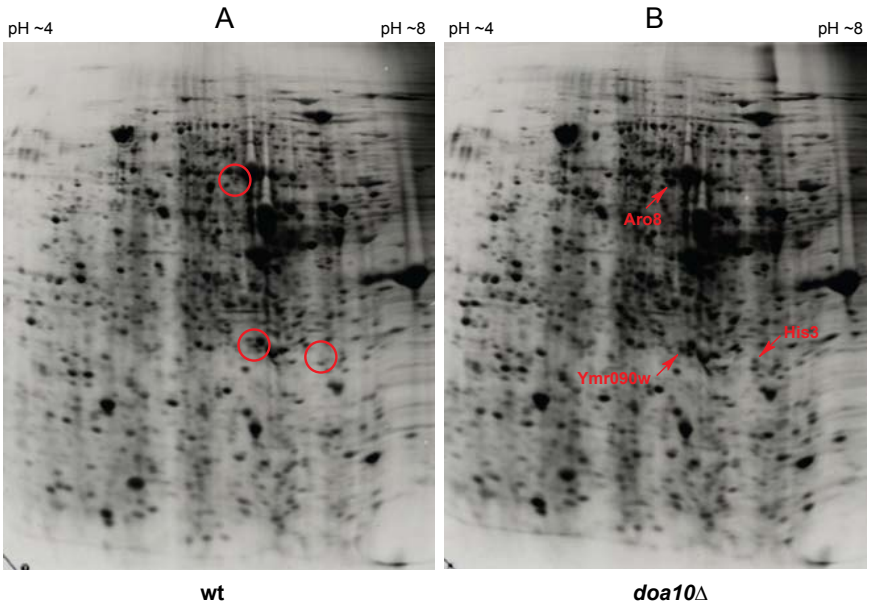

Figure A2.8. ^{35}S-pulse-chase of *S. cerevisiae* proteins fractionated by 2-D electrophoresis. (A) Wild-type *S. cerevisiae* were pulse-labeled for 15 min at 30°C with ^{35}S-methionine/cysteine, followed by extraction of proteins, 2-D electrophoresis and autoradiography (see Methods). (B) Same as in A but in a *doa10Δ* cells. As described in the main text, these and related ^{35}S-pulse-chase patterns (panels A, B, and data not shown) contained a number of protein spots with significantly higher relative levels of ^{35}S in samples from *doa10Δ* versus wild-type cells. Three of these spots (this survey continues to expand) were examined using standard MALDI-MS fingerprinting techniques, thereby identifying His3, Aro8, and Ymr090w (see Methods and the main text) as putative substrates of the Doa10 Ub ligase. The spots of His3, Aro8 and Ymr090w are indicated by red arrows in B. Red circles in A demarcate the regions containing these ^{35}S-labeled proteins in extract from wild-type *S. cerevisiae*, at lower levels than in *doa10Δ* cells (panel A and data not shown).

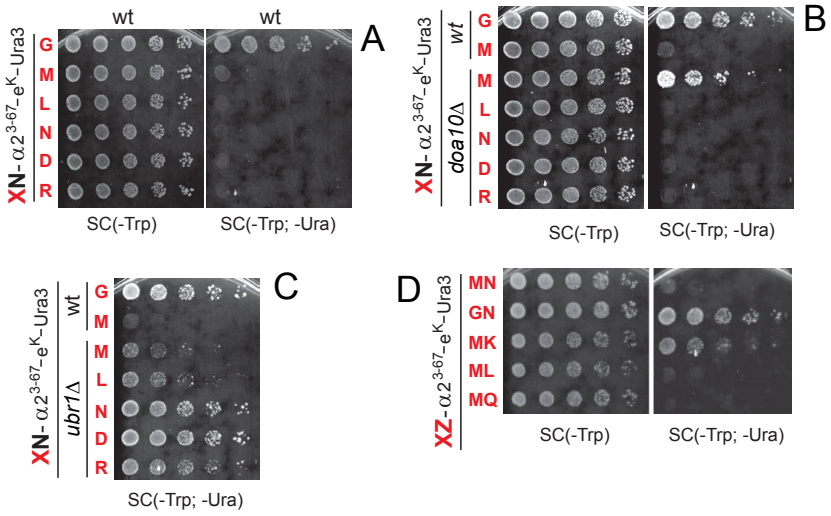

Figure A2.9. Cell growth assays with XZ-α2$^{3\text{-}67}$-e^{K}-Ura3 in wild-type and mutant yeast. In vivo levels of Ura3 determine *S. cerevisiae* growth rates in the absence of uracil in the medium, making it possible to compare the rates of degradation of Ura3 fusions through the use of growth assays (25). We carried out such assays, shown here, in wild-type, *doa10Δ* and *ubr1Δ,* and also in cells lacking specific subunits of Nt-acetylases. The reporters were Deg1-bearing XZ-α2$^{3\text{-}67}$-e^{K}-Ura3 fusions (X=Met, Gly, Leu, Asn, Asp, Arg; Z=Asn, Lys, Leu, Gln), with cell growth rates compared by serial dilutions on uracil-containing (SC(-Trp) versus uracil-lacking (SC(-Trp, -Ura)) plates. The results of these assays (panels A-D) were entirely consistent with other findings, including the necessity of Nt-acetylation of N-terminal Met for the recognition of MZ-α2$^{3\text{-}67}$-e^{K}-Ura3 by Doa10. (A) XN-α2$^{3\text{-}67}$-e^{K}-Ura3 (X= Gly, Met, Leu, Asn, Asp, Arg) in wild-type (wt) cells. (B) XN-α2$^{3\text{-}67}$-e^{K}-Ura3 (X= Gly, Met) and XN-α2$^{3\text{-}67}$-e^{K}-Ura3 (X=Met, Leu, Asn, Asp, Arg) in wild-type and *doa10Δ* cells, respectively. (C) XN-α2$^{3\text{-}67}$-e^{K}-Ura3 (X=Gly, Met) and XN-α2$^{3\text{-}67}$-e^{K}-Ura3 (X=Met, Leu, Asn, Asp, Arg) in wild-type and *ubr1Δ* cells, respectively. (D) XZ-α2$^{3\text{-}67}$-e^{K}-Ura3 (XZ=

Met-Asn, Gly-Asn, Met-Lys, Met-Leu, Met-Gln) in wild-type cells.

APPENDIX 3:

SUPPLEMENTARY MATERIAL FOR CHAPTER 5

Figure A3.1

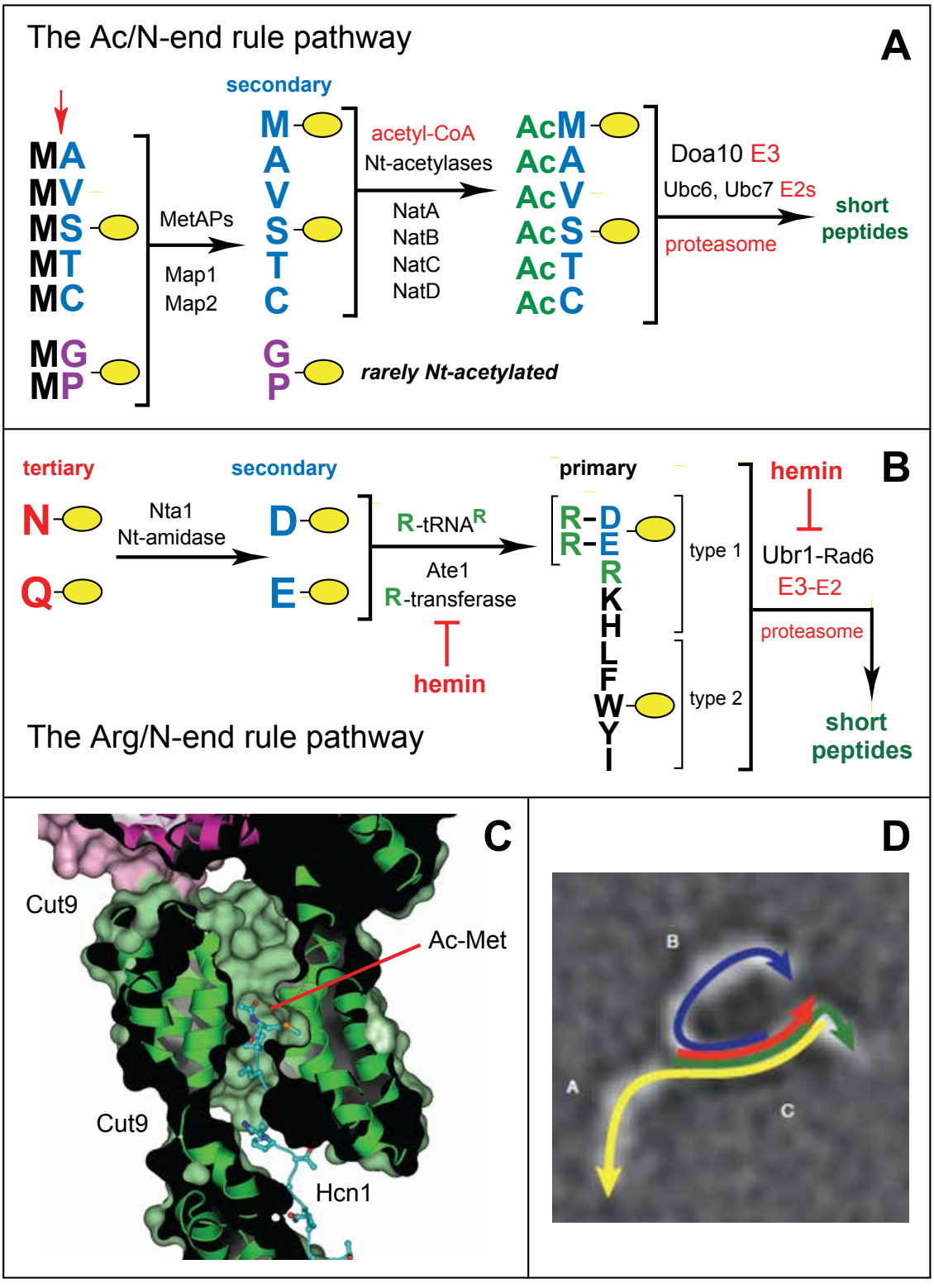
The Ac/N-end rule pathway
A
secondary
MA
MV
MS
MT
MC
MG
MP
MetAPs
Map1
Map2
M
A
V
S
T
C
G
P
acetyl-CoA
Nt-acetylases
NatA
NatB
NatC
NatD
AcM
AcA
AcV
AcS
AcT
AcC
Doa10 E3
Ubc6, Ubc7 E2s
proteasome
short peptides
rarely Nt-acetylated
tertiary
secondary
primary
B
N
Q
Nta1
Nt-amidase
D
E
R-tRNA^R
Ate1
R-transferase
hemin
R-D
R-E
R
K
H
L
F
W
Y
I
type 1
type 2
hemin
Ubr1-Rad6
E3-E2
proteasome
short peptides
The Arg/N-end rule pathway
C
Cut9
Ac-Met
Cut9
Hcn1
D
B
A
C

Figure A3.S1. The Ac/N-End Rule Pathway, the Arg/N-End Rule Pathway, and the Steric Sequestration of N^{α}-Terminally Acetylated N-Termini of Cellular Proteins.

(A) The Ac/N-end rule pathway in the yeast *Saccharomyces cerevisiae* (95,96). N-terminal residues are indicated by single-letter abbreviations for amino acids. A yellow oval denotes the rest of a protein substrate. E3 ubiquitin (Ub) ligases of the N-end rule pathway are called N-recognins. Red arrow on the left indicates the removal of N-terminal Met by Met-aminopeptidases (MetAPs). N-terminal Met is retained if a residue at position 2 is nonpermissive (too large) for MetAPs ((96) and references therein). If the retained N-terminal Met or N-terminal Ala, Val, Ser, Thr, and Cys are followed by acetylation-permissive residues, the cited N-terminal residues are usually N^{α}-terminally acetylated (Nt-acetylated) by the Nt-acetylases NatA-NatD, the bulk of which is associated with the ribosomes (86,87,89). Although second-position Gly or Pro can be made N-terminal by MetAPs and although the Doa10 E3 N-recognin can recognize Nt-acetylated Gly or Pro (95), few proteins with N-terminal Gly or Pro are Nt-acetylated. See Figure S2 for a summary of Nt-acetylation vis-à-vis specific N-terminal residues. The Nt-acetylation-mediated N-degrons are called Ac/N-degrons, to distinguish them from other N-degrons. The term “secondary” refers to the requirement for a modification (Nt-acetylation) of a destabilizing N-terminal residue before a protein can be recognized by a cognate N-recognin. Nearly 90% of human proteins are Nt-acetylated. Thus, most eukaryotic proteins harbor a specific degradation signal from the moment of their birth (95,96). Physiological roles of the Ac/N-end rule pathway are considered in the main text.

(B) The Arg/N-end rule pathway in S. cerevisiae (96,98-102,133-135). The Ubr1/Rad6 E3-E2 N-recognin Ub ligase directly recognizes (binds to) the "primary" destabilizing N-terminal residues Arg, Lys, His, Leu, Phe, Tyr, Trp and Ile. In contrast, N-terminal Asn, Gln, Asp, and Glu (as well as Cys, under some metabolic conditions) are destabilizing owing to their preliminary enzymatic modifications. These include the Nt-deamidation of N-terminal Asn and Gln by the Nta1 Nt-amidase and the Nt-arginylation of N-terminal Asp and Glu by the Ate1 arginyltransferase (R-transferase), which can also Nt-arginylate oxidized Cys, either Cys-sulfinate or Cys-sulfonate. These derivatives of N-terminal Cys can form in cells that produce nitric oxide (NO) and may also form in *S. cerevisiae*. One aspect of the *S. cerevisiae* Arg/N-end rule pathway that is not illustrated in this diagram is that there is a physical and functional interaction between the Ubr1 E3 of the Arg/N-end rule pathway and the Ufd4 E3 of the previously known Ub-fusion-degradation (UFD) pathway. Specifically, the targeting apparatus of the Arg/N-end rule pathway comprises a physical complex of the RING-type E3 Ubr1 N-recognin and the HECT-type E3 Ufd4, together with their cognate E2 enzymes Rad6 and Ubc4 (or Ubc5), respectively (102). In addition to its two distinct binding sites that recognize type 1 (basic) and type 2 (bulky hydrophobic) destabilizing N-terminal residues, the *S. cerevisiae* Ubr1 N-recognin also contains (similarly to its counterparts in multicellular eukaryotes) at least one more binding site, which recognizes substrates that are targeted through their internal (non-N-terminal) degradation signals. One example of such a substrate is the Cup9 transcriptional repressor (136-138). Polyubiquitylated N-end rule substrates are processively destroyed to short

peptides by the 26S proteasome. Hemin (Fe^{3+}-heme) binds to R-transferase and inhibits its Nt-arginylation activity. Hemin also binds to Ubr1 and alters its functional properties, in ways that remain to be understood (139).

Regulated degradation of specific proteins by the Arg/N-end rule pathway mediates the sensing of heme, NO, oxygen and short peptides; the selective elimination of misfolded proteins; the regulation of DNA repair; the cohesion/segregation of chromosomes; the signaling by transmembrane receptors; the control of peptide import; the regulation of apoptosis, meiosis, viral and bacterial infections, fat metabolism, cell migration, actin filaments, cardiovascular development, spermatogenesis, neurogenesis and memory; the functioning of adult organs, including the brain, muscle, testis and pancreas; and the regulation of leaf and shoot development, leaf senescence, and many other functions in plants ((96-100,102-104,133-135,139-153) and references therein).

(C) Steric shielding of the Nt-acetylated N-terminal residue of a subunit in a protein complex. Shown here is a part of the crystal structure, by the Barford laboratory, of a complex between the Hcn1 and Cut9 subunits of the *Schizosaccharomyces pombe* APC/C Ub ligase (128). In this structure, the (indicated) Nt-acetylated N-terminal Met residue of Hcn1 is enclosed within a deep cleft formed by the Cut9 subunit, in the heterotetramer of Hcn1 and Cut9. The N-terminal region of Hcn1 is shown in cyan as a stick model, and Cut9 is depicted as a cut-out surface representation, to show the chamber's interior (128).

(D) Model for interactions, based on single-particle electron microscopy by the Hughson laboratory, among the subunits Cog1-Cog4 that form a specific

subcomplex of the S. cerevisiae COG complex (120). The head of an arrow and its blunt end indicate the C-terminus and the N-terminus of a protein, respectively. The green, red, yellow, and blue arrows denote Cog1, Cog2, Cog3 and Cog4, respectively (120).

Figure A3.2

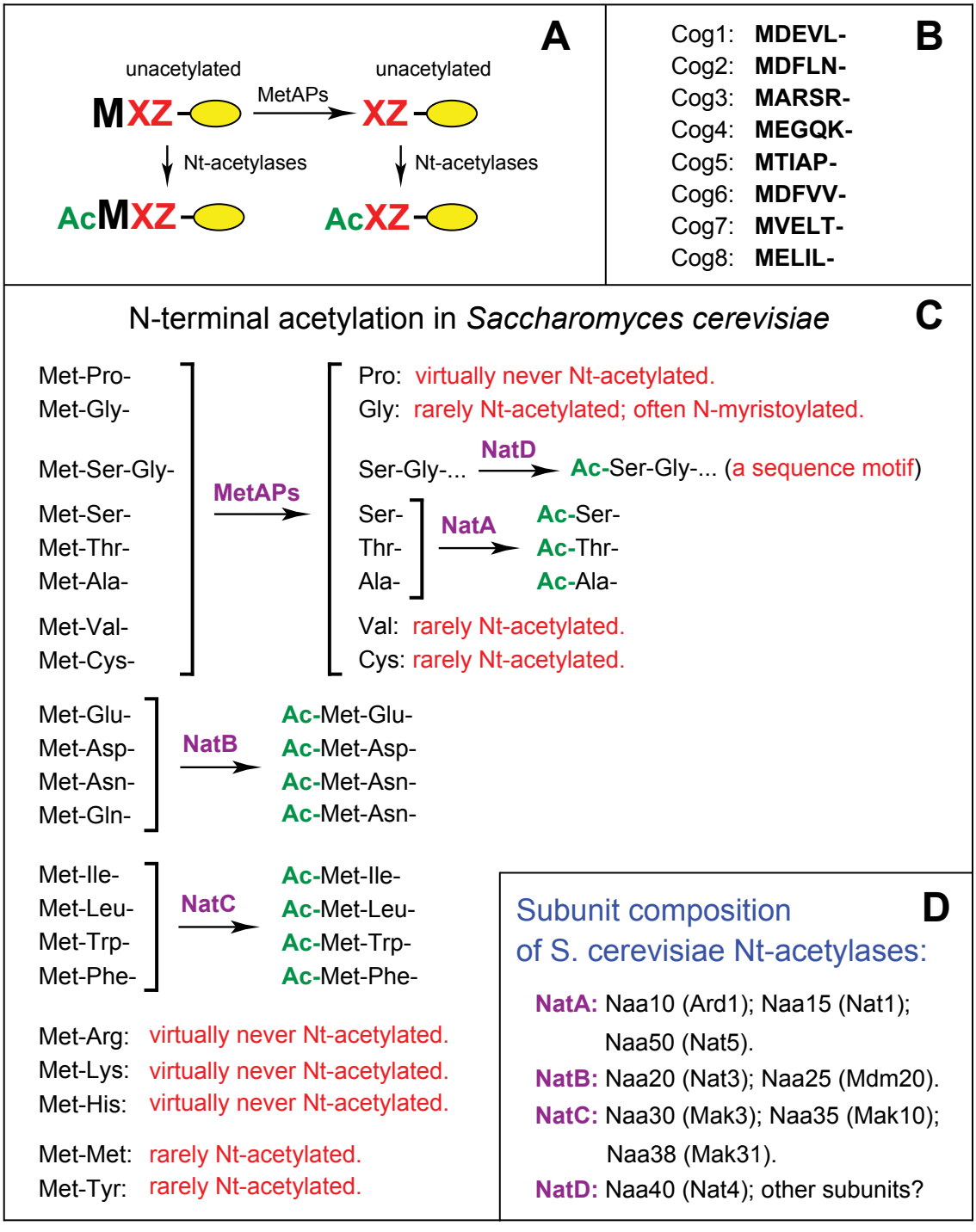

Figure A3.S2. N-terminal Processing of Nascent Proteins, the N-termini of COG Subunits, and the N$^{\alpha}$-Terminal Acetylation in *S. cerevisiae*.

(A) N-terminal processing of nascent cellular proteins by N^{α}-terminal acetylases (Nt-acetylases) and Met-aminopeptidases (MetAPs). “Ac” denotes the N^{α}-terminal acetyl moiety. M, Met. X and Z, single-letter abbreviations for any amino acid residue. Yellow ovals denote the rest of a protein.

(B) The first five encoded N-terminal residues of the Cog1-Cog8 subunits of the Conserved Oligomeric Golgi (COG) complex in S. cerevisiae (117,118).

(C) Substrate specificities and subunit compositions of *S. cerevisiae* Nt-acetylases. This compilation is derived from data in the literature ((86-89,129) and references therein). The present paper uses the revised nomenclature for specific subunits of Nt-acetylases (154) and cites the older names of these subunits in parentheses.

Figure A3.3

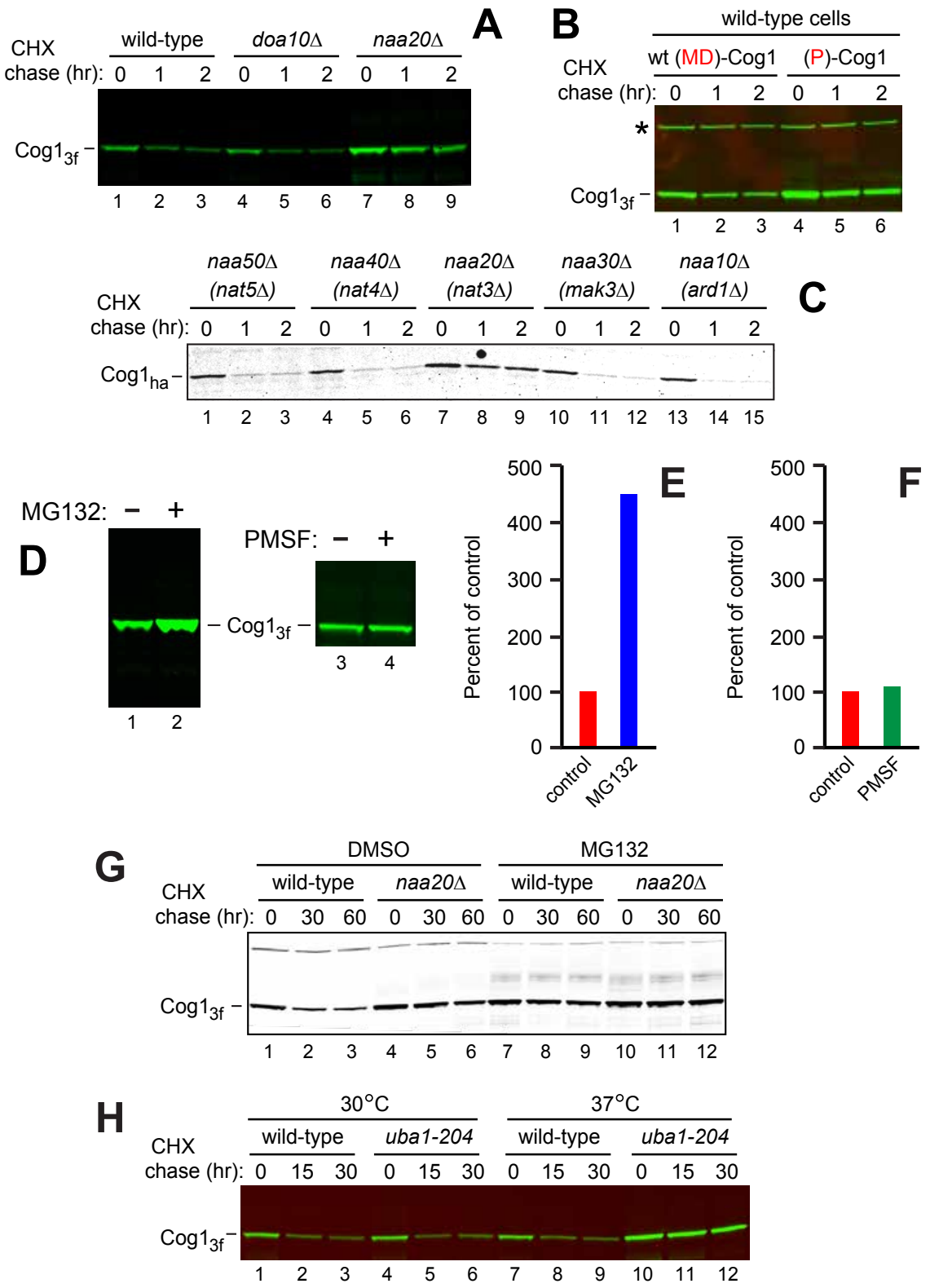
A
CHX
chase (hr):
wild-type
doa10Δ
naa20Δ
0 1 2 0 1 2 0 1 2
Cog1 3f
1 2 3 4 5 6 7 8 9
B
wild-type cells
wt (MD)-Cog1
(P)-Cog1
CHX
chase (hr): 0 1 2 0 1 2
*
Cog1 3f
1 2 3 4 5 6
C
naa50Δ (nat5Δ)
naa40Δ (nat4Δ)
naa20Δ (nat3Δ)
naa30Δ (mak3Δ)
naa10Δ (ard1Δ)
CHX
chase (hr): 0 1 2 0 1 2 0 1 2 0 1 2 0 1 2
Cog1 ha
1 2 3 4 5 6 7 8 9 10 11 12 13 14 15
D
MG132: − +
PMSF: − +
Cog1 3f
1 2
3 4
E
Percent of control
500
400
300
200
100
0
control
MG132
F
Percent of control
500
400
300
200
100
0
control
PMSF
G
DMSO
MG132
CHX
chase (hr):
wild-type
naa20Δ
wild-type
naa20Δ
0 30 60 0 30 60 0 30 60 0 30 60
Cog1 3f
1 2 3 4 5 6 7 8 9 10 11 12
H
30°C
37°C
CHX
chase (hr):
wild-type
uba1-204
wild-type
uba1-204
0 15 30 0 15 30 0 15 30 0 15 30
Cog1 3f
1 2 3 4 5 6 7 8 9 10 11 12

Figure A3.S3. Degradation of Cog1 by the Ac/N-End Rule Pathway.

(A) Cycloheximide (CHX)-chases (related to the ones described in Figure 1) were carried out at 30°C with wild-type (wt) (lanes 1-3), *doa10Δ* (lanes 4-6) and *naa20Δ* (*nat3Δ*) (lanes 7-9) *S. cerevisiae* strains that expressed wt Cog1, termed MD-Cog1^{wt}, which was C-terminally tagged with three flag epitopes. At the indicated times of chase, proteins in cell extracts were fractionated by SDS-PAGE and assayed by immunoblotting with anti-flag antibody.

(B) CHX-chases as in A, with wt cells that expressed MD-Cog1^{wt} (lanes 1-3) or its non-Nt-acetylatable P-Cog1 mutant (lane 4-6), both of which were C-terminally tagged with three flag epitopes. See the main text for descriptions of P-Cog1. Asterisk on the left denotes a crossreacting protein.

(C) CHX-chases as in A, with MD-Cog1^{wt} C-terminally ha-tagged and examined in *naa50Δ* (*nat5Δ*) (lanes 1-3), *naa40Δ* (*nat4Δ*) (lanes 4-6), *naa20Δ* (*nat3Δ*) (lanes 7-9), *naa30Δ* (*mak3Δ*) (lanes 10-12), and *naa10Δ* (*ard1Δ*) (lanes 13-15) S. cerevisiae strains. Each of these strains lacked the activity of a specific Nt-acetylase (see Figure S2C), including the cognate (for MD-Cog1^{wt}) NatB Nt-acetylase (lanes 7-9).

(D) Left panel: Expression of MD-Cog1^{wt} C-terminally tagged with three flag epitopes in *pdr5Δ S. cerevisiae*. Cells were incubated for 1 hr in SD medium containing either 0.5% dimethylsulfoxide (DMSO) (the solvent for a stock solution of the proteasome inhibitor MG132) (lane 1), or both 50 μM MG132 and 0.5% DMSO (lane 2). The incubation was followed by preparation of extracts, SDS-PAGE and immunoblotting with anti-flag antibody. Right panel: same procedures as in

experiments of the left panel but with *erg6Δ S. cerevisiae* incubated in SD containing either 1% isopropanol (the solvent for a stock solution of phenylmethylsulfonyl fluoride (PMSF), an inhibitor of serine proteases) (lane 1), or both 1 mM PMSF and 1% isopropanol (lane 2).

(E) Quantification of data in D, left panel.

(F) Quantification of data in D, right panel.

(G) CHX-chases with wt (lanes 1-3, 7-9) or *naa20Δ* (*nat3Δ*) (lanes 4-6, 10-12) *S. cerevisiae* strains expressing MD-Cog1^{wt} C-terminally tagged with three flag epitopes. Cells were grown for 3 hrs in SD medium containing 0.003% SDS (to allow for the entry of MG132) and either 0.5% DMSO (control, lanes 1-6) or both 50 μM MG132 and 0.5% DMSO. Note the metabolic stabilization of MD-Cog1^{wt} in wild-type cells by MG132 (lanes 1-3 vs. lanes 7-9) and the metabolic stabilization of MD-Cog1^{wt} in *naa20Δ* cells (lacking the NatB Nt-acetylase) irrespective of the absence or presence of MG132 (lanes 4-6 vs. lanes 10-12).

(H) CHX-chases with either wt or *uba1-204 S. cerevisiae* (the latter containing a temperature-sensitive mutant of the Ub-activating (E1) enzyme (125)) expressing MD-Cog1^{wt} C-terminally tagged with three flag epitopes. Lanes 1-3, wt cells at 30°C. Lanes 4-5, *uba1-204* cells at 30°C. Lanes 7-8, same as in lanes 1-3 but at 37°C (nonpermissive temperature for *uba1-204* cells). Lanes 10-12, same as lanes 4-6 but at 37°C. Note the metabolic stabilization of MD-Cog1^{wt} in *uba1-204* cells at 37°C (lanes 10-12).

Figure A3.4.

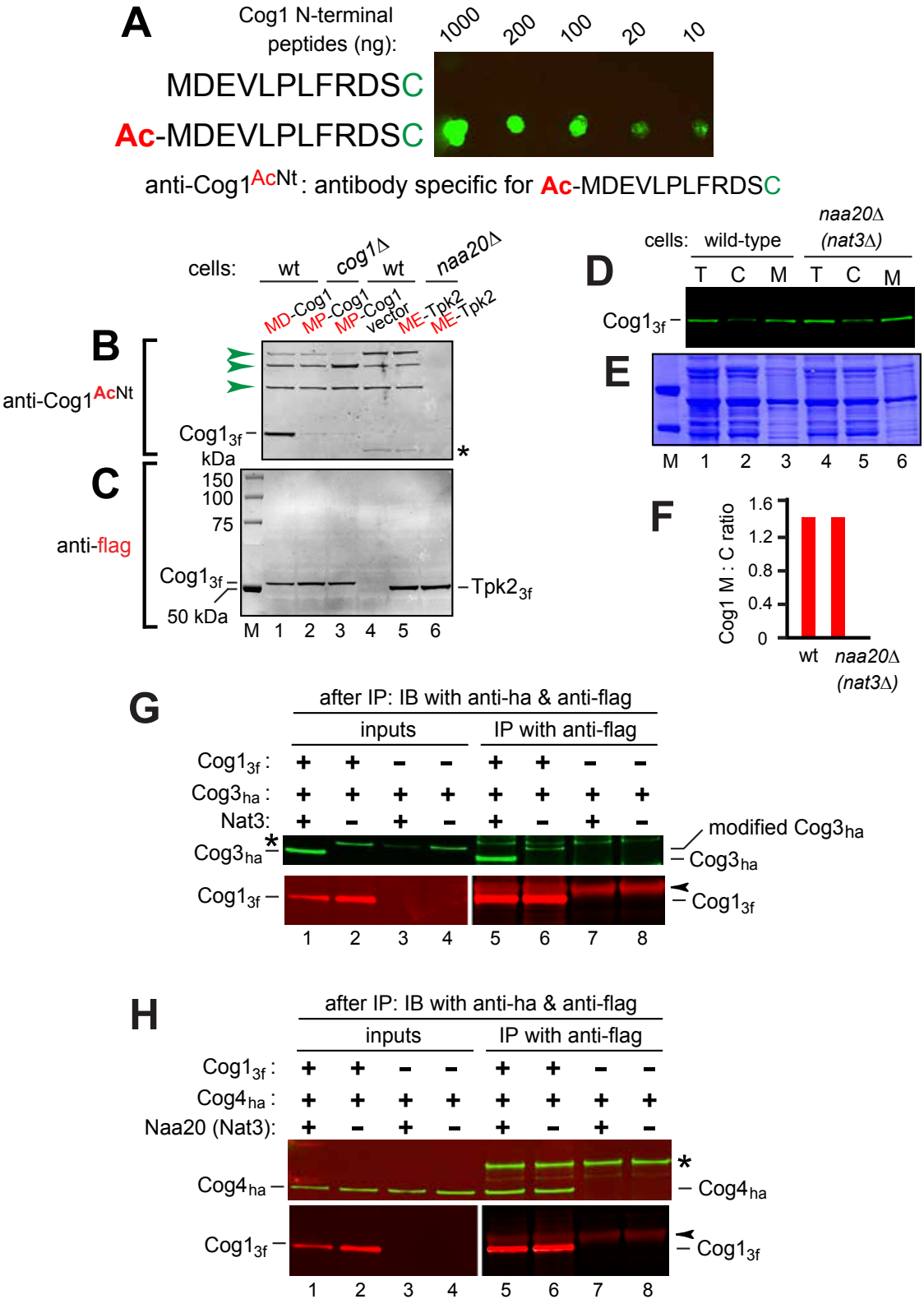
A
Cog1 N-terminal peptides (ng):
1000
200
100
20
10
MDEVLPLFRDSC
Ac-MDEVLPLFRDSC
anti-Cog1AcNt: antibody specific for Ac-MDEVLPLFRDSC
B
anti-Cog1AcNt
cells:
wt
cog1Δ
wt
naa20Δ
MD-Cog1
MP-Cog1
MP-Cog1
vector
ME-Tpk2
ME-Tpk2
Cog13f
kDa
*
C
anti-flag
150
100
75
Cog13f
50 kDa
Tpk23f
M 1 2 3 4 5 6
D
cells:
wild-type
naa20Δ (nat3Δ)
T C M T C M
Cog13f
E
M 1 2 3 4 5 6
F
Cog1 M : C ratio
1.6
1.2
0.8
0.4
0
wt
naa20Δ (nat3Δ)
G
after IP: IB with anti-ha & anti-flag
inputs
IP with anti-flag
Cog13f: + + – – + + – –
Cog3ha: + + + + + + + +
Nat3: + – + – + – + –
Cog3ha
*
modified Cog3ha
Cog3ha
Cog13f
Cog13f
1 2 3 4 5 6 7 8
H
after IP: IB with anti-ha & anti-flag
inputs
IP with anti-flag
Cog13f: + + – – + + – –
Cog4ha: + + + + + + + +
Naa20 (Nat3): + – + – + – + –
Cog4ha
*
Cog4ha
Cog13f
Cog13f
1 2 3 4 5 6 7 8

Figure A3.4. Antibody Specific for Nt-Acetylated Cog1, and Interactions of Nt-Acetylated and Unacetylated Cog1 with Subunits of the COG Complex or with Membranes.

(A) Characterization of the anti-^{AcNt}Cog1 antibody using a dot assay. Increasing amounts of the Nt-acetylated Ac-MDEVLPLFRDSC peptide and its non-acetylated counterpart MDEVLPLFRDSC were spotted onto a nitrocellulose membrane, followed by immunoblotting with the rabbit anti-^{AcNt}Cog1 antibody that was raised against the Ac-MDEVLPLFRDSC peptide and was then affinity-purified both "positively" (against Ac-MDEVLPLFRDSC) and "negatively" (against MDEVLPLFRDSC) (see Extended Experimental Procedures).

(B) Wt, *cog1Δ*, and *naa20Δ* (*nat3Δ*) S. cerevisiae strains overexpressed either MD-Cog1^{wt}, P-Cog1, or ME-Tpk2 (an Nt-acetylated protein whose N-terminal sequence is different from that of MD-Cog1^{wt}; a negative control) from the P_{CUP1} promoter on low copy plasmids. Equal amounts of total protein in the extracts were fractionated by SDS-PAGE and immunoblotted with the anti-^{AcNt}Cog1 antibody. Lane 1, MD-Cog1^{wt} (C-terminally tagged with three flag epitopes) was expressed in wt cells. Lane 2, same as in lane 1 but the identically tagged P-Cog1 (MP-Cog1). Lane 3, same as in lane 2 but in *cog1Δ* cells. Lane 4, same as in lane 1 but vector alone (no exogenously expressed MD-Cog1^{wt}). Lane 5, ME-Tpk2 (C-terminally tagged with three flag epitopes) was expressed in wt cells. Lane 6, same as in lane 5 but ME-Tpk2 was expressed in *naa20Δ* (*nat3Δ*) cells lacking the cognate NatB Nt-acetylase.

Anti-^{AcNt}Cog1 detected the band of Nt-acetylated MD-Cog1^{wt} in lane 1. Consistently, there was virtually no signal in other lanes, except for the barely

detectable band in lanes 4 and 5 (marked by asterisk on the right) that is likely to be the endogenous Nt-acetylated MD-Cog1^{wt} (endogenous MD-Cog1^{wt} was expressed at levels significantly below those of exogenous MD-Cog1^{wt}). Consistent with the absence of three flag epitopes in the endogenous MD-Cog1^{wt}, its band migrated faster than the band of the exogenous (tagged) MD-Cog1^{wt} (lane 1 vs. lanes 4 and 5). Note the absence of crossreaction of anti-^{AcNt}Cog1 with Nt-acetylated ME-Tpk2 in wt cells (lane 5). The anti-^{AcNt}Cog1 antibody also detected proteins larger than MD-Cog1^{wt}; they are marked by green arrowheads on the left. These proteins were not derivatives of MD-Cog1^{wt}, as they were present in cells not expressing MD-Cog1^{wt} (lane 4). The three proteins were Nt-acetylated by NatB, as they were absent in *naa20Δ* (*nat3Δ*) cells (lane 6). A likely and parsimonious interpretation is that the anti-^{AcNt}Cog1 antibody detected three specific Nt-acetylated proteins whose cognate Nt-acetylase (NatB) is the same as the one that Nt-acetylates MD-Cog1^{wt} and whose N-terminal sequences are sufficiently close to that of MD-Cog1^{wt} to have resulted in a crossreaction.

(C) Same as in B, but the same membrane was re-probed with anti-flag antibody, to detect the bulk of triply flag-tagged MD-Cog1^{wt} and ME-Tpk2.

(D) Equal amounts of total detergent-free cell extracts from wt or *naa20Δ* (*nat3Δ*) *S. cerevisiae* were fractionated to yield the cytosolic (C) and membrane (M) fractions, followed by SDS-PAGE and immunoblotting with anti-flag antibody to detect the triply flag-tagged MD-Cog1^{wt}. Lanes 1-3, wt total (T) extract and its C and M fractions, respectively. Lanes 4-6, same as in lanes 1-3 but from *naa20Δ* (*nat3Δ*) cells.

(E) Coomassie Blue staining of membrane probed by anti-flag in D.

(F) Quantification of the ratio of MD-Cog1^{wt} in the membrane versus cytosolic fractions in panel D, using Odyssey (Li-Cor) (see Extended Experimental Procedures).

(G) Coimmunoprecipitation of MD-Cog1^{wt} and Cog3 in the presence and absence of Nt-acetylation. Wt and *naa20Δ* (*nat3Δ*) *S. cerevisiae* strains carried either a P_{CUP1} promoter-containing low copy plasmid, or the otherwise identical plasmid expressing MD-Cog1^{wt} (C-terminally tagged with three flag epitopes), or the plasmid expressing Cog3 (C-terminally ha-tagged), in the indicated combinations of test proteins and genetic backgrounds of strains in which they were expressed. Extracts from these strains were immunoprecipitated using anti-flag beads, followed by SDS-PAGE and immunoblotting with anti-ha (to detect Cog3; the upper panel, green color) or with anti-flag (to detect MD-Cog1^{wt}; the lower panel, red color). As described in the main text, most Cog3 in *naa20Δ* (*nat3Δ*) cells was converted into a derivative of lower electrophoretic mobility, indicated on the right as "modified Cog3". The asterisk on the left indicates a protein crossreacting with anti-ha antibody. The arrowhead on the right marks the position of the heavy IgG chain, above the band of immunoprecipitated MD-Cog1^{wt}.

(H) Same as in G (including the same notations), but coimmunoprecipitation of MD-Cog1^{wt} (C-terminally tagged with three flag epitopes) and Cog4 (C-terminally ha-tagged). The asterisk in the top panel on the right indicates a protein crossreacting with anti-ha.

Figure A3.5.

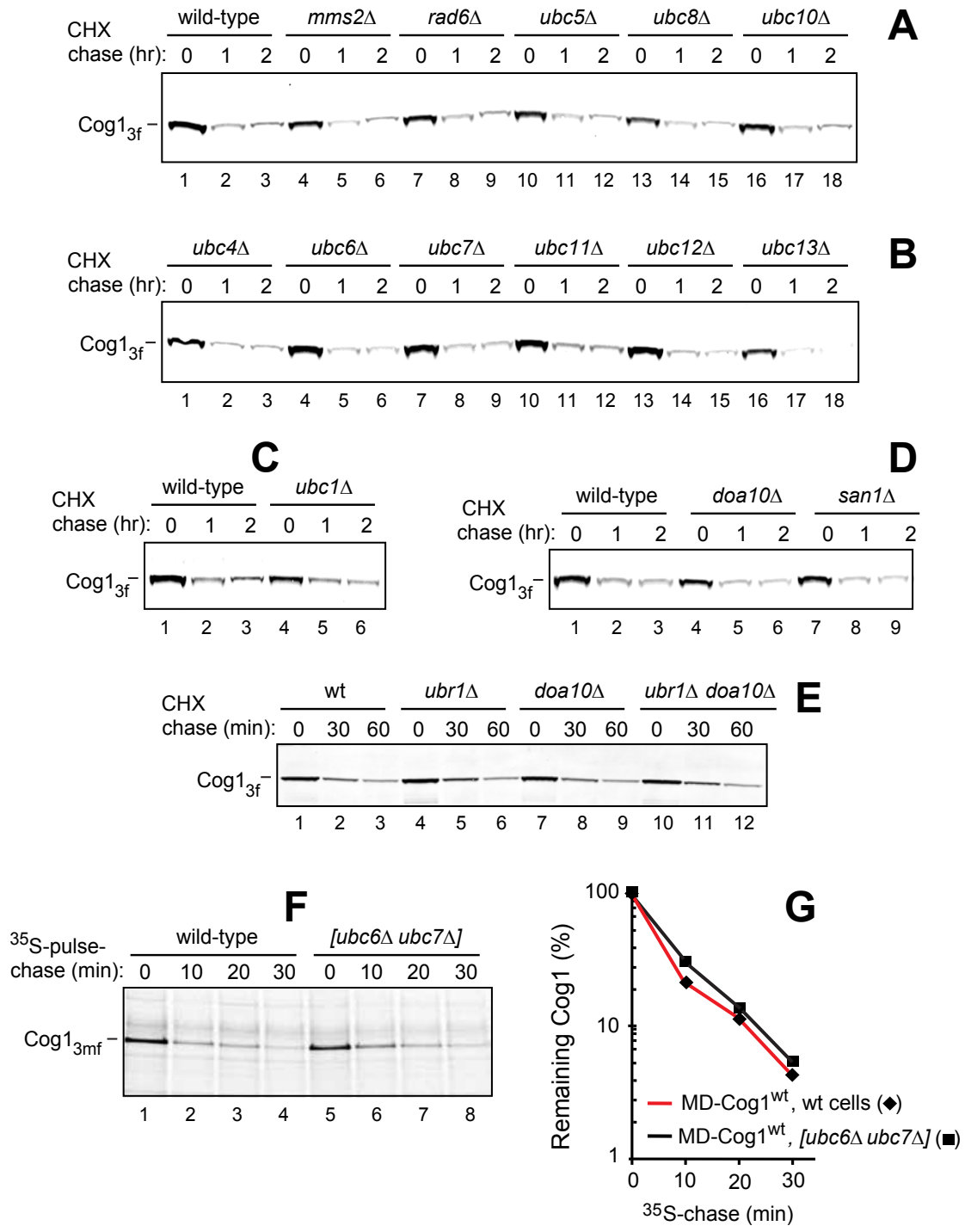

Figure A3.5. Degradation of MD-Cog1^{wt} by the Ac/N-End Rule Pathway in *S. cerevisiae* Mutants Lacking Specific E2 or E3 enzymes.

(A) CHX-chases with *S. cerevisiae* mutants in specific Ub-conjugating (E2) enzymes that expressed MD-Cog1^{wt} C-terminally tagged with three flag epitopes. Wt (lanes 1-3), *mms2Δ* (lanes 4-6), *rad6Δ* (lanes 7-9), *ubc5Δ* (lanes 10-12), *ubc8Δ* (lanes 13-15), and *ubc10Δ* (lanes 16-18) *S. cerevisiae* strains.

(B) Same as in A but with *ubc4Δ* (lanes 1-3), *ubc6Δ* (lanes 4-6), *ubc7Δ* (lanes 7-9), *ubc11Δ* (lanes 10-12), *ubc12Δ* (lanes 13-15), and *ubc13Δ* (lanes 16-18) S. cerevisiae strains.

(C) Same as in A but with wt (lanes 1-3) and *ubc1Δ* (lanes 4-6) *S. cerevisiae* strains.

(D) CHX-chases with mutants in two specific E3 enzymes. Same as in A but with wt (lanes 1-3), *doa10Δ* (lanes 4-6), and *san1Δ* (lanes 7-9) *S. cerevisiae* strains.

(E) Same as in D but with wt (lanes 1-3), *ubr1Δ* (lanes 4-6), *doa10Δ* (lanes 7-9), and double-mutant *ubr1Δ doa10Δ* (lanes 10-12) *S. cerevisiae* strains.

(F) Lanes 1-4, ^{35}S-pulse chase with wt S. cerevisiae and MD-Cog1^{wt} (C-terminally tagged with three flag epitopes modified to contain a Met residue in each epitope, to increase ^{35}S in Cog1; see Extended Experimental Procedures). Lanes 5-8, same as lanes 1-4 but with a double mutant *ubc6Δ ubc7Δ*.

(G) Quantification of data in F.

Note the absence of significant effects of the tested mutant backgrounds on the degradation of MD-Cog1^{wt} by the Ac/N-end rule pathway (see also Figure 1 and the main text).

EXTENDED EXPERIMENTAL PROCEDURES

Yeast Strains, Media, and Genetic Techniques

S. cerevisiae strains used in this study are described in Table S1. Standard techniques (155,156) were employed for strain construction and transformation. *S. cerevisiae* media included YPD (1% yeast extract, 2% peptone, 2% glucose; only most relevant components are cited); SD medium (0.17% yeast nitrogen base, 0.5% ammonium sulfate, 2% glucose); and synthetic complete (SC) medium (0.17% yeast nitrogen base, 0.5% ammonium sulfate, 2% glucose), plus a drop-out mixture of compounds required by a given auxotrophic strain. The COG1-3HA strains were made by standard PCR of the 3HA-HIS3MX6 module (157) targeted to the 3' coding region of COG1. The PCR product was transformed into BY4742, BY17299, and BY15546 to create ASY101, ASY102, and ASY103, respectively. The double mutant *ubc6Δubc7Δ* (ASY104) was made by transforming BBY67.3 with a PCR product of the KanMX6 module (157) targeted to the 5' and 3' regions of UBC7, thereby replacing the ORF of Ubc7 with KanMX6. The ASY105 strain was made by the standard integration of a PCR fragment derived from pFA6a-13MYC with the HIS3MX6 marker targeted to the 3' end of the *COG1* gene. Proper tagging of *COG1* and its product was verified by PCR and immunoblotting with anti-myc antibody. The resulting ASY105 strain was transformed with pAS118 or the control YEPlac181 plasmid (Table S2). E1, E2, E3 and Nt-acetylase mutant strains used in this study were from the Varshavsky lab stock (CHY345, CHY346, BBY67.3), the

T. Sommer lab stock (YW05), the Deshaies lab stock (RJD3268, RJD3269) or all others from Open Biosystems. Strains used in the proteasome and vacuole inhibitor studies were obtained from Open Biosystems (BY10568) or from the Varshavsky lab stock (JD52, CHY49). The *cog1Δ* mutant (BY14589) was obtained from Open Biosystems.

Construction of Plasmids

The *S. cerevisiae* Cog1-coding sequence was amplified by PCR from genomic DNA and the triple flag-coding sequence was then added by PCR. Additional Met-coding sequences were added in between the Cog1-coding sequence and the triple flag-coding sequence to increase the labeling of MD-Cog1^{wt} with ^{35}S-Met. The 3 extra Met-coding DNA sequences were separated by short Gly-Ser linker sequences, the complete Met-enriching sequence being MSGMGAM. pAS101 was constructed by ligating the BamHI/Not1 digested PCR fragment of Cog1-3flag DNA into the low-copy (CEN) plasmid pRS316 with the P_{CUP1} promoter (p316Cup1). pAS117 was made by standard site-directed mutagenesis of pAS101 to insert a coding sequence for proline (P) in between the initiator Met (M) and Asp (D). pAS105 was made by amplifying the Cog1-coding sequence with a sequence encoding a single C-terminal ha tag and ligating this PCR product into the BamHI/NotI-cut p316Cup1 plasmid. pAS118 was made by standard point mutagenesis of pAS105 to mutate the aspartic acid (D) coding sequence to lysine (K). pAS102 was made by adding the 3flag sequence to the 3' end of the Cog2 PCR product and ligating that product into p316Cup1. pAS115 was made by inserting the Cog2-3f sequence and the Cog3-HA

sequence on opposite sides of the $P_{GAL1/10}$ bidirectional promoter. pAS116 was made by inserting the Cog4-ha-coding sequence into pRS425Gal1/10. pAS118 was made by ligating the XbaI/PstI-derived, PCR-produced DNA fragment into XbaI/PstI-cut pRB208.

To construct pAS112 (Table S2), the *S. pombe HCN1* coding sequence was amplified from pGAD424-Hcn1. The triple flag-coding DNA sequence was then added to the 3' region of *HCN1*. The resulting PCR-produced DNA fragment was ligated into the high copy plasmid pRS423 (155) containing the P_{CUP1} promoter. The same PCR fragment from pAS112 was ligated into p413Met25 to produce pAS113. The *S. cerevisiae* DNA encoding Cdc26 was amplified from genomic DNA and the triple flag-coding DNA sequence was added by PCR. The resulting DNA fragment was cloned into pRS423 as described above to produce pAS119. DNA encoding *S. pombe* Cut9 was amplified from pGAD424-Cut9, and the triple flag-coding DNA sequence was added to the 3' region of *CUT9* by PCR. The resulting DNA fragment was ligated into the high copy pRS425 plasmid containing the P_{GAL1} promoter, yielding pAS114.

Cycloheximide Chase Degradation Assays

S. cerevisiae were grown to A_{600} of 0.8 to 1.0 in plasmid-maintaining (selective) liquid media at 30°C, followed by treatment with cycloheximide (CHX), at the final concentration of 0.1 mg/ml. At indicated times, cell samples (corresponding to 1 ml of cell suspension at A_{600} of 1) were harvested by centrifugation for 1 min at 11,200*g*, and resuspended in 1 ml of 0.2 M NaOH, for 20

min on ice, or for 5 min at room temperature, followed by centrifugation for 1 min at 11,200*g*. Pelleted cells were resuspended in 50 µl of 1X LDS buffer (Invitrogen, Carlsbad, CA) with 1X reducing agent and 1x protease inhibitor cocktail "for use with fungal and yeast extracts" (Sigma), and heated for 10 min at 70°C. After centrifugation at 5 min at 11,200g, 10 µl of supernatant was fractionated by SDS-4-12% NuPAGE, followed by immunoblotting with an appropriate antibody. The antibodies used included anti-ha (Sigma), anti-flag (Stratagene, La Jolla, CA), anti-tubulin (used for loading controls) (Sigma), and anti-^{Nt}Cog1, prepared and purified as described below. Immunoblots were processed using secondary antibodies labeled with different fluorophores. Visualized protein bands were quantified using the Odyssey Imaging System (Li-Cor, Lincoln, NE). The near-infrared fluorescence range and other features of the Odyssey scanner facilitate quantification of immunoblots.

^{35}S-Pulse-Chase Degradation Assays

These experiments were performed essentially as described previously (95,102,133). Unless stated otherwise, *S. cerevisiae* strains were grown at 30°C to A_{600} of ~1 in 10 ml of SD medium with components required for auxotrophic growth. Cells were pelleted by centrifugation, gently resuspended, and washed in 0.8 ml of SD medium with required amino acids but without L-Met and L-Cys. Cell pellets were gently resuspended again in 0.4 ml of the same medium and labeled for 5 min at 30°C with 0.16 mCi of ^{35}S-EXPRESS (Perkin-Elmer). Cells were pelleted again and resuspended in 0.3 ml of SD medium containing unlabeled 10 mM L-Met,

5 mM unlabeled L-Cys, and required amino acids. Samples (0.1 ml) were taken at the indicated time points, followed by preparation of extracts by bead beating (FastPrep, 20 seconds at 6.5 M/s, 4 times each), immunoprecipitation with anti-flag magnetic beads (Sigma), SDS-4-12% NuPAGE, electrophoretic transfer of proteins to a PVDF membrane (Invitrogen) and autoradiography. Quantification of ^{35}S-pulse-chases was carried out using Storm PhosphorImager and ImageQuant (GE Healthcare, Pittsburgh, PA).

Antibody Specific for Nt-Acetylated Cog1

Ac-MDEVLPLFRDS, the Nt-acetylated N-terminal peptide of MD-Cog1^{wt}, was used to produce a rabbit antibody, termed anti-Cog1^{AcNt}, that recognized Ac-MDEVLPLFRDS but not its unacetylated counterpart (Figures 1E-H and S4A-C). The Nt-acetylated synthetic peptide AcMDEVLPLFRDSC and its unacetylated counterpart MDEVLPLFRDSC (they bore C-terminal Cys for crosslinking these peptides to the keyhole limpet hemocyanin carrier protein) were synthesized and purified by Abgent (San Diego, CA). Standard procedures were employed by Abgent to produce rabbit antisera to AcMDEVLPLFRDSC. The resulting antibody (its IgG fraction, produced using immobilized Protein A) was affinity-purified, "positively" at first, against the immobilized AcMDEVLPLFRDSC peptide. The peptide-bound antibody was eluted and thereafter "negatively" purified against the MDEVLPLFRDSC peptide (immobilized using SulfoLink Coupling Resin (Pierce)), with collection, this time, of the unbound antibody fraction. The resulting antibody, termed anti-^{AcNt}Cog1, was highly specific for Nt-acetylated MD-Cog1^{wt} (see Results). Immunoblotting with anti-

^{AcNt}Cog1 (1:500 dilution) was carried out for 3 h at room temperature (RT) in 5% skim milk in PBST (PBS containing 0.5% Tween-20). The bound anti-^{AcNt}Cog1 was detected using the Odyssey Imaging System and a goat anti-rabbit antibody (at 1:5,000 dilution) that was conjugated to IRDye-800 (Li-Cor).

Partitioning of Nt-Acetylated and Unacetylated MD-Cog1^{wt} Between Membranes and Cytosol

This assay (Figure S4D-F) used a slight modification of the previously described procedure (119). Wild-type and *naa20Δ* (*nat3Δ*) *S. cerevisiae* expressing MD-Cog1^{wt} (C-terminally tagged with three flag epitopes) were grown at 30°C in 200 ml of SD to A_{600} between 1 and 2. Cells were collected by centrifugation and washed twice with ice-cold distilled water. Cells were disrupted in 1 ml of lysis buffer (1 mM dithiothreitol (DTT), 20 mM HEPES, (pH 7.0), 1 mM PMSF, and protease inhibitor cocktail (Sigma)), using 1 ml of glass beads and vortexing 3 times for 1 min each. The extract was clarified by centrifugation at 3000*g* for 5 min, followed by centrifugation in the TL100 ultracentrifuge (Beckman) at 150,000*g* for 1 h to obtain crude "cytosolic" (supernatant) and "membrane" (pellet) fractions. Membrane fractions were resuspended in 1 ml of Tris-Buffered Saline (TBS). Total clarified extracts and equal total protein amounts of cytosolic and membrane fractions (as determined by the Bradford assay) were fractionated by SDS-4-12% NuPAGE (Invitrogen), followed by immunoblotting with anti-flag antibody. The relative amounts of MD-Cog1^{wt} in cytosolic and membrane fractions were quantified using the Odyssey Imaging System.

Coimmunoprecipitation of Cog1 with Cog3 and Cog4

Wild-type and *naa20Δ* (*nat3Δ*) *S. cerevisiae* expressing specific combinations of either vector alone, MD-Cog1^{wt} (C-terminally tagged with three flag epitopes), Cog3 (C-terminally ha-tagged), or Cog4 (C-terminally ha-tagged) (Figure S4G, H) were grown at 30°C to A_{600} of ~1 in 50 ml of SD containing or lacking appropriate metabolic markers. Cells were collected by centrifugation and resuspended in 0.8 ml of lysis buffer (0.1% NP-40, 10% glycerol, 0.1 M NaCl, 0.5 mM EDTA, 25 mM HEPES, pH 7.5) containing 1X protease inhibitor cocktail and 1 mM PMSF. Cells were disrupted using the FastPrep lysing matrix and bead beating (FastPrep). The extract was clarified by centrifugation at 12,000*g* for 15 min at 4°C. The total protein concentration was measured by the Bradford assay. Equal amounts of total protein were incubated with anti-flag magnetic beads (Sigma) for 2 hrs at 4°C. The beads were washed 3 times with lysis buffer, followed by the elution of beads-bound proteins with 12 µl of 2X NuPAGE LDS sample buffer (containing lithium dodecyl sulfate instead of SDS) with protease inhibitors. Sample were heated at 95°C for 5 min, clarified by centrifugation, and fractionated by SDS-4-12% NuPAGE, followed by immunoblotting with anti-ha antibody and thereafter with anti-flag antibody.

Assays with Protease Inhibitors

MD-Cog1^{wt} C-terminally tagged with three flag epitopes was expressed from the low copy plasmid pRS316Cup1-Cog1-3flag and its P_{CUP1} promoter in *pdr5Δ S. cerevisiae* (the absence of the Pdr5 pump in this mutant allowed for the intracellular

retention of MG132, a proteasome inhibitor). Cells were incubated for 1 hr in SD medium containing either 0.5% dimethylsulfoxide (DMSO) (the solvent for a stock solution of MG132), or both 50 μM MG132 and 0.5% DMSO. The incubation was followed by preparation of extracts, SDS-PAGE and immunoblotting with anti-flag antibody. The same procedures were employed using *erg6Δ S. cerevisiae* to examine effects of phenylmethylsulfonyl fluoride (PMSF), an inhibitor of serine proteases, on the degradation of MD-Cog1^{wt}. Cells were incubated either in the presence of 1% isopropanol (the solvent for a stock solution of PMSF), or both 1 mM PMSF and 1% isopropanol, followed by preparation of extracts, SDS-PAGE and immunoblotting with anti-flag antibody (Figure S3D-F).

Table S1: *S. cerevisiae* Strains Used in This Study

Strain	Relevant Genotype	Source
BY4742	*MATα his3-1 leu2-0 lys2-0 ura3-0 can1-100,*	Open Biosystems
BY10976	*ard1Δ::KanMX6 in* BY4742	Open Biosystems
BY15470	*mak3Δ::KanMX6 in* BY4742	Open Biosystems
BY15546	*nat3Δ::KanMX6 in* BY4742	Open Biosystems
BY17299	*doa10Δ:KanMX6 in* BY4742	Open Biosystems
BY4741	*MATa his3-1 leu2-0 met15-0 ura3-0*	Open Biosystems
BY4425	*rad6Δ:: KanMX4* in BY4741	Open Biosystems
BY14589	*cog1Δ::KanMX4* in BY4742	Open Biosystems
ASY101	COG1-3HA::HIS3MX6 in BY4742	This Study
ASY102	COG1-3HA::HIS3MX6 in BY17299	This Study
ASY103	COG1-3HA::HIS3MX6 in BY15546	This Study
ASY105	COG1-13MYC::HIS3MX6 in BY4742	This Study
YW05	*ubc1Δ:: HIS3* JD52	T. Sommers lab collection
BY4454	*mms2Δ::KanMX6* in BY4741	Open Biosystems
BY3994	*ubc5Δ::KanMX6* in BY4741	Open Biosystems
BY3219	*ubc4Δ::KanMX6* in BY4741	Open Biosystems
BBY67.3	*ubc6Δ::HIS3* in JD52	Varshavsky lab collection
BY597	*ubc7Δ::KanMX6* in BY4741	Open Biosystems
BY6577	*ubc8Δ:: KanMX6* in BY4741	Open Biosystems
BY4763	*ubc10Δ:: KanMX6* in BY4741	Open Biosystems
BY1636	*ubc11Δ:: KanMX6* in BY4741	Open Biosystems
BY5214	*ubc12Δ:: KanMX6* in BY4741	Open Biosystems
BY4027	*ubc13Δ:: KanMX6* in BY4741	Open Biosystems
AS104	*ubc6Δ::HIS3, ubc7Δ::KanMX6* in JD52	This Study
BY10568	*erg6Δ::KanMX6* in BY4742	Open Biosystems
RJD3268	*MATa, uba1::KANMX [pRS313 - UBA1-HIS], can1-100, leu2-3, -112, his3-11, -15, trp1-1, ura3-1, ade2-1*	(125)
RJD3269	*MATa, uba1Δ*::*KanMX* [*pRS313-uba1-204-HIS*], *can1-100, leu2-3, -112, his3-11, -15, trp1-1, ura3-1, ade2-1*	(125)
JD52	*MATa trp1- 63 ura3-52 his3- 200 leu2-3112. lys2-801*	(95)
CHY49	*pdr5Δ::KanMX6 in JD52*	(158)
CHY345	*ubr1Δ::LEU2* in BY4742	This Study
CHY346	*ubr1Δ::LEU2 doa10Δ::KANMX6* in BY4742	This Study

Table S2: Plasmids Used in This Study

Plasmid	Description	Source
p316Cup1	pRS316 with P_{CUP1} promoter	This study
p313Cup1	pRS313 with P_{CUP1} promoter	This study
pAS101	Cog1-3flag in p316CUP1	This study
pAS117	MPCog1-3flag in p316Cup1	This study
pAS102	Cog2-3flag in p316CUP1	This study
pAS103	Cog1-3flag in p313CUP1	This study
pAS104	Cog1-3HA in p316CUP1	This study
pAS105	Cog1-HA in p316CUP1	This study
pAS106	Cog3-HA in p316CUP1	This study
pAS107	Cog4-HA in p316CUP1	This study
pAS108	Cog5-HA in p316CUP1	This study
pAS109	Cog6-HA in p316CUP1	This study
pAS110	Cog8-HA in p316CUP1	This study
pAS111	Cog1-3flag in p425GAL1	This study
p413MET25	pRS413 with P_{MET25} promoter	(159)
pAS112	Hcn1-3flag in p423CUP1	This study
pAS113	Hcn1-3flag in p413MET25	This study
p425Gal1	pRS425 with P_{GAL1} promoter	(159)
pAS114	Cut9-3flag in p425GAL1	This study
pAS115	Cog2-3flag, Cog3-HA in p423GAL1,10	This study
pAS116	Cog4-HA in p425GAL1,10	This study
pAS118	Cog1-3flag in YEPlac181 with pAdh1	This study
YEPlac181	2μ LEU2 plasmid	Varshavsky lab collection

SUPPLEMENTAL REFERENCES

1. Varshavsky, A. (2011) *Protein science : a publication of the Protein Society*
2. Ang, X. L., and Wade Harper, J. (2005) *Oncogene* **24**, 2860-2870
3. Finley, D., Ulrich, H. D., Sommer, T., and Kaiser, P. (2012) *Genetics* **192**, 319-360
4. Varshavsky, A. (2006) *Protein science : a publication of the Protein Society* **15**, 647-654
5. Varshavsky, A. (1991) *Cell* **64**, 13-15
6. Finley, D. (2009) *Annual review of biochemistry* **78**, 477-513
7. Kravtsova-Ivantsiv, Y., and Ciechanover, A. (2012) *Journal of cell science* **125**, 539-548
8. Hochstrasser, M. (2006) *Cell* **124**, 27-34
9. Kulathu, Y., and Komander, D. (2012) *Nature reviews. Molecular cell biology* **13**, 508-523
10. Behrends, C., and Harper, J. W. (2011) *Nature structural & molecular biology* **18**, 520-528
11. Gallastegui, N., and Groll, M. (2010) *Trends in biochemical sciences* **35**, 634-642
12. Marques, A. J., Palanimurugan, R., Matias, A. C., Ramos, P. C., and Dohmen, R. J. (2009) *Chemical reviews* **109**, 1509-1536
13. Xie, Y., and Varshavsky, A. (2000) *Proceedings of the National Academy of Sciences of the United States of America* **97**, 2497-2502

14. Metzger, M. B., Hristova, V. A., and Weissman, A. M. (2012) *Journal of cell science* **125**, 531-537

15. Deshaies, R. J., and Joazeiro, C. A. (2009) *Annual review of biochemistry* **78**, 399-434

16. Rotin, D., and Kumar, S. (2009) *Nature reviews. Molecular cell biology* **10**, 398-409

17. Bachmair, A., Finley, D., and Varshavsky, A. (1986) *Science* **234**, 179-186

18. Bachmair, A., and Varshavsky, A. (1989) *Cell* **56**, 1019-1032

19. Varshavsky, A., Bachmair, A., and Finley, D. (1987) *Biochemical Society transactions* **15**, 815-816

20. Varshavsky, A., Bachmair, A., Finley, D., Gonda, D. K., and Wunning, I. (1989) *Biotechnology* **13**, 109-143

21. Varshavsky, A. (2004) *Current biology : CB* **14**, R181-183

22. Choi, W. S., Jeong, B. C., Joo, Y. J., Lee, M. R., Kim, J., Eck, M. J., and Song, H. K. (2010) *Nature structural & molecular biology* **17**, 1175-1181

23. Matta-Camacho, E., Kozlov, G., Li, F. F., and Gehring, K. (2010) *Nature structural & molecular biology* **17**, 1182-1187

24. Tasaki, T., and Kwon, Y. T. (2007) *Trends in biochemical sciences* **32**, 520-528

25. Xia, Z., Webster, A., Du, F., Piatkov, K., Ghislain, M., and Varshavsky, A. (2008) *The Journal of biological chemistry* **283**, 24011-24028

26. Hu, R. G., Brower, C. S., Wang, H., Davydov, I. V., Sheng, J., Zhou, J., Kwon, Y. T., and Varshavsky, A. (2006) *The Journal of biological chemistry* **281**, 32559-32573

27. Wang, H., Piatkov, K. I., Brower, C. S., and Varshavsky, A. (2009) *Molecular cell* **34**, 686-695

28. Hu, R. G., Sheng, J., Qi, X., Xu, Z., Takahashi, T. T., and Varshavsky, A. (2005) *Nature* **437**, 981-986

29. Xia, Z., Turner, G. C., Hwang, C. S., Byrd, C., and Varshavsky, A. (2008) *The Journal of biological chemistry* **283**, 28958-28968

30. Du, F., Navarro-Garcia, F., Xia, Z., Tasaki, T., and Varshavsky, A. (2002) *Proceedings of the National Academy of Sciences of the United States of America* **99**, 14110-14115

31. Dohmen, R. J., Madura, K., Bartel, B., and Varshavsky, A. (1991) *Proceedings of the National Academy of Sciences of the United States of America* **88**, 7351-7355

32. Hwang, C. S., Shemorry, A., Auerbach, D., and Varshavsky, A. (2010) *Nature cell biology* **12**, 1177-1185

33. Hwang, C. S., Shemorry, A., and Varshavsky, A. (2009) *Proceedings of the National Academy of Sciences of the United States of America* **106**, 2142-2147

34. Johnson, E. S., Ma, P. C., Ota, I. M., and Varshavsky, A. (1995) *The Journal of biological chemistry* **270**, 17442-17456

35. Johnson, E. S., Bartel, B., Seufert, W., and Varshavsky, A. (1992) *The EMBO journal* **11**, 497-505

36. Park, Y., Yoon, S. K., and Yoon, J. B. (2009) *The Journal of biological chemistry* **284**, 1540-1549

37. Park, Y., Yoon, S. K., and Yoon, J. B. (2008) *Biochemical and biophysical research communications* **374**, 294-298

38. Hu, R. G., Wang, H., Xia, Z., and Varshavsky, A. (2008) *Proceedings of the National Academy of Sciences of the United States of America* **105**, 76-81

39. Varshavsky, A. (2008) *The Journal of biological chemistry* **283**, 34469-34489

40. Mogk, A., Schmidt, R., and Bukau, B. (2007) *Trends in cell biology* **17**, 165-172

41. Graciet, E., and Wellmer, F. (2010) *Trends in plant science* **15**, 447-453

42. An, J. Y., Seo, J. W., Tasaki, T., Lee, M. J., Varshavsky, A., and Kwon, Y. T. (2006) *Proceedings of the National Academy of Sciences of the United States of America* **103**, 6212-6217

43. Kwon, Y. T., Xia, Z., An, J. Y., Tasaki, T., Davydov, I. V., Seo, J. W., Sheng, J., Xie, Y., and Varshavsky, A. (2003) *Molecular and cellular biology* **23**, 8255-8271

44. Kwon, Y. T., Kashina, A. S., Davydov, I. V., Hu, R. G., An, J. Y., Seo, J. W., Du, F., and Varshavsky, A. (2002) *Science* **297**, 96-99

45. Kwon, Y. T., Xia, Z., Davydov, I. V., Lecker, S. H., and Varshavsky, A. (2001) *Molecular and cellular biology* **21**, 8007-8021

46. Kwon, Y. T., Balogh, S. A., Davydov, I. V., Kashina, A. S., Yoon, J. K., Xie, Y., Gaur, A., Hyde, L., Denenberg, V. H., and Varshavsky, A. (2000) *Molecular and cellular biology* **20**, 4135-4148

47. Hwang, C. S., and Varshavsky, A. (2008) *Proceedings of the National Academy of Sciences of the United States of America* **105**, 19188-19193

48. Brower, C. S., and Varshavsky, A. (2009) *PloS one* **4**, e7757

49. Graciet, E., Walter, F., Maoileidigh, D. O., Pollmann, S., Meyerowitz, E. M., Varshavsky, A., and Wellmer, F. (2009) *Proceedings of the National Academy of Sciences of the United States of America* **106**, 13618-13623

50. Eisele, F., and Wolf, D. H. (2008) *FEBS letters* **582**, 4143-4146

51. Heck, J. W., Cheung, S. K., and Hampton, R. Y. (2010) *Proceedings of the National Academy of Sciences of the United States of America* **107**, 1106-1111

52. Prasad, R., Kawaguchi, S., and Ng, D. T. (2010) *Molecular biology of the cell* **21**, 2117-2127

53. Nillegoda, N. B., Theodoraki, M. A., Mandal, A. K., Mayo, K. J., Ren, H. Y., Sultana, R., Wu, K., Johnson, J., Cyr, D. M., and Caplan, A. J. (2010) *Molecular biology of the cell* **21**, 2102-2116

54. Ouyang, Y., Kwon, Y. T., An, J. Y., Eller, D., Tsai, S. C., Diaz-Perez, S., Troke, J. J., Teitell, M. A., and Marahrens, Y. (2006) *Mutation research* **596**, 64-75

55. Yoshida, S., Ito, M., Callis, J., Nishida, I., and Watanabe, A. (2002) *The Plant journal : for cell and molecular biology* **32**, 129-137

56. Holman, T. J., Jones, P. D., Russell, L., Medhurst, A., Ubeda Tomas, S., Talloji, P., Marquez, J., Schmuths, H., Tung, S. A., Taylor, I., Footitt, S., Bachmair, A., Theodoulou, F. L., and Holdsworth, M. J. (2009) *Proceedings of the National Academy of Sciences of the United States of America* **106**, 4549-4554

57. Rai, R., Wong, C. C., Xu, T., Leu, N. A., Dong, D. W., Guo, C., McLaughlin, K. J., Yates, J. R., 3rd, and Kashina, A. (2008) *Development* **135**, 3881-3889

58. Zhang, F., Saha, S., Shabalina, S. A., and Kashina, A. (2010) *Science* **329**, 1534-1537

59. Kurosaka, S., Leu, N. A., Zhang, F., Bunte, R., Saha, S., Wang, J., Guo, C., He, W., and Kashina, A. (2010) *PLoS genetics* **6**, e1000878

60. Saha, S., Mundia, M. M., Zhang, F., Demers, R. W., Korobova, F., Svitkina, T., Perieteanu, A. A., Dawson, J. F., and Kashina, A. (2010) *Molecular biology of the cell* **21**, 1350-1361

61. de Groot, R. J., Rumenapf, T., Kuhn, R. J., Strauss, E. G., and Strauss, J. H. (1991) *Proceedings of the National Academy of Sciences of the United States of America* **88**, 8967-8971

62. Lloyd, A. G., Ng, Y. S., Muesing, M. A., Simon, V., and Mulder, L. C. (2007) *Virology* **360**, 129-135

63. Mulder, L. C., and Muesing, M. A. (2000) *The Journal of biological chemistry* **275**, 29749-29753

64. Lecker, S. H., Solomon, V., Price, S. R., Kwon, Y. T., Mitch, W. E., and Goldberg, A. L. (1999) *The Journal of clinical investigation* **104**, 1411-1420

65. Lecker, S. H., Solomon, V., Mitch, W. E., and Goldberg, A. L. (1999) *The Journal of nutrition* **129**, 227S-237S

66. Carpio, M. A., Lopez Sambrooks, C., Durand, E. S., and Hallak, M. E. (2010) *The Biochemical journal* **429**, 63-72

67. Zenker, M., Mayerle, J., Lerch, M. M., Tagariello, A., Zerres, K., Durie, P. R., Beier, M., Hulskamp, G., Guzman, C., Rehder, H., Beemer, F. A., Hamel, B., Vanlieferinghen, P., Gershoni-Baruch, R., Vieira, M. W., Dumic, M., Auslender, R., Gil-da-Silva-Lopes, V. L., Steinlicht, S., Rauh, M., Shalev, S. A., Thiel, C., Ekici,

A. B., Winterpacht, A., Kwon, Y. T., Varshavsky, A., and Reis, A. (2005) *Nature genetics* **37**, 1345-1350

68. Hwang, C. S., Shemorry, A., and Varshavsky, A. (2010) *Science* **327**, 973-977
69. Moerschell, R. P., Hosokawa, Y., Tsunasawa, S., and Sherman, F. (1990) *The Journal of biological chemistry* **265**, 19638-19643
70. Li, X., and Chang, Y. H. (1995) *Proceedings of the National Academy of Sciences of the United States of America* **92**, 12357-12361
71. Van Damme, P., Lasa, M., Polevoda, B., Gazquez, C., Elosegui-Artola, A., Kim, D. S., De Juan-Pardo, E., Demeyer, K., Hole, K., Larrea, E., Timmerman, E., Prieto, J., Arnesen, T., Sherman, F., Gevaert, K., and Aldabe, R. (2012) *Proceedings of the National Academy of Sciences of the United States of America* **109**, 12449-12454
72. Starheim, K. K., Gevaert, K., and Arnesen, T. (2012) *Trends in biochemical sciences* **37**, 152-161
73. Van Damme, P., Arnesen, T., and Gevaert, K. (2011) *The FEBS journal* **278**, 3822-3834
74. Helsens, K., Van Damme, P., Degroeve, S., Martens, L., Arnesen, T., Vandekerckhove, J., and Gevaert, K. (2011) *Journal of proteome research* **10**, 3578-3589
75. Arnesen, T., Van Damme, P., Polevoda, B., Helsens, K., Evjenth, R., Colaert, N., Varhaug, J. E., Vandekerckhove, J., Lillehaug, J. R., Sherman, F., and Gevaert, K. (2009) *Proceedings of the National Academy of Sciences of the United States of America* **106**, 8157-8162

76. Polevoda, B., Brown, S., Cardillo, T. S., Rigby, S., and Sherman, F. (2008) *Journal of cellular biochemistry* **103**, 492-508

77. Kreft, S. G., and Hochstrasser, M. (2011) *The Journal of biological chemistry* **286**, 20163-20174

78. Ravid, T., Kreft, S. G., and Hochstrasser, M. (2006) *The EMBO journal* **25**, 533-543

79. Kreft, S. G., Wang, L., and Hochstrasser, M. (2006) *The Journal of biological chemistry* **281**, 4646-4653

80. Behnia, R., Panic, B., Whyte, J. R., and Munro, S. (2004) *Nature cell biology* **6**, 405-413

81. Setty, S. R., Strochlic, T. I., Tong, A. H., Boone, C., and Burd, C. G. (2004) *Nature cell biology* **6**, 414-419

82. Jackson, C. L. (2004) *Nature cell biology* **6**, 379-380

83. Hofmann, I., and Munro, S. (2006) *Journal of cell science* **119**, 1494-1503

84. Graham, T. R. (2004) *Current biology : CB* **14**, R483-485

85. Coulton, A. T., East, D. A., Galinska-Rakoczy, A., Lehman, W., and Mulvihill, D. P. (2010) *Journal of cell science* **123**, 3235-3243

86. Arnesen, T., Van Damme, P., Polevoda, B., Helsens, K., Evjenth, R., Colaert, N., Varhaug, J. E., Vandekerckhove, J., Lillehaug, J. R., Sherman, F., and Gevaert, K. (2009) *Proc. Natl. Acad. Sci. USA* **106**, 8157-8162

87. Starheim, K. K., Gevaert, K., and Arnesen, T. (2012) *Trends Biochem. Sci.* **37**, 152-161

88. Polevoda, B., and Sherman, F. (2003) *J. Mol. Biol.* **325**, 595-622

89. Van Damme, P., Lasac, M., Polevoda, B., Gazquezc, C., Elosegui-Artolae, A., Kim, D. S., De Juan-Pardoe, E., Demeyera, K., Holef, K., Larreac, E., Timmermana, E., Prietoc, J., Arnesenf, T., Shermand, F., Gevaerta, K., and Aldabec, R. (2012) *Proc. Natl. Acad. Sci. USA* **109**, 12449-12454

90. Scott, D. C., Monda, J. K., Bennett, E. J., Harper, J. W., and Schulman, B. A. (2011) *Science* **334**, 674-678

91. Choudhary, C., Kumar, C., Gnad, F., Nielsen, M. L., Rehman, M., Walther, T. C., Olsen, J. V., and Mann, M. (2009) *Science* **325**, 834-840

92. Gautschi, M., Just, S., Mun, A., Ross, S., Rücknagel, P., Dubaquié, Y., Ehrenhofer-Murray, A., and Rospert, S. (2003) *Mol. Cell. Biol.* **23**, 7403-7414

93. Mullen, J. R., Kayne, P. S., Moerschell, R. P., Tsunasawa, S., Gribskov, M., Colavito-Shepanski, M., Grunstein, M., Sherman, F., and Sternglanz, R. (1989) *EMBO J.* **8**, 2067-2075

94. Park, E. C., and Szostak, J. W. (1992) *EMBO J.* **11**, 2087-2093

95. Hwang, C.-S., Shemorry, A., and Varshavsky, A. (2010) *Science* **327**, 973-977

96. Varshavsky, A. (2011) *Prot. Sci.* **20**, 1298-1345

97. Piatkov, K. I., Brower, C. S., and Varshavsky, A. (2012) *Proc. Natl. Acad. Sci. USA* **109**, E1839-E1847

98. Tasaki, T. S., Sriram, S. M., Park, K. S., and Kwon, Y. T. (2012) *Annu. Rev. Biochem.* **81**, 261-289

99. Dougan, D. A., Micevski, D., and Truscott, K. N. (2011) *Biochim. Biophys. Acta* **1823**, 83-91

100. Mogk, A., Schmidt, R., and Bukau, B. (2007) *Trends Cell Biol.* **17**, 165-172

101. Varshavsky, A. (2008) *J. Biol. Chem.* **283**, 34469-34489

102. Hwang, C.-S., Shemorry, A., and Varshavsky, A. (2010) *Nat. Cell Biol.* **12**, 1177-1185

103. Wang, H., Piatkov, K. I., Brower, C. S., and Varshavsky, A. (2009) *Mol. Cell* **34**, 686-695

104. Brower, C. S., and Varshavsky, A. (2009) *PLoS ONE* **4**, e7757

105. Piatkov, P. I., Colnaghi, L., Bekes, M., Varshavsky, A., and Huang, T. T. (2012) *(submitted for publication)*

106. Halbach, A., Zhang, H., Wengi, A., Jablonska, Z., Gruber, I. M., Halbeisen, R. E., Dehé, P. M., Kemmeren, P., Holstege, F., Géli, V., Gerber, A. P., and Dichtl, B. (2009) *EMBO J.* **28**, 2959-2570

107. Duncan, C. D., and Mata, J. (2011) *PLoS Genet.* **7**, e1002398

108. Brandman, O., Stewart-Ornstein, J., Wong, D., Larson, A., Williams, C. C., Li, G. W., Zhou, S., King, D., Shen, P. S., Weibezahn, J., Dunn, J. G., Rouskin, S., Inada, T., Frost, A., and Weissman, J. S. (2012) *Cell* **151**, 1042-1054

109. Hartl, F. U., Bracher, A., and Hayer-Hartl, M. (2011) *Nature* **475**, 324-332

110. Wolf, D. H., and Stolz, A. (2012) *Biochim. Biophys. Acta* **1823**, 117-124

111. Guerriero, C. J., and Brodsky, J. L. (2012) *Physiol Rev.* **92**

112. Ravid, T., and Hochstrasser, M. (2008) *Nat. Rev. Mol. Cell Biol.* **9**, 679-689

113. Fredrickson, E. K., and Gardner, R. G. (2012) *Semin. Cell Dev. Biol.* **23**, 530-537

114. Varshavsky, A. (2012) *Annu. Rev. Biochem.* **81**, 167-176

115. Finley, D., Ulrich, H. D., Sommer, T., and Kaiser, P. (2012) *Genetics* **192**, 319-360

116. Smith, M. H., Ploegh, H. L., and Weissman, J. S. (2011) *Science* **334**, 1086-1090

117. Sztul, E., and Lupashin, V. (2009) *FEBS Lett.* **583**, 3770-3783

118. Miller, V. J., and Ungar, D. (2012) *Traffic* **13**, 891-897

119. Fotso, P., Koryakina, Y., Pavliv, O., Tsiomenko, A. B., and Lupashin, V. V. (2005) *J. Biol. Chem.* **280**, 27613-27623

120. Lees, J. A., Yip, C. K., Walz, T., and Houghton, F. M. (2010) *Nat. Struct. Mol. Biol.* **11**, 1292-1298

121. Barford, D. (2011) *Q. Rev. Biophys.* **44**, 153-190

122. Hershko, A. (2010) *Mol. Biol. Cell* **15**, 1645-1647

123. Pines, J. (2011) *Nat. Rev. Mol. Cell Biol.* **12**, 427-438

124. Goetze, S., Qeli, E., Mosimann, C., Staes, A., Gerrits, B., Roschitzki, B., Mohanty, S., Niederer, E. M., Laczko, E., Timmerman, E., Lange, V., Hafen, E., Aebersold, R., Vandekerckhove, J., Basler, K., Ahrens, C. H., Gevaert, K., and Brunner, E. (2009) *PLoS Biol.* **7**, e1000236

125. Ghaboosi, N., and Deshaies, R. J. (2007) *Mol. Biol. Cell.* **18**, 1953-1963

126. Setty, S. R. G., Strochlic, T. I., Tong, A. H. Y., Boone, C., and Burd, C. G. (2004) *Nat. Cell Biol.* **6**, 414-419

127. Monda, J. K., Scott, D. C., Miller, D. J., Lydeard, J., King, D., Harper, J. W., Bennett, E. J., and Schulman, B. A. (2012) *Structure* **21**, 1-12

128. Zhang, Z., Kulkarni, K., Hanrahan, S. J., Thompson, A. J., and Barford, D. (2010) *EMBO J.* **29**, 3733-3744

129. Helbig, A. O., Gauci, S., Raijmakers, R., van Breukelen, B., Slijper, M., Mohammed, S., and Heck, A. J. R. (2010) *Mol Cell Proteom.* **9**, 928-939

130. Chen, J., and Archer, T. (2005) *Mol. Cell. Biol.* **25**, 9016-9027

131. Siegel, J. J., and Amon, A. (2012) *Annu. Rev. Cell. Dev Biol.* **28**, 189-214

132. Forte, G. M. A., Pool, M. R., and Stirling, C. J. (2011) *PLoS Biol.* **9**, e1001073

133. Hwang, C.-S., Shemorry, A., and Varshavsky, A. (2009) *Proc. Natl. Acad. Sci. USA* **106**, 2142-2147

134. Hwang, C.-S., and Varshavsky, A. (2008) *Proc. Natl. Acad. Sci. USA* **105**, 19188-19193

135. Xia, Z., Webster, A., Du, F., Piatkov, K., Ghislain, M., and Varshavsky, A. (2008) *J. Biol. Chem.* **283**, 24011-24028

136. Xia, Z., Turner, G. C., Hwang, C.-S., Byrd, C., and Varshavsky, A. (2008) *J. Biol. Chem.* **283**, 28958-28968

137. Turner, G. C., Du, F., and Varshavsky, A. (2000) *Nature* **405**, 579-583

138. Byrd, C., Turner, G. C., and Varshavsky, A. (1998) *EMBO J.* **17**, 269-277

139. Hu, R.-G., Wang, H., Xia, Z., and Varshavsky, A. (2008) *Proc. Natl. Acad. Sci. USA* **105**, 76-81

140. Eisele, F., and Wolf, D. H. (2008) *FEBS Lett.* **582**, 4143-4146

141. Heck, J. W., Cheung, S. K., and Hampton, R. Y. (2010) *Proc. Natl. Acad. Sci. USA* **107**, 1106-1111

142. Graciet, E., and Wellmer, F. (2010) *Trends Plant Sci.* **15**, 447-453

143. Varshavsky, A. (1996) *Proc. Natl. Acad. Sci. USA* **93**, 12142-12149

144. Hu, R.-G., Sheng, J., Xin, Q., Xu, Z., Takahashi, T. T., and Varshavsky, A. (2005) *Nature* **437**, 981-986

145. Hwang, C.-S., Sukalo, M., Batygin, O., Addor, M. C., Brunner, H., Aytes, A. P., Mayerle, J., Song, H. K., Varshavsky, A., and Zenker, M. (2011) *PLoS One* **6**, e24925

146. Zenker, M., Mayerle, J., Lerch, M. M., Tagariello, A., Zerres, K., Durie, P. R., Beier, M., Hülskamp, G., Guzman, C., Rehder, H., Beemer, F. A., Hamel, B., Vanlieferinghen, P., Gershoni-Baruch, R., Vieira, M. W., Dumic, M., Auslender, R., Gil-da-Silva-Lopes, V. L., Steinlicht, S., Rauh, R., Shalev, S. A., Thiel, C., Winterpacht, A., Kwon, Y. T., Varshavsky, A., and Reis, A. (2005) *Nat. Genet.* **37**, 1345-1350

147. Prasad, R., Kawaguchi, S., and Ng, D. T. W. (2010) *Mol. Biol. Cell* **21**, 2117-2127

148. Kurosaka, S., Leu, N. A., Zhang, F., Bunte, R., Saha, S., Wang, J., Guo, C., He, W., and Kashina, A. (2010) *PLoS Genet.* **6**, e1000878

149. Zhang, F., Saha, S., Shabalina, S. A., and Kashina, A. (2010) *Science* **329**, 1534-1537

150. Lee, M. J., Tasaki, T., Moroi, K., An, J. Y., Kimura, S., Davydov, I. V., and Kwon, Y. T. (2005) *Proc. Natl. Acad. Sci. USA* **102**, 15030-15035

151. Piatkov, K. I., Colnaghi, L., Bekes, M., Varshavsky, A., and Huang, T. T. (2012) *Mol. Cell* **(in press)**

152. Kwon, Y. T., Kashina, A. S., Davydov, I. V., Hu, R.-G., An, J. Y., Seo, J. W., Du, F., and Varshavsky, A. (2002) *Science* **297**, 96-99

153. Lee, M. J., Kim, D. E., Zakrzewska, A., Yoo, Y. D., Kim, S. H., Kim, S. T., Seo, J. W., Lee, Y. S., Dorn, G. W., 2nd, Oh, U., Kim, B. Y., and Kwon, Y. T. (2012) *J. Biol. Chem.* **287**, 24043-24052

154. Polevoda, B., Arnesen, T., and Sherman, F. (2009) *BMC Proceedings* **3**, S2

155. Ausubel, F. M., Brent, R., Kingston, R. E., Moore, D. D., Smith, J. A., Seidman, J. G., and Struhl, K. (2010) *Current Protocols in Molecular Biology.*, Wiley-Interscience, New York

156. Sherman, F. (1991) *Meth. Enzymol.* **194**, 3-21

157. Longtine, M. S., McKenzie, A., 3rd., Demarini, D. J., Shah, N. G., Wach, A., Brachat, A., Philippsen, P., and Pringle, J. R. (1998) *Yeast* **14**, 953-961

158. Dohmen, R. J., Stappen, R., McGrath, J. P., Forrová, H., Goffeau, A., and Varshavsky, A. (1995) *J. Biol. Chem.* **270**, 18099-18109

159. Mumberg, D., Muller, R., and Funk, M. (1994) *Nucleic Acids Res.* **22**, 5767-5768